NATIONAL TECHNICAL UNIVERSITY OF ATHENS

School of Civil Engineering

Laboratory for Earthquake Engineering

Modal Parameter Identification using the Continuous Wavelet Transform

Hera Yanni

A dissertation submitted in partial fulfillment of the requirements for the degree of Master of Science in
Analysis and Design of Earthquake Resistant Structures (ADERS)

Supervisor
Dr. Michalis Fragiadakis
Associate Professor NTUA

Athens, February 2022

Abstract

   Modal parameter identification is a fundamental procedure in structural engineering, applied both in the design phase of new structures as well as the monitoring or the assessment of existing structures.

The objective of this thesis is the application of the Continuous Wavelet Transform (CWT) on the free decay responses of damped linear structural systems, with the aim of the identification of their modal parameters. Both single degree of freedom (s.d.o.f.) and multi degree of freedom (m.d.o.f.) systems were examined, under the assumptions of weak damping and of linear behaviour. The condition of weak damping allowed the consideration of the processed signals as a sum of components consisting of asymptotic frequency modulated signals. Consequently, the concept of the analytic signal with the terms of instantaneous amplitude, phase and frequency was applied and the modal parameter identification was performed directly, by employing procedures and equations involving these signals.

The CWT is a multi-scale time-frequency signal processing method, based on a set of family wavelets formed by scaling and translation of a prototype mother wavelet. Two complex mother wavelets were employed, the Complex Morlet wavelet and the Cauchy wavelet of order n. The CWT using a complex mother wavelet returns information about both the instantaneous amplitude and instantaneous phase of each component within the processed signals, as the calculated data tends to "concentrate" near a series of curves in the time-frequency domain, called the ridges of the transform. Ridges can be defined as the place where the instantaneous frequency of the signal is equal to the analyzing wavelet's center frequency. Each ridge corresponds to a component of the signal, and thus, the identification of the ridges allows for the estimation of the corresponding instantaneous frequencies, the damping rations and the mode shapes. The algorithms implemented for the identification of ridges focus on *differential methods*, specifically the *"Simple"* method that employs the modulus of the CWT and the *"Marseille"* method that employs the phase of the CWT.

The thesis is structured into three thematic sections: The first thematic section presents the essential engineering, physical and mathematical theoretical background, with emphasis in signal processing techniques and the fundamental definitions and properties of the CWT. The second thematic section focuses on the methods and algorithms that are applied for modal parameter identification using the CWT and the third involves two numerical applications of the provided methods, one over a s.d.o.f system and one on a m.d.o.f. system.

The implementation of the algorithms, the calculations and the visualizations are done with MATLAB ver.R2021a, using the standard features and additionally the Signal Processing Toolbox and the Wavelet Toolbox.

Περίληψη

Ο προσδιορισμός των ιδιοχαρακτηριστικών (ιδιοσυχνότητες, ποσοστά απόσβεσης, ιδιομορφές) μιας κατασκευής είναι μια θεμελιώδης διαδικασία στη δομική μηχανική, η οποία εφαρμόζεται τόσο στη φάση του σχεδιασμού νέων κατασκευών όσο και στην παρακολούθηση της δομικής ακεραιότητας (Structural Health Monitoring) ή την αποτίμηση υφιστάμενων κατασκευών (Damage detection).

Τα κύρια βήματα μιας τέτοιας διαδικασίας είναι τρία: Πρώτο βήμα είναι η διέγερση της κατασκευής και η συλλογή δεδομένων, η οποία μπορεί να γίνει μέσω Πειραματικής ιδιομορφικής ανάλυσης (Experimental Modal Analysis) ή μέσω Λειτουργικής ιδιομορφικής ανάλυσης (Operational Modal Analysis). Το δεύτερο βήμα είναι η ανάλυση αυτών των δεδομένων με μεθόδους επεξεργασίας σημάτων (Signal Processing Methods), οι οποίες περιλαμβάνουν μεθόδους στο πεδίο του χρόνου (Time domain), στο πεδίο της συχνότητας (Frequency Domain) και στο πεδίο της χρονο-συχνότητας (Time-Frequency domain). Το τρίτο βήμα είναι ο υπολογισμός των ιδιοχαρακτηριστικών με εφαρμογή κατάλληλων αλγορίθμων και εξισώσεων.

Η παρούσα μεταπτυχιακή εργασία εστιάζεται στην εκτίμηση των ιδιοχαρακτηριστικών σε υφιστάμενες κατασκευές με χρήση μιας μεθόδου στο πεδίο της χρονο-συχνότητας, τον Συνεχή Κυματιδιακό Μετασχηματισμό (Continuous Wavelet Transform - CWT).

Εξετάζονται τόσο συστήματα ενός βαθμού ελευθερίας (s.d.o.f.) όσο και συστήματα πολλαπλών βαθμών ελευθερίας (m.d.o.f.) με την παραδοχή γραμμικής ελαστικής συμπεριφοράς και υποκρίσιμης απόσβεσης, στα οποία αφού εισάγονται κάποιες αρχικές συνθήκες, στη συνέχεια αφήνονται να ταλαντωθούν ελεύθερα και καταγράφονται οι αποκρίσεις της μετατόπισης, της ταχύτητας και της επιτάχυνσης με τον χρόνο.

Οι αποκρίσεις των μονοβαθμίων συστημάτων είναι σήματα που περιέχουν μία συνιστώσα (monocomponent), ενώ των πολυβαθμίων συντίθενται από πολλές συνιστώσες (multicomponent) από τις οποίες κάθε μια αντιστοιχεί σε μια ιδιομορφή. Τα σήματα των αποκρίσεων έχουν επιπλέον το χαρακτηριστικό ότι είναι μη-στάσιμα, δηλαδή το συχνοτικό τους περιεχόμενο μεταβέλλεται με τον χρόνο.

Η ανάλυση και επεξεργασία τέτοιων σημάτων απαιτεί την έκφρασή τους σε συνάρτηση με τον χρόνο. Η παραδοχή της υποκρίσιμης απόσβεσης, επιτρέπει την εφαρμογή της έννοιας του αναλυτικού σήματος (Analytic Signal) εισάγοντας τις έννοιες του στιγμιαίου πλάτους (Instantaneous amplitude), της στιγμιαίας φάσης (Instantaneous phase) και της στιγμιαίας συχνότητας (Instantaneous frequency), οι οποίες μπορούν να εφαρμοστούν κατάλληλα σε αλγορίθμους και σχέσεις ώστε να υπολογιστούν τα ιδιοχαρακτηριστικά του συστήματος.

Τα αποτελέσματα μιας ανάλυσης στο πεδίο της χρονο-συχνότητας είναι τρισδιάστατα και συνήθως απεικονίζονται σε ένα δισδιάστατο γράφημα όπου ο οριζόντιος άξονας είναι ο χρόνος και ο κατακόρυφος άξονας είναι η συχνότητα, επομένως μπορούν να ληφθούν για το επεξεργασμένο σήμα πληροφορίες και για τη συμπεριφορά των συνιστωσών του ως προς τον χρόνο αλλά και για το συχνοτικό του περιεχόμενο.

Μια τέτοια απεικόνιση στο πεδίο της χρονο-συχνότητας έχει το χαρακτηριστικό ότι τα υ-πολογιζόμενα δεδομένα τείνουν να "συγκεντρώνονται" σε περιοχές του γραφήματος, σχηματίζοντας "κορυφές" (Ridges). Κάθε κορυφή, αντιστοιχεί σε μια συνιστώσα του σήματος με συγκεκριμένη συχνότητα, επομένως, ο προσδιορισμός των κορυφών αυτών επιτρέπει τον υπολογισμό των αντίστοιχων στιγμιαίων συχνοτήτων και των αντίστοιχων ποσοστών αποσβέσεως και ιδιομορφών με χρήση σχέσεων του αναλυτικού σήματος.

Ο Συνεχής Κυματιδιακός Μετασχηματισμός είναι μια μέθοδος επεξεργασίας σήματος με μεταβαλλόμενη ευκρίνεια η οποία βασίζεται σε ένα σύνολο ομοειδών συναρτήσεων (κυματιδίων-(wavelets» οι οποίες παράγονται από την κλιμάκωση (scaling) και τη χρονική μετάθεση (translation) μιας πρωτότυπης (μητρικής) συνάρτησης (mother wavelet) η οποία έχει μορφή κυματιδίου. Επομένως Ο Συνεχής Κυματιδιακός Μετασχηματισμός είναι συνάρτηση δύο παραμέτρων: της κλίμακας a και της χρονικής μετάθεσης b.

Στην παρούσα εργασία χρησιμοποιήθηκαν δύο μιγαδικά μητρικά κυματίδια, το μιγαδικό κυματίδιο Morlet (Complex Morlet wavelet) και το κυματίδιο Cauchy (Cauchy wavelet) τάξης n.

Ο Συνεχής Κυματιδιακός Μετασχηματισμός που χρησιμοποιεί μιγαδικό μητρικό κυματίδιο παράγει πληροφορίες τόσο για το στιγμιαίο πλάτος όσο και για τη στιγμιαία φάση κάθε συνιστώσας στο επεξεργασμένο σήμα. Κάθε συνιστώσα αναλύεται ξεχωριστά.

Για τον προσδιορισμό των κορυφών υπάρχουν διάφορες μέθοδοι οι οποίες μπορούν να καταταχθούν σε δύο κατηγορίες: Differential Methods και Integral Methods. Οι differential μέθοδοι βασίζονται στην εύρεση ενός ζεύγους (α,b) για το οποίο η στιγμιαία συχνότητα του σήματος ταυτίζεται με τη κεντρική συχνότητα του κυματιδίου. Οι integral μέθοδοι βασίζονται στην θεώρηση των κορυφών ως συναρτήσεις οι οποίες έχουν ως χαρακτηριστικό ότι η ενέργειά τους τείνει να συγκεντρώνεται στις περιοχές των κορυφών στο διάγραμμα του χρόνου-συχνότητας. Εισάγοντας μια κατάλληλη συνάρτηση ποινής (penalty function), οι κορυφές εκτιμώνται ως οι συναρτήσεις αυτές που ελαχιστοποιούν αυτή τη συνάρτηση.

Στην παρούσα μεταπτυχιακή εργασία εφαρμόστηκαν δύο differential μέθοδοι , η Simple Method και η Marseille method. Η Simple Method βασίζεται στο διάγραμμα του μέτρου του συνεχή κυματιδιακού μετασχηματισμού και αναζητεί τις περιοχές όπου εμφανίζεται το τοπικό μέγιστο, που αντιστοιχεί στην συχνότητα της αντίστοιχης συνιστώσας. Η Marseille Method είναι ένας επαναληπτικός αλγόριθμος και βασίζεται στο διάγραμμα της φάσης του συνεχή κυματιδιακού μετασχηματισμού. Η Marseille Method αναζητεί την κλίμακα στην οποία αντιστοιχεί η εξεταζόμενη κορυφή και υπολογίζει την συχνότητα ως την κλίση του διαγράμματος της φάσης με τον χρόνο για την κλίμακα αυτή.

Με γνωστές τις κορυφές, μπορεί να βρεθεί η τιμή του συνεχή κυματιδιακού μετασχηματισμού στις θέσεις αυτές και υπολογίζονται τα αναλυτικά σήματα. Η συσχέτιση της λύσης της εξίσωσης της κίνησης για ελεύθερη ταλάντωση με απόσβεση με το στιγμιαίο πλάτος και τη στιγμιαία φάση του αναλυτικού σήματος, επιτρέπει την εξαγωγή εξισώσεων που υπολογίζουν τα ποσοστά απόσβεσης και τις ιδιομορφές.

Η παρούσα μεταπτυχιακή εργασία διαρθρώνεται σε τρεις θεματικές ενότητες: Η πρώτη θεματική ενότητα παρουσιάζει το βασικό τεχνικό, φυσικό και μαθηματικό θεωρητικό υπόβαθρο, με έμφαση σε σημαντικές έννοιες της επεξεργασίας σήματος όπως η δειγματοληψία (sampling) και η αναδίπλωση (aliasing), καθώς και σε θεμελιώδεις ορισμούς και ιδιότητες του συνεχή κυματιδιακού μετασχηματισμού, αναλύοντας τις έννοιες της ευκρίνειας (resolution), της επιλογής των μητρικών κυματιδίων, της κανονικοποίησης (normalization), της παραμέτρου της κλίμακας (scaling), της παραμέτρου (Q), της επιρροής των φαινομένων των άκρων (edge effects) και του υπολογισμού του μετασχηματισμού σε Η/Υ. Η δεύτερη θεματική ενότητα επικεντρώνεται στις μεθόδους και τους αλγορίθμους που εφαρμόζονται για τον προσδιορισμό των ιδιοχαρακτηριστικών μιας κατασκευής με τη χρήση συνεχή κυματιδιακού μετασχηματισμού όπως αναλύθηκε προηγουμένως και η τρίτη περιλαμβάνει δύο αριθμητικές εφαρμογές των μεθόδων αυτών, μία σε ένα μονοβάθμιο σύστημα και μία σε ένα πολυβάθμιο σύστημα.

Η υλοποίηση των αλγορίθμων, οι υπολογισμοί και οι απεικονίσεις έγιναν με το πρόγραμμα MATLAB ver.R2021a, χρησιμοποιώντας επιπλέον και τα Signal Processing Toolbox και Wavelet Toolbox.

Preface and Acknowledgements

Preface

This master thesis signals the end of my journey in the MSc program "Analysis and Design of Earthquake Resistant Structures" (ADERS) of the School of Civil Engineering, NTUA, and the successful completion of a personal goal: Years ago, on the second year of my undergraduate studies at the School of Civil Engineering, NTUA, I came across a leaflet that promoted the ADERS program. I felt extremely interested and drawn by it's subjects, so from that moment I had decided that I would do my best and succeed my admission to the program. Now, being at the finish line and seeing how far I have come and how much I have achieved, I can only feel great happiness, pride and immense gratitude for everything.

Acknowledgements

First of all, I would like to express my gratitude to my supervisor, Associate Professor Michalis Fragiadakis, for offering me this thesis and introducing me into the exiting world of the wavelets. This topic was quite new to me and it really sparked my interest. I am very thankful for his continuous help, guidance and support during the course of this thesis, always providing me with helpful advice and material to study. I am also grateful for him believing in me and choosing to continue our collaboration as my supervisor in my PhD. I truly appreciate his support and advice.

I am also grateful to all the professors of the program for all the knowledge that they provided us through this program.

Special thanks also to my parents, Ilias and Mailinta, for their dear support through the years. I truly appreciate their confidence in my decisions and I am extremely grateful for them always making making sure that I have the precious time to work and follow my dreams.

As endings always signal new beginnings, I will conclude this preface with just a phrase:

"To the infinity and beyond!"

Contents

List of Figures

List of Tables

Listings

Acronyms, Abbreviations and Symbols

CWT	Continuous Wavelet Transform
WT	Wavelet Transform
DOF	Degree of Freedom
FFT	Fast Fourier Transform
FT	Fourier Transform
FRF	Frequency Response Function
TF	Time Frequency
EMA	Experimental Modal Analysis
OMA	Operational Modal Analysis
MDOF	Multi Degree of Freedom system
SDOF	Single Degree of Freedom system
STFT	Short Time Fourier Transform

$sgn(\omega)$ Sign function of a real number, equal to:

$$sgn(\omega) = \begin{cases} -1, & \text{if } \omega < 0. \\ 0, & \text{if } \omega = 0. \\ 1, & \text{if } \omega > 0. \end{cases}$$

$\Theta(\omega)$ Heaviside step function, equal to:

$$\Theta(\omega) = \begin{cases} 1, & \text{if } \omega \geq 0. \\ 0, & \text{if } \omega < 0. \end{cases}$$

ω	Angular frequency [rad/sec]
f	Frequency [Hz]
Fs	Sampling frequency [Hz]
T	Period [sec]
dt	Sampling period [sec]

ω	Undamped angular frequency [rad/sec]
$\widetilde{\omega}$	Damped angular natural frequency of the system [rad/sec]
m	Mass

c	Damping constant
c_{cr}	Critical damping coefficient
k	Stiffness
ξ	Damping ratio
$\boldsymbol{u}(t)$	Displacement vector
$\dot{\boldsymbol{u}}(t)$	Velocity vector
$\ddot{\boldsymbol{u}}(t)$	Acceleration vector
$\boldsymbol{M}$	Mass matrix
$\boldsymbol{C}$	Damping matrix
$\boldsymbol{K}$	Stiffness matrix
$\boldsymbol{\Phi}$	Mode shape matrix
$u(t)$	Real valued signal
$Z_u(t)$	Analytic signal
$T_\psi[u](b,a)$	Continuous wavelet transform of a signal u(t)
$A(t)$	Instantaneous amplitude
$\varphi(t)$	Instantaneous phase
$\omega(t)$	Instantaneous angular frequency
$\psi(t)$	Mother wavelet defined in the time domain
$\widehat{\psi}(\omega)$	Mother wavelet defined in the frequency domain
t_ψ	Mother wavelet center time
ω_ψ	Mother wavelet center frequency
Δt_ψ	Duration of the mother wavelet
$\Delta \omega_\psi$	Bandwidth of the mother wavelet
a	Scale parameter of the CWT
b	Time translation parameter of the CWT
$a_r(b)$	Ridge of the CWT
$\overline{z}$	Complex conjugate of a complex number z
$x * y$	Convolution of x and y
$\widehat{g}$	Fourier transform of a function g
$\langle x, y \rangle$	Inner product of x and y
$\lVert \cdot \rVert$	Norm of a function, vector or matrix

$\angle$	Phase of the function/signal
$Re()$	Real part of a complex number
$Im()$	Imaginary part of a complex number
$\mathbb{C}$	The set of all complex numbers
$\mathbb{R}$	The set of all real numbers
$\mathbb{R}_+^*$	The set of all real positive numbers excluding zero
$\mathbb{Z}$	The set of integers (positive, negative, zero)

Chapter 1

Introduction

1.1 Overview

Modal analysis is the process of identifying the inherent dynamic characteristics of a structural system - also known as modal parameters - which include the natural frequencies, the damping ratios, and the mode shape vectors. Modal parameter identification is a fundamental part of structural engineering, used in the design phase of new structures as well as the monitoring or the assessment of existing structures under dynamic loading conditions.

When designing a new structure, the mass, damping, and stiffness matrix are known and used as inputs to modal analysis, the results (outputs) of which provide the prediction of the structure's response to external loading, allowing the evaluation and optimization of the design. For example, assessing the structure's natural periods and mode shapes might result in a design decision to modify the structure's stiffness matrix to avoid unwanted behavior. For existing structures, the knowledge of the structure's current modal parameters is important for its monitoring and/or assessment through dynamic analysis, structural health monitoring, detection of structural modifications In these cases, the problem is inverse, meaning that the damping and stiffness matrix are not known in advance. Consequently, modal parameter identification is essential for the description of an existing structural system by a model, based on data recorded by instruments. For example, structural damage caused by earthquake results in observable changes in the vibratory responses of the structure, hence the analysis of these outputs can allow the estimation of the decreased stiffness matrix. Furthermore, measured vibration data can be employed for validating and updating finite-element-models used in the analysis, even in the design phase for some cases of complex and large-scale structures where experiments and tests are also performed.

In existing structures, modal parameter identification consists in general of three main steps: excitation and data acquisition, signal processing, and modal parameters estimation. Focusing on the first step, vibration measurements can be obtained by performing Experimental Modal Analysis (EMA) or Operational Modal Analysis (OMA). Experimental Modal Analysis or Modal testing is an experimental process where the structure is subjected to a controlled input (excitation) and its output (response) is being recorded. This testing procedure is generally made under carefully-controlled conditions and consequently yields more accurate and detailed information. However, EMA methods have some disadvantages, including the requirement of special equipment that might make the testing quite costly, the difficulties and expenses of implementing such testing in large-scale structures, and the need for evacuation before any testing. Operational Modal Analysis aims at identifying the modal properties of a structure based on vibration data collected during operating conditions of the structure under study, i.e., no initial excitation or known artificial excitation is applied. OMA methods are output-only methods, since the system's input is unknown (wind, traffic, machine vibration etc.). In many

cases, OMA is used instead of classical modal analysis, as it provides the advantages of not requiring special equipment and evacuation of the structure during the measurements and it can be applied in situations where it is difficult or impossible to artificially excite the structure. Additionally, OMA methods make possible the ongoing structural health monitoring and damage detection. Yet, OMA methods do have disadvantages; since the ambient vibration is random, there is a chance that some of the modes appearing in the measured response might not originate from the structure itself, but might actually be input modes that have been filtered through the structural system. Thus, the methods should be able to distinguish the system's natural frequencies from excitation frequencies through stochastic procedures.

Continuing in the second and third step of modal parameter identification, signal processing techniques are used for the estimation of modal parameters. The most common classification of these methods is done according to the domain where the data are processed: time domain, frequency domain and time-frequency domain. Early methods used to work in the frequency domain, but problems associated with frequency resolution, leakage and high modal densities led to the developing of time domain methods as a promising alternative. In general, time domain models tend to provide the best results when a wide frequency range or large number of modes exist in the data, whereas frequency domain models tend to provide the best results when the frequency range of interest is limited and the number of modes is relatively small. However, time domain methods have a major disadvantage in that they can only estimate modes inside the frequency range of analysis, and take no account on the residual effects of modes that lie outside that range [19]. Frequency domain methods still have the difficulties mentioned, plus they do not provide any information about the time where the components of the frequency content of the under signal are present. For a long time, frequency domain identification and time domain identification were considered as competing methods to solve the same problem. A main conclusion of Ljung and Glover [17] back in 1979, was that these two approaches are complementary rather than rivalling. Thus, taking it one step further, the need to overcome the inability of the frequency domain approach to capture time-varying features of a structure but retain the advantage of the frequency content information, led to the development of the time-frequency domain methods. These methods study a signal in both the time and frequency domains simultaneously; subsequently they were widely applied and used in system identification and damage detection.

The wavelet transform (WT) originated in the early 1980s in the works of Morlet [25] who used it in seismology and then Grossman and Morlet [26] who developed the geometrical formalism of the continuous wavelet transform. The Continuous wavelet transform (CWT) is a time-frequency domain output-only modal identification method and was first proposed by Staszewski and Cooper [36] in 1995 to estimate structural parameters. Since then, the potential of modal parameter identification using the CWT has been receiving considerable attention in the literature (see from [37] to [52] and [13], [33]). Early works were focused on exploring and developing methods and techniques for the estimation of a system's natural frequencies, damping ratios and gradually mode shapes, e.g. Ruzzene et al. [39] in 1997 showed that the CWT applied to free responses of m.d.o.f system represents a consistent improvement for the estimation of instantaneous frequencies and viscous damping ratios compared to the Hilbert transform (HT), Staszewski also in 1997 [37] proposed three different damping estimation procedures for MDOF systems, based on

the CWT. Le and Argoul in 2003 [13] focused on improving the use of continuous wavelet transform for modal identification purposes from the free-decay responses of structures by exploring the choice of the mother wavelet and of its localization properties and making efforts to remedy the problem of edge effect appearing during the numerical computation of the CWT. Progressively these methods were expanded to process free responses of nonlinear systems, e.g. by Staszewski [38] and Argoul and Le [43]. In recent years there has been a great focus on the practical utilization of the CWT in structural health monitoring (SHM) for modal parameter identification through ambient excitation measurements, e.g. Le and Paultre [48] in 2012 proposed a new method that allows a straightforward CWT calculation from raw data of ambient tests and the direct use of all available procedures that are valid for free decay response in identifying modal parameters, while Wijesundara et al. [51] in 2015 explored the estimation of modal parameters of low-rise buildings using ambient excitation measurements.

The CWT is a linear transform by definition and thus, appropriate for multi-component signals. Compared with other identification techniques, CWT has two fundamental advantages in structural parameter identification [52]. The first is the multi-resolution ability inherent to wavelet analysis. This property enables the separation of the close frequency components of a coupled frequency signal, allowing MDOF systems to be handled directly. Additionally this ability ensures that CWT can work as a band-pass filter and automatically filter out noise from the signal; hence this method can handle very noisy measurements. The second advantage is that CWT can resolve multiple structural parameters from a single signal without knowledge of the applied force acting on the structure. This advantage makes it a promising output-only identification method that is widely utilized in both EMA and OMA. Another important advantage of the CWT is that it can be used to analyze time series that contain nonstationary power at many different frequencies [5], and therefore it can process nonstationary vibration measurements. Lastly, the use of the CWT allows to determine the time variation of instantaneous amplitude and phase of each component within the signal [13] a property that facilitates the identification procedure of modal parameters through the identification of ridges and the reconstruction of the signal; procedures that will be applied in this thesis.

1.2   Objective

The objective of this thesis is the application of the Continuous Wavelet Transform (CWT) on the free decay responses of damped linear structural systems, with the aim of the identification of their modal parameters. Both SDOF and MDOF systems are examined, under the assumptions of weak damping and of linear behaviour. The condition of weak damping allows the consideration of the processed signals as a sum of components consisting of asymptotic frequency modulated signals. Consequently, the concept of the analytic signal with the terms of instantaneous amplitude, phase and frequency can be applied and the modal parameter identification can be performed directly, by employing procedures and equations involving these signals. The CWT is a multi-scale time-frequency analysis method, based on a set of family wavelets formed by scaling and translation of a prototype mother wavelet. Two complex mother wavelets are employed, the Complex Morlet wavelet and the Cauchy wavelet of order n. The CWT using a complex mother wavelet returns information about both the instantaneous amplitude and

instantaneous phase of each component within the processed signals, as the calculated data tends to "concentrate" near a series of curves in the time-frequency domain, called the ridges of the transform. Ridges can be defined as the place where the instantaneous frequency of the signal is equal to the analyzing wavelet's center frequency. Each ridge corresponds to a component of the signal, and thus, the identification of the ridges allows for the estimation of the corresponding instantaneous frequencies, the damping rations and the mode shapes. The algorithms implemented for the identification of ridges focus on *differential methods*, specifically the *"Simple"* method that employs the modulus of the CWT and the *"Marseille"* - as referred by Carmona in [2] - method that employs the phase of the CWT.

1.3 Thesis outline

This thesis is divided into 7 Chapters and is structured in such way that:

- Chapters 1 to 3 present the essential engineering, physical and mathematical theoretical background that is required to comprehend the contents and the methods applied in the following Chapters. Specifically:

  ✤ Chapter 1 illustrates a general overview of modal parameter identification methods.

  ✤ Chapter 2 presents basic ideas and definitions used in signal processing that will be applied for the analysis of the signals.

  ✤ Chapter 3 provides the fundamental definitions and properties needed to understand the wavelet theory and its application to the estimation of modal parameters, plus information on the implementation of the CWT in the MATLAB environment for the calculations.

- Chapter 4 describes the methods and algorithms that will be applied for modal parameter identification using the CWT.

- Chapter 5 provides an essential background on structural dynamics and presents the techniques used in obtaining the modal parameters from the results of the CWT analysis.

- Chapter 6 presents two numerical applications of the method, one over a s.d.o.f system and one on a m.d.o.f. system.

- Chapter 7 concludes, summarizes this thesis and presents some remarks and suggestions for further work.

1.4 Programs applied

- ***MATLAB ver.2021a***

The implementation of the algorithms, the calculations and the visualizations are done with MATLAB ver.R2021a, using the standard features and additionally the Signal Processing Toolbox and the Wavelet Toolbox.

The Signal Processing Toolbox provides functions and apps to analyze, preprocess, and extract features from uniformly and nonuniformly sampled signals, while the Wavelet Toolbox provides apps and functions for analyzing and synthesizing signals and images[21]. There are two cwt commands, one called new version and one the old of the legacy one; their main difference in the calculation of the CWT is on the choice of normalization of the mother wavelet. In this thesis, the old cwt command was employed as it allowed to insert user defined mother wavelets. More will be discussed thoroughly on Chapter 6.

1.5 Modal parameter identification techniques

As mentioned in the overview, the dynamic properties of existing structures, such as natural periods, mode shapes and damping ratios, can be estimated by applying modal identification methods on vibration measurements. Modal parameter identification based on vibration measurements represents a challenge because the recorded data is non-stationary and is usually embedded in high-level noise. Furthermore, the estimation of closely-spaced modal parameters present in a structure is an additional challenge in those methods. Over the past decades, many modal identification methods have been developed and can be found in the literature. A classification of such methods, influenced by Maia et al.[19] is the following:

- ***Time domain, frequency domain and time-frequency domain methods***

The most common classification of modal parameter identification techniques is done according to the domain where the data are processed; therefore they can be categorized into three main groups: *time domain*, *frequency domain* and *time-frequency domain*.

Time domain methods do not employ any form of transform space to process a time series. Modal parameters are estimated with techniques that use correlation functions of the signals, or the signals directly. Time domain methods can be categorized in subspace methods, free decay-based methods and statistical time series [29]. Some examples are the Random Decrement (RD) method, the Least-Squares Complex Exponential (LSCE), the Polyreference Complex Exponential (PRCE), the Ibrahim Time Domain (ITD), the Single-Station Time Domain (SSTD), and the Eigensystem Realization Algorithm (ERA) [19]. However, a crucial problem with many time domain methods is the incapacity for distinguishing structural modes from uncorrelated modes and the fact that they are often very sensitive to noise in the data since all frequency components present in the data are included into the analysis.

Frequency domain methods are based on the frequency response function (FRF). A FRF is a function used to quantify in the frequency domain the response of a system to an excitation and is usually graphically represented by Bode type diagrams. Frequency domain methods can be categorized in Fourier transform-based methods and high-resolution methods [29]. Some examples are the Frequency Domain Decomposition method (FDD), the Enhanced Frequency Domain Decomposition (EFDD), the Curve Fit frequency Domain Decomposition (CFDD), the Peak Picking Method (PPM), the Polyreference Least Squares Complex Frequency Domain method (p-LCSF) and the Complex mode indication function method (CMIF). However, frequency response methods require the application

of signal processing techniques as transformation of the data from the time domain to the frequency domain is prone to leakage errors: noiseless data in the time domain might result in noisy FRFs. Additionally, problems in frequency domain methods also arise for nonlinear or lightly damped structural systems.

Time-frequency (TF) domain methods process a signal in both the time and frequency domains simultaneously: The signal is treated as a function whose domain is the two-dimensional real plane, obtained from the signal via a time–frequency transform. The most basic TF methods are the short-time Fourier transform (STFT) and the Gabor transform. More sophisticated techniques already established are the wavelet transform (WT - Continuous wavelet transform and Discrete wavelet transform), the Hilbert-Huang transform (HHT), the Blind Source Separation (BSS) and the Wigner–Ville distribution (WVD), however still new methods and further improvements are developed and explored such as the Local Characteristic-scale Decomposition (LCD), the Compact Empirical Mode Decomposition (CEMD), the music-Empirical Wavelet Transform and the Novel blind source separation algorithm [29].

Summarizing, table 1.1, influenced by [29] presents a summary of the main advantages and disadvantages of the signal processing techniques used for modal parameter identification.

- ### *Direct and Indirect methods*

Time domain and frequency domain methods can be further divided into *direct* and *indirect* (or modal) methods, while the time-frequency domain methods belong only to the indirect methods. In *direct methods*, the identification procedure is directly based on the spatial model, i.e., on the general matrix equation of dynamic equilibrium. In *indirect methods* the identification procedure is based on the modal model, i.e., on the modal parameters (natural frequencies, damping ratios, modal constants and their phases) which are the quantities in the characteristic solutions of the dynamic equations of equilibrium.

- ### *Single Degree Of Freedom and Multiple Degrees Of Freedom*

A further division refers to the number of modes which can be analysed. *Single Degree Of Freedom analysis* (SDOF) considers only one mode in the analysis, whereas in *Multiple Degrees Of Freedom* (MDOF) analysis more than one modes are considered. In the time domain, only MDOF analysis can be performed, whereas in the frequency domain, both types of analysis: SDOF and MDOF can be performed in the indirect methods. Direct methods only apply to MDOF analysis.

Table 1.1: Advantages and disadvantages of the signal processing techniques used in modal parameter identification

Domain	Method	Advantages	Disadvantages
Time domain methods	STSM	Straightforward use. Modal parameters can be directly obtained from the model. Can deal with small noise-level signals.	Linear and stationary model. Accuracy depends on the level of noise. Model order selection can be a time-consuming procedure.
	Free-decay methods	Filtering properties. Can process raw ambiental responses. Simplicity. Easy implementation.	Multi-stage schemes. Increased computational burden. Sensitive to noise. Used mainly to process stationary responses.
	SSI methods	Noise immunity. Closely-spaced modes detection. Modal parameters are directly obtained. Can process slightly non-stationary signals.	Heavy computational burden. Require calibration. Generation of spurious modes.
Frequency domain methods	FT-based methods	Straightforward use. Modal parameters are directly obtained. Simplicity (PP). Non a-priori knowledge of the number of modes is required. Filtering properties (FRF).	Fixed resolution. Can deal with only stationary signals. Sensitive to noise. Closely-spaced modes are not detected. The input excitation should be available for FRF estimation. If the excitation source is a harmonic signal, the estimated natural frequency can be biased (FDD).
	High-resolution methods	Noise immunity. Closely-spaced modes can be detected.	Computational burden. Require calibration.

Time-Frequency domain methods	Wavelet transform	Multi-resolution time-frequency analysis. Detection of sudden frequency changes and transients. Closely-spaced modes can be detected. Can process non-stationary signals. Can handle noisy signals. Output-only method. Modal parameters are directly obtained.	Accuracy depends on the mother wavelet choice. Require calibration. Computational burden for very fine analysis. DWT method lacks translation-invariance.
	HHT and its variants	Adaptive method. Straightforward use. The individual modes are extracted. No user interaction is required.	Mode-mixing. EMD variants require calibration. Its computational burden and accuracy depends on selected algorithm: EMD (lower), ensemble EMD (higher).
	BSS	Good accuracy to separate frequency components. Can identify modes with low energy.	A pre-filtered stage is required for signal embedded in high-level noise. High damping ratios cannot be accurately estimated.

- ***Single-Input-Single-Output, Single-Input-Multi-Output and Multi-Input-Multi-Output methods***

In *Input-output* methods, used in EMA, modal parameter identification is based in the use of both input (excitation) and output (response) measurements, whereas in *output-only* methods, used in OMA, only output signals are used for estimating the modal parameters.

While collecting the measured data, FRFs can also be calculated from the recorded responses. These FRFs are the result of exciting the structure at each selected point and measuring the response at several locations across that structure. *Single-Input-Single-Output methods* refer to modal analysis methods that can be applied only to a single FRF at a time. Other methods allow for several FRFs to be analysed simultaneously, with responses taken at various points on the structure, but using one excitation point.

These methods are called *Single-Input-Multi-Output* (SIMO) methods. The philosophy behind this category of methods is that the natural frequencies and damping ratios do not vary (theoretically) from FRF to FRF (they are global properties of a structure) and, thus, it should be possible to obtain a consistent and unique set of those properties by processing several FRFs at the same time. Finally, there are methods that can process all the available FRFs simultaneously, from various excitation and response locations. These methods are called *Multi-Input-Multi-Output* (MIMO) methods [19].

- ***Wavelet Analysis***

Referring to the classification of Maia et al [19], wavelet analysis for modal identication is added as a time-frequency domain processing method allows modal identication through applying the indirect MDOF and SIMO methods.

Chapter 2

Signal Processing Basics

This chapter presents some fundamental concepts and definitions used in signal processing, so that they can be utilized for the wavelet analysis theory and its application on the estimation of modal parameters (natural frequencies, damping ratios and mode shapes) that will be described in the following chapters.

2.1 Signal definition and examples

A signal can be defined as a physical quantity that varies with time, space, or any other independent variable (or variables) [31]. In signal processing, a signal is a function that conveys information about a phenomenon and can be represented in the time domain, the frequency domain, and the time-frequency domain.

Typical examples of signals are: human speech, whale song, music, photographs and videos, electrocardiograms, encephalograms, etc. Noise is also a signal, but the information conveyed by it, is unwanted in general, hence it is considered as undesirable. In structural dynamics, the most commonly used signals are those that provide information about the acceleration, velocity, and displacement response of structures during an earthquake or any other kind of vibration. One example of such a signal is an accelerogram.

A system may be defined as a physical device that performs an operation such as analysis, modification, filtering, synthesis, etc. on a signal. "Passing" a signal through a system is called *Signal Processing*.

2.2 Traditional Signal Representation

2.2.1 *Time domain representation*

A typical representation of a signal u is as a function of time, called temporal or time-domain representation $u(t)$ (see figure 2.2(a)). The time-domain representation, $u(t)$, provides information about the actual presence of the signal, its start and end time point, it's duration in time, its strength and temporal evolution, and it indicates how the signal's energy (see equations 2.21 and 2.22) is distributed along the t axis. The observation and recording of physical phenomena from instruments is usually performed in relation to time, and therefore the signals obtained are in the time-domain, for example an accelerogram or the displacement response of a structure during an earthquake.

2.2.2 *Frequency domain representation*

Another typical representation of a signal u is as a function of frequency, called the spectral or frequency-domain representation $u(\omega)$ (see figure 2.2(b)). The frequency-domain representation, $u(\omega)$, provides information about which frequencies are present in the signal, their relative magnitudes, minimum frequency, maximum frequency, and the

bandwidth formed by their difference. A signal represented in time-domain can be also represented in the frequency-domain by applying a pair of mathematical operators called a transform. An example is the Fourier Transform (FT) (see equation 3.9) which decomposes a function into the sum of a (potentially infinite) number of sine wave frequency components. The inverse Fourier transform (see equation 3.10) converts the frequency domain function back to a time function.

2.2.3 *Time – frequency representation*

Most signals from the nature are intrinsically non-stationary, in the sense that their frequencies vary along time. Using a time-frequency representation, the signal is represented on a time-frequency plane, providing both temporal information and spectral information simultaneously. This illustration on the time-frequency plane allows the determination of the variation of the instantaneous amplitude and phase of each component within a signal in time.

Depending on the application, a time-frequency representation is more advantageous: the time-domain representation does not provide information about the frequency content of a signal and the frequency domain representation dos not not locate in time the frequency content of the signal, whereas the time-frequency representation illustrates information on both variables, see figures 2.1 and 2.2.

Example 2.1. Consider a non stationary sinusoidal function composed of the sum of three sine functions, with frequencies $F_1 = 1Hz$, $F_2 = 3Hz$ and $F_3 = 10Hz$: respectively, defined as,

$$u(t) = u_1(t) + u_2(t) + u_3(t)$$

where

$$
\begin{aligned}
u_1(t) &= \sin(2\pi t) &&, && t \in [0, 10] \ sec \\
u_2(t) &= \sin(6\pi t) &&, && t \in (2, 7) \ sec \\
u_3(t) &= \sin(8\pi t) &&, && t \in (5, 10] \ sec
\end{aligned}
$$

The signal $u(t)$ is illustrated in the TF plane in figure 2.1. As it can be observed, both information about time and frequency can be extracted: The frequency components at 1, 3, and 10 Hz are clearly shown in the frequency axis, while information about the presence of each component in time is clearly illustrated: component $u_1(t)$ is present for all the signal's duration, $u_2(t)$ is present from 2sec to 7sec and $u_3(t)$ is present from 5sec until the end of the signal.
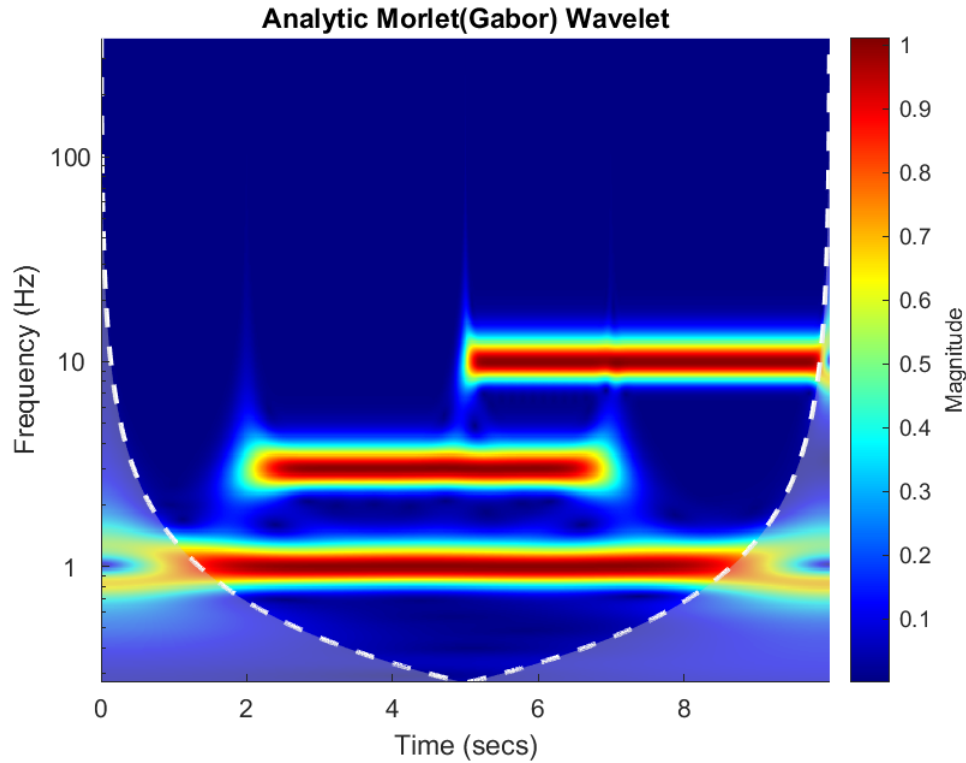
Figure 2.1: Time-frequency domain representation of a non stationary signal. It can be observed that it illustrates information on both time t and frequency f.

Example 2.2. Consider the displacement response of a SDOF signal with natural frequency $f = 3Hz$ and duration $L = 10sec$. The three representations of the signal are shown in figure 2.2. a) time domain, (b) frequency domain, and (c) joint time-frequency domain.

As it can be observed, (a) provides information only about the signal's duration which is $L = 10sec$, (b) provides information about the system's natural frequency $f = 3Hz$, whereas (c) illustrates information on both variables t and f.
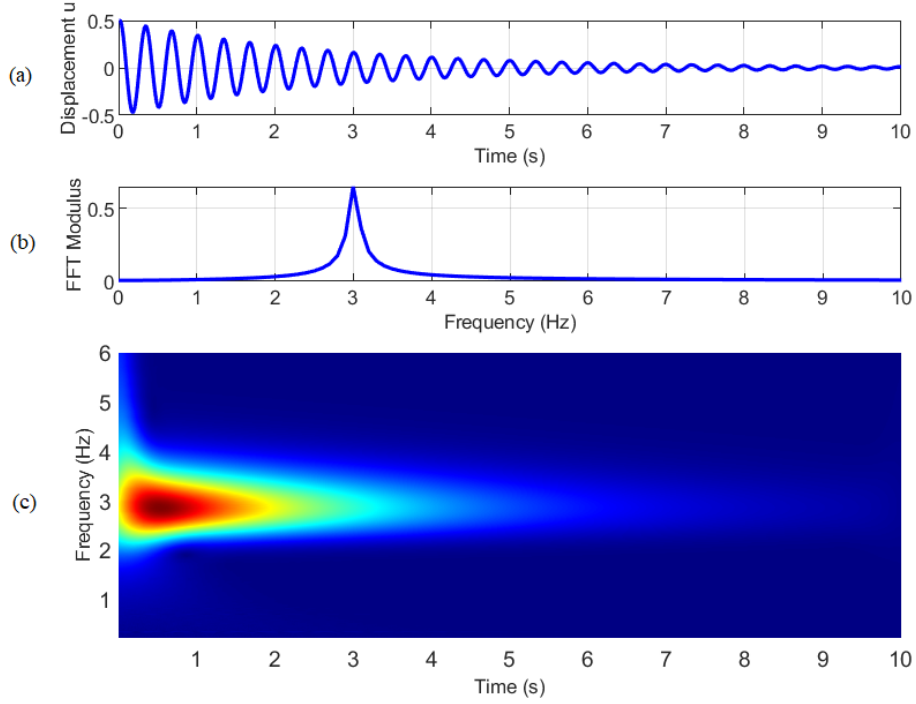
Figure 2.2: Three representations of free decay response u of a s.d.o.f. system: (a) time domain, (b) frequency domain, and (c) joint time-frequency domain.

2.3 Complex Numbers

Fundamental concepts of oscillatory motion involve the use of complex numbers. Additionally, the mother wavelets used in this thesis are complex, which results in the CWT also being complex. Therefore, this section provides a brief reference to basic definitions and properties of complex numbers.

Definition 2.1 (Complex number). Let $i^2 = -1$. A complex number is of the form:

$$z = x + yi \tag{2.1}$$

where $Re(z) = x$ and $Im(z) = y$ are real numbers.

Definition 2.2. (Modulus and argument)

    i. The modulus of a complex number $z = x + yi$, is defined as:

$$r = ||z|| = \sqrt{x^2 + y^2} \tag{2.2}$$

    ii. The argument of a complex number $z = x + yi$, denoted $\varphi = \arg(z)$, is defined as:

$$\varphi = \arctan\left(\frac{y}{x}\right), \quad or \quad \varphi = atan2[Re(z), Im(z)] = atan2(y, x) \tag{2.3}$$

13

Definition 2.3 (Euler's formula)**.** Euler's formula, establishes the fundamental relationship between the trigonometric functions and the complex exponential function and is expressed as:

$$e^{i\varphi} = \cos\varphi + i\sin\varphi \tag{2.4}$$

Using Euler's formula, trigonometric functions can be expressed as:

$$\cos\varphi = \frac{e^{i\varphi} + e^{-i\varphi}}{2} \tag{2.5}$$

and

$$\sin\varphi = \frac{e^{i\varphi} - e^{-i\varphi}}{2i} \tag{2.6}$$

Definition 2.4 (Polar form)**.** The polar form of a complex number with modulus r and argument φ denoted as: $z = r\angle\varphi$, is defined:

$$z = |z|e^{i\varphi} = |z|(\cos\varphi + i\sin\varphi) \tag{2.7}$$

Definition 2.5 (Complex conjugate)**.** The complex conjugate of a complex number $z = x + yi$ is defined as:

$$\overline{z} = x - yi, \quad or \quad z = |z|e^{-i\varphi} \tag{2.8}$$

2.4 Simple Harmonic Motion

Simple harmonic motion (a special class of oscillatory motion) can serve as a mathematical model for a variety of phenomena as it provides a basis for the characterization of more complicated periodic motion. Thus, this section provides some basic definitions and concepts which will be used in the following chapters.

2.4.1 *Trigonometric Notation for Simple Harmonic Motion*

Let the motion of a given point be described by the equation:

$$u(t) = A\sin(\omega t + \varphi) \quad or \quad u(t) = A\cos(\omega t + \varphi) \tag{2.9}$$

where
$u(t)$ is the displacement from the equilibrium position in m, cm, etc.,
A the displacement magnitude of the oscillation in m, cm, etc.,
ω the angular frequency in rad/s,
φ the phase angle in rad,
and t the time.
The quantity A is the single-peak amplitude; $u(t)$ moves between the limits $\pm A$, so the peak-to peak amplitude (also known as double amplitude) is $2A$. The time history of this simple harmonic displacement is shown in figure 2.3.
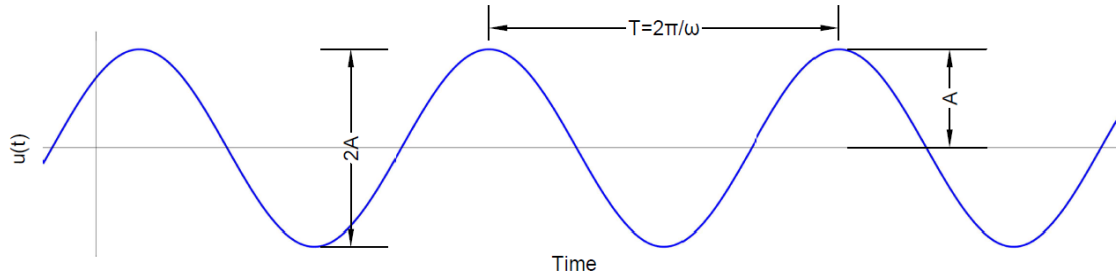
Figure 2.3: Time history of simple harmonic displacement.

The angular frequency ω is is the rate of change of the phase angle φ with time t:

$$\omega = \frac{d\varphi}{dt} \tag{2.10}$$

The angular frequency ω is also related with the frequency $f = 1/T$ (units in hertz) and the period $T = 1/f$ (units in seconds) through the following relations:

$$\omega = 2\pi f \tag{2.11}$$

and

$$\omega = \frac{2\pi}{T} \tag{2.12}$$

Simple harmonic motion can also be described as the sum of a sine function and a cosine function, that is:

$$u(t) = a\cos(\omega t) + b\sin(\omega t) \tag{2.13}$$

As seen in figure 2.4 the sum of the sine and cosine functions is also a sinusoid that oscillates at angular frequency, ω. The motion described by equation 2.13 can be expressed in the form of equation 2.9, with amplitude $A = \sqrt{a^2 + b^2}$ and phase angle $\varphi = \arctan(a/b)$.
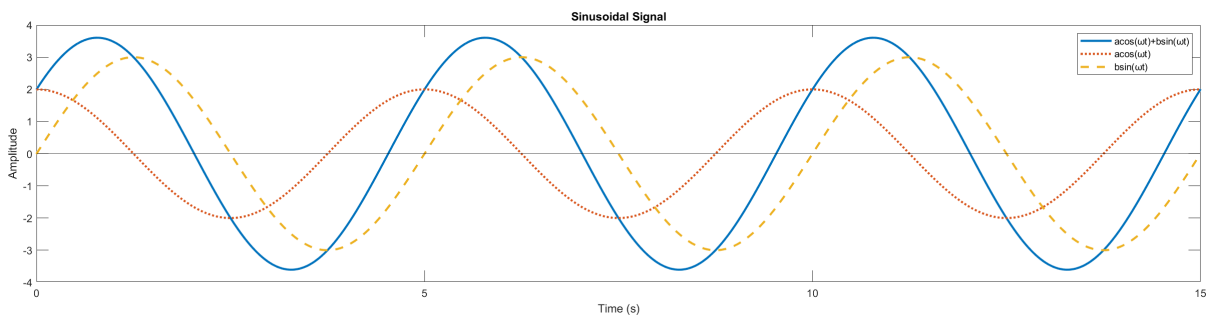
Figure 2.4: Summation of sine and cosine functions of the same frequency produces a sinusoid of the same frequency. Amplitude and phase of the sinusoid depends on the amplitudes of the sine and cosine functions.

15

2.4.2 Complex Notation for Simple Harmonic Motion

Trigonometric descriptions of simple harmonic motion use familiar functions that are easy to visualize. However, for many dynamic analyses, the use of trigonometric notation complicates considerably many operations, particularly the solution of differential equations. These analyses become much simpler when motions are described using complex notation, which can be derived directly from trigonometric notation using Euler's formula (see equation 2.4)., by substituting equations 2.5 and 2.6 in equation 2.13:

$$u(t) = \frac{a - ib}{2}e^{i\omega t} + \frac{a + ib}{2}e^{-i\omega t} \tag{2.14}$$

2.4.3 Displacement, Velocity, Acceleration

Differentiating with respect to time the expression for simple harmonic displacement produces expression for velocity and differentiating again produces the expression for acceleration, i.e for $\varphi = 0$:
In trigonometric notation:

$$u(t) = A\sin(\omega t) \tag{2.15}$$

$$\dot{u}(t) = \omega A\cos(\omega t) = \omega A\sin(\omega t + \frac{\pi}{2}) \tag{2.16}$$

$$\ddot{u}(t) = -\omega^2 A\sin(\omega t) = \omega^2 A\sin(\omega t + \pi) \tag{2.17}$$

In complex notation:

$$u(t) = Ae^{i\omega t} \tag{2.18}$$

$$\dot{u}(t) = i\omega Ae^{i\omega t} \tag{2.19}$$

$$\ddot{u}(t) = -\omega^2 Ae^{i\omega t} \tag{2.20}$$

2.5 Classification of signals

The methods employed in processing a signal depend heavily on the characteristics of that particular signal, for example, there are techniques that apply only to specific families of signals. Consequently, any investigation in signal processing requires knowledge of the classification of the signals that are involved in each application.

Signals can be classified according to many criteria into the following categories:

- **Continuous-time and Discrete-time signals.**

This classification's criteria is based on the characteristics of the time (independent) variable and the values they take. Let $u(t)$ be a function (signal) of the independent variable t, defined in the time domain:

If the independent variable t is continuous, $t \in \mathbb{R}$, i.e. between any two points in time there is an infinite number of other points in time, then the corresponding signal is a *continuous-time signal*, often called an analog signal. Any signal value can be found at any arbitrary point in time. Mathematically, these signals can be described by functions of a continuous variable and they are related to operations with integrals. A simple example of a continuous-time signal is a sinusoidal function $u(t) = sin(\omega t)$, where $t \in \mathbb{R}$, see figure 2.5.
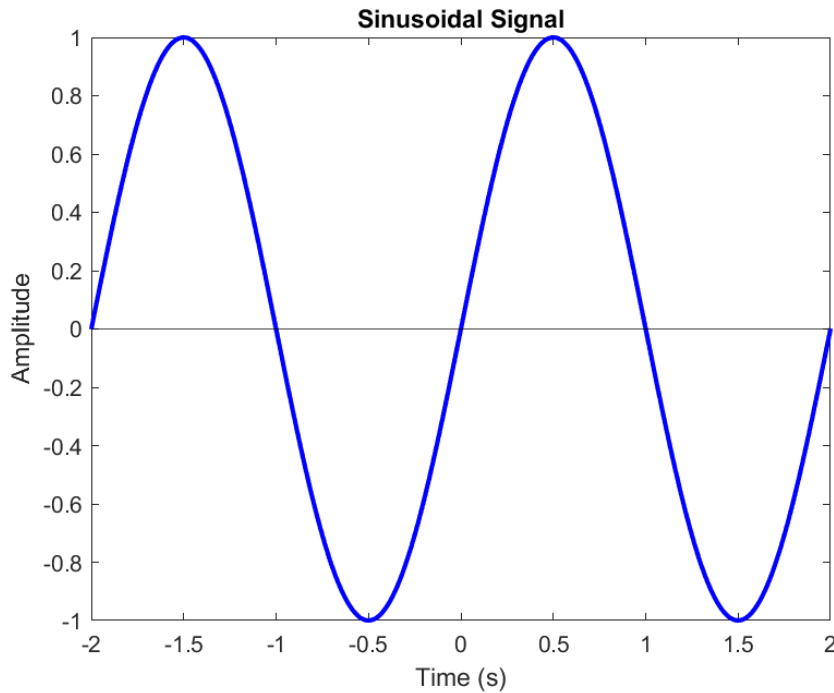
Figure 2.5: Example of a continuous time signal: Sinusoidal signal $u(t) = sin(\omega t)$, $t \in \mathbb{R}$, with angular frequency $\omega = \pi \; rad/sec$.

If the independent variable t takes on only discrete integer values, $t \in \mathbb{Z}$, for example $t = \pm 1$, ± 2, ± 3,..., then the corresponding signal is a *discrete-time signal*. A discrete-time signal is not defined at instants between two successive points in time, therefore mathematically it can be represented by a sequence of real or complex numbers. To emphasize the discrete-time nature of these signals, they can be denoted as $u(n)$ instead of $u(t)$. A simple example of a discrete-time signal is a sinusoidal sequence $u(n) = sin(\omega n)$, where $n \in \mathbb{Z}$, see figure 2.6.

Generally, discrete-time signals may arise in two ways:

1. By selecting values of a continuous-time signal at discrete-time instants. This process is called sampling and the values selected samples. As an example, figure 2.6 can be acquired by sampling the continuous-time signal of figure 2.5. This is a fundamental process, as most signals of practical interest in nature (e.g. seismic signals, speech) are analog; consequently, they must be converted into a discrete-time form to be able to be processed by digital means (e.g. computers). More will be discussed in detail in section 2.7.

2. By accumulating a variable's values over a period of time. For example, the daily rainfall data of a specific area or the hourly number of cars passing through a certain street result in discrete-time signals.
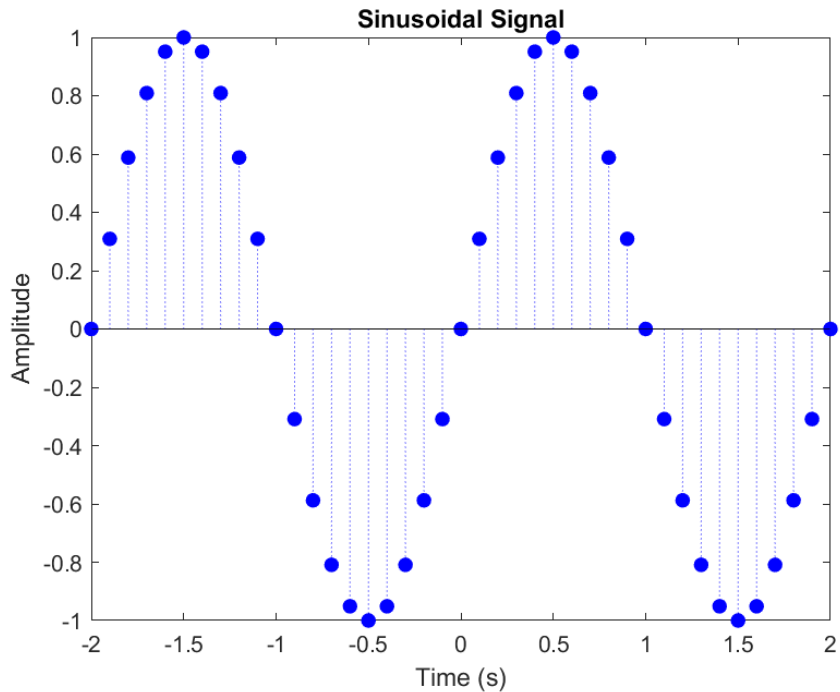
Figure 2.6: Example of a discete-time signal: Sinusoidal signal $u(n) = sin(\omega n)$, $n \in \mathbb{Z}$, with angular frequency $\omega = \pi \ rad/sec$.

- **Deterministic and Random Signals**

Mathematical analysis and processing of signals demands the availability of a mathematical expression of the signal itself. This requirement leads to another important classification of signals, in relation to the existence of not of this formula:

Deterministic signals are those whose values are predictable at any time and can be described exactly by a mathematical formula, a table of data, or a well-defined rule. It is worth mentioning that true deterministic signals are very rare in nature because unknown and uncontrollable factors (e.g. noise) usually influence the signal as well.

Random signals are signals that take on random values at any given time instant, therefore they are modeled stochastically, in probabilistic terms. Seismic signals and speech signals are examples of random signals.

- **Stationary and Non-stationary signals**

This classification results from the observation of the signal's frequency content over time:

Stationary signals are those whose frequency content remains unchanged in time. All

frequency components exist at all times.

Non-stationary signals are those whose frequency content varies in time. These kinds of signals are the ones that are found in nature.

- **Periodic and aperiodic signals**

Periodic signals. These signals have waveforms whose pattern repeats at equal increments of time; this is expressed mathematically as: $u(t + T) = u(t)$, where T is the period of continuous-time signals, or $u(n + N) = u(n)$, where N is the period for discrete-time signals.

Non-periodic or aperiodic signals, which are signals that are not periodic.

- **Energy signals and Power signals.**

This classification is based on the signal total energy E and signal average power P, definitions which are used to characterize a signal.

The total energy E of a signal is defined as:

For continuous-time signals u(t):

$$E = \int_{-\infty}^{+\infty} |u(t)|^2 dt \tag{2.21}$$

For discrete-time signals u(n):

$$E = \sum_{n=-\infty}^{+\infty} |u(t)|^2 \tag{2.22}$$

The average power P of a signal is defined as:

For continuous-time signals u(t):

$$P = \lim_{T \to \infty} \frac{1}{2T} \int_{-T}^{T} |u(t)|^2 dt \tag{2.23}$$

For discrete-time signals u(n):

$$P = \lim_{N \to \infty} \frac{1}{2N + 1} \sum_{n=-N}^{N} |u(t)|^2 \tag{2.24}$$

Hence, the classification goes as follows:

Energy signals are those whose total energy is equal to a finite positive value, i.e. $0 < E < +\infty$, and their average power is zero ($P = 0$). Aperiodic signals are an example of

energy signals.

Power signals are those whose average power P is finite, i.e. $0 < P < +\infty$, and their energy is infinite ($E = +\infty$). Periodic signals are examples of power signals.

- **Monocomponent and multicomponent signals**

This classification is based on the time-frequency domain, a concept which it will be discussed in the following section (see subsection 2.2.3) and Chapter 4, but it is presented here for the purpose of completeness.
A *monocomponent signal* is described in the time-frequency plane by a single "ridge" corresponding to an elongated region of energy concentration.[1] For example, the displacement response u(t) of a s.d.o.f system is a monocomponent signal (see figure 2.8).

A *multicomponent signal* may be described as the sum of two or more monocomponent signals. For example, the displacement response u(t) of a m.d.o.f system's d.o.f. is a multicomponent signal(see figure 2.9).

- **Noise**

The term noise originates from radio engineering, where it describes the unwanted signal that it is heard when the radio is not tuned exactly to a radio station. In signal processing, noise is a general term for unwanted (and, in general, unknown) modifications that interfere and degrade the desirable information of a signal. This can happen during capture, storage, transmission, processing, or conversion of a signal.[35]
Signals within which the presence of noise is insignificant, can be characterized as pure, while signals with significant noise present within them can be characterized as noisy. In real-life applications, signals are not "clean" in general and most often are embedded in noise. Noise can be eliminated by filtering of the signal. A filter is a system that removes unwanted components or features from a signal.

Example 2.3. Figure 2.7 shows the time-domain representations of six continuous-time signals (left hand side) and their respective frequency-domain representations (only the modulus plot is presented, right hand side): (a) is simple sinusoidal signal with a constant frequency f: pure, deterministic, periodic signal. (b) is a sum of sinusoids: a "multicomponent" pure signal containing several "components". (c) is monocomponent, nonstationary signal: has a single "component" whose local frequency $f(t)$ changes as time profresses. In this case, the dominant frequency at a certain time t is a linear function of time t, which it is called *"instantaneous frequency"* $f(t)$. (d) is a multicomponent, nonstationary signal.
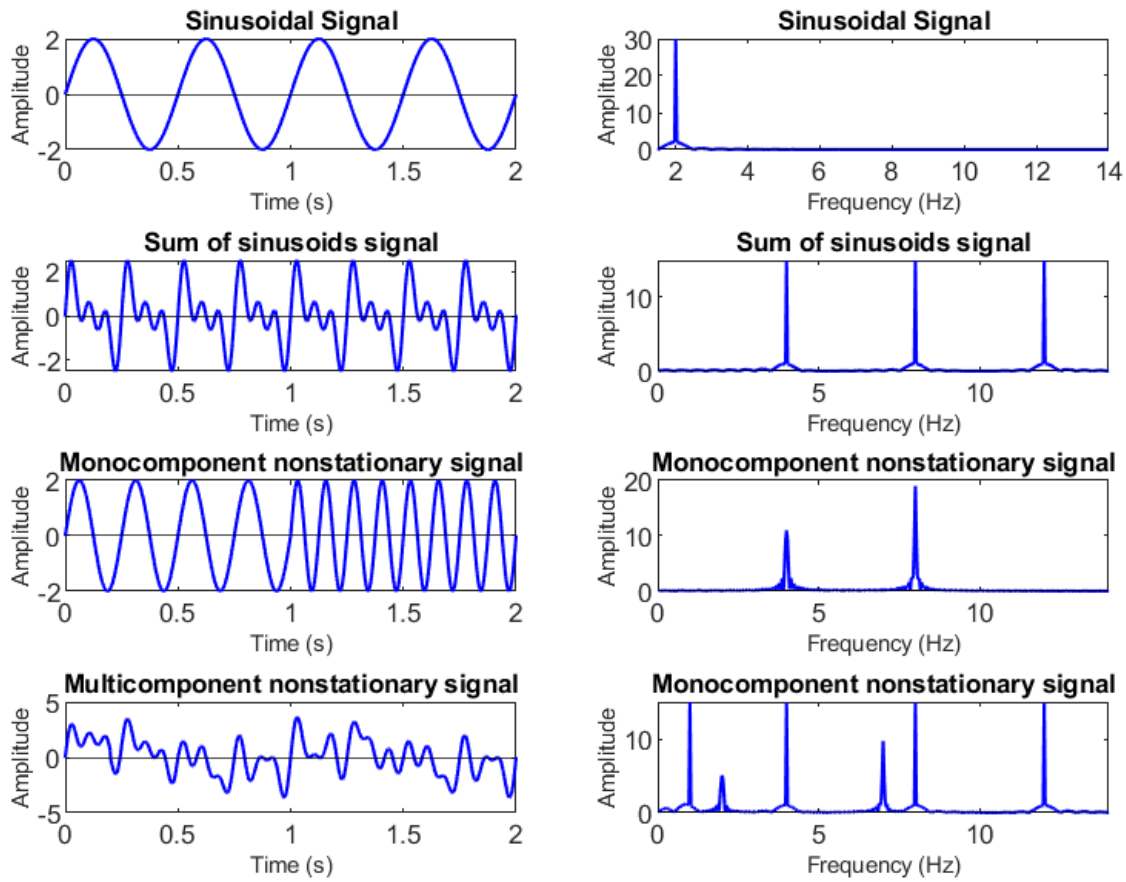
Figure 2.7: Example of time-domain representations of six continuous-time signals (left hand side) and their respective frequency-domain representations modulus plot (right hand side).

2.6 The Time-Frequency Approach

The basic product of a time-frequency analysis is a set of data represented in the 2D time-frequency plane as in figures 2.8, 2.9 and 2.10.

- *Instantaneous amplitude, phase and frequency*

As it was mentioned in Chapter 1, time-frequency methods have the ability to analyze non-stationary signals efficiently. The frequency of a sinusoidal signal is a well defined quantity, as it was seen in section 2.4. However, often in practice, signals are not truly sinusoidal, or even aggregates of sinusoidal components. Non-stationary signals do not lend themselves well to decomposition into sinusoidal. For such signals, the notion of frequency loses its effectiveness, and one needs to use a parameter which accounts for the time-varying nature of the process [1]. Following the thought process of the simple harmonic motion in equation 2.9 and 2.13, such signals can be expressed as:

For monocomponent, frequency modulated (FM) signal:

$$u(t) = A(t) \cos \varphi(t) \tag{2.25}$$

21

For a multicomponent, frequency modulated (FM) signal:

$$u(t) = \sum_{j=1}^{N} A(t) \cos \varphi(t) \tag{2.26}$$

Where $A(t)$ is the instantaneous amplitude and $\varphi(t)$ is the instantaneous phase of the signal.

Consequently, the instantaneous frequency (IF) is the temporal rate of the instantaneous phase and equation 2.10 becomes:

$$\omega(t) = \frac{\varphi(t)}{dt} = 2\pi f(t) \tag{2.27}$$
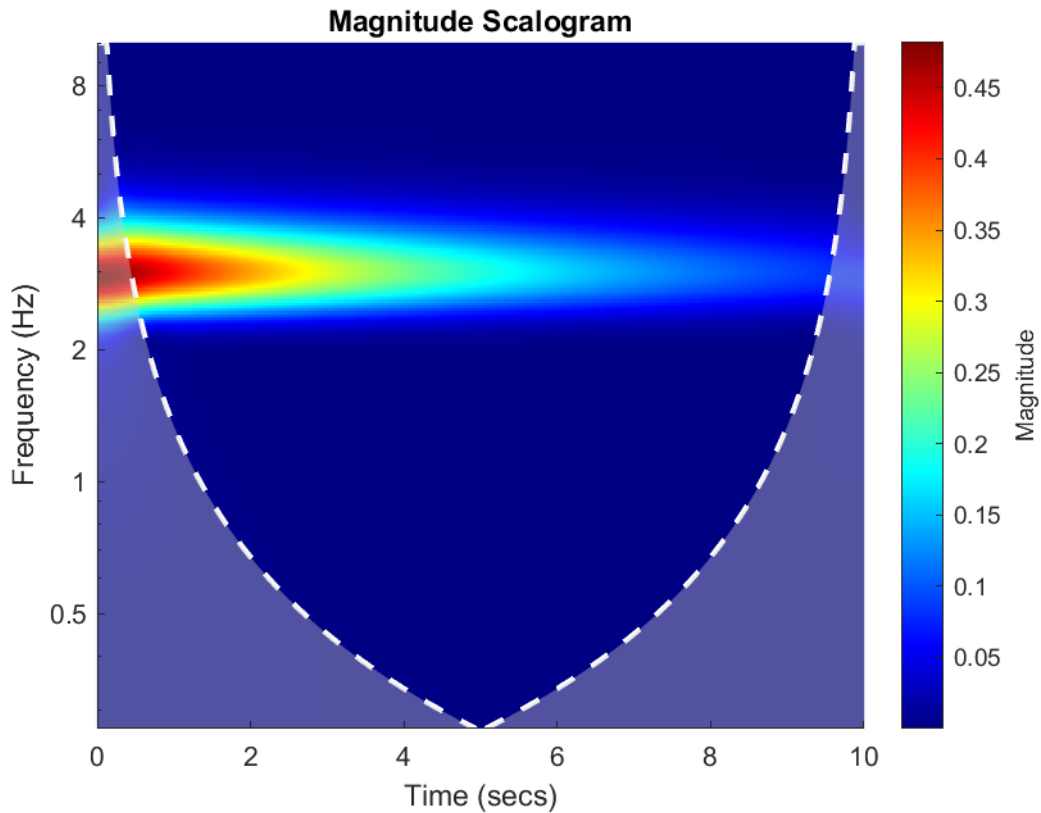
Figure 2.8: Example of time-frequency analysis of a monocomponent signal: Magnitude (Modulus) Scalogram of the CWT
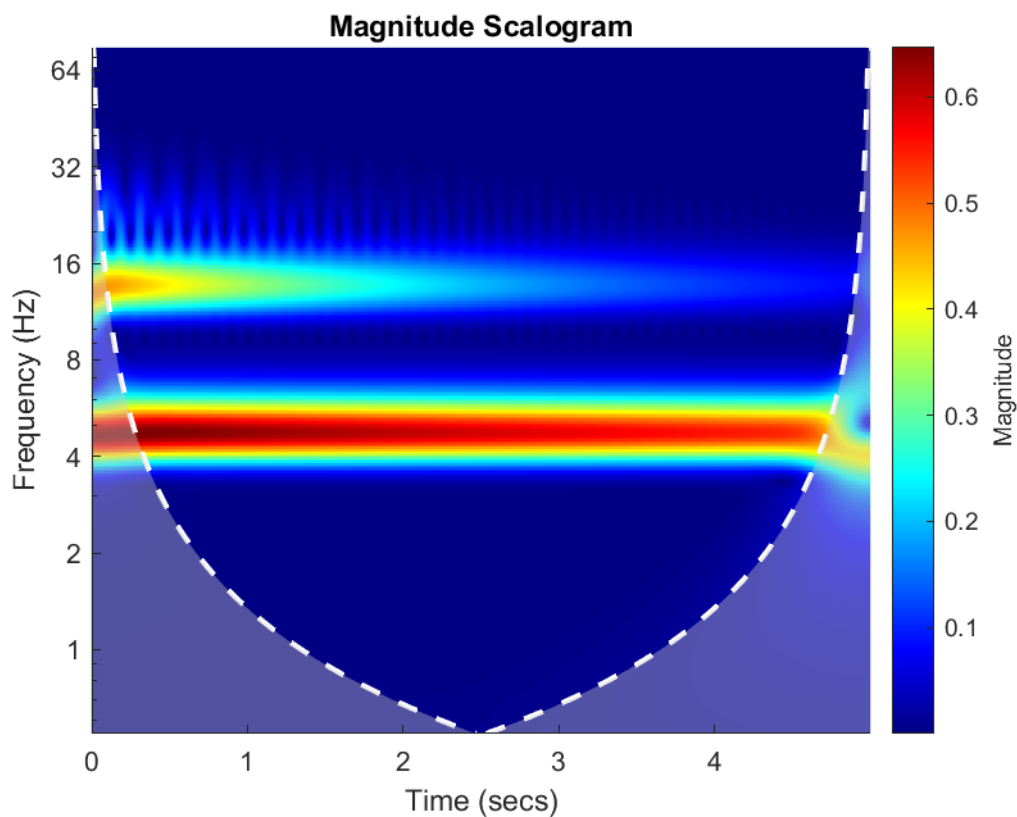
Figure 2.9: Example of time-frequency analysis of a multicomponent signal: Magnitude (Modulus) Scalogram of the CWT
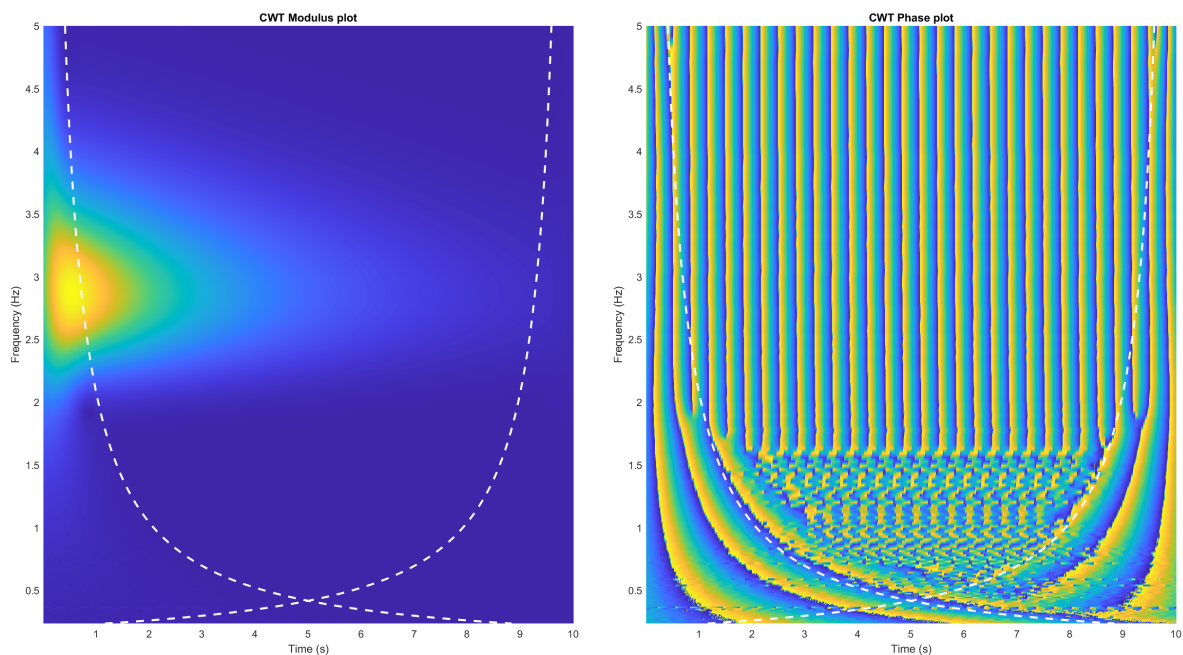
Figure 2.10: Example of time-frequency analysis of a monocomponent signal: Magnitude (Modulus) (left) and Phase Plot (right) of the CWT

- **Ridges**

The IF of a signal at time t_0 indicates the dominant frequency of the signal at that specific time, therefore it describes the frequency modulation law of the signal. For a monocomponent FM signal, the peak of the cross-sections parallel to the frequency axis of the time-frequency plane gives the IF law which describes the signal FM law, while for a multicomponent FM signal, the dominant peaks of the cross-sections parallel to the frequency axis of the time-frequency plane reflect the components' respective FM laws. Those peaks in the cross-sections parallel to the frequency axis correspond to elongated regions of energy concentration in the time-frequency plot, called *ridges*. For example, the signal of figure 2.8, is a monocomponent signal with frequency $f = 3Hz$; the ridge can be observed clearly as a function of time fixed around the frequency point $f = 3Hz$. Same in figure 2.9: the signal is multicomponent, containing the frequencies $f_1 = 4.75Hz$ and $f_2 = 13.60Hz$, the two ridges are clearly visible.

- **Positive and negative frequencies**

Mathematically, the frequency f ranges from $-\infty$ to $+\infty$, yet in practice only the positive frequencies are used, as it can be seen from the plots shown in the previous figures. The intuitive explanation is that f represents the number of oscillations per second, therefore is expected to be positive. Mathematically, this is based on a property of the FT: if $u(t)$ is real, its FT $\hat{u}(\omega)$ has Hermitian symmetry (see section 3.2.2), thus, the information contained in the negative frequencies is a duplication of the information contained in the positive frequencies. Therefore, in practice, negative frequencies are considered redundant and the analysis is done with positive frequencies. This is achieved by introducing a particular complex signal $Z(t)$ called the "analytic signal," which contains only positive frequencies.

More on analytic signals, ridges and instantaneous amplitude, phase and frequency will be discussed extensively in Chapter 4.

2.7 Sampling and Aliasing – Nyquist's Theorem

As referred in the previous section, most signals of practical interest in nature are continuous-time signals, and therefore they must be converted into a discrete-time form to be able to be processed by digital means. This conversion of a continuous time signal to a discrete-time signal is done through a procedure called *sampling*.

The sampling type that is used most often in practice is the periodic (or uniform) sampling, where the discrete-time signal is obtained by "taking samples" of the continuous-time signal every T_s seconds. The time interval T_s between successive samples is called the *sampling period*. Its reciprocal $F_s = 1/T_s$ is called the sampling rate (how many samples per second are recorded) or the *sampling frequency*.

Example 2.4. The figure 2.6 illustrates a discrete-time sinusoidal signal $u(n) = sin(\omega n)$ with angular frequency $\omega = \pi \ rad/sec$. The sampling frequency is $F_s = 10Hz$ and the sampling period $T_s = 0.1sec$. The figure can be produced by the following matlab script:

Listing 2.1: Creating the discrete-time sinusoidal signal of figure 2.6

```
1  % Discrete time Sine Signal
2  Fy=0.5                %signal frequency in Hz
3  omega=2*pi*Fy         %signal angular frequency in rad/s
4
5  Fs=10                 %sampling frequency in Hz
6  dt=1/Fs               %sampling period;
7  t=-10:dt:10;          %time intervals set
8  y=sin(omega*t);       %signal data set
9
10 figure()
11 hold on;  box on;
12 stem(t,y,'filled','b','LineStyle',':')
13 yline(0,'k')
14 title('Sinusoidal Signal');
15 xlabel('Time (s)')
16 ylabel('Amplitude')
17 xlim([-2 2])
```

The sampling rate has a significant effect on the reconstruction of the continuous real signal in the time domain. Insufficient sampling frequency results to a phenomenon called *aliasing*. Aliasing is an effect that causes different signals to become indistinguishable (or aliases of one another) when sampled. It also often refers to the distortion or artifact that results when a signal reconstructed from samples is different from the original continuous-time signal. Generally, a high F_s is desired, because as F_s increases, the effectiveness of sampling increases too, but after a certain value, no further improvement is achieved, and instead the computational time is increased.

Example 2.5. Consider two different sinusoidal signals have different frequencies, $F_1 = 1/8Hz$ and $F_2 = -7/8Hz$:

$$u_1(t) = \sin\left(\frac{2\pi}{8}t\right)$$

and

$$u_2(t) = \sin\left(-\frac{14\pi}{8}t\right)$$

The two signals are plotted in figure 2.11, together with a third signal, which is the second one calculated with a sampling frequency $F_s = 1Hz$. It can be clearly observed that choosing a sampling frequency $F_s = 1Hz$ results in the second signal to be illustrated almost the same as the first one, when in reality they are completely different. This is an example of aliasing.

Listing 2.2: Example of aliasing of figure 2.11

```
1  % Signal 1
2  Fy1=1/8;              %signal frequency in Hz
3  omega1=2*pi*Fy1       %signal frequency in rad/s
4  % Signal 2
```

```
 5   Fy2=-7/8;              %signal frequency in Hz
 6   omega2=2*pi*Fy2        %signal frequency in rad/s
 7   % Efficient sampling rate
 8   Fs=70;                 %sampling frequency in Hz
 9   dt=1/Fs;               %sampling period
10   t=0:dt:20;             %time intervals set
11   u1=sin(omega1*t);      %signal 1 data set
12   u2=sin(omega2*t);      %signal 2 data set
13   % Non efficient sampling rate
14   Fs3=1;                 %sampling frequency in Hz
15   dt3=1/Fs3;             %sampling period
16   t3=0:dt3:20;           %time intervals set
17   u3=sin(omega2*t3);     %signal data set
18
19   figure()
20   hold on; box on;
21   plot(t,u1,'b','LineWidth',2);
22   plot(t,u2,'c','LineWidth',2);
23   plot(t3,u3,'r--','LineWidth',2);
24   yline(0,'k')
25   xlabel('Time (s)','FontSize',14)
26   ylabel('Amplitude','FontSize',14)
27   legend('Signal 1','Signal 2','Signal 2 with inefficient Fs')
```
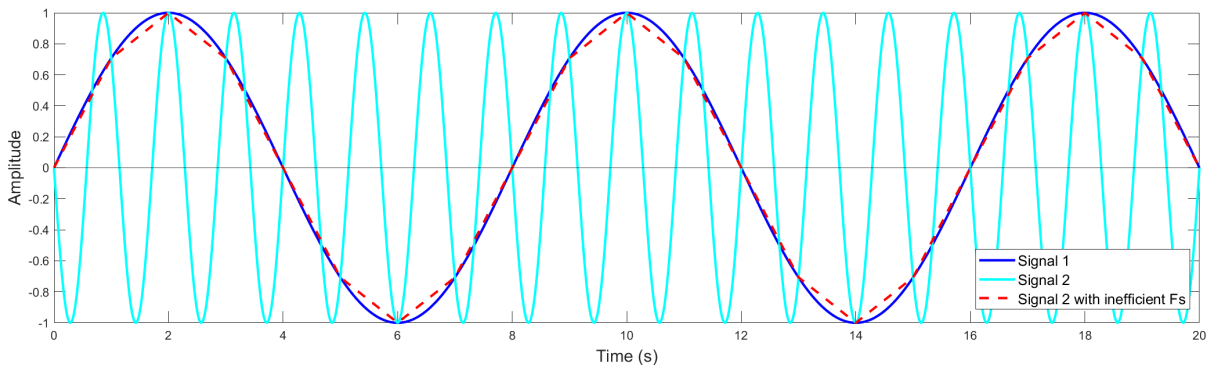

Figure 2.11: Example of aliasing

Consequently, to avoid the ambiguities resulting from aliasing, the sampling rate must be selected to be sufficiently high; this is solved by following the *Nyquist–Shannon sampling theorem*.

Theorem 2.1 (Nyquist–Shannon sampling theorem)**.** Sampling frequency F_s must be at least two times greater than the signal's highest frequency F_{max}:

$$F_s \geq 2F_{max} \tag{2.28}$$

The theorem establishes a sufficient condition for a sample rate that permits a discrete sequence of samples to capture all the information from a continuous-time signal of finite bandwidth. Usually the general frequency content of the signal is known, thus the signal's highest frequency can be estimated.

Definition 2.6 (Nyquist frequency). The previous theorem leads to the definition of the Nyquist frequency as the maximum frequency in the frequency domain of the analysis:

$$F_{Nyquist} = \frac{F_s}{2} \tag{2.29}$$

Chapter 3

Wavelet Analysis – The Continuous Wavelet Transform (CWT)

This chapter presents an overview of the background of the continuous wavelet transform. It provides the basic definitions and properties needed to understand the wavelet theory and its application to modal parameter identification.

3.1 Function Spaces

This section provides a brief description of the function spaces used in wavelet theory[6].

3.1.1 *Normed Spaces*

The concept of *norm* in a vector space is an abstract generalization of the length of a vector in the $\mathbb{R}^3$ set and is defined axiomatically; i.e. any real-valued function that satisfies some particular conditions can be defined as a norm.

Definition 3.1 (Norm). A real-valued function $||x||$ defined on a vector space X, where $x \in X$, is called a norm on X if the following conditions are satisfied:

    i. $||x|| = 0$ if and only if $x = 0$,

    ii. $||ax|| = |a| \; ||x||$ for every $a \in \mathbb{R}$ and $x \in X$,

    iii. $||x + y|| \leq ||x|| + ||y||$ for all $x \in X$ (also known as the *triangle equality*).

Combining i, ii, and iii, follows that: $0 = ||0|| = ||x - x|| \leq ||x|| + ||-x|| = 2||x||$, therefore $||x|| \geq 0$ for every $x \in X$.

Definition 3.2 (Normed Space). A normed space is a pair $(X, ||\cdot||)$ where X is a vector space and $||\cdot||$ is a norm defined on X.
Note: It is possible to define different norms on the same vector space.

Example 3.1.   i. $\mathbb{R}$ is a real normed space with the norm defined by the absolute values: $||x|| = |x|$.

    ii. $\mathbb{C}$ is a complex normed space with the norm defined by the modulus: $||z|| = |z|$.

Example 3.2. The sequence space $\ell^p (1 \leq p \leq +\infty)$ is the set of all sequences $x = [x_n]_{n=1}^{+\infty}$ of real (or complex) numbers such that $\left(\sum_{n=1}^{+\infty} |x_n|^p \right) < \infty$ is a normed space with a norm defined as:

$$||x||_p = \left[\sum_{n=1}^{+\infty} |x_n|^p \right]^{1/p} \tag{3.1}$$

Example 3.3. $\mathbb{R}^N = \left[(x_1, x_2, ..., x_N) : x_1, x_{2,.}.., x_N \in \mathbb{R} \right]$ is a vector spase with norm defined by setting p=2 at equation 3.1:

$$||x||_2 = \sqrt{(x_1^2 + x_2^2 + \cdots + x_N^2)} \tag{3.2}$$

where $x = (x_1, x_{2,.}.., x_N) \in \mathbb{R}$. This norm is called the *Euclidean Norm.*

3.1.2 L^p *Spaces*

Definition 3.3. If $p \geq 1$ is any real number, the vector space of all complex-valued Lebesgue integrable functions f defined on $\mathbb{R}$ is denoted by $L^p(\mathbb{R})$ with a norm:

$$||f||_p = \left[\int_{-\infty}^{+\infty} |f(x)|^p dx \right]^{1/p} \tag{3.3}$$

where $||f||_p$ is the L^p-norm.

Remarks:

1. The range of p is $1 \leq p \leq +\infty$, as for values $0 < p < 1$ the function $|| \cdot ||_p$ does not satisfy the triangle inequality (see Definition 3.1) [18].

2. Equation 3.1 is the discrete version of equation 3.3.

3. The case p $=$ 2 warrants special attention: it is a Hilbert space, more will be discussed in subsection 4.3.

4. Elements of $L^2(\mathbb{R})$ are called square integrable functions.

5. The term "signal of finite energy" in the following, refers to a generic element of $L^2(\mathbb{R})$.

6. The equation of the total energy of a function (see equations2.21 and 2.22) can be defined as the square of the L^2 norm of the function.

3.1.3 *The Complex Hardy Space*

The Complex Hardy space $H^2(\mathbb{R})$ -sometimes called the space of analytic signals-, is made of signals which do not have negative frequency components, and is defined as:

$$H^2(\mathbb{R}) = \left[f \in L^2(\mathbb{R}); \ \widehat{f}(\omega) = 0 \ for \ \omega \leq 0 \right] \tag{3.4}$$

3.1.4 *Convolution*

Definition 3.4 (Convolution)**.** Let f and g be functions in $L^1(\mathbb{R})$. Then the (continuous-time) *convolution* of f and g is also an $L^1(\mathbb{R})$ function $h \in L^1(\mathbb{R})$ defined by:

$$h(x) = (f * g)(x) = \int_{-\infty}^{+\infty} f(x-y)g(y)dy \tag{3.5}$$

whenever the integral is well-defined. The convolution's properties are that it is commutative, associative and distributive.

Theorem 3.1. If f and $g \in L^1(\mathbb{R})$, then the function $f(x-y)g(y)dy$ is integrable for almost all $x \in \mathbb{R}$. Furthermore, the convolution h is an integrable function and the following equality holds:

$$||h||_1 = ||f * g||_1 \le ||f||_1\, ||g||_1 \tag{3.6}$$

3.1.5 *Inner product*

Definition 3.5. Let f and $g \in L^2(\mathbb{R})$. The *inner product* and *norm* for the space $L^2(\mathbb{R})$ is given by:

$$\langle f, g \rangle = \int_{-\infty}^{+\infty} f(x)\overline{g(x)}dx \tag{3.7}$$

$$||f||_2 = \langle f, f \rangle^{1/2} \tag{3.8}$$

3.2 From Fourier analysis to Wavelet analysis

3.2.1 *The Fourier Transform*

As mentioned in Chapter 2, the Fourier Transform (FT) converts a signal from the time domain to the frequency domain by decomposing it into the sum of a (potentially infinite) number of sine wave frequency components.

Definition 3.6 (Fourier Transform)**.** For finite energy signals $u(t) \in L^1(\mathbb{R}) \cap L^2(\mathbb{R})$ the FT is defined as:

$$\widehat{u}(\omega) = \mathcal{F}[u] = \int_{-\infty}^{+\infty} u(t)e^{-i\omega t}dt \tag{3.9}$$

And the inverse FT as:

$$u(t) = \mathcal{F}^{-1}[u] = \frac{1}{2\pi} \int_{-\infty}^{+\infty} \widehat{u}(\omega)e^{i\omega t}d\omega \tag{3.10}$$

The function $\widehat{u}(\omega)$ is complex, and can be expressed in polar form as $\widehat{u}(\omega) = Ae^{i\varphi}$ to express the amplitude spectrum $A(\omega)$ (frequency-amplitude plot), and phase spectrum $\varphi(\omega)$ (frequency-phase angle plot).

It is important to mention that the Parseval identity allows the extension of the definition of FT from $L^1(\mathbb{R})$ to $L^2(\mathbb{R})$ to include finite energy signals:

Definition 3.7 (Parseval's Identity). Let $f \in L^1(\mathbb{R}) \cap L^2(\mathbb{R})$. Then the FT $\widehat{f}$ of f is in $L^2(\mathbb{R})$, and satisfies the following Parseval's Identity:

$$||f||_2^2 = \frac{1}{2\pi}||\widehat{f}||_2^2 \tag{3.11}$$

which by substituting equation 3.3 of norm, Parseval's Identity becomes:

$$\int_{-\infty}^{+\infty} |f(t)|^2 dt = \frac{1}{2\pi} \int_{-\infty}^{+\infty} |\widehat{f}(\omega)|^2 d\omega \tag{3.12}$$

It can be observed that the left hand side part of the equation is the energy of a signal (see equation 2.21). Consequently, Parseval's Identity states a conservation of energy between the time and the frequency domains.

Then, for all f and $g \in L^1(\mathbb{R}) \cap L^2(\mathbb{R})$ (signals of finite energy), the following identity is easily obtained from Parseval's identity using the inner product definition (see equation 3.7):

$$\int_{-\infty}^{+\infty} f(t)\overline{g(t)}dt = \frac{1}{2\pi} \int_{-\infty}^{+\infty} \widehat{f}(\omega)\overline{\widehat{g}(\omega)}d\omega \quad or \quad \langle f, g \rangle = \frac{1}{2\pi} \left\langle \widehat{f}, \widehat{g} \right\rangle \tag{3.13}$$

which emphasizes the fact that the Fourier transform preserves the Hilbert spaces inner products.

3.2.2 Properties of the Fourier Transform

Some basic properties of the FT are (mentioned because they will be extended to wavelet analysis):

- **Linearity**

$$\mathcal{F}\left[\sum_{j=1}^{N} u_j\right] = \sum_{j=1}^{N} \mathcal{F}[u_j] \tag{3.14}$$

- **Time scaling**

$$\mathcal{F}[u(at)](\omega) = \frac{1}{|a|}\widehat{u}\left(\frac{\omega}{a}\right), \quad a \neq 0 \tag{3.15}$$

- *Translation / time shifting*

  For any real number $t_0 \in \mathbb{R}$:

  $$\mathcal{F}[u(t - t_0)](\omega) = e^{-i\omega t_0}\widehat{u}(\omega) \tag{3.16}$$

- *Modulation / frequency shifting*

  For any real number $\omega_0 \in \mathbb{R}$:

  $$\mathcal{F}[e^{-i\omega_0 t}u(t)](\omega) = \widehat{u}(\omega - \omega_0) \tag{3.17}$$

- *Hermitian symetry*

  For a real function $u(t) \in \mathbb{R}$:

  $$\widehat{u}(-\omega) = \overline{\widehat{u}(\omega)} \tag{3.18}$$

- *Convolution*

  $$(u_1 * u_2)(t) = \mathcal{F}^{-1}[\widehat{u_1}(\omega)\widehat{u_2}(\omega)] \tag{3.19}$$

3.2.3 The Fast Fourier Transform

FT is implemented in digital means by the discrete form of equation 3.9, the Discrete Fourier Transform (DFT). The DFT of a discrete-time signal $u(n)$ is:

$$\widehat{u}(k) = \frac{1}{N} \sum_{n=0}^{N-1} u(n)e^{-i\left(\frac{2\pi k n}{N}\right)} \tag{3.20}$$

where $k = 0, 1, ..., N - 1$ is the frequency index.
However, the calculation of the DFT with equation 3.20 requires performing approximately N^2 multiplications, which becomes impractical when large amounts of data (large values of N) are required for processing.

As it is implied by its name, the Fast Fourier Transform (FFT) is an algorithm that determines the DFT of a signal significantly faster than computing it directly, as it performs an N-term DFT in $2N \log{(N)}$ calculations allowing the analysis of large data sets. FFT can be implemented in MATLAB using the fft command.

3.2.4 Spectral leakage

Signals that are used in practice are of finite length. Due to this finite duration, signals that are converted from the time domain to the frequency domain are subject to spectral leakage. When the DFT is applied to an aperiodic signal of finite length, it assumes that any existing frequency components are periodic and infinite, i.e the same finite signal is repeated infinite times. So, when a spectral component that is not a harmonic of the fundamental frequency for the observation window exists, the repetition

of that finite component by the transform creates discontinuities at the boundaries of the iterations. Since that component is not a harmonic, and no longer a smooth wave due to the discontinuities, the energy of that component cannot be expressed on a single basis and instead is distributed among the other harmonic frequency bases. This "smearing" of energy manifests on the amplitude spectrum as low amplitude frequency components that are not actually present. Introducing a proper window function into the transform can reduce the degree of spectral leakage in the spectrum. [10].

Example 3.4. Consider a sinusoidal function composed of the sum of three sine functions, with frequencies $F_1 = 1Hz$, $F_2 = 3Hz$ and $F_3 = 4Hz$: respectively, defined as,

$$u(t) = \sin(2\pi t) + \sin(6\pi t) + \sin(8\pi t) \quad , \quad t \in [0, 10] \; sec$$

The signal $u(t)$ is displayed in figure 3.1 with respective Fourier amplitude spectrum normalized by the sampling period and its phase spectrum. The signal $u(t)$ is real, therefore the spectrum is symmetric, so the one-sided spectrum is illustrated. The peaks in the plot of Figure 3.1 (b) indicate the presence of frequency components at 1, 3, and 4 Hz. Since the present frequency components have equivalent amplitudes (all have an amplitude of one), the relative power for each of the frequencies within the signal is also equivalent. This can be observed by the uniform amplitude of the peaks.

The effect of leakage can be observed by making the signal u(t) non-stationary:

$$u(t) = u_1(t) + u_2(t) + u_3(t)$$

where

$$u_1(t) = \sin(2\pi t) \quad , \quad t \in [0, 10] \; sec$$
$$u_2(t) = \sin(6\pi t) \quad , \quad t \in (2, 7) \; sec$$
$$u_3(t) = \sin(8\pi t) \quad , \quad t \in (5, 10] \; sec$$

As it can be observed in figure 3.2, the Fourier amplitude is distorted by spectral leakage, i.e. low amplitude frequency components.

Listing 3.1: FFT computation: amplitude spectrum and phase spectrum

```
1  %% FFT
2  Fs=2^10;                % sampling frequency in Hz
3  dt=1/Fs                 % sampling period
4  t=0:dt:10-dt;           % time intervals set
5  Ny = Fs/2;              % nyquist frequency
6
7  % Generate the signal
8  F1 = 1;        % Hz
9  F2 = 3;        % Hz
10 F3 = 4;        % Hz
11 ut = sin(2*pi*F1*t)+sin(2*pi*F2*t)+sin(2*pi*F3*t);
12 %ut = sin(2*pi*F1*t)+sin(2*pi*F2*t).*(t>2 & t<7)+sin(2*pi*F3*t).*(t>5);
13
14 NbSpl = length(t) % number of samples in the time domain (in power of 2)
```

```matlab
15
16  min_omega = 0;                                    % min angular frequency
17  max_omega = 2*pi*Ny;                              % max angular frequency
18  delta_omega = 2*pi*Fs/NbSpl;                      % frequency step
19  omega = (min_omega:delta_omega:max_omega);        % frequency range rad/sec
20
21  % Transform u from time domain u(t) to frequency domain u(w)
22  uw = fft(ut);
23  uw = uw';
24
25  Nw_max = 1+fix(max_omega*NbSpl/(2*pi*Fs));  % Single sided
26  uw = uw(1:Nw_max);
27
28  % Amplitude Spectrum
29  A = abs(uw).*dt;           % Amplitude
30  F = omega./(2*pi);         % Frequency range in Hz
31  % Phase spectrum
32  phi =-angle(uw);
33  %plots
34  figure()
35  subplot(3,1,1)
36  hold on; box on; grid on;
37  plot(t,ut,'b','LineWidth',2)
38  xlabel('Time (s)')
39  ylabel('Amplitude')
40  title('Simulated signal u(t)')
41
42  subplot(3,1,2)
43  hold on; box on; grid on;
44  plot(F,A,'b','LineWidth',2)
45  xlim([0 5])
46  xlabel('Frequency (Hz)')
47  ylabel('Amplitude')
48  title('Fourier Amplitude Spectrum of u(t)')
49
50  subplot(3,1,3)
51  hold on; box on; grid on;
52  plot(F,phi,'b','LineWidth',2)
53  xlim([0 5])
54  xlabel('Frequency (Hz)')
55  ylabel('Phase')
56  title('Fourier Phase Spectrum of u(t)')
57  set(gca,'YTick',-pi:pi/2:pi)
58  set(gca,'YTickLabel',{'-\pi','-\pi/2','0','\pi/2','\pi'})
```
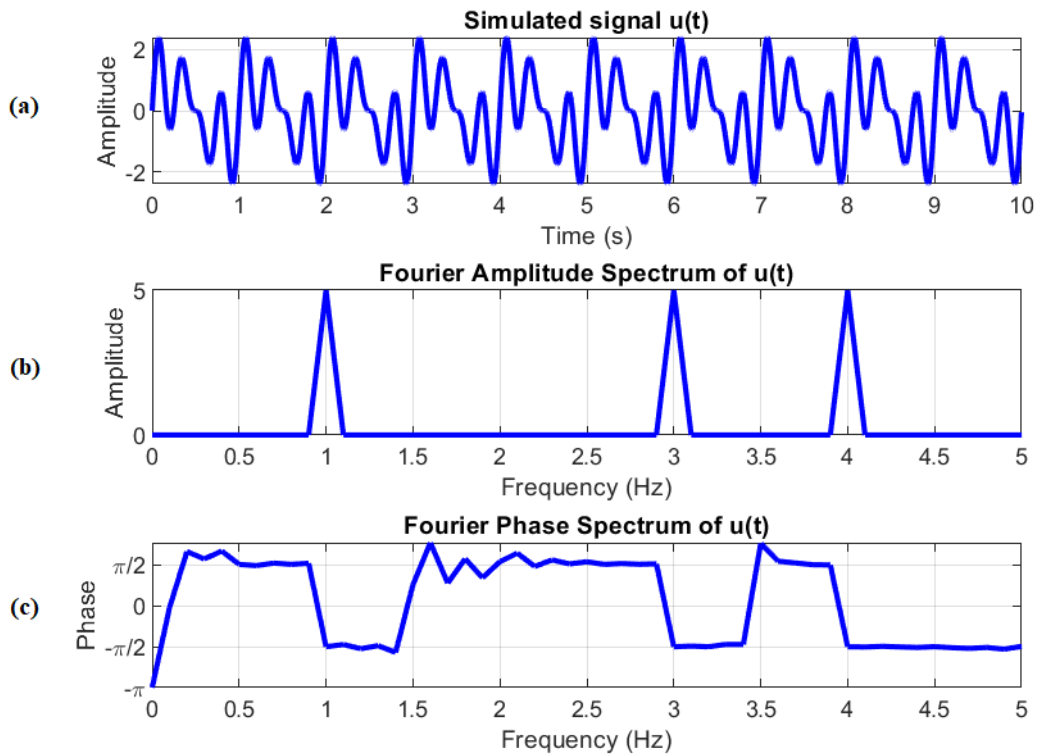
Figure 3.1: A sine wave with three frequency components,its corresponding Fourier amplitude spectrum and phase spectrum. (a) A sinusoidal function $u(t)$ with frequencies 1, 3, and 4 Hz. (b) The Fourier amplitude spectrum of $u(t)$. Frequency components emerge at 1, 3, and 4 Hz. (c) The Fourier phase spectrum of $u(t)$.
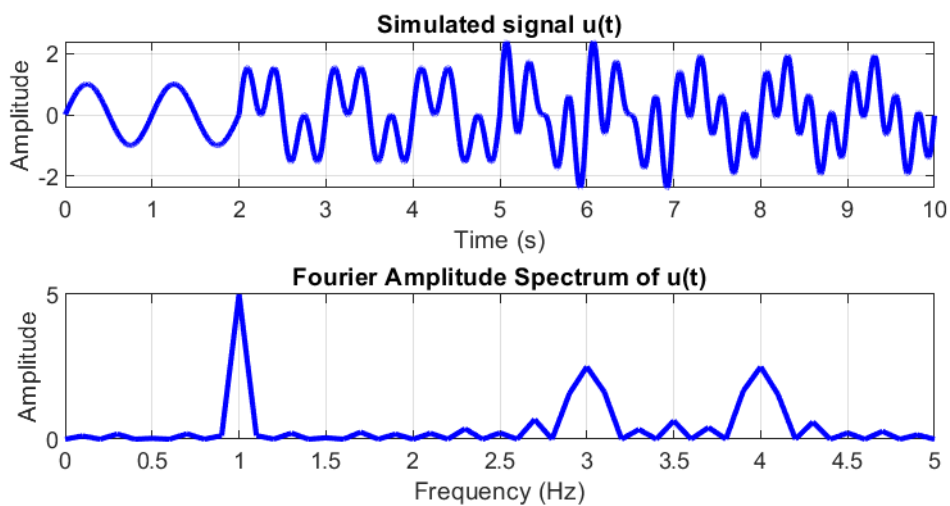
Figure 3.2: Example of spectral leakage. As it can be observed, the Fourier amplitude is distorted by spectral leakage.

3.2.5 *Window function*

As it was mentioned, the problem of spectral leakage can be reduced with the use of a proper window function. Window functions operate by multiplying the time signal by a finite-length window with an amplitude that varies smoothly and gradually toward zero at the edges.

In signal processing, a window function is a mathematical function that is zero-valued outside of some chosen interval, normally symmetric around the middle of the interval, usually near a maximum in the middle, and usually tapering away from the middle.

Definition 3.8. A nontrivial function $\psi \in L^2(\mathbb{R})$ is called a window function if $x\psi(x)$ is also in $L^2(\mathbb{R})$. The center x_ψ and radius Δx_ψ of a window function w are defined respectively by:

$$x_\psi = \int_{-\infty}^{+\infty} x \frac{|\psi(x)|^2}{||\psi||_2^2} dx \tag{3.21}$$

and

$$\Delta x_\psi = \frac{1}{||\psi||_2} \sqrt{\int_{-\infty}^{+\infty} (x - x_\psi)^2 |\psi(x)|^2 dx} \tag{3.22}$$

Note that the radius Δx_ψ expression is equivalent to standard deviation in statistics. The width of the window function is defined as $2\Delta x_\psi$.

Most popular window functions are bell-shaped curves, for example the Hann window or a Gaussian window (see figure 3.3. These are just presented for the sake of completeness as a passage to the Short Time Fourier Transform (time-frequency domain).
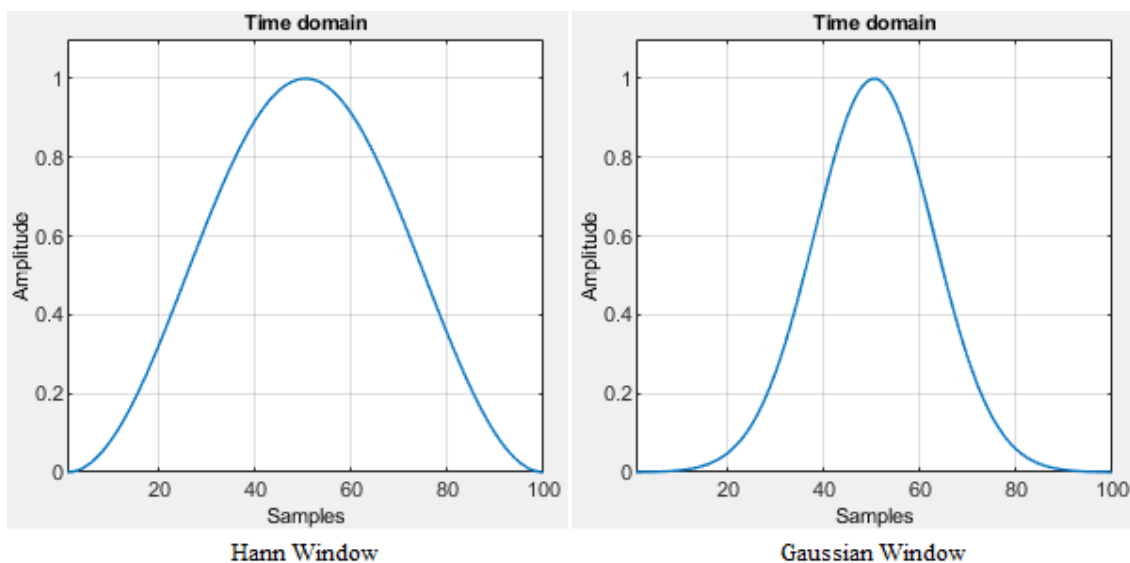
Figure 3.3: Example of two window functions in the time domain as generated by MATLAB with the signal processing toolbox.

3.2.6 *Short Time Fourier Transform (or Windowed Fourier Transform)*

As demonstrated in Example 3.4, the FT converts a signal from the time domain into the frequency domain and does not provide any information about the time localization of the frequency components. In Chapter 1, was mentioned that the need to overcome the inability of the frequency domain approach to capture time-varying features of a structure but retain the advantage of the frequency content information, plus the problem of spectral leakage, led to the development of the time-frequency domain methods.

Gabor in 1946 developed and introduced the Short Time Fourier Transform (STFT, otherwise known as the windowed Fourier transform, or Gabor transform). The STFT is nothing but a simple localization of the FT via the introduction of a sliding window function. The existence of this window makes this transform into a function of two parameters: a time parameter giving the location of the center of the window and a frequency parameter for the computation of the Fourier transform of the windowed signal[2].

Introducing now the *time-frequency window* ψ, with time center and frequency center respectively defined as:

$$t_\psi = \int_{-\infty}^{+\infty} t \frac{|\psi(t)|^2}{||\psi||_2^2} dt \tag{3.23}$$

and

$$\omega_\psi = \int_{-\infty}^{+\infty} \omega \frac{|\widehat{\psi}(\omega)|^2}{||\widehat{\psi}||_2^2} d\omega \tag{3.24}$$

And with time radius and frequency radius respectively defined as:

$$\Delta t_\psi = \frac{1}{||\psi||_2} \sqrt{\int_{-\infty}^{+\infty} (t - t_\psi)^2 |\psi(t)|^2 dt} \tag{3.25}$$

and

$$\Delta \omega_\psi = \frac{1}{||\widehat{\psi}||_2} \sqrt{\int_{-\infty}^{+\infty} (\omega - \omega_\psi)^2 |\widehat{\psi}(t)|^2 d\omega} \tag{3.26}$$

The window function now is in the time-frequency plane and has dimensions $2\Delta t$ and $2\Delta \omega$.

Definition 3.9 (Heisenberg uncertainty principle)**.** The Heisenberg uncertainty principle states that:

$$\mu_\psi = \Delta t \Delta \omega \geq \frac{1}{2} \tag{3.27}$$

Consequently, an improvement of the time localization (i.e., a decrease of Δt) is accompanied by a deterioration in the frequency localization (i.e., an increase of $\Delta\omega$), thus it is not possible to achieve optimal localization simultaneously in the time and the fre-

quency domains. Note that the inequality becomes an equality in the case of Gaussian (or modulated Gaussian) functions.

Definition 3.10. The STFT of a function $u(t)$, $STFT_u$ consists of multiplying $u(t)$ by a (usually real) window function ψ shifted in time. If $\psi(t)$ is a prototype window, symmetric about $t = 0$, then $STFT_u$ is calculated as:

$$STFT_u = \int_{-\infty}^{+\infty} u(t)\psi(t-b)e^{-i\omega t}dt \tag{3.28}$$

where the parameter b is used to translate the window in order to cover the whole time-domain, for extracting local information of the Fourier transform of the signal.

Definition 3.11 (Mother function)**.** Given a window function $g \in L^2(\mathbb{R})$ the corresponding family $[g_{b,\omega}; b \in \mathbb{R}, \omega \in \mathbb{R}]$ of Gabor functions is obtained by shifting and modulating copies of g:

$$g_{b,\omega}(t) = g(t-b)e^{i\omega(t-b)} \tag{3.29}$$

Examples of two such functions are illustrated in figure 3.4. Once the window g is fixed, the associated continuous Gabor transform is defined as follows.
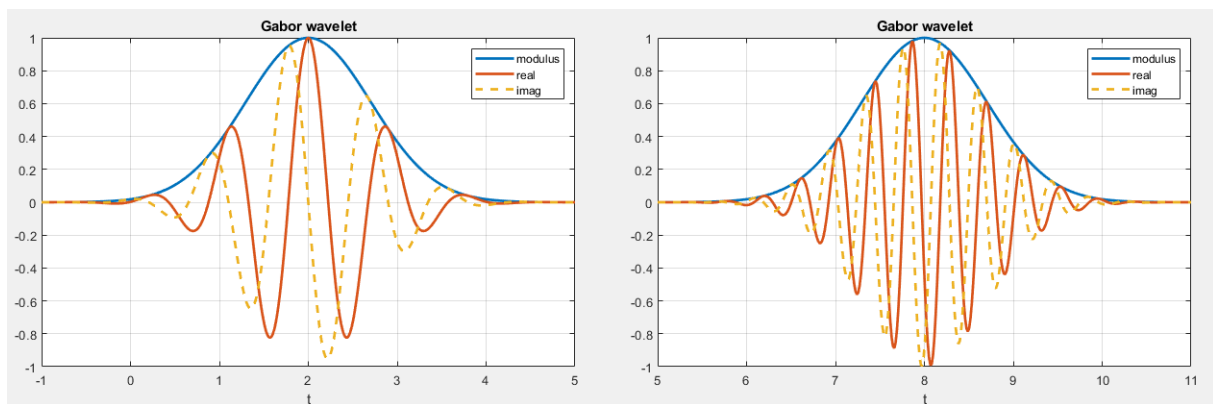
Figure 3.4: Examples of two $g_{b,\omega}(t)$ functions in the time domain.

Definition 3.12. Let $g \in L^2(\mathbb{R})$ a window function. The continuous Gabor Transform of a finite-energy signal $u(t) \in L^2(\mathbb{R})$ is defined by:

$$G_u(b,\omega) = \langle u, g_{b,\omega} \rangle = \int_{-\infty}^{+\infty} u(t)\overline{g}_{b,\omega}(t)dt \tag{3.30}$$

Consequently, the Gabor transform is essentially a STFT with a Gaussian window. As it can be observed by the previous definitions, changing the values of t simply corresponds to translating the window in time while its width is kept fixed. Similarly, as the mod-

ulation parameter ω varies, the transform translates in frequency, retaining a constant width. Thus, the resolution windows in the time–frequency plane have dimensions $2\Delta t$ and $2\Delta\omega$, which are fixed for all t and ω, thus, STFT and Gabor transform the fixed-duration window function is accompanied by a fixed frequency resolution. Consequently, this transform allows only a fixed time–frequency resolution. This is shown in figure 3.5 in which the mother function is illustrated centered at (t_0, ω_0) and the sliding time window are centered at integral multiples of t_0 and the transforms are evaluated at frequencies centered at integral multiples of ω_0.
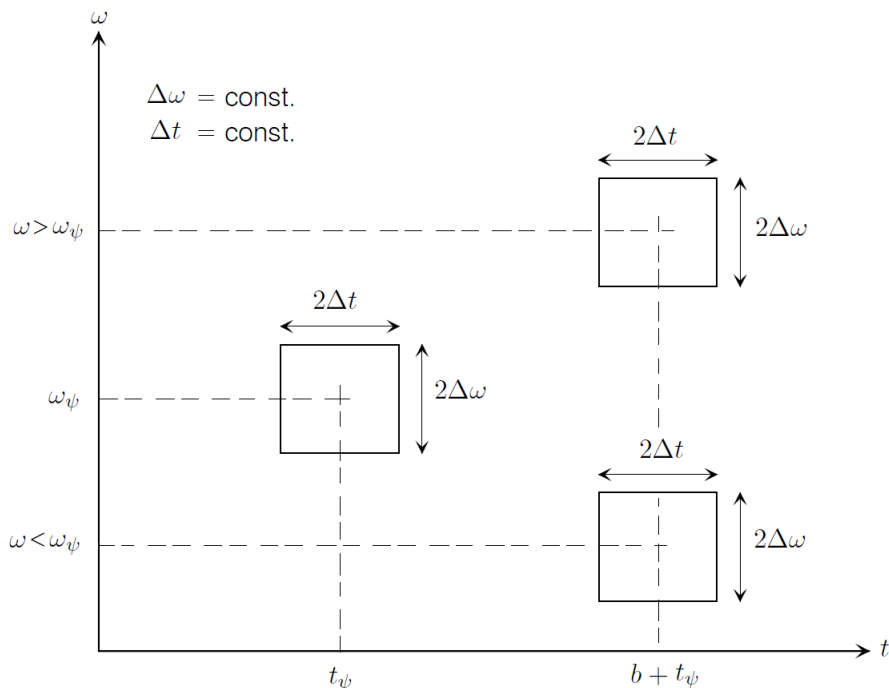
Figure 3.5: Fixed time-frequency resolution for the Gabor Transform.

However, the STFT represents an inaccurate and inefficient method of time–frequency localization, as it imposes a scale or "response interval" $2\Delta t$ into the analysis. The inaccuracy arises from the aliasing of high- and low-frequency components that do not fall within the frequency range of the window [34].

Since frequency is directly proportional to the number of cycles per unit time, it requires a narrow time-window to locate high frequency phenomena more precisely and a wide time-window to analyze low frequency behaviors more spectral information. In other words, it is important to have a flexible time-frequency window that automatically narrows at high *center-frequency* and widens at low center-frequency. Hence, the STFT is not suitable for analyzing signals with both very high and very low frequencies [3]. This constraint led to the development of the *Wavelet transform* where a dilation (or scale) parameter a is introduced to make the time-frequency window flexible.

Summarizing, the Gabor transform is based upon time and frequency translations, as opposed to time translations and scalings as in the case of the wavelet transform which is presented in the next section.

3.3 The Continuous Wavelet Transform

This section provides a presentation on the basic theory of the continuous wavelet transform. The main idea is that the wavelet transform is based on a set of basis functions (wavelet family) formed by dilation and translation of a prototype mother function (wavelet) $\psi(t)$ and is used to decompose a function (signal) $u(t)$ into the time-frequency domain.

Definitions in the literature vary slightly and depend on the choice of normalization of the wavelets. However, normalization is irrelevant to the basic theory [11], thus, in order to present the basic theory, the definition by Carmona et al.[2] is used for the wavelet definition; the differences and the influence of normalization are described in the "Normalization" section.

3.3.1 *Definitions and basic properties*

Definition 3.13 (Mother wavelet). Let $\psi \in L^1(\mathbb{R}) \cap L^2(\mathbb{R})$ be a window function. This function is called the mother (analyzing) wavelet, and the corresponding family of wavelets is the family $[\psi_{b,a}; b \in \mathbb{R}, a \in \mathbb{R}_+^*]$ of shifted and scaled (dilated) copies of ψ defined as:

$$\psi_{b,a}(t) = \frac{1}{a}\psi\left(\frac{t-b}{a}\right) \quad , \quad t \in \mathbb{R} \tag{3.31}$$

where $a > 0$ is a scaling parameter that defines the dilation of the mother wavelet $\psi(t)$ and b is the translation parameter related to time. Scale factor $a > 1$ corresponds to dilation and $0 < a < 1$ corresponds to compression (see figure 3.10). The mother wavelet is the member of the family where $b = 0$ and $a = 1$. Consequently, in terms of a window function, the $\psi_{b,a}(t)$ wavelet can be viewed as a copy of the original mother wavelet with center frequency rescaled by a, that is, ω_ψ/a and centered around the time $t_\psi + b$.
Common mother wavelets are the Morlet wavelet, the Meyer wavelet, the Mexican Hat, the Paul wavelet, the Cauchy wavelet, the Daubechies wavelets, the Gaussian Derivatives Family (DOG), the generalized Morse wavelets etc. (see figure 3.6).

For a window function $\psi(t)$ to be accepted as a mother wavelet,it must fulfill the admissibility condition:
Let $\psi \in L^1(\mathbb{R}) \cap L^2(\mathbb{R})$ be such that the number C_ψ defined by:

$$0 < C_\psi = \int_0^{+\infty} |\widehat{\psi}(a\omega)|^2 \frac{da}{a} < +\infty \tag{3.32}$$

So, the constant C_ψ finite, non-zero and independent of $\omega \in \mathbb{R}$. The finiteness of this constant restricts the class of $L^2(\mathbb{R})$ functions that can be used as "mother wavelets" in the definition of the integral wavelet transform. In particular, if $\psi(t)$ must also be a window function, then is necessarily in $L^1(\mathbb{R})$ [3], meaning:

$$\int_{-\infty}^{+\infty} |\psi(t)|^2 dt < +\infty \tag{3.33}$$

and the integral of the mother wavelet $\psi(t)$ has to vanish, so that the graph in the time domain to be a small wave:

$$\int_{-\infty}^{+\infty} \psi(t)dt = 0 \qquad (3.34)$$
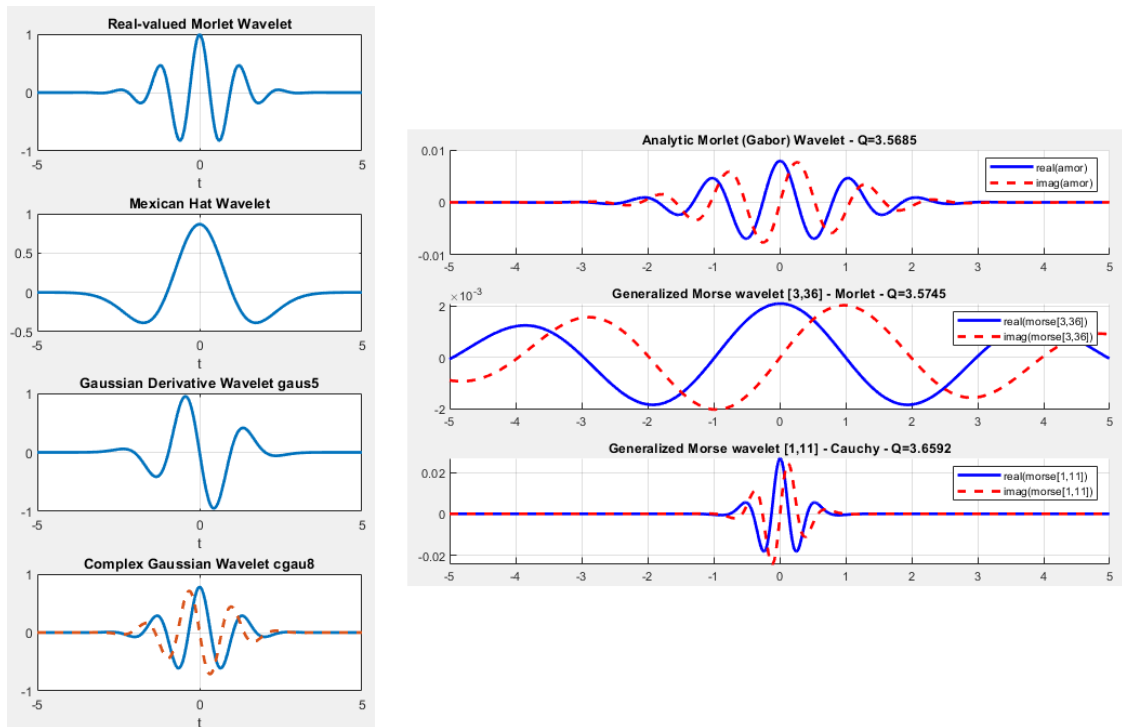
Figure 3.6: Example of different mother wavelets in the time domain, real and two complex. For the complex wavelets the plots illustrate the real part (solid) and imaginary part (dashed) for the wavelets.

Definition 3.14. A wavelet $\psi(t)$ is progressive, when $\psi(t) \in H^2(\mathbb{R})$. That is, its FT $\widehat{\psi}(\omega)$ vanishes for $\omega \leq 0$.

Definition 3.15 (Continuous wavelet transform). Let $u(t)$ be a signal that is of finite energy and a piece-wise continuous function of t. Given a mother wavelet $\psi(t)$, the continuous wavelet transform of this signal is given by the integral:

$$T_\psi[u](b,a) = \frac{1}{a}\int_{-\infty}^{+\infty} u(t)\overline{\psi}\left(\frac{t-b}{a}\right)dt \qquad (3.35)$$

where $a > 0$ is a scaling parameter that defines the dilation of the mother wavelet $\psi(t)$ and b is the translation parameter related to time. As it can be observed by the equation 3.35, CWT transforms a one-dimensional (time domain) signal $u(t)$ to a two-dimensional representation: the time-scale plane. Scales are directly linked with frequencies: a scale a corresponds to a scaled version of the mother wavelet with center frequency ω_ψ/a, thus bringing the CWT on the time-frequency plane.

Remark 3.1. The CWT, as defined by equation 3.35, can be interpreted as:

- The convolution of $u(t)$ with $\frac{1}{a}\overline{\psi}\left(-\frac{b-t}{a}\right)$, based on equation 3.5.

- The inner product of of $u(t)$ with the shifted and scaled copies of the mother wavelet, $\psi_{b,a} = \frac{1}{a}\psi\left(\frac{t-b}{a}\right)$, based on equation 3.7.

Consequently, the CWT can be viewed as a tool that measures the similarity between a signal $u(t)$ and the shifted and scaled copies $\psi_{b,a}$ of a mother wavelet $\psi(t)$. A general illustration of how the CWT works can be seen in figure 3.7. This concept now allows for a more simple definition of the ridges as the region where the frequency of the scaled mother wavelet is equal to the instantaneous frequency of the signal. Thus, in the ridges' regions of the TF plane, the CWT coefficients have (locally) relatively larger values, as the level of similitude is high, creating peaks in the TF representation as it can be seen in figure figure 3.8.
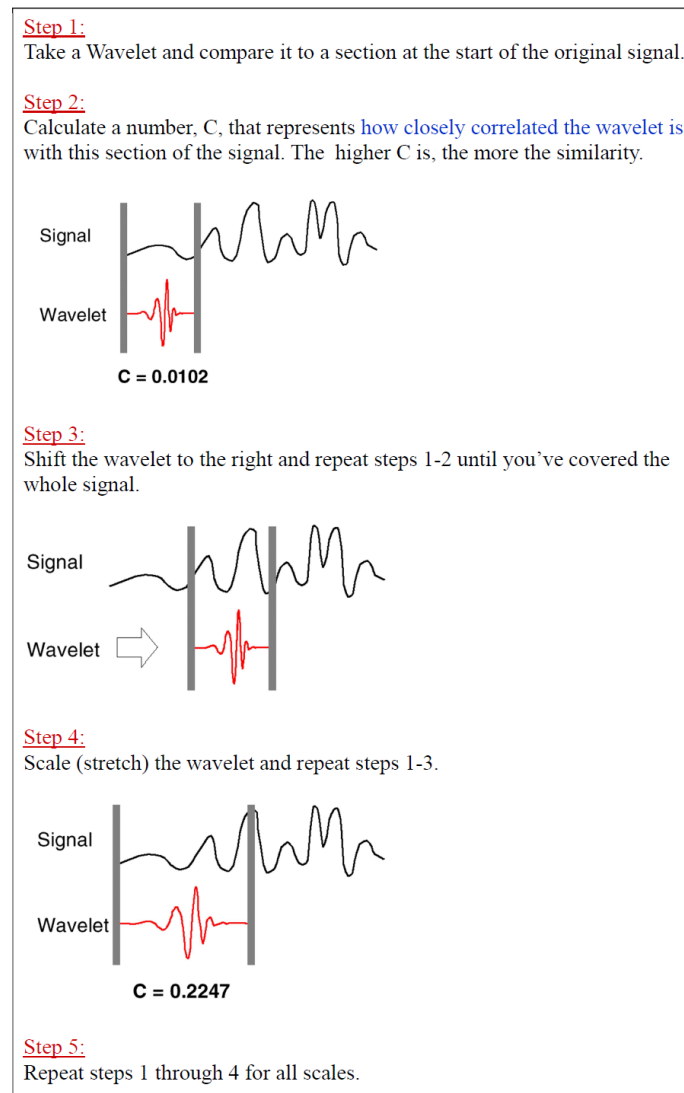
Figure 3.7: General illustration of how the CWT works. Source, class notes from [30]
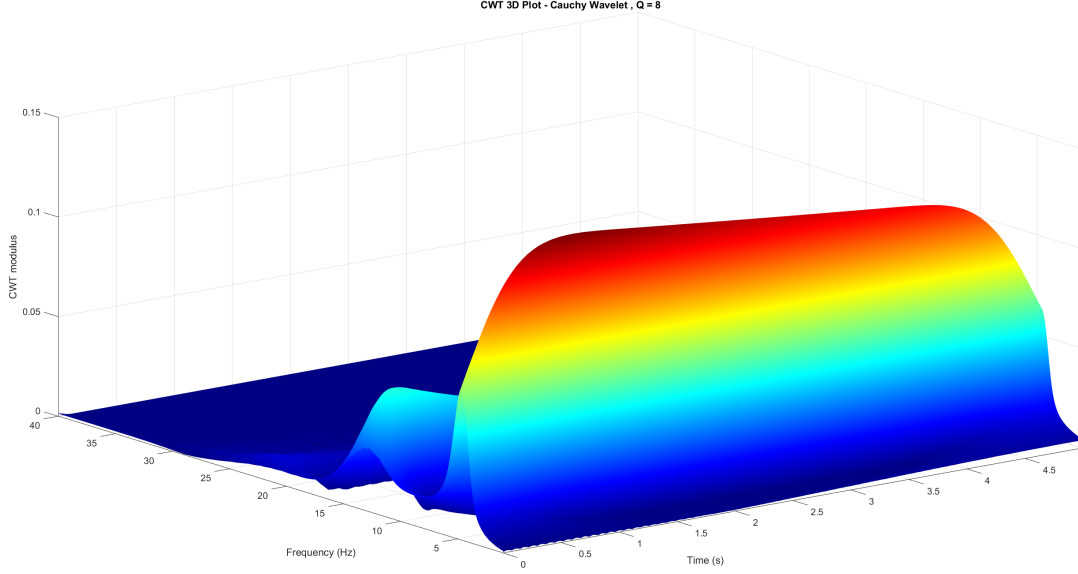
Figure 3.8: 3D representation of the TF plane to observe the ridges.

Definition 3.16 (Inverse Continuous wavelet transform)**.** When the admissibility condition is fulfilled, the signal $u(t)$ can be reconstructed as:

$$u(t) = \frac{1}{C_\psi} \int_{-\infty}^{+\infty} \int_{0}^{+\infty} T_\psi[u](b, a) \overline{\psi}\left(\frac{t - b}{a}\right) \frac{da}{a} db \qquad (3.36)$$

Remark 3.2. A simple application of Parseval's relation gives the wavelet coefficients in terms of the Fourier transforms of the signal and the mother wavelet using the definition of the inverse Fourier transform:

$$T_\psi[u](b, a) = \frac{1}{2\pi} \int_{-\infty}^{+\infty} \widehat{u}(\omega) \overline{\widehat{\psi}}(a\omega) e^{i\omega b} d\omega \qquad (3.37)$$

3.3.2 CWT Properties

• *Linearity*

$$T_\psi\left[\sum_{j=1}^{N} u_j\right](b, a) = \sum_{j=1}^{N} T_\psi[u_j](b, a) \qquad (3.38)$$

Consequently, multicomponent signals can be processed and a particular component $u_j(t)$ can be extracted by using the localization properties of the mother wavelets, in both time and frequency domains.

• *CWT of $u(t)$, $\dot{u}(t)$, $\ddot{u}(t)$ relations*

Generally, the free responses that are recorded are displacement, velocity or acceleration, so the relation between their CWT can be useful. If $\psi(t)$ and $u(t)$ are continuous and piece-wise differentiable, the integration by parts theorem allows equation 3.35 to

43

be rewritten as:

$$T_\psi[\dot u](b,a) = \frac{1}{a}\left[u(t)\overline{\psi}\left(\frac{t-b}{a}\right)\Big|_{-\infty}^{+\infty} - \frac{1}{a}\int_{-\infty}^{+\infty} u(t)\overline{\dot\psi}\left(\frac{t-b}{a}\right) dt\right] \tag{3.39}$$

$\psi(t)$ is a window function, so:

$$\lim_{t\to+\infty}|\psi(t)| = \lim_{t\to-\infty}|\psi(t)| = 0 \tag{3.40}$$

Consequently, it follows that:

$$\lim_{t\to+\infty}\left| u(t)\overline{\psi}\left(\frac{t-b}{a}\right)\right| = \lim_{t\to-\infty}\left| u(t)\overline{\psi}\left(\frac{t-b}{a}\right)\right| = 0 \ , \tag{3.41}$$

$$\lim_{t\to+\infty} u(t)\overline{\psi}\left(\frac{t-b}{a}\right) = \lim_{t\to-\infty} u(t)\overline{\psi}\left(\frac{t-b}{a}\right) = 0 \tag{3.42}$$

Therefore,

$$\lim_{t\to+\infty} u(t)\overline{\psi}\left(\frac{t-b}{a}\right) - \lim_{t\to-\infty} u(t)\overline{\psi}\left(\frac{t-b}{a}\right) = u(t)\overline{\psi}\left(\frac{t-b}{a}\right)\Big|_{-\infty}^{+\infty} = 0 \tag{3.43}$$

So, when $\dot\psi(t)$ is square and absolutely integrable and $\dot u(t)$ is of finite energy, the CWT of $\dot u(t)$ with $\psi(t)$ is then related to the CWT of $u(t)$ with $\dot\psi(t)$:

$$T_\psi[\dot u](b,a) = -\frac{1}{a}T_{\dot\psi}[u](b,a) \tag{3.44}$$

This relation can be easily extended to the finite energy signal $\ddot u(t)$ when $\ddot\psi(t)$ is square and absolutely integrable:

$$T_\psi[\ddot u](b,a) = -\frac{1}{a}T_{\dot\psi}[u](b,a) = \frac{1}{a^2}T_{\ddot\psi}[u](b,a) \tag{3.45}$$

3.3.3 Resolution

The value of $T_\psi[u](b,a)$ contains the information of the level of similitude of the signal $u(t)$ with the scaled wavelet at scale a around the time point b. The scaled wavelet at scale a has a duration Δt and frequency bandwidth $\Delta\omega$, thus the local resolution of the CWT in time and in frequency depends on the scale parameter a and is determined, respectively, by the duration Δt_ψ and bandwidth $\Delta\omega_\psi$ of the mother wavelet.

The resolution of the time-frequency window can be constructed by considering:
Time localization: Considering the time shifting property, equation 3.16:

$$\psi_b(t) = \psi(t-b) \text{ and } \widehat{\psi_b}(\omega) = e^{-i\omega b}\widehat{\psi}(\omega) \tag{3.46}$$

Consequently, if the mother wavelet is localized around the time $t = t_\psi$, with temporal resolution Δt_ψ, the translation property gives the temporal localization of $\psi_b(t)$ around $t = b + t_\psi$ with the same time resolution Δt_ψ.

Frequency localization: In the STFT, the frequency localization of the analyzing wavelet was changing by translating the value of the frequency in the frequency axis. In CWT, where the concept of scale is applied, the frequency localization of the mother wavelet is obtained considering the time scaling property, equation 3.15:

$$\psi_a(\cdot) = \frac{1}{a}\left(\frac{\cdot}{a}\right) \ \text{ and } \ \widehat{\psi}_a(\omega) = \widehat{\psi}(a\omega) \tag{3.47}$$

Consequently, if the mother wavelet is localized around t_ψ and ω_ψ with time and frequency resolution Δt_ψ and $\Delta\omega_\psi$ respectively, the scaled copy $\psi_{b,a}$ is localized around:

$$t = b + at_\psi \quad , \quad \omega = \frac{\omega_\psi}{a} \tag{3.48}$$

with time and frequency resolution Δt_ψ and $\Delta\omega_\psi$ respectively:

$$\Delta t = a\Delta t_\psi \quad , \quad \Delta\omega = \frac{\Delta\omega_\psi}{a} \tag{3.49}$$

Thus, looking ω_ψ/a as the frequency variable ω, then the $t - \omega$ plane can be considered as the time-frequency plane. The localization domain for the CWT at point $(b + at_\psi \ , \ \omega_\psi/a)$ is the time-frequency window (see figure 3.9):

$$[b + at_\psi - a\Delta t_\psi \ , \ b + at_\psi + a\Delta t_\psi] \times \left[\frac{\omega_\psi}{a} - \frac{\Delta\omega_\psi}{a} \ , \ \frac{\omega_\psi}{a} + \frac{\Delta\omega_\psi}{a}\right] \tag{3.50}$$

where

$$[b + at_\psi - a\Delta t_\psi \ , \ b + at_\psi + a\Delta t_\psi] \tag{3.51}$$

is the time-window, which narrows for small values of a and widens for large values of a, and

$$\left[\frac{\omega_\psi}{a} - \frac{\Delta\omega_\psi}{a} \ , \ \frac{\omega_\psi}{a} + \frac{\Delta\omega_\psi}{a}\right] \tag{3.52}$$

is the frequency-window, which widens for small values of a and narrows for large values of a.

Hence, this window automatically narrows for detecting rapidly changing details, i.e. high-frequency phenomena (small a), and widens for investigating slowly changing details, i.e. low-frequency behavior (large a). This is exactly what is most desirable in time-frequency analysis, and makes the use of the CWT appropriate for analyzing non-stationary signals. This can be observed clearly in figure 3.9.
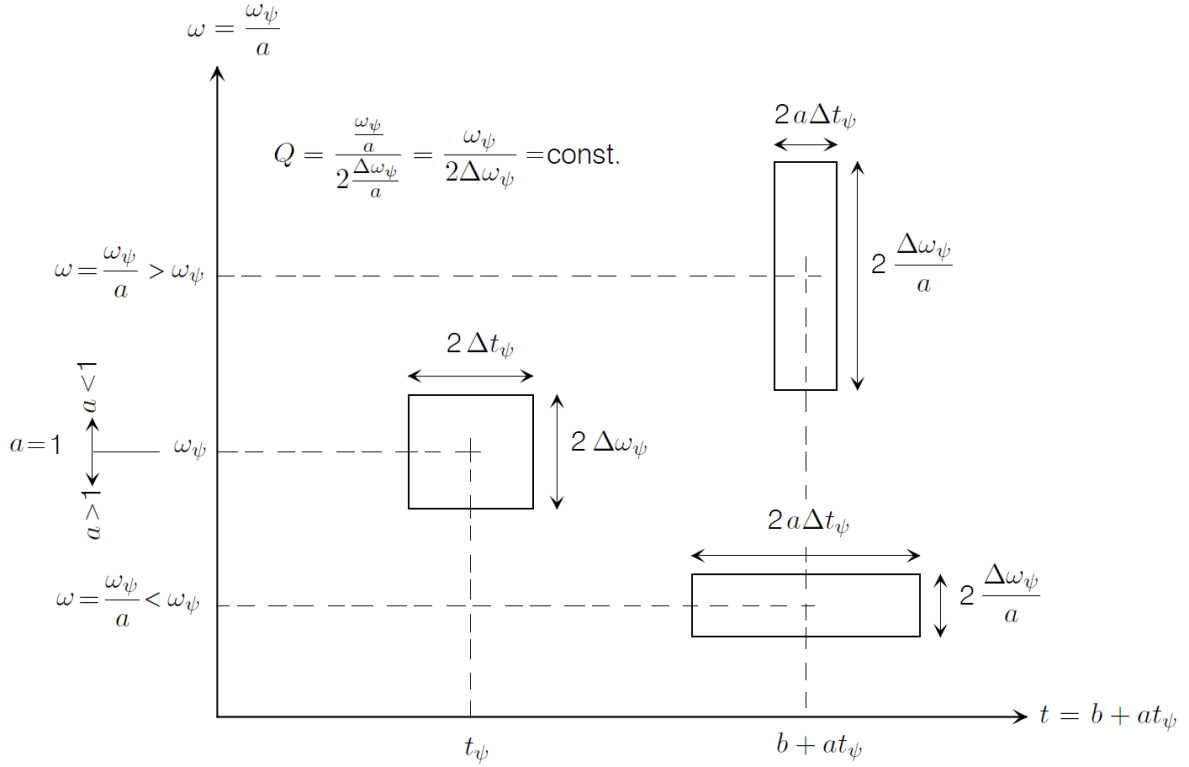
Figure 3.9: Time-frequency resolution for the CWT. The mother wavelet is illustrated at (t_ψ, ω_ψ), as $a = 1$ and $b = 0$ by definition. Scaled wavelets at points $(b + at_\psi, \omega_\psi/a)$ for scales $a > 1$ and scales $0 < a < 1$

Example 3.5. Consider the Complex Morlet wavelet, defined in the time domain in the frequency domain respectively as:

$$\psi(t) = e^{-t^2/(2\delta^2)} e^{i\beta t} \quad , \quad \widehat{\psi}(\omega) = \delta\sqrt{2\pi} e^{-(\omega-\beta)^2\delta^2/2}$$

The center time is considered zero, $t_\psi = 0$ and the center frequency is equal to β, $\omega_\psi = \beta$. δ controls the rate at which the time-domain wavelet and frequency domain spectrum are driven towards zero. The effect of scaling is as: $\omega = \omega_\psi/a$ and $\delta = a\delta_\psi$.

Let the mother wavelet have $\omega_\psi = 10 rad/sec$ and $\delta = 0.5$. Consider two scaled wavelets, one with scale $a = 2 > 1$ with center frequency $\omega_\psi = 10/2 = 5 rad/sec$ and one with scale $0 < a = 0.5 < 1$ with center frequency $\omega_\psi = 10/0.5 = 20 rad/sec$. Figure 3.10 shows the results. The plots on the left hand side illustrate the real part (solid) and imaginary part (dashed) for the wavelets in the time domain. The plots on the right hand illustrate the corresponding wavelets in the frequency domain. (a) Shows the mother wavelet $\omega_\psi = 10 rad/sec$, (b) Illustrates a scaled version with $a > 1$. It can be observed that it is the original wavelet stretched in time, while the frequency bandwidth narrows. (c) Illustrates a scaled version with $0 < a < 1$. It can be observed that it is the original wavelet compressed in time. It can be clearly observed that a wide spread in time (high time resolution) corresponds with a narrow spread in frequency (low frequency resolution). Conversely, a narrow spread in time (low time resolution) corresponds with a wide spread in frequency (high frequency resolution)
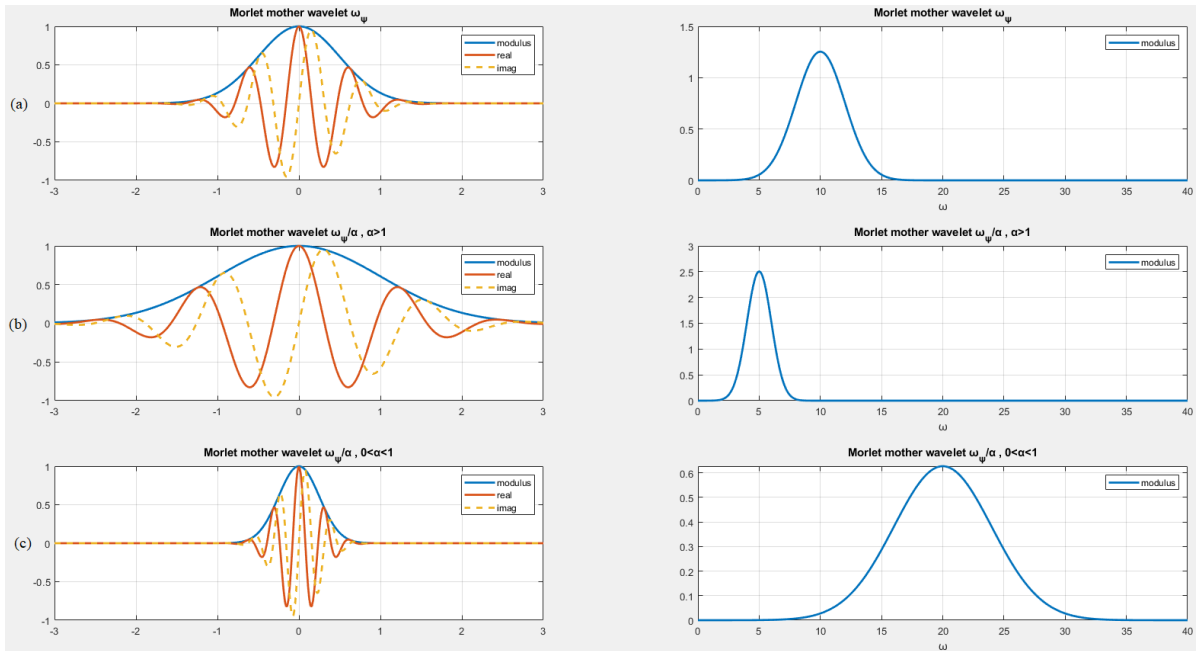
Figure 3.10: Example of the effect of scaling on a Morlet wavelet. (a) Mother wavelet, (b) Scaled version with $a > 1$. (c) Scaled version with $0 < a < 1$.

Listing 3.2: Effect of scaling on a Morlet wavelet

```matlab
clc; clearvars; close all;

% Morlet Wavelet
% Specify the morlet wavelet
beta = 10
delta = 0.5
% Q parameter
Q2 = beta*delta/sqrt(2)

% Mother wavelet parameters
m=400;                                    % mother wavelet points to calculate

% time domain
t2 = linspace(-3,3,m);
m_w_morlet=exp(-t2.^2./(2.*delta^2)).*exp(1i.*beta.*t2);

% frequency domain
omega2 = linspace(0,40,m);
m_w_morlet_w=delta.*sqrt(2*pi).*exp(-(omega2-beta).^2.*(delta^2)./2);


% Scale a>1
a1 = 2
betaSc1 = beta/a1
deltaSc1 = delta*a1

% time domain
m_w_morlet_Sc1=exp(-t2.^2./(2.*deltaSc1^2)).*exp(1i.*betaSc1.*t2);

```

```matlab
30  % frequency domain
31  m_w_morlet_w_Sc1=deltaSc1.*sqrt(2*pi).*exp(-(omega2-betaSc1).^2.*(
        deltaSc1^2)./2);
32
33
34  % Scale 0<a<1
35  a2 = 0.5
36  betaSc2 = beta/a2
37  deltaSc2 = delta*a2
38
39  % time domain
40  m_w_morlet_Sc2=exp(-t2.^2./(2.*deltaSc2^2)).*exp(1i.*betaSc2.*t2);
41
42  % frequency domain
43  m_w_morlet_w_Sc2=deltaSc2.*sqrt(2*pi).*exp(-(omega2-betaSc2).^2.*(
        deltaSc2^2)./2);
44
45  % plot the morlet wavelet
46  figure()
47  subplot(3,2,1)
48  hold on; grid on; box on;
49  plot(t2,abs(m_w_morlet),'-','LineWidth',2)
50  plot(t2,real(m_w_morlet),'-','LineWidth',2)
51  plot(t2,imag(m_w_morlet),'--','LineWidth',2)
52  legend('modulus','real','imag')
53  title('Morlet mother wavelet omega_psi')
54  xlabel('t')
55
56  subplot(3,2,2)
57  hold on; grid on; box on;
58  plot(omega2,abs(m_w_morlet_w),'-','LineWidth',2)
59  legend('modulus')
60  title('Morlet mother wavelet omega_psi')
61  xlabel('omega')
62
63  subplot(3,2,3)
64  hold on; grid on; box on;
65  plot(t2,abs(m_w_morlet_Sc1),'-','LineWidth',2)
66  plot(t2,real(m_w_morlet_Sc1),'-','LineWidth',2)
67  plot(t2,imag(m_w_morlet_Sc1),'--','LineWidth',2)
68  legend('modulus','real','imag')
69  title('Morlet mother wavelet omega_psi/alpha , alpha>1')
70  xlabel('t')
71
72  subplot(3,2,4)
73  hold on; grid on; box on;
74  plot(omega2,abs(m_w_morlet_w_Sc1),'-','LineWidth',2)
75  legend('modulus')
76  title('Morlet mother wavelet omega_psi/alpha , alpha>1')
77  xlabel('omega')
78
79  subplot(3,2,5)
80  hold on; grid on; box on;
81  plot(t2,abs(m_w_morlet_Sc2),'-','LineWidth',2)
82  plot(t2,real(m_w_morlet_Sc2),'-','LineWidth',2)
83  plot(t2,imag(m_w_morlet_Sc2),'--','LineWidth',2)
```

```
84  legend('modulus','real','imag')
85  title('Morlet mother wavelet omega_psi/alpha , 0<alpha<1')
86  xlabel('t')
87
88  subplot(3,2,6)
89  hold on; grid on; box on;
90  plot(omega2,abs(m_w_morlet_w_Sc2),'-','LineWidth',2)
91  legend('modulus')
92  title('Morlet mother wavelet omega_psi/alpha , 0<alpha<1')
93  xlabel('omega')
```

3.3.4 *Normalization*

To ensure that the wavelet transforms at each scale a are directly comparable to each other and to the transforms of other time series, the wavelet function at each scale a is normalized.

Different normalizations can be found in the literature. Attempting now to give a general definition in order to explore the choice of normalization, let the mother wavelet $\psi(t)$ and an arbitrary number $q \geq 0$. The corresponding family of wavelets is the family $[\psi_{b,a}; b \in \mathbb{R}, a \in \mathbb{R}_+^*]$ of shifted and scaled (dilated) copies of ψ defined as:

$$\psi_{b,a}(t) = |a|^{-q}\psi\left(\frac{t-b}{a}\right) \quad , \quad t \in \mathbb{R} \tag{3.53}$$

where a is the scaling parameter and b is the translation parameter. This definition associates the normalization choice with the just the value of q. Different values have been selected in the literature, for example, Carmona et al. [2], Delprat et al. [7] use $q = 1$. Chui [3] and Daubechies [5] use $q = 1/2$. When dealing with orthonormal bases of wavelets, the choice $q = 0$ is sometimes convenient [11]. Thus, these three values will be explored and presented in the next.
Starting with $q = 1$, equation 3.53 becomes:

$$\psi_{b,a}(t) = \frac{1}{a}\psi\left(\frac{t-b}{a}\right) \quad , \quad t \in \mathbb{R} \tag{3.54}$$

The scaled wavelets $\psi_{b,a}(t)$ have been normalized in such a way that:

$$||\psi_{b,a}(t)||_1 = \int_{-\infty}^{+\infty} |\psi_{b,a}(t)| = ||\psi(t)||_1 = constant \tag{3.55}$$

Thus, all the scaled wavelets, $\psi_{b,a}(t)$, at every scale, a, enclose the same area.

For $q = 1/2$, equation 3.53 becomes:

$$\psi_{b,a}(t) = \frac{1}{\sqrt{a}}\psi\left(\frac{t-b}{a}\right) \quad , \quad t \in \mathbb{R} \tag{3.56}$$

The scaled wavelets $\psi_{b,a}(t)$ have been normalized in such a way that:

$$||\psi_{b,a}(t)||_2 = \int_{-\infty}^{+\infty} |\psi_{b,a}(t)|^2 = ||\psi(t)||_2 = constant \qquad (3.57)$$

Thus, all the scaled wavelets, $\psi_{b,a}(t)$, at every scale, a, have the same energy.

For $q = 0$, equation 3.53 becomes:

$$\psi_{b,a}(t) = \psi\left(\frac{t-b}{a}\right) \quad , \quad t \in \mathbb{R} \qquad (3.58)$$

The scaled wavelets $\psi_{b,a}(t)$ have been normalized in such a way that:

$$||\psi_{b,a}(t)||_\infty = constant \qquad (3.59)$$

Thus, all the scaled wavelets, $\psi_{b,a}(t)$, at every scale, a, have merely the same maximum value.

Example 3.6. Consider the Complex Morlet wavelet of the previous example, defined in the time domain as $\psi(t) = e^{-t^2/(2\delta^2)}e^{i\beta t}$. Let the mother wavelet have $\omega_\psi = 10\,rad/sec$ and $\delta = 0.5$. Consider two scaled wavelets, one with scale $a = 2 > 1$ and one with scale $0 < a = 0.5 < 1$ and $b = 0$ for both. The three presented cases of normalization are considered, $q = 1$ (same area), $q = 1/2$ (same energy), and $q = 0$ (same peak amplitude).
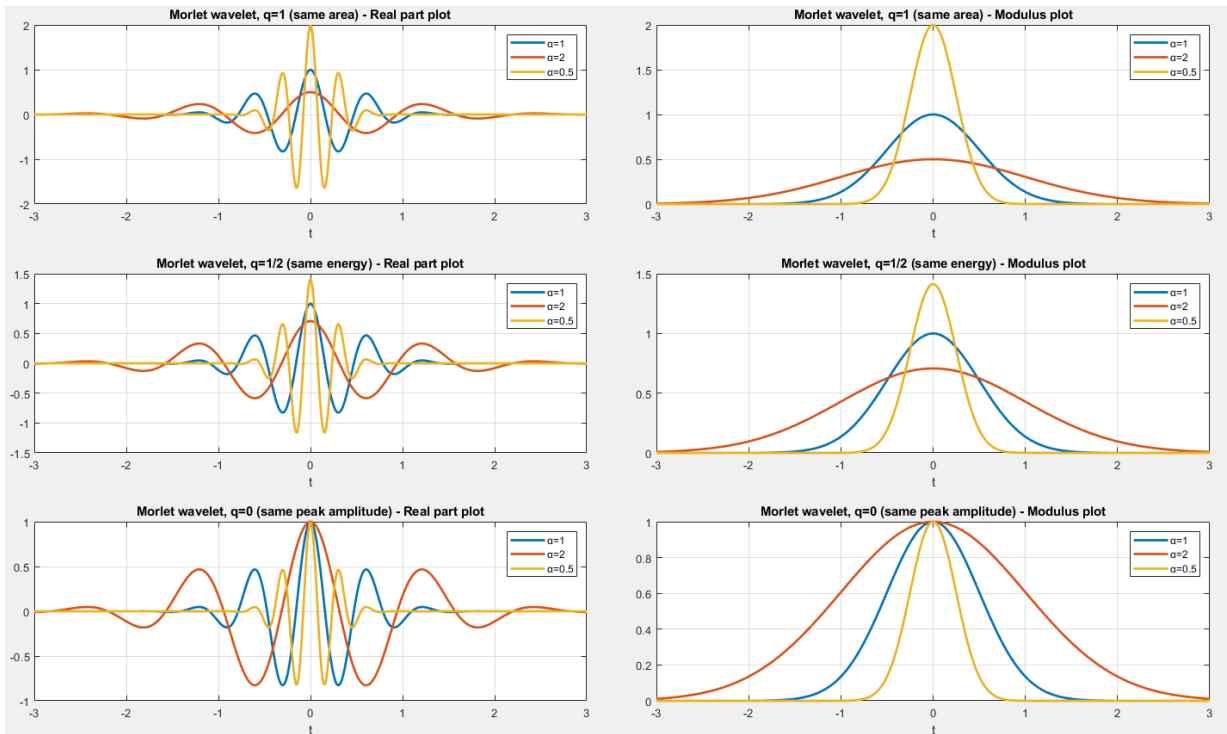
Figure 3.11: Example of the effect of normalization for $q = 1$ (same area), $q = 1/2$ (same energy), and $q = 0$ (same peak amplitude) on a Morlet wavelet.

Figure 3.11 shows the results. The plots on the left hand side illustrate the real part of the wavelets in the time domain. The plots on the right hand illustrate the modulus of the wavelets in the time domain, which give a more clear picture of the situation. Notice that for $q = 0$ how all the wavelets have the same peak amplitude $= 1$, as expected.

Listing 3.3: The effect of normalization on a Morlet wavelet script

```
1  clc; clearvars; close all;
2
3  % Morlet Wavelet
4  % Specify the morlet wavelet
5  beta = 10;
6  delta = 0.5;
7
8  % Mother wavelet parameters
9  m=400;                                  % mother wavelet points to calculate
10
11 % time domain
12 t2 = linspace(-3,3,m);
13 m_w_morlet=exp(-t2.^2./(2.*delta^2)).*exp(1i.*beta.*t2);
14
15 % frequency domain
16 omega2 = linspace(0,40,m);
17 m_w_morlet_w=delta.*sqrt(2*pi).*exp(-(omega2-beta).^2.*(delta^2)./2);
18
19 % Scale a>1
20 a1 = 2;
21 betaSc1 = beta/a1;
22 deltaSc1 = delta*a1;
23
24 % time domain
25 m_w_morlet_Sc1=(exp(-t2.^2./(2.*deltaSc1^2)).*exp(1i.*betaSc1.*t2));
26
27 % q = 1 (same area)
28 m_w_morlet_Sc1_q1 = m_w_morlet_Sc1/a1;
29
30 % q = 1/2 (same energy)
31 m_w_morlet_Sc1_q2 = m_w_morlet_Sc1/sqrt(a1);
32
33
34 % Scale 0<a<1
35 a2 = 0.5;
36 betaSc2 = beta/a2;
37 deltaSc2 = delta*a2;
38
39 % time domain
40 m_w_morlet_Sc2 = (exp(-t2.^2./(2.*deltaSc2^2)).*exp(1i.*betaSc2.*t2));
41
42 % q = 1 (same area)
43 m_w_morlet_Sc2_q1 = m_w_morlet_Sc2/a2;
44
45 % q = 1/2 (same energy)
46 m_w_morlet_Sc2_q2 = m_w_morlet_Sc2/sqrt(a2);
47
48
49 % plot the morlet wavelet
```

```matlab
50   figure()
51   subplot(3,2,1)
52   hold on; grid on; box on;
53   plot(t2,real(m_w_morlet),'-','LineWidth',2)
54   plot(t2,real(m_w_morlet_Sc1_q1),'-','LineWidth',2)
55   plot(t2,real(m_w_morlet_Sc2_q1),'-','LineWidth',2)
56   legend('a=1','a=2','a=0.5')
57   title('Morlet wavelet, q=1 (same area) - Real part plot')
58   xlabel('t')
59
60   subplot(3,2,2)
61   hold on; grid on; box on;
62   plot(t2,abs(m_w_morlet),'-','LineWidth',2)
63   plot(t2,abs(m_w_morlet_Sc1_q1),'-','LineWidth',2)
64   plot(t2,abs(m_w_morlet_Sc2_q1),'-','LineWidth',2)
65   legend('a=1','a=2','a=0.5')
66   title('Morlet wavelet, q=1 (same area) - Modulus plot')
67   xlabel('t')
68
69   subplot(3,2,3)
70   hold on; grid on; box on;
71   plot(t2,real(m_w_morlet),'-','LineWidth',2)
72   plot(t2,real(m_w_morlet_Sc1_q2),'-','LineWidth',2)
73   plot(t2,real(m_w_morlet_Sc2_q2),'-','LineWidth',2)
74   legend('a=1','a=2','a=0.5')
75   title('Morlet wavelet, q=1/2 (same energy) - Real part plot')
76   xlabel('t')
77
78   subplot(3,2,4)
79   hold on; grid on; box on;
80   plot(t2,abs(m_w_morlet),'-','LineWidth',2)
81   plot(t2,abs(m_w_morlet_Sc1_q2),'-','LineWidth',2)
82   plot(t2,abs(m_w_morlet_Sc2_q2),'-','LineWidth',2)
83   legend('a=1','a=2','a=0.5')
84   title('Morlet wavelet, q=1/2 (same energy) - Modulus plot')
85   xlabel('t')
86
87   subplot(3,2,5)
88   hold on; grid on; box on;
89   plot(t2,real(m_w_morlet),'-','LineWidth',2)
90   plot(t2,real(m_w_morlet_Sc1),'-','LineWidth',2)
91   plot(t2,real(m_w_morlet_Sc2),'-','LineWidth',2)
92   legend('a=1','a=2','a=0.5')
93   title('Morlet wavelet, q=0 (same peak amplitude) - Real part plot')
94   xlabel('t')
95
96   subplot(3,2,6)
97   hold on; grid on; box on;
98   plot(t2,abs(m_w_morlet),'-','LineWidth',2)
99   plot(t2,abs(m_w_morlet_Sc1),'-','LineWidth',2)
100  plot(t2,abs(m_w_morlet_Sc2),'-','LineWidth',2)
101  legend('a=1','a=2','a=0.5')
102  title('Morlet wavelet, q=0 (same peak amplitude) - Modulus plot')
103  xlabel('t')
```

3.3.5 *Choice of mother wavelets*

There are a lot of mother wavelets in the literature, some examples are shown in figure 3.6. The choice of the mother wavelet is dictated by the characteristics of the signal under study and the nature of the application. It is important to use a wavelet that is the best fit for the analysis that will follow. Consequently, there are several factors which should be considered in the choice of the mother wavelet [34]:

1. ***Complex or Real***. A complex wavelet function will return information about both amplitude and phase and is better adapted for capturing oscillatory behavior. A real mother wavelet returns only a single component and can be used to isolate peaks or discontinuities.

2. ***Shape***. The wavelet function should reflect the type of features present in the time series. For example, in the analysis of free responses of structures, wave-like mother wavelets with an increased number of oscillations such as the Morlet wavelet and the Cauchy wavelet are preferred. For time series with sharp jumps or steps, one would choose a boxcar-like function such as the Harr, while for smoothly varying time series one would choose a smooth function such as a damped cosine. If one is primarily interested in wavelet power spectra, then the choice of wavelet function is not critical, and one function will give the same qualitative results as another. Conversely, the wavelet function can also be chosen to uncover specific signal features that are hypothesized to exist in the signal but may not be directly evident upon initial inspection.

3. ***Width***. The resolution of a wavelet function is determined by the balance between the width in real space and the width in Fourier space. A narrow (in time) function will have good time resolution but poor frequency resolution, while a broad function will have poor time resolution, yet good frequency resolution.

4. ***Orthogonal or nonorthogonal***. This refers to the DWT. In orthogonal wavelet analysis, the number of convolutions at each scale is proportional to the width of the wavelet basis at that scale. This produces a wavelet spectrum that contains discrete "blocks" of wavelet power and is useful for signal processing as it gives the most compact representation of the signal. Unfortunately for time series analysis, an aperiodic shift in the time series produces a different wavelet spectrum. Conversely, a nonorthogonal analysis is highly redundant at large scales, where the wavelet spectrum at adjacent times is highly correlated. The nonorthogonal transform is useful for time series analysis, where smooth, continuous variations in wavelet amplitude are expected.

The optimal mother wavelet ψ for modal identification purposes using the free responses of a m.d.o.f system should satisfy the following conditions [13]:

1. ψ is admissible. Obvious, required by definition.

2. ψ is progressive. Several reasons suggest the use of progressive wavelets instead of real ones for the analysis of real signals:

   i. It allows the direct connection between a real signal and its associated analytic signal.

ii. The wavelet transform of real signals using real wavelets yields real wavelet co-efficients, and there is no natural way of making a connection with some "local spectrum" which one would like associate with a given signal.

3. ψ has good time and frequency localization properties. This condition is very important in the context of time–frequency analysis as presented in the section of resolution.

4. The first and the second derivatives of ψ satisfy the three previous conditions. This condition makes the processing by CWT of displacement, velocity and acceleration easier without differential and integral operations.

Example 3.7 (Complex Morlet wavelet and Cauchy wavelet of order n)**.** Two important complex mother wavelets and their properties are presented in table 3.1, the complex Morlet wavelet and the Cauchy wavelet of order n.

The Complex Morlet wavelet, is defined in the time domain in the frequency domain respectively as:

$$\psi(t) = e^{-t^2/(2\delta^2)}e^{i\beta t} \qquad , \qquad \widehat{\psi}(\omega) = \delta\sqrt{2\pi}e^{-(\omega-\beta)^2\delta^2/2} \tag{3.60}$$

where β is a frequency parameter controlling the number of oscillations of the wavelet and δ is a parameter that controls the spread of the wavelet.

The Cauchy wavelet of order n, is defined in the time domain in the frequency domain respectively as:

$$\psi(t) = \left(\frac{i}{t+i}\right)^{n+1} = \left(\frac{1}{\sqrt{t^2+1}}\right)^{n+1}e^{i(n+1)arctan(t)} \qquad , \qquad \widehat{\psi}(\omega) = \frac{2\pi\omega^n e^{-\omega}}{n!}\Theta(\omega) \tag{3.61}$$

Figure 3.12: (a) The complex Morlet wavelet for $\beta = 37.5$ and $\delta = 0.1629$ and (b) the Cauchy wavelet for $n = 7$.

These two wavelets are applied in this thesis. An essential aspect of these mother wavelets is that they have parameters in their definitions that strongly influence the localization properties, i.e. β and δ for the Complex Morlet wavelet and n for the Cauchy wavelet. It can be observed that the more the ω_ψ increases, the closer the Cauchy and the Morlet wavelet curves become in both time-frequency domains.

The first and the second condition are verified by the Cauchy wavelet. The Morlet wavelet is only numerically admissible and progressive when the product of the two parameters $\beta\delta$ is large enough ($\beta\delta \geq 5$ in practice). According to the third condition, the Morlet wavelet has its time–frequency window with the smallest area allowable (1/2) by the Heisenberg inequality. The uncertainty μ_ψ of the Cauchy wavelet behaves asymptotically with this threshold when its order parameter n tends towards infinity. The last condition is easily verified by the definition of the Cauchy wavelet. The first and second derivatives of the Cauchy wavelet ψ_n are also Cauchy wavelets:

$$\dot{\psi}_n(t) = \frac{d\psi_n(t)}{dt} = (n+1)\left(\frac{i}{t+i}\right)^n \frac{d(i/(t+i))}{dt}$$

$$= (n+1)\left(\frac{i}{t+i}\right)^n \frac{-1i}{(t+i)^2}$$

$$= (n+1)\frac{i^n}{(t+i)^n}\frac{i^2 i}{(t+i)^2}$$

$$= i(n+1)\frac{i^{n+2}}{(t+i)^{n+2}}$$

$$= i(n+1)\left(\frac{i}{t+i}\right)^{n+2}$$

$$= i(n+1)\psi_{n+1}(t) \tag{3.62}$$

thus,

$$\dot{\psi}_n(t) = i(n+1)\psi_{n+1}(t) \qquad \text{and} \qquad \ddot{\psi}_n(t) = -(n+1)(n+2)\psi_{n+2}(t) \tag{3.63}$$

Consequently an identification procedure using $\dot{u}$ and $\ddot{u}$ can be simplified. The first and second derivatives of the Morlet wavelet also satisfy the fourth condition, but they are not the Morlet wavelets and their time–frequency localization are no longer as good as the Morlet wavelet [13].

Table 3.1: Definition and main properties of the Complex Morlet wavelet and the Cauchy wavelet of order n.

	Morlet wavelet	Cauchy wavelet
$\psi(t)$	$e^{-t^2/(2\delta^2)}e^{i\beta t}$	$\left(\dfrac{i}{t+i}\right)^{n+1}$
$\hat{\psi}(\omega)$	$\delta\sqrt{2\pi}e^{-(\omega-\beta)^2\delta^2/2}$	$\dfrac{2\pi\omega^n e^{-\omega}}{n!}\Theta(\omega)$
C_ψ:	∞	$4\pi^2\dfrac{1}{2^{2n}}\dfrac{(2n-1)!}{(n!)^2}$
t_ψ	0	0
ω_ψ	β	$n+\dfrac{1}{2}$
$\Delta\omega_\psi$:	$\dfrac{1}{\delta\sqrt{2}}$	$\dfrac{\sqrt{2n+1}}{2}$
Δt_ψ:	$\dfrac{\delta}{\sqrt{2}}$	$\dfrac{1}{\sqrt{2n-1}}$
μ_ψ:	$\dfrac{1}{2}$	$\dfrac{1}{2}\sqrt{1+\dfrac{2}{2n-1}}$
$Q=\dfrac{\omega_\psi}{2\Delta\omega_\psi}$	$\dfrac{\beta\delta}{\sqrt{2}}$	$\dfrac{n+\dfrac{1}{2}}{\sqrt{2n+1}}$

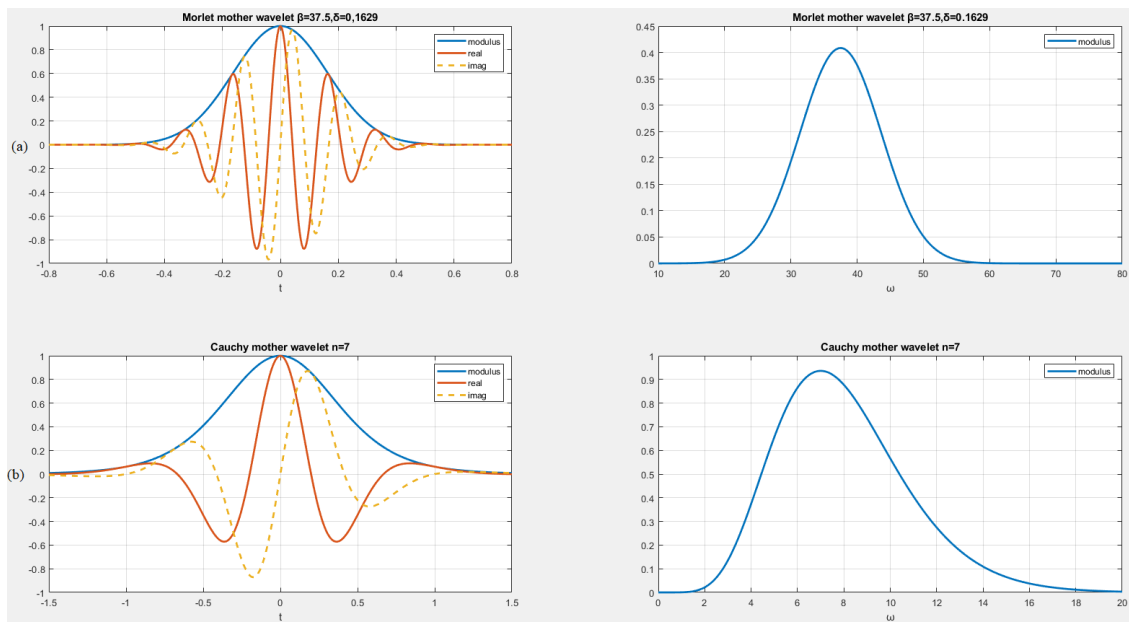Figure 3.13: Example of when the two wavelets have the same center frequency ω_ψ(a) The complex Morlet wavelet for $\beta = 37.5$ and $\delta = 0.1629$ and (b) the Cauchy wavelet for $n = 37$.

3.3.6 Scales and Converting scale to frequency

By definition the CWT decomposes signals based on time and scale parameters. However in many applications, including the modal parameter identification, the results are preferred to be on the time-frequency plane. Therefore,it is important to define a relationship between scale and frequency. As it was presented in the Resolution section a scaled wavelet's frequency is $\omega = \frac{\omega_\psi}{a}$, thus scale and frequency are inversely proportional and related through the center frequency ω_ψ, and can be theoretically computed as:

$$f = \frac{f_\psi}{a} \tag{3.64}$$

where f_ψ is the center frequency of the mother wavelet, and a the scale.
In a more intuitive sense, the center frequency of a wavelet is a simplified approximation of the dominant frequency component contained in the function. The center frequency can be determined and visualized by superimposing a sine wave onto the wavelet and determining the frequency value for which the sinusoid best parallels the wavelet's main oscillation. MATLAB, in the built in cwt command, determines the center frequency by this approximation and makes a slight variation of the theoretical equation, adding the sampling period dt:

$$f = \frac{f_\psi}{a} \frac{1}{dt} \tag{3.65}$$

Example 3.8. Consider a Cauchy wavelet with $n = 37$ and $\omega_\psi = 37.5 rad/sec$, that is $f_\psi = 5.97 Hz$. This wavelet is inserted in MATLAB as user defined. As it can be observed

by figure 3.14, MATLAB "tailors" a sine wave into the wavelet, so the center frequency estimated by MATLAB $f_\psi = 5.7Hz$ is very close to the original.
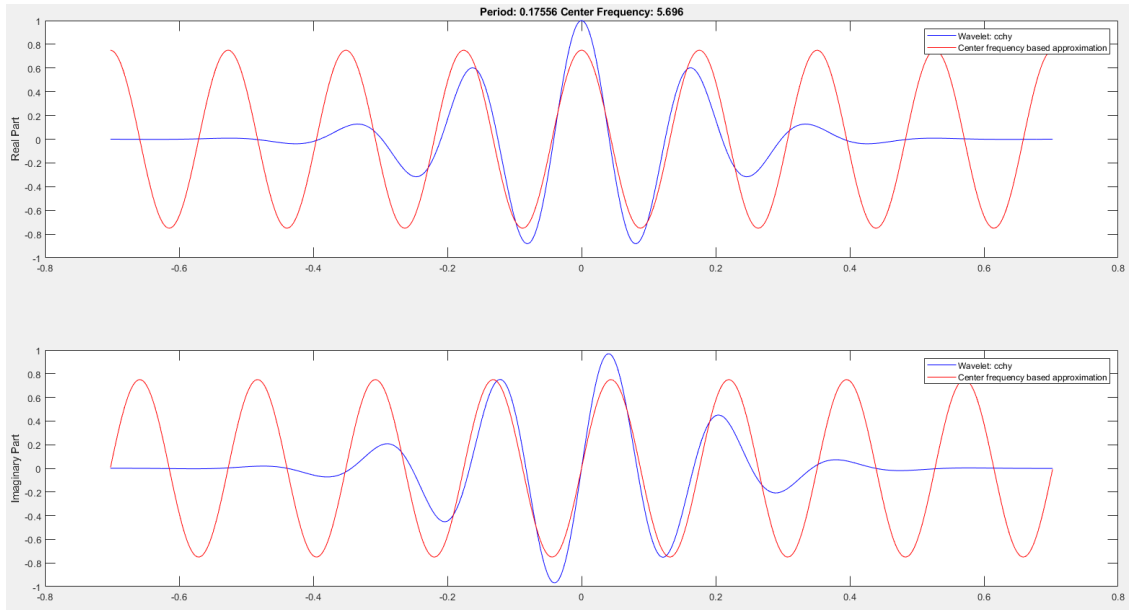
Figure 3.14: Approximation of the wavelet to a sine wave and its frequency.

As the frequency variable is identified as a constant multiple of $1/a$, then the mother wavelet ψ can be considered as an adaptive bandpass filter, with pass-band given by 3.52. Thus, the series of the scaled copies of ψ can be viewed as a bandpass filterbank. The number of scales used in an analysis defines the number of scaled copies of the mother wavelet that will be generated; the finer the scales, the finer the frequency resolution.

Octave is a notion from acoustics and refers to a duplication of frequency, e.g. a frequency range $[10\ 20]Hz$ is one octave, as $log_2(fmax/fmin) = log_2(20/10) = 1$. Number of Voices per Octave is a term commonly used to designate the number of scaled wavelets per octave, i.e. the number of scales per octave. Therefore, number of voices per octave determines the number of scales between a frequency duplication.

Summarizing, the number of octaves determines the span of frequencies being analyzed, while the number of voices per octave determines the number of scales (i.e. samples) across this span. The appropriate range of octaves and scales depends on the spectral content of the data, and the highest requested frequency in the CWT [16].

Example 3.9 (Scales and frequencies relationship)**.** The following script computes the scales for the analysis of a signal, using the Cauchy wavelet, that has $\omega_\psi = n + 0.5$. The max and min frequencies are defined by the user; here the Nyquist frequency is considered as max frequency. The relationship $f = \frac{f_\psi}{a}$ it can be observed clearly (considering the same corresponding index): Lower frequencies correspond to larger scales, e.g. see index 100, while higher frequencies correspond to smaller scales, e.g. see index 20.
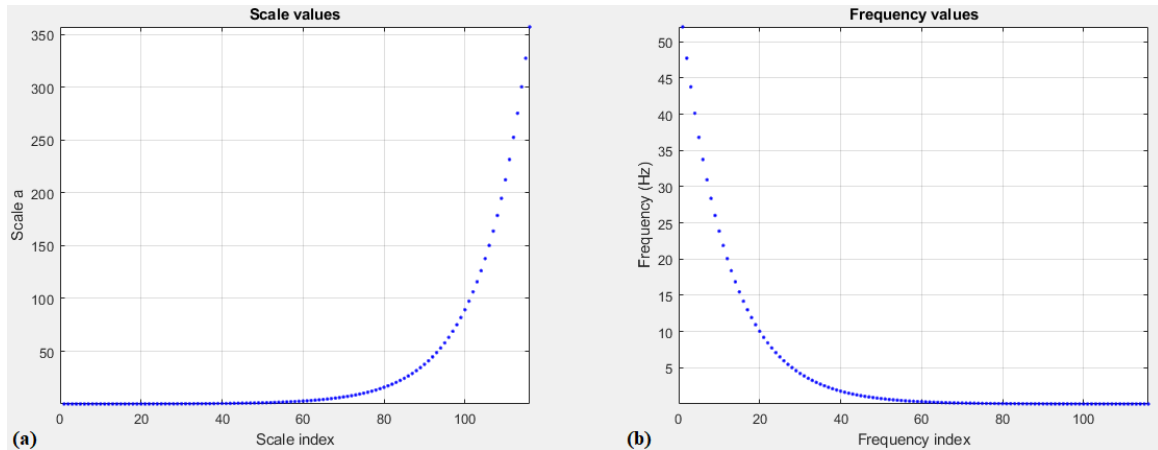
Figure 3.15: Plot of scale index vs scale value, 16 voices per octave

Listing 3.4: Scale and frequency relationship script

```
1  clc; close all; clearvars;
2  % Signal processing
3  dt = 0.01;         % sampling period
4  Fs = 1/dt;         % sampling frequency
5  Fn = Fs/2;         % Nyquist frequency
6
7  % Wavelet center frequency
8  n=5;
9  omega_psi = n+1/2;                    % center frequency in rad/sec - Cauchy
       wavelet
10 CentFreq = omega_psi/(2*pi)   % center frequency in Hz
11
12 % Analysis frequencies for scale calculation
13 min_freq = dt/4;     % min freq of analysis
14 max_freq = Fn;       % max freq of analysis
15
16 % Define proper scales
17 NumVoices = 8;                            % voices per octave
18 a0 = 2^(1/NumVoices);
19 min_scale = CentFreq/(max_freq*dt);
20 max_scale = CentFreq/(min_freq*dt);
21 min_scale = floor(NumVoices*log2(min_scale));
22 max_scale = ceil(NumVoices*log2(max_scale));
23 scales = a0.^(min_scale:max_scale).*dt;
24 frequencies = CentFreq./scales;
25
26 figure()
27 subplot(1,2,1)
28 hold on; grid on; box on;
29 plot(scales,'b.')%,'LineWidth',2)
30 title('Scale values')
31 xlabel('Scale index')
32 ylabel('Scale a')
33 xlim([0,length(scales)])
34 ylim([min(scales),max(scales)])
35
36 subplot(1,2,2)
```

59

```
37  hold on; grid on; box on;
38  plot(frequencies,'b.')%,'LineWidth',2)
39  title('Frequency values')
40  xlabel('Frequency index')
41  ylabel('Frequency (Hz)')
42  xlim([0,length(frequencies)])
43  ylim([min(frequencies),max(frequencies)])
```

Example 3.10 (Number of scales influence to frequency resolution). The following script computes the cwt of a signal ut, using the Morlet wavelet. The focus is on the frequency range frequency range $[10\ \ 20]Hz$,i.e. in one octave. The signal $u(t)$ is the free response of a SDOF system with :
mass m = 1 kg, stiffness k = 7 kN/m, damping coefficient c = 2 N s/m,
initial conditions: u(0) = 1 m and $\dot{u}(0)$ = 0 m/s,
length of the signal is L = 5 s and the sampling period dt = 0.001 s.
Two cases are presented: the first considers 4 number of voices per octave, while the second 48 number of voices per octave. The new cwt command is used for this. It should be metniones that it also calls the matlab function sdfLcdf to solve the SDOF system.

As it can be clearly observed in figure 3.17, 4 number of voices per octave correspond to 4 scaled wavelets (+1 the mother wavelet), while 48 number of voices per octave correspond to 48 scaled wavelets (+1 the mother wavelet). In figure 3.18 the effect of the number of scales can be clearly observed. Low number of scales (Nv=4) result in poor frequency resolution and unclear information about the signal, whlie high number of scales (Nv=48) result in good frequency resolution and clear information about the signal.
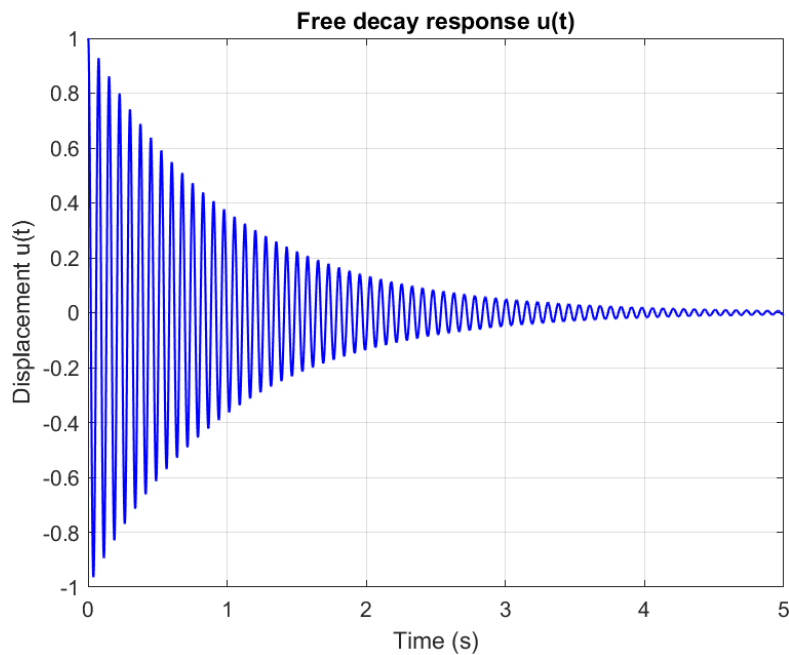
Figure 3.16: Signal u(t). Free decay response of the SDOF system
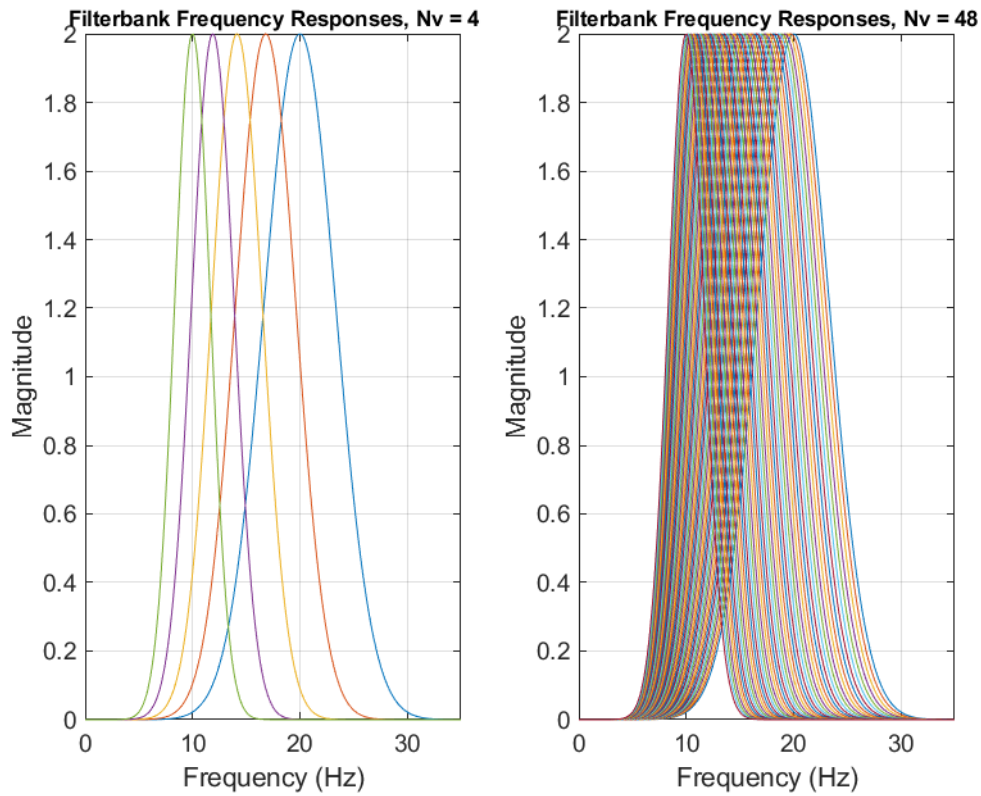
Figure 3.17: Filterbank frequency respones. On the left hand side is the case with 4 number of voices per octave and on the right hand side is the case with 48 number of voices per octave.
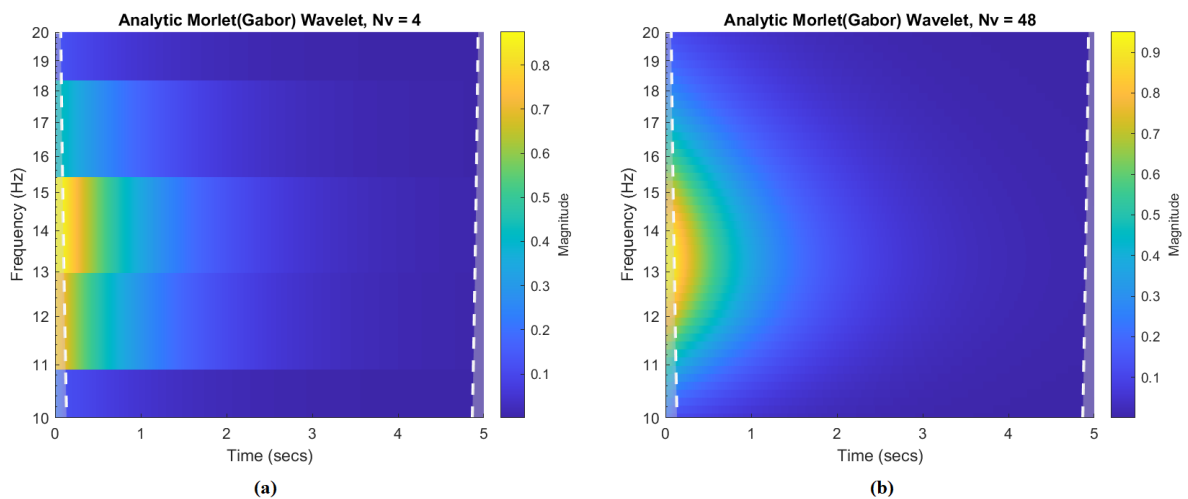
Figure 3.18: CWT modulus Scalogram. (a) 4 number of voices per octave (b) 48 number of voices per octave.

Listing 3.5: Number of scales influence to frequency resolution

```
1  clc; clearvars; close all;
```

```matlab
2
3  % Solve the SDOF system
4  M = 1;                          % kg
5  K = 7000;                       % N/m
6  omega_exact = sqrt(K/M)
7  T_exact=2*pi/omega_exact        % natural period
8  f_exact=1/T_exact
9  C = 2;                          % N*s/m
10 xi_exact=C/(2*M*omega_exact)    % damping ratio
11
12 % initial conditions
13 u0 = 1.0;
14 v0 = 0;
15
16 L = 5;                          % length of signal - sec
17 dt = 0.001;                     % sampling period sec
18 F = zeros(floor(L/dt),1);
19 irec = 0;
20 [amax,vmax,umax,ut,uv,ua] = sdfLcdf(T_exact,F,xi_exact,dt,irec,u0,v0);
21
22 t = (1:length(ut))*dt;
23 t = t';
24
25 %Plot the free decay response
26 figure()
27 hold on; box on; grid on;
28 h3 = plot(t,ut,'b','LineWidth',2);
29 title('Free decay response u(t)')
30 xlabel('Time (s)')
31 ylabel('Displacement u(t)')
32 xlim([0,L])
33
34 % Filterbank creation
35 fb_morlet1 = cwtfilterbank('SignalLength',numel(ut),'SamplingFrequency'
      ,1/dt,'FrequencyLimits',[10 20],'VoicesPerOctave',4,'Wavelet','amor')
      ;
36 fb_morlet2 = cwtfilterbank('SignalLength',numel(ut),'SamplingFrequency'
      ,1/dt,'FrequencyLimits',[10 20],'VoicesPerOctave',48,'Wavelet','amor'
      );
37 % As the number of voices per octave increases, the scale resolution
      becomes finer
38
39 % plot the magnitude frequency responses for the CWT filter bank
40 figure()
41 subplot(1,2,1)
42 hold on; grid on; box on;
43 [psidft1,frqfb1] = freqz(fb_morlet1);
44 plot(frqfb1,psidft1)
45 title('Filterbank Frequency Responses, Nv = 4','FontSize',8)
46 xlabel('Frequency (Hz)')
47 ylabel('Magnitude')
48 xlim ([0,35])
49
50 subplot(1,2,2)
51 hold on; grid on; box on;
52 [psidft2,frqfb2] = freqz(fb_morlet2);
```

```
53  plot(frqfb2,psidft2)
54  title('Filterbank Frequency Responses, Nv = 48','FontSize',8)
55  xlabel('Frequency (Hz)')
56  ylabel('Magnitude')
57  xlim ([0,35])
58
59
60  figure()
61  cwt(ut,'Filterbank',fb_morlet1) %Analytic Morlet(Gabor) Wavelet
62  title('Analytic Morlet(Gabor) Wavelet, Nv = 4')
63
64
65  figure()
66  cwt(ut,'Filterbank',fb_morlet2) %Analytic Morlet(Gabor) Wavelet
67  title('Analytic Morlet(Gabor) Wavelet, Nv = 48')
```

3.3.7 Edge effect - Cone of influence

The CWT works as described in figure 3.7, i.e, the mother wavelet is scaled, then translated in time and covers the whole signal. Inevitably, when the wavelets are near the beginning or end of the data "catch" data outside the observation interval, thus the computed wavelet coefficients near the beginning and end of the data are affected by the fact that there wavelets are extending outside the boundary. This is called the *edge effect problem*, which arises due to the finite length and to the discretization of measured data record and to the nature of the CWT [13]. Furthermore, the extent of the wavelet coefficients affected by data outside the observation interval depends on the scale (frequency). Low frequencies correspond to wavelets of larger scale, while higher frequencies correspond to wavelets of smaller scale. The edge effect persists longer in time with large scaled wavelets, that is why the affected area takes the shape of a cone [23]. Various techniques have been developed to remedy the edge effect, however it cannot be removed and the interpretation of wavelet coefficients near the boundaries must be handled with great caution. Thus, a domain D in the TF plane, must be determined, where the edge effect can be neglected. The *cone of influence* (COI) is the region of the wavelet spectrum in which edge effects become important.

However, there is no closed mathematical formula to determine the extent of the cone of influence at each scale. Nobach et al. [28] define the extent of the cone of influence at each scale as the point where the wavelet transform magnitude decays to 2% of its peak value. Because many of the wavelets used in continuous wavelet analysis decay exponentially in time, Torrence and Compo [34] use the time constant $1/e$ to delineate the borders of the cone of influence at each scale. For Morse wavelets, Lilly [15] uses the concept of the "wavelet footprint", which is the time interval that encompasses approximately 95% of the wavelet's energy. Lilly delineates the COI by adding $1/2$ the wavelet footprint to the beginning of the observation interval and subtracting $1/2$ the footprint from the end of the interval at each scale.

Le and Argoul [13] introduced two real coefficients $c_t \geq 1$ and $c_f \geq 1$ that have the property that:

when t is outside the interval $I_{c_t} = [t_\psi - c_t \Delta t_\psi \ , \ t_\psi + c_t \Delta t_\psi]$

and when ω is outside the interval $I_{c_f} = [\omega_\psi - c_f \Delta \omega_\psi \ , \ \omega_\psi + c_f \Delta \omega_\psi]$,

$\psi(t)$ and $\widehat{\psi}(\omega)$ have good decreasing properties, i.e. have null or very "small" values. They explored the effect of the different values of c_t and c_f and concluded that the choice of $c_t = 5$ and $c_f = 5$ seem to yield good results. Consequently, they proposed to define the domain D as an "extended" time–frequency localization domain for the CWT as expressed in equation 3.50 around the point b_j , $\omega_j = \omega_\psi/a_j$: Using the coefficients c_t and c_f and the progressive property of the mother wavelet, D becomes:

$$\left[b_j + \frac{\omega_\psi}{\omega_j}t_\psi - \frac{\omega_\psi}{\omega_j}c_t\Delta t_\psi \ , \ b_j + \frac{\omega_\psi}{\omega_j}t_\psi + \frac{\omega_\psi}{\omega_j}c_t\Delta t_\psi \right] \times \left[max\left(0, \omega_j\left(1 - c_f\frac{\Delta\omega_\psi}{\omega_\psi} \right) \right), \omega_j\left(1 + c_f\frac{\Delta\omega_\psi}{\omega_\psi} \right) \right]$$
(3.66)

The domain D must be included into $[0, L] \times [2\pi f_{Nyquist}]$, this leads to the following system of inequalities:

$$\begin{cases} \dfrac{\omega_\psi}{\omega_j}c_t\Delta t_\psi - \dfrac{\omega_\psi}{\omega_j}t_\psi \leq b_j \leq L - \dfrac{\omega_\psi}{\omega_j}c_t\Delta t_\psi - \dfrac{\omega_\psi}{\omega_j}t_\psi \\[4mm] 0 < \omega_j \leq \dfrac{2\pi f_{Nyquist}}{1 + c_f\frac{\Delta\omega_\psi}{\omega_\psi}} \end{cases}$$
(3.67)

where L is the signal's duration.

Example 3.11 (Application on the complex Morlet and the Cauchy wavelets). As mentioned in table 3.1, $t_\psi = 0$ for both the complex Morlet and the Cauchy wavelets, thus the domain D becomes:

$$\begin{cases} \dfrac{\omega_\psi}{\omega_j}c_t\Delta t_\psi \leq b_j \leq L - \dfrac{\omega_\psi}{\omega_j}c_t\Delta t_\psi \\[4mm] 0 < \omega_j \leq \dfrac{2\pi f_{Nyquist}}{1 + c_f\frac{\Delta\omega_\psi}{\omega_\psi}} \end{cases}$$

Solving for ω, four equations are obtained, which delimit the useful domain D:

$$\begin{cases} \omega_1 = \dfrac{\omega_\psi}{b}c_t\Delta t_\psi \\[4mm] \omega_2 = \dfrac{\omega_\psi}{L - b}c_t\Delta t_\psi \\[4mm] \omega_3 = 0 \\[4mm] \omega_4 = \dfrac{2\pi f_{Nyquist}}{1 + c_f\frac{\Delta\omega_\psi}{\omega_\psi}} \end{cases}$$

ω_1 and ω_2 are two hyperbolae and ω_3 and ω_4 are two horizontal lines, see figure 3.19.Due to the introduction of the two parameters $c_t \geq 1$ and $c_f \geq 1$, the useful time interval is smaller than L and the maximum useful frequency is smaller than $f_{Nyquist}$.

64

Figure 3.19 illustrates the modulus scalogram of a SDOF system with natural period $T = 0.5sec$. The white lines are the ω_1 and ω_2 hyperbolae limits. Notice the cone of influence on the region where the data begins that manifests as a spread of energy along the frequency axis. Observe that the white line follows that shape.
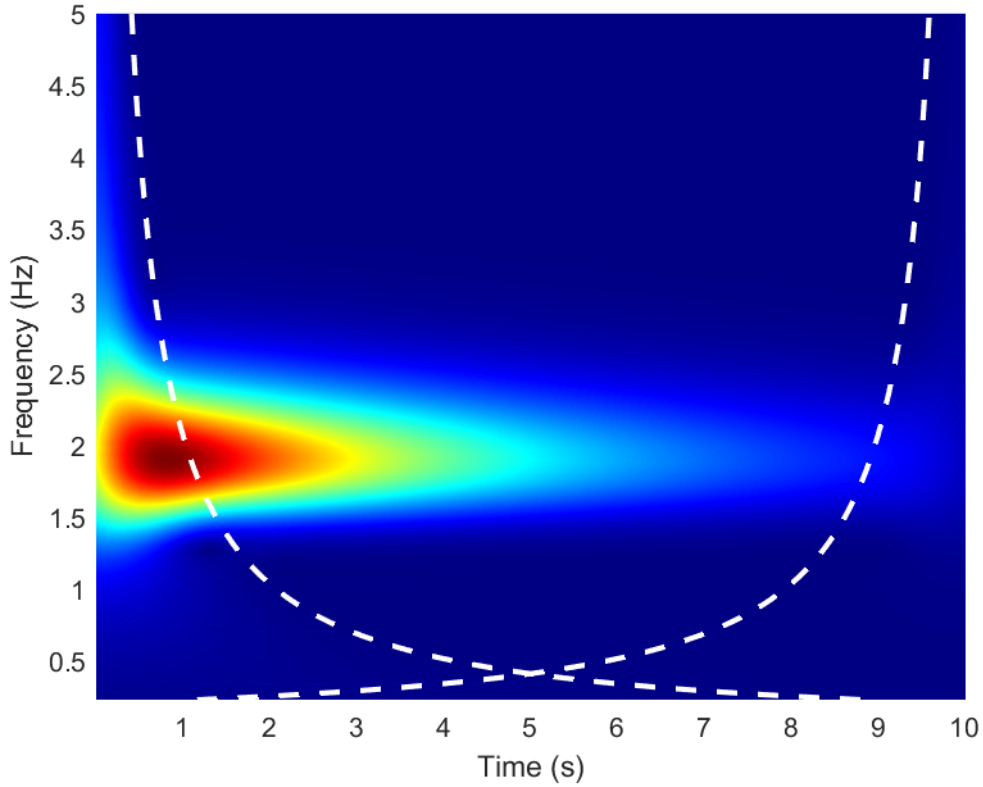
Figure 3.19: CWT modulus Scalogram. Illustration of edge effects, $c_t = 3$ and $c_f = 3$.

3.3.8 *Q factor and it's influence*

In figure 3.9, a parameter Q is presented and stated that it remains constant. As it was mentioned in the previous, the center frequency ω_ψ of is assumed to be positive. This enables the consideration on the frequency window of 3.52 as a frequency band (or octave) with center-frequency ω_ψ/a and bandwidth $2\Delta\omega_\psi/a$. The importance of this identification is that it allows the introduction of the following ratio (Q factor):

$$Q = \frac{\dfrac{\omega_\psi}{a}}{2\dfrac{\Delta\omega_\psi}{a}} = \frac{\omega_\psi}{2\Delta\omega_\psi} \tag{3.68}$$

Q is independent of the scaling a. Hence, if the frequency variable is identified as a constant multiple of $1/a$, then an adaptive bandpass filter, with pass-band given by 3.52, has the property that the center-frequency to bandwidth ratio is independent of the location of the center-frequency, thus it remains constant. This is called *constant-Q filtering*, where Q, once set in the beginning of the analysis, remains the same for all

scaled and shifted wavelets. Q depends only at the mother wavelet choice.

Gram-Hansen and Dorize [9] associate this Q value to the filterbank of a $(1/N)th$ octave as:

$$Q = \frac{1}{2^{1/(2N)} - 2^{-1/(2N)}} \tag{3.69}$$

where an $(1/N)th$ of center frequency ω_ψ is a band $[\omega_1, \omega_2]$ with $\omega_1 = 2^{-1/(2N)}$ and $\omega_2 = 2^{1/(2N)}$.

As it follows by it's definition in 3.68, the Q factor can be associated with the mother wavelet parameters and define their tuning. Higher Q produce narrower wavelets, with more oscillations within their waveform. Consequently applying the CWT with a high Q factor allows a multiscale analysis with high frequency resolution (at the expense of a lower time resolution), making it appropriate for analyzing oscillatory signals such as the displacement response of a structure. Therefore, the choice of Q depends on the spectral components contained in the signal as well as the sampling frequency Fs and the duration of the signal.

Example 3.12 (Q and mother wavelet definition parameters). Consider the previously mentioned complex Morlet wavelet and the Cauchy wavelet of order n, defined as: The Complex Morlet wavelet, is defined in the time domain in the frequency domain respectively as:

$$\psi(t) = e^{-t^2/(2\delta^2)}e^{i\beta t} \quad , \quad \widehat{\psi}(\omega) = \delta\sqrt{2\pi}e^{-(\omega-\beta)^2\delta^2/2}$$

The Cauchy wavelet of order n, is defined in the time domain in the frequency domain respectively as:

$$\psi(t) = \left(\frac{i}{t+i}\right)^{n+1} = \quad , \quad \widehat{\psi}(\omega) = \frac{2\pi\omega^n e^{-\omega}}{n!}\Theta(\omega)$$

Their Q value from table 3.1 is:

$$Q = \frac{\beta\delta}{\sqrt{2}} \text{ , for the Morlet wavelet}$$

and

$$Q = \frac{n + \frac{1}{2}}{\sqrt{2n+1}} \text{ , for the Cauchy wavelet}$$

In order to find the relationship between Q and mother wavelet definition parameters, the following problem is set: For a given parameter of Q, find the corresponding value of the mother wavelet.

Starting with the Morlet wavelet:

For the Morlet wavelet, $\widehat{\psi}(0) \neq 0$ but $\widehat{\psi}(0)$ tends towards 0 when the product $\beta\delta$ increases. Additionally, at a given ω_j of a scaled wavelet, the localizations in time and in frequency

obtained from equation 3.49 and the definition of Q from table 3.1 are:

$$\frac{\beta\delta}{\sqrt{2}} = \frac{\omega_j}{2\Delta\omega_j}, \qquad \text{solving for } \Delta\omega_j,$$

$$\Delta\omega_j = \frac{\omega_j\sqrt{2}}{2\beta\delta} = \frac{\omega_j}{\beta\delta\sqrt{2}}$$

and, as $\Delta t_j \Delta\omega_j = \mu_\psi = 1/2$, thus $\Delta\omega_j = \frac{1}{2\Delta t_j}$ and the previous equation becomes:

$$\frac{1}{2\Delta t_j} = \frac{\omega_j\sqrt{2}}{2\beta\delta}, \qquad \text{solving for } \Delta t_j,$$

$$\Delta t_j = \frac{\beta\delta}{\omega_j\sqrt{2}}$$

Consequently, $\Delta\omega_j$ and Δt_j depend only on the product $\beta\delta$ and thus on the Q value. So, without loss of generality, one can assign $\delta = 1$ and β varying to reach the expected value of Q, so:

$$Q = \frac{\beta}{\sqrt{2}}, \qquad \text{solving for } \beta,$$

$$\beta = Q\sqrt{2}$$

For the Cauchy wavelet, the equation $Q = \dfrac{n + \dfrac{1}{2}}{\sqrt{2n+1}}$ is solved for n:

$$Q = \frac{n + \dfrac{1}{2}}{\sqrt{2n+1}}$$

$$Q\sqrt{2n+1} = n + \frac{1}{2}$$

$$\left(Q\sqrt{2n+1}\right)^2 = \left(n + \frac{1}{2}\right)^2$$

$$Q^2(2n+1) = n^2 + n + \frac{1}{4}$$

$$n^2 + n + \frac{1}{4} - 2nQ^2 - Q^2 = 0$$

$$n^2 + n(1 - 2Q^2) + (0.25 - Q^2) = 0$$

solving the quadratic equation:

$$n = \frac{-(1 - 2Q^2) \pm \sqrt{(1 - 2Q^2)^2 - 4(0.25 - Q^2)}}{2}$$

$$n = \frac{-1 + 2Q^2 \pm \sqrt{1 - 4Q^2 + 4Q^4 - 1 - 4Q^2}}{2}$$

$$n = \frac{-1 + 2Q^2 \pm \sqrt{4Q^4}}{2}$$

$$n = \frac{-1 + 2Q^2 \pm 2Q^2}{2}$$

$n > 0$, so only positive solutions are accepted:

$$n = \frac{-1 + 4Q^2}{2}$$

$$n = 2Q^2 - \frac{1}{2}$$

Now the next step is to implement the problem in MATLAB: Setting a avalue of Q, compute the parameters β for the Morlet wavelet, n for the Cauchy wavelet, compute and visualise the mother wavelets. Figure 3.20 illustrates the Morlet wavelet, in the time domain and in the frequency domain, for Q = 4.3185, 8.6514 and 17.3099. As $\delta = 1 = constant$ the spread of the wavelet in the time domain (time bandwidth) does not change, but as Q increases, ω_j increases, thus more oscillations occur in the waveform. Figure 3.21 illustrates the Cauchy wavelet, in the time domain and in the frequency domain, for Q = 1.4142, 2.8710 and 4.3185. As Q increases, more oscillations occur in the waveform and the time bandwidth decreases while the frequency bandwidth increases.

As it follows again by it's definition, the Q factor affects the edge effects. The higher the Q, the more significant the edge effect become, thus the cone of influence becomes larger, as illustrated in the next example.
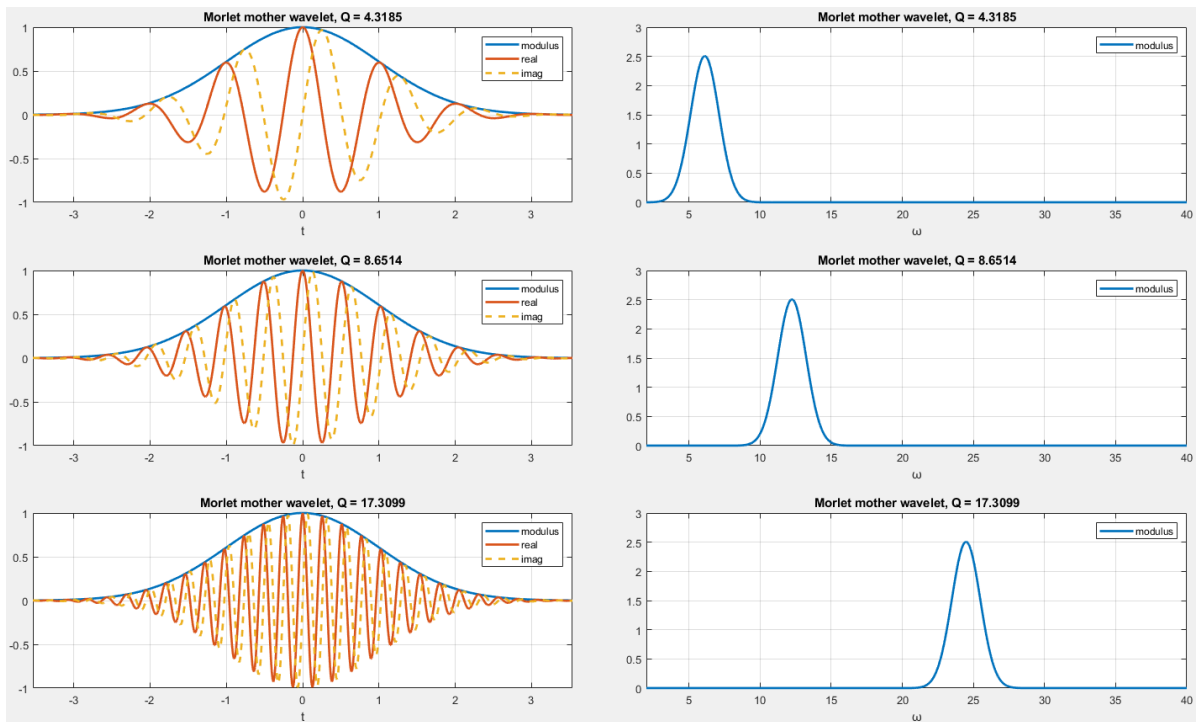
Figure 3.20: Example of the effect of Q factor on a Morlet wavelet.
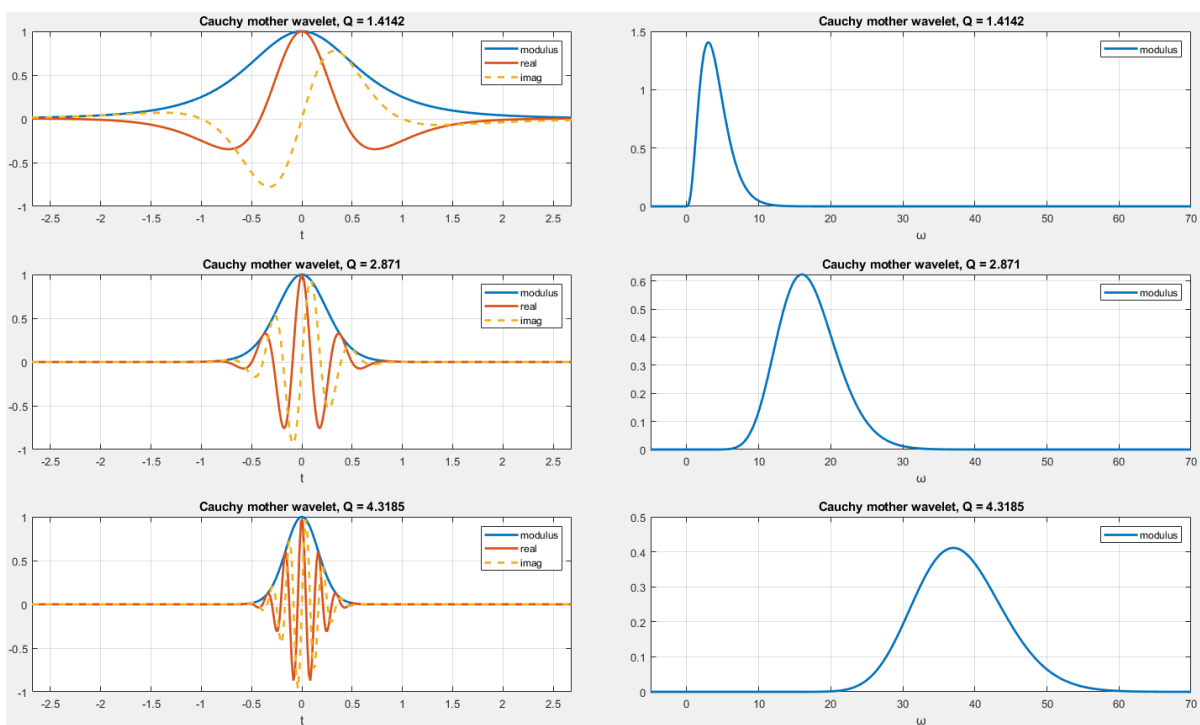
Figure 3.21: Example of the effect of Q factor on a Cauchy wavelet.

69

Example 3.13 (Q and edge effects). Continuing the example 3.11, to implement the factor Q. As it was mentioned, the four equations which delimit the useful domain D are:

$$
\begin{cases}
\omega_1 = \dfrac{\omega_\psi}{b} c_t \Delta t_\psi \\[2em]
\omega_2 = \dfrac{\omega_\psi}{L-b} c_t \Delta t_\psi \\[2em]
\omega_3 = 0 \\[2em]
\omega_4 = \dfrac{2\pi f_{Nyquist}}{1 + c_f \frac{\Delta\omega_\psi}{\omega_\psi}}
\end{cases}
$$

Setting $Q = \dfrac{\omega_\psi}{2\Delta\omega_\psi}$ and $\mu_\psi = \Delta\omega_\psi \Delta t_\psi$, follows that $\omega_\psi \Delta t_\psi = 2Q\mu_\psi$.

Additionally, now, $\dfrac{\Delta\omega_\psi}{\omega_\psi} = \dfrac{1}{2Q}$, thus the previous equations become:

$$
\begin{cases}
\omega_1 = \dfrac{1}{b} 2 c_t Q \mu_\psi \\[2em]
\omega_2 = \dfrac{1}{L-b} 2 c_t Q \mu_\psi \\[2em]
\omega_3 = 0 \\[2em]
\omega_4 = \dfrac{2\pi f_{Nyquist}}{1 + c_f \frac{1}{2Q}}
\end{cases}
$$

This useful domain D will be used for the modal identification procedure. Implementing these equations in MATLAB, the influence of Q can be observed: Consider the signal $u(t)$ is the free response of a SDOF system with :

mass $m = 1$ kg, damping ratio $\xi = 2\%$,

initial conditions: u(0) = 0.5 m and $\dot{u}(0) = 0$ m/s,

length of the signal is L = 10 s and the sampling period dt = 0.01 s.

Two cases are presented: the first considers $Q = 2.871$, while the second $Q = 8.6514$. Figure 3.22 illustrates the CWT modulus scalogram of the two cases, zoomed by 2 to show clearly the edge effect. It can be observed that when the Q value increases, the edge effect become more significant, thus the useful time interval for modal identification is reduced.
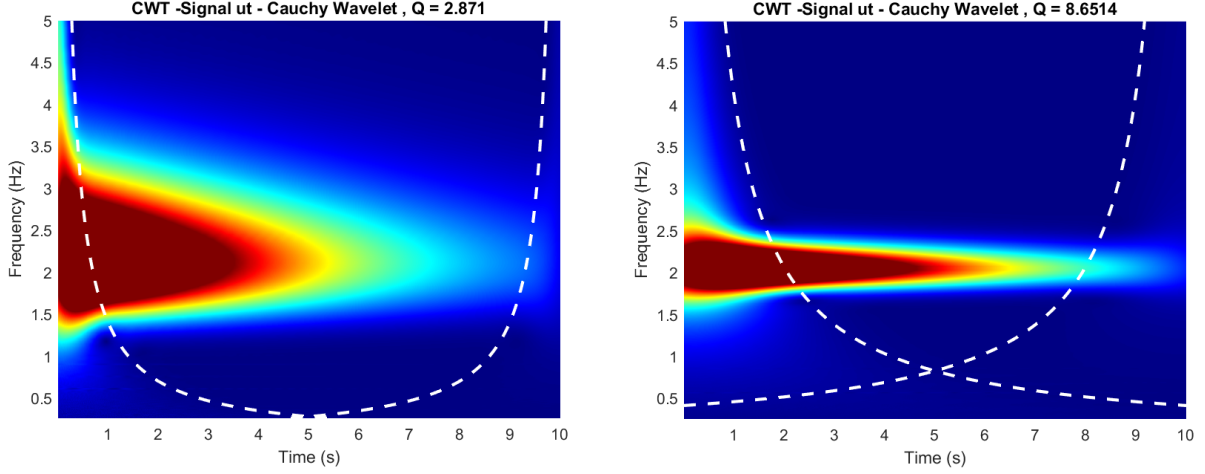
Figure 3.22: Example of the effect of Q factor on the edge effect.

The Q factor value has also another significant property, it can be used to correctly extract two close ridges corresponding to two coupled modes, which is of great importance in the modal parameter identification of MDOF systems. Continuing with the method proposed by Le and Argoul [13], the problem is set as: ω_j the angular eigenfrequency and $d\omega_j$ the frequency discrepancy from which the effect of the modal coupling must be avoided. In order to solve this problem, the frequency localization domain of the CWT along a ridge, as modified to take into account the edge effects in relation 3.66 is assumed to be included into a bandwidth $[\omega_j - d\omega_j, \omega_j + d\omega_j]$ This leads to bounding the Q as:

$$Q \geq c_f \frac{\omega_j}{2d\omega_j} \tag{3.70}$$

Let $d\omega_j = min[(\omega_j - \omega_{j-1}), (\omega_{j+1} - \omega_j)]$ for $1 \leq j \leq N$ with $\omega_0 = 0$, $\omega_{N+1} = 2\pi f_{Nyquist}$.

Consequently, the edge effect delimiting inequality

$$0 \leq \omega_j \leq \frac{2\pi f_{Nyquist}}{1 + c_f \frac{1}{2Q}} \tag{3.71}$$

is immediately checked, since $d\omega_j < \pi f_{Nyquist}$. Then, the edge effect delimiting inequality

$$\frac{1}{\omega_j} 2c_t Q\mu_\psi \leq b_j \leq L - \frac{1}{\omega_j} 2c_t Q\mu_\psi \tag{3.72}$$

combined with the Heisenberg's inequality gives:

$$Q \leq \frac{L\omega_j}{2c_t} \tag{3.73}$$

Concluding, the parameter Q can be bounded as:

$$c_f \frac{\omega_j}{2d\omega_j} \leq Q \leq \frac{L\omega_j}{2c_t} \tag{3.74}$$

71

Where L is the signal's length and the contained ω_js in a signal can be obtained by applying FFT, then classified in an increasing order. Finally, c_t and c_f must fulfill the following inequality:

$$c_t c_f \leq L d\omega_j \tag{3.75}$$

Le and Argoul prospose to start with $c_t = c_f = 5$. When the inequality 3.75 is not satisfied, c_t and c_f should be reduced until it becomes true. Then the value of Q can be chosen between the limits posed in 3.74.

Example 3.14 (Q, mode decoupling and edge effects)**.** Consider the signal $u_k(t)$ is the free response of a dof k, of a MDOF system with 4 dofs:
masses $m_1 = m_2 = m_3 = m_4 = 1$ kg, natural periods $T_1 = 0.2509sec, T_2 = 0.0880sec, T_3 = 0.0570sec, T_4 = 0.0465sec$, stiffness $k_1 = k_2 = k_3 = k_4 = 5$ kN/m
initial conditions: $[u_1(0) = 1, u_2(0) = 0.75, u_3(0) = 0.50, u_4(0) = 0.25]^T m$,
length of the signal is $L = 5s$ and the sampling period dt $= 0.005$ sec.
Two cases are presented: the first considers $Q = 8$, while the second $Q = 30$. Figure 3.23 illustrates the CWT modulus scalogram of the two cases, zoomed by 2. It can be observed that when the $Q = 8$ the two higher modes (3 and 4) are coupled (not distinguishable). Setting $Q = 8$, the cone of influence increases, but the two previously coupled modes now are decoupled and clearly distinguishable.
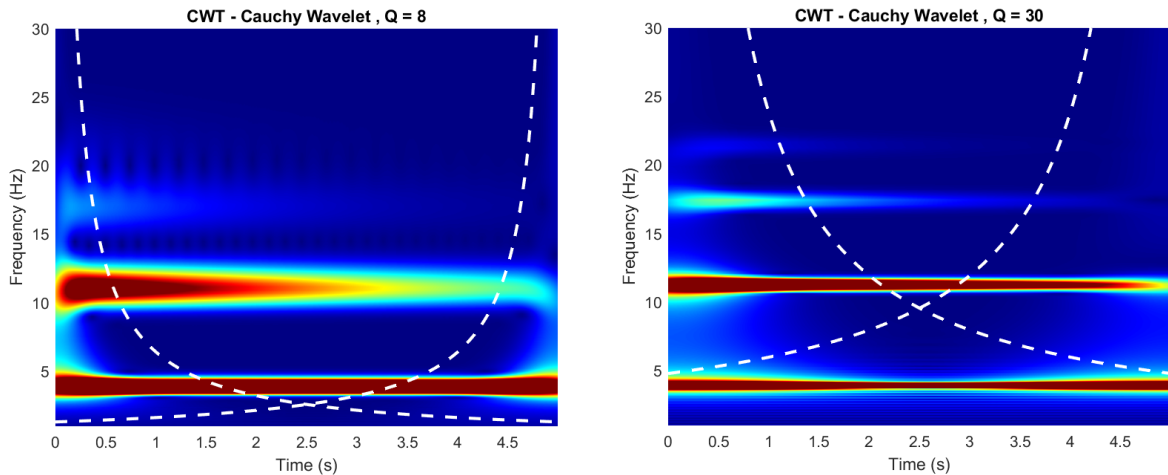
Figure 3.23: Example of the effect of Q factor on mode decoupling.

3.3.9 *Numerical implementation of the Continuous Wavelet Transform*

The CWT computation can be performed by different algorithms: quadrature rule, fast Fourier transform (FFT) with or without zero padding, convolution product and the chirp Z transform. These algorithms are based on different expressions of the definition of the CWT [14]. In the following, two algorithms are presented for numerical implementation in MATLAB, plus the CWT computation of the MATLAB built in cwt command.

- *Computation as a convolution product*

Based on the remark 3.1, the CWT can be defined as:

$$T_\psi[u](b,a) = \frac{1}{a} \int_{-\infty}^{+\infty} u(t)\overline{\psi}\left(-\frac{b-t}{a}\right) dt \qquad (3.76)$$

Setting a parity operator: $P{:}s \longmapsto P$ such that $(Ps)(t) = s(-t)$, then the restriction of $T_\psi[u](.,a)$ is the convolution product of $u(t)$ with $P\overline{\psi}_a$:

$$T_\psi[u](b,a) = \frac{1}{a}[u * P\overline{\psi}_a(b)] \qquad (3.77)$$

This remark leads us to the use of the convolution algorithm conv available in MATLAB. The algorithm as it is proposed by [14] is shown in figure 3.24. For the test of a simple cosine signal, this procedure needs 4.34 seconds of calculation [14].

- *Calculation via FFT*

Equation 3.37, suggests that the CWT can be computed with the inverse Fourier transform. This remark provides the opportunity to use the FFT on the algorithm, thus making the analysis much faster than the one using the convolution. Using the the fft and ifft commands of MATLAB, the algorithm it is proposed by [14] is shown in figure 3.25. The computation time of the previous test is only 0.3 seconds.[14].

3.3.10 *Implementation in MATLAB*

MATLAB Wavelet Toolbox has it's own built in cwt command, which employs a discretized version of the CWT and computes the coefficients as a convolution product with conv.

There are two versions of cwt, a new one and the old one, their main difference is in the normalization used for the mother wavelets. Their basic differences are presented in table 3.2. Throughout this thesis, both the new and the old command are used for the examples, each is stated in the example description. However, for the numerical applications of Chapter 6 are implemented with the old cwt command because it allows the definition of user defined mother wavelets. The new command provides only the choice of Morse, Morlet(Gabor), and Bump mother wavelets with parameter tuning allowed only in the Morse wavelets. However, the focus of this thesis is on the complex Morlet wavelet and the Cauchy wavelet and the definition of their parameters with the Q factor. Attempts where made to tune Morse wavelets accordingly to fit the desired mother wavelets for given values of Q, but no successful correspondence was achieved.

Continuing with the old cwt command, as it was referred in the section of Scaling, there is a conflict between the scales as defined in the theory, with the scales calculated in the built in command. This was addressed here because it was distorting the results of the analytic signal. This was solved by setting the scales a equal to aDT on the convolution computation line (DT is the sampling period).
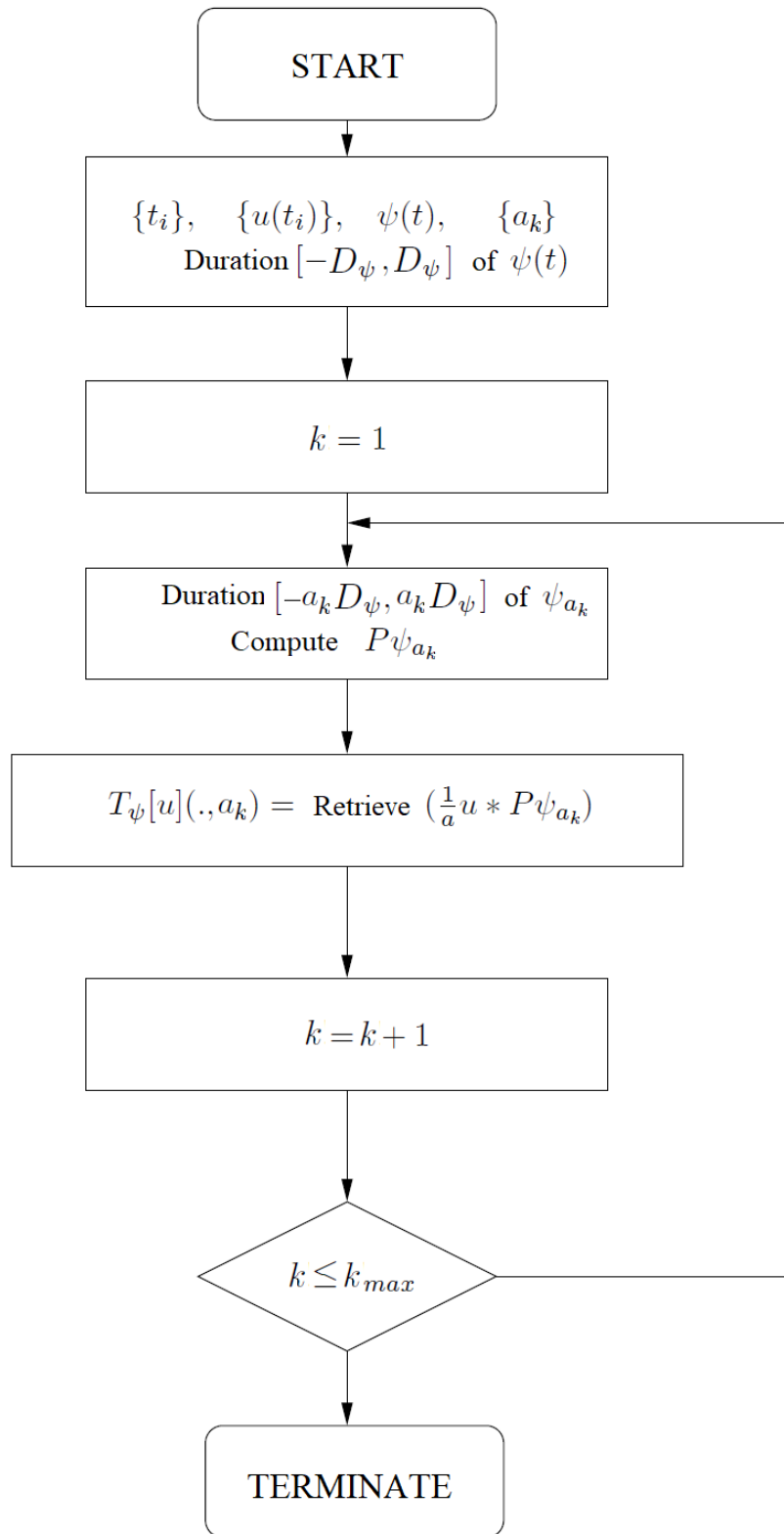
Figure 3.24: Algorithm for the computation of CWT as a convolution product.
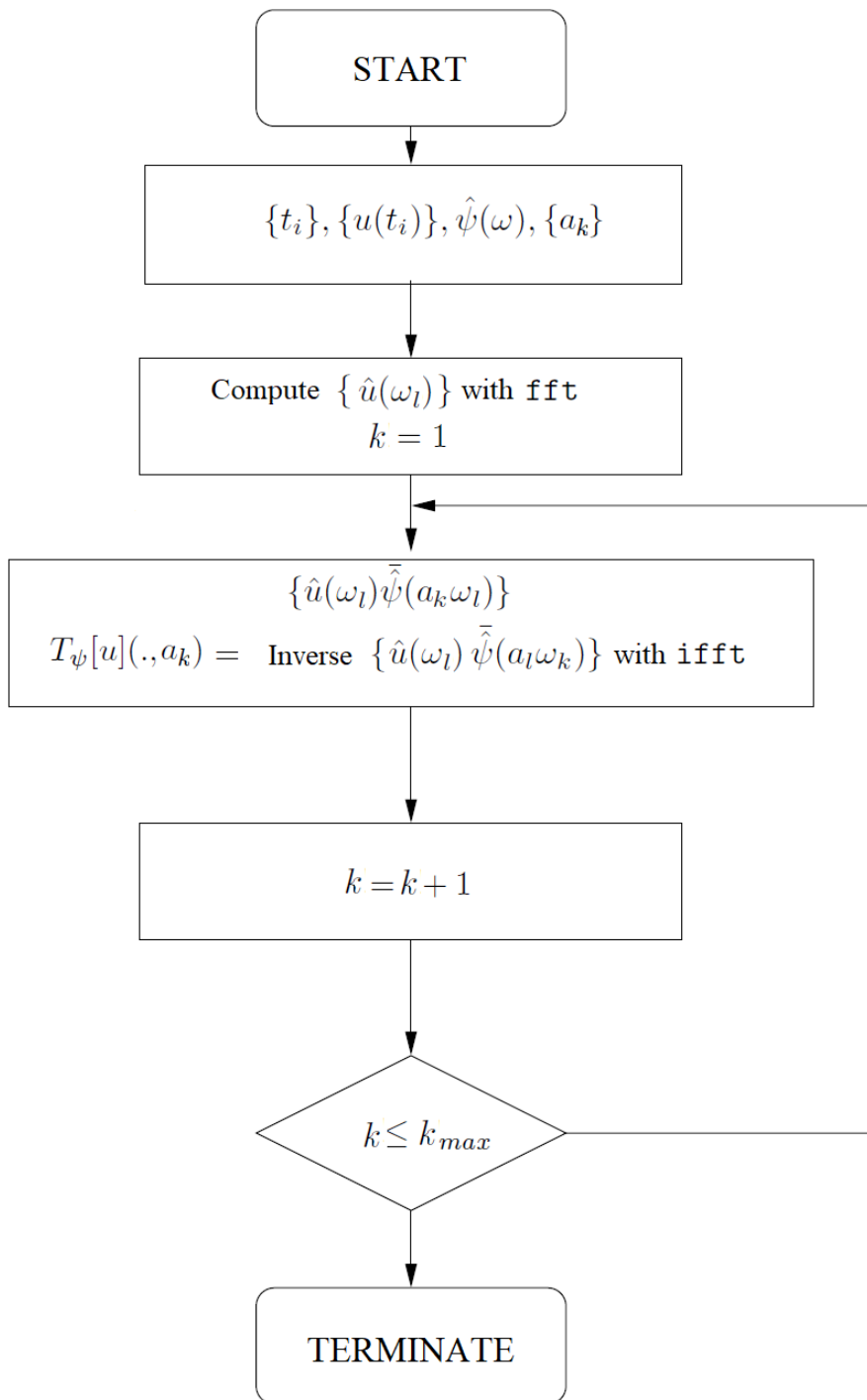
Figure 3.25: Algorithm for the computation of CWT with the FFT.

Table 3.2: MATLAB old vs. new cwt command

Old cwt	New cwt
Mother wavelets : wavelets within the toolbox, allows to add user defined wavelets.	Mother wavelets : only Morse, Morlet (Gabor), and Bump wavelet.
Allows parameter tuning of wavelets.	Allows parameter tuning only for Morse wavelets.
Uses L^2 normalization	Uses L^1 normalization
Is specified by user defined scales	Is specified by the sampling frequency Fs
Returns the frequencies f	Returns the frequencies f
Does not return the cone of influence	Returns the cone of influence

Listing 3.6: MATLAB old CWT correction for scales

```
1  for k = 1:nb_SCALES
2      a = scales(k);
3      a_SIG = a/stepSIG;
4      j = 1+floor((0:a_SIG*xMaxWAV)/(a_SIG*stepWAV));
5      if length(j)==1 , j = [1 1]; end
6      f          = fliplr(val_WAV(j));
7      coefs(ind,:) = -sqrt(a*DT)*wkeep1(diff(wconv1(ySIG,f)),lenSIG);
8      ind        = ind+1;
9  end
```

Another important remark is the addition of user mother wavelets, which is described in the following script for a Cauchy wavelet.

Listing 3.7: Adding user mother wavelets

```
1  % Specify the Cauchy wavelet
2  % n
3  n = round(2*Q^2 - 1/2);    % n is an integer > 0
4
5  % Mother wavelet parameters
6  Dt_psi = 1/sqrt(2*n-1);              % duration
7  Dtw = 6*Dt_psi;
8  omega_psi = n+1/2;                   % center frequency
9  m1=ceil(60*omega_psi);               % sample rate 60 points per
        oscilation
10 t1 = linspace(-Dtw,Dtw,m1);          % time interval to calculate t
        values
```

```matlab
11
12  % mother wavelet
13  m_w_cauchy=(1i./(t1+1i)).^(n+1);        % Le-Argoul paper equation
14
15  % plot the cauchy wavelet
16  figure()
17  hold on; grid on; box on;
18  plot(t1,abs(m_w_cauchy),'-','LineWidth',2)
19  plot(t1,real(m_w_cauchy),'-','LineWidth',2)
20  plot(t1,imag(m_w_cauchy),'--','LineWidth',2)
21  legend('modulus','real','imag')
22  title(['Cauchy mother wavelet , Q = ' num2str(Q)])
23
24  % Adding a wavelet
25  % familyName      = 'Cauchy';    Can be whatever name
26  % familyShortName = 'cchy';        The number of characters must be <= 4
27  % familyWaveType  = 5;
28  % Wavelet family type, specified as one of the following:
29  % 1  Orthogonal wavelets
30  % 2  Biorthogonal wavelets
31  % 3  Wavelet with a scaling function
32  % 4  Wavelet without a scaling function
33  % 5  Complex wavelet without a scaling function :
34  % Complex wavelets without FIR filter and without scale function.
35  % These wavelets can be defined through the definition of the wavelet
       function.
36  % Same applies for type 4.
37  % familyNums      = '';  % If the family consists of a single wavelet,
       NUMS is the empty string ''
38  % fileWaveName    = 'Cauchy.mat';
39  % effective support : is valid only for wavelets of type 3, 4, and 5.
40  % It represents the time interval where the wavelet is non zero.
41
42  X=linspace(-Dtw,Dtw,length(m_w_cauchy));
43  Y=m_w_cauchy ;
44  save('Cauchy.mat','X','Y')
45
46  % wavemngr('add',familyName,familyShortName,familyWaveType,familyNums,
       ...
47              ...fileWaveName,effectiveSupport)
48   wavemngr('add','Cauchy','cchy',5,'','Cauchy.mat',[-Dtw Dtw])
```

Chapter 4

Instantaneous frequency identification using the CWT

As referred in Chapter 3, if the Fourier transform of a mother wavelet $\psi(t)$ is sharply concentrated near a fixed value $\omega = \omega_j$ of frequency, the continuous wavelet transform tends to "concentrate" near a series of curves in the time-frequency domain, called the ridges of the transform. The ridge, let it be referred to as $a_r(b)$, has an interesting property: it describes the frequency modulation law of the signal. This property can be utilized to extract important features of the original signal which can be associated with the modal parameters of the s.d.o.f or m.d.o.f system under study, as will be described in this chapter.

4.1 Ridge estimation methods

There are several algorithms developed for the detection of ridges, depending on what problem they are called to solve: signals with a unique component or several components, pure or noisy signals. These algorithms can be classified into two categories, the "Integral" methods and the "Differential" methods. Integral methods are more stable than differential ones, consequently they are preferred in cases where significant noise is present within the signal, whereas differential methods are usually applied to pure signals where the noise component is relatively small in the regions occupied by the ridges.

"Differential" methods are based on a local analysis either of the extrema of the modulus of the CWT or the search for the points (b,a) -scale a and time point b- where the instantaneous frequency of the signal is equal to the frequency of the scaled mother wavelet. Two such methods reviewed in this thesis are:

- **The "Simple" method**, which uses the modulus of the CWT:

This method is based on CWT's modulus scalogram to extract a cross-section parallel to the scale (or frequency) axis of the plot, for a fixed value of the time variable b.

In the simple case where the signal is monocomponent, it possesses a unique ridge (see figure 4.1), so an estimation of the ridge is obtained by looking for the global maxima in the scale variable:

$$|T_\psi[u](b, a_r(b))| = \max_a |T_\psi[u](b, a)| \qquad (4.1)$$

In the case of multicomponent signals, more than one ridge are present - one for each mode - (see figure 4.2); therefore the estimation of each ridge focuses on local maxima, still with respect to the scale variable:

$$\frac{\partial |T_\psi[u](b, a_r(b))|}{\partial a} = 0 \qquad (4.2)$$
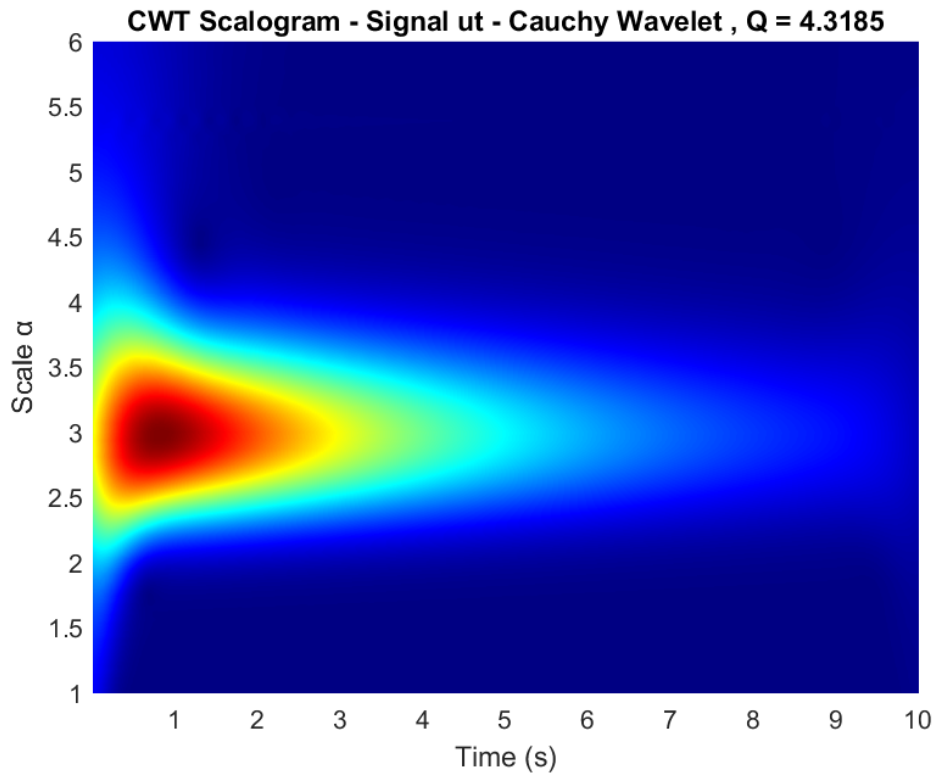
Figure 4.1: Example: Modulus scalogram of $T_\psi[u](b, a)$ in the case of a s.d.o.f. system. The ridge, defined as $a_r(b) = \frac{\dot\varphi(0)}{\omega_u(b)}$, is unique and it can be estimated by looking for the *global* maxima in the scale variable
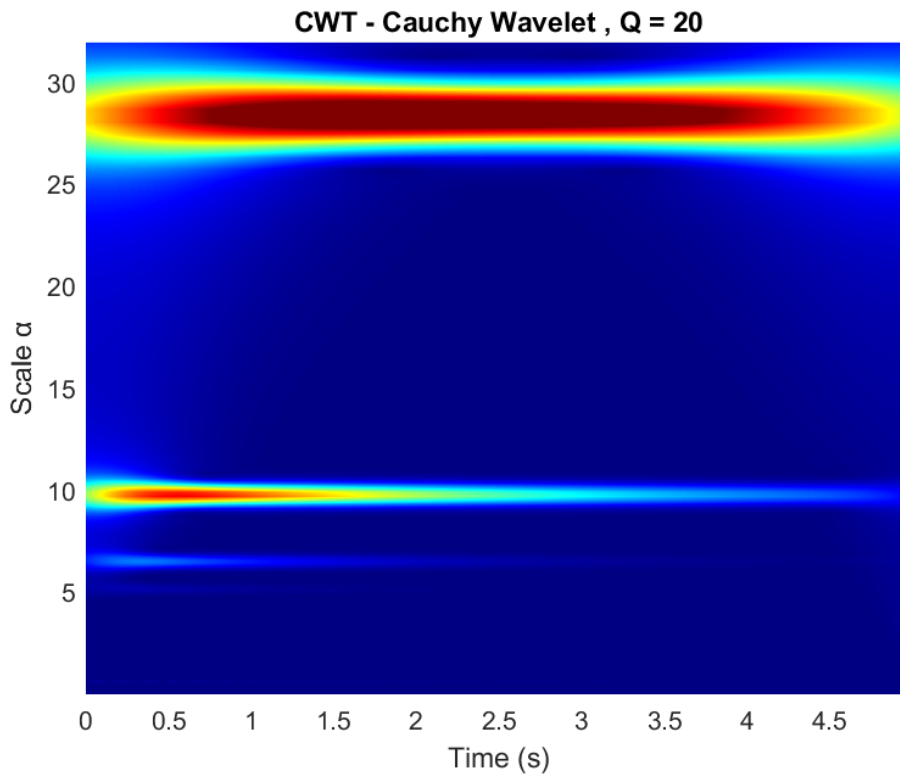
Figure 4.2: Example: Modulus scalogram of $T_\psi[u](b, a)$ in the case of a m.d.o.f. system (here a 4 d.o.f. system). Each ridge corresponds to a mode of the m.d.o.f. system. The ridges, defined as $a_r(b) = \frac{\dot\varphi(0)}{\omega_u(b)}$, are estimated for each mode by looking for *local* maximas in the scale variable

However, the Simple method turns out to be unstable in the presence of noise; the noise creates additional local maxima, and to determine the ridge, one has to discriminate between the local maxima which come from a "true" ridge and those that are noise artifacts [2].

- **The "Marseille" method**, which uses the phase of the CWT:

This method is based on the definition of the ridges, as the place where the frequency of the scaled mother wavelet is equal to the instantaneous frequency of the signal; therefore it can be calculated as the first derivative of the CWT's phase with respect to time:

$$\frac{\partial \angle(T_\psi[u](b, a_r(b)))}{\partial b} \approx \omega_u(b) \tag{4.3}$$

Graphically the first derivative of a function provides the slope of a tangent line to the function's graph at any instant. Utilizing this property, equation 4.3 can be interpreted (and easily calculated) as the slope of the phase-time data extracted from the phase plot of the CWT on the time-frequency plane, at the wavelet's ridge, see figure 4.3.
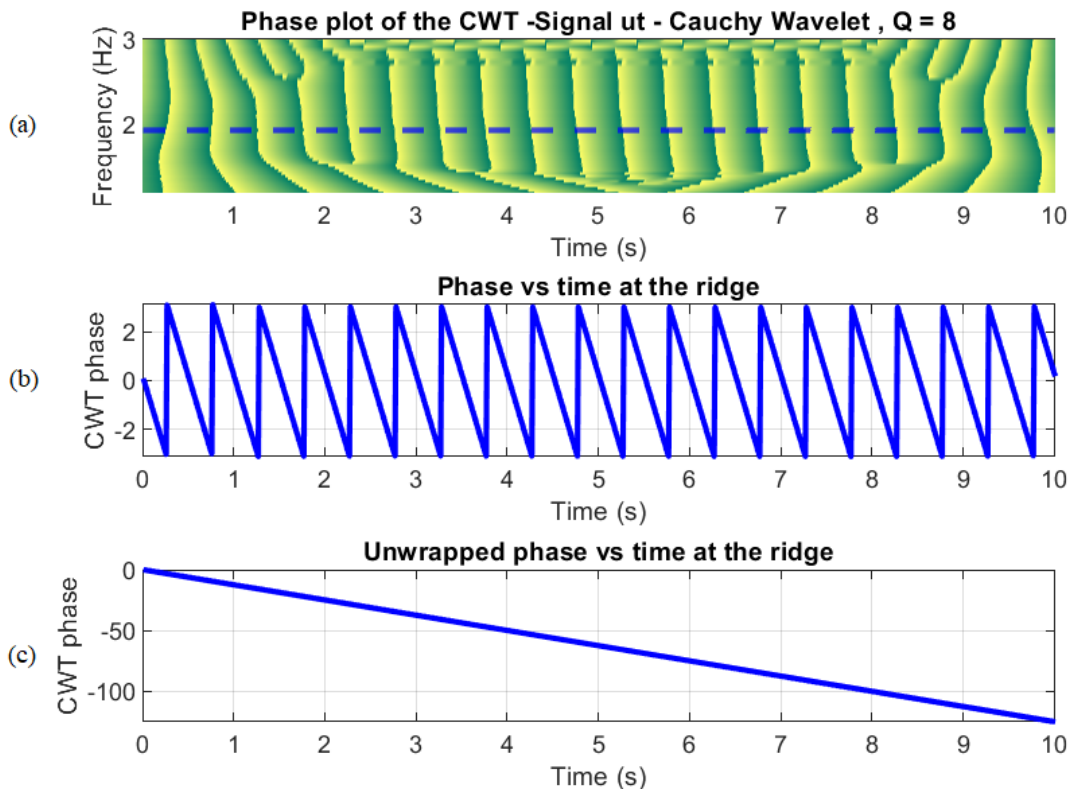
Figure 4.3: Example: (a) Phase plot of $T_\psi[u](b, a)$ on the time-frequency plane, (b) Phase-time plot on the ridge, (c) Unwrapped phase-time plot on the ridge: The slope of the phase of $T_\psi[u](b, a)$, equal to $\frac{\partial \angle(T_\psi[u](b, a_r(b)))}{\partial b}$ is the instantaneous frequency $\omega_u(b)$.

In *"Integral"* methods, ridges are considered as smooth and slowly varying functions where the energy has a tendency to localize in the time–frequency map. An appropriate penalty function is introduced on the set of possible ridges, and it estimates the ridge as the one that minimizes the penalty. There are various techniques that can be used to minimize the penalty function, for example the simulated annealing algorithm. Examples of integral methods are the "Corona" method and the "Crazy Climbers" method. However, integral methods have drawbacks too: when abrupt changes of parameters – such as natural frequency of time-variant systems – are involved, detection of time instant for which these changes appear is not a trivial task and often impossible [50].

4.2 Canonical representation of a real signal

Physical signals $u(t)$ obtained from vibration measurement are real valued and in the time domain. Following the concepts presented in Chapter 2 and since by definition the instantaneous angular frequency is the derivative of phase with respect to time (see equation 4.3), there is a need for the signal to be expressed by canonical representation.

An arbitrary real monocomponent signal $u(t)$ can always be represented in terms of instantaneous modulus $A_u(t)$ and instantaneous phase $\varphi_u(t)$, in the form :

$$u(t) = A_u(t) \cos\left[\varphi_u(t)\right] \tag{4.4}$$

where $A_u(t) \geq 0$ and $\varphi_u(t) \in [0, 2\pi)$.

Multicomponent signals then may be expressed canonically as the sum of two or more monocomponent signals:

$$u(t) = \sum_{j=1}^{N} A_u(t) \cos\left[\varphi_u(t)\right] \tag{4.5}$$

As referred in section 3.3.8, choosing an appropriate value of Q allows to isolate coupled modes, therefore it can be assumed that multicomponent signals have components which do not interact. Consequently, the analysis can be restricted to a domain where the wavelet coefficients of all but one component are negligible, allowing to treat each component as a monocomponent signal (which is one of the advantages of employing a time-frequency analysis). That being the case, the following theory focuses on monocomponent signals.

Continuing with equation 4.4, differentiating the phase $\varphi_u(t)$ with respect to time gives the instantaneous angular frequency:

$$\omega_u(t) = \frac{d\varphi_u(t)}{dt} = \dot{\varphi}_u(t) \tag{4.6}$$

However, there is a problem with this representation: the pair of $[A_u(t), \varphi_u(t)]$ is far from unique since there are infinite such pairs that can be associated with the real signal $u(t)$. This obstacle can be overcome with the use of the Hilbert Transform, which can be utilized as described in the following two sub-chapters.

4.3 Hilbert Transform

The Hilbert transform of u can be considered as the convolution of the function (or signal) $u(t)$ with the function $h(t) = \frac{1}{\pi t}$, known as the Cauchy kernel. Because $\frac{1}{t}$ is not integrable across $t = 0$, the integral defining the convolution does not always converge. Therefore, the Hilbert transform is given by:

$$H_u(t) = u(t) * \frac{1}{\pi t}$$

$$= \frac{1}{\pi} \; p.v. \int_{-\infty}^{+\infty} \frac{u(\tau)}{t - \tau} d\tau \quad , \quad t \in \mathbb{R} \tag{4.7}$$

where p.v.[·] denotes the Cauchy principal value of the improper integral (i.e., to account for the $t = \tau$ situation).

In the frequency domain, the Hilbert transform has a very useful form:

$$\widehat{H}_u(\omega) = -i sgn(\omega) \widehat{u}(\omega) \quad , \quad \omega \in \mathbb{R} \tag{4.8}$$

where $sgn(\omega)$ is the sign function of a real number.

4.4 Analytic Signals and Instantaneous Frequency

An analytic signal is defined as a complex-valued function that has no negative frequency components, therefore, the analytic signal $Z_u(t)$ associated with a real-valued signal of finite energy $u(t)$ is obtained by a linear filtering of $u(t)$ canceling its negative frequencies. By using the Hilbert transform, $Z_u(t)$ can be defined (up to a factor 2) as $u(t)$ signal's orthogonal projection onto the subspace $H^2(\mathbb{R})$ of $L^2(\mathbb{R})$:

$$Z_u(t) = u(t) + i H_u(t) \tag{4.9}$$

Note that $Re[Z_u(t)] = u(t)$. It should be mentioned also that, although an analytic signal contains no negative frequencies, it may have a spectral component at zero frequency. Considering the previous sub-chapter's observation, the Fourier Transform of an analytic signal is given by:

$$\widehat{Z}_u(\omega) = \widehat{u}(\omega) + i\widehat{H}_u(\omega)$$

$$\stackrel{eq.4.8}{=} \widehat{u}(\omega) - i^2 sgn(\omega) \widehat{u}(\omega)$$

$$= \widehat{u}(\omega) + sgn(\omega) \widehat{u}(\omega)$$

$$= \begin{cases} 2\widehat{u}(\omega), & \text{if } \omega \geq 0. \\ 0, & \text{if } \omega < 0. \end{cases}$$

$$= 2\widehat{u}(\omega)\Theta(\omega) \tag{4.10}$$

where $\Theta(\omega)$ denotes the Heaviside step function.

By definition, $Z_u(t)$ is an analytic function in the upper half complex plane (hence the term analytic). If one assumes a pair $[A_u(t), \varphi_u(t)]$, where $A_u(t) = |Z_u(t)| \geq 0$ and $\varphi_u(t) = \angle[Z_u(t)] \in [0, 2\pi)$, the function $Z_u(t)$ has a unique polar coordinate representation:

$$Z_u(t) = A_u(t)e^{i\varphi_u(t)} \tag{4.11}$$

where

$$A_u(t) = |Z_u(t)| = \sqrt{\left[Re(Z_u(t))\right]^2 + \left[Im(Z_u(t))\right]^2} \tag{4.12}$$

and

$$\varphi_u(t) = \angle(Z_u(t)) = \arctan\left(\frac{Im(Z_u(t))}{Re(Z_u(t))}\right) \tag{4.13}$$

Applying this canonical pair $[A_u(t), \varphi_u(t)]$ to equation 4.4, a unique representation of the form can be determined and it is defined as the canonical representation of a real signal.

The instantaneous angular frequency then can be defined by setting $\varphi_u(t) = \angle[Z_u(t)]$ in equation 4.6 as:

$$\omega_u(t) = \frac{d\varphi_u(t)}{dt} = \frac{d\angle(Z_u(t))}{dt} \tag{4.14}$$

Remark 4.1. This is the most direct method for determination of instantaneous frequency, and is easy to implement. However it is important to note that although this definition of the instantaneous frequency is always valid mathematically, its physical meaning can be doubtful in some particular situations, especially when the signal $u(t)$ is not oscillating enough, i.e. when $\varphi_u(t)$ varies slowly compared to $A_u(t)$, or when the frequency $\omega_u(t)$ itself has fast variations [2],[33].

4.5 Asymptotic Signals

For some real finite energy signals $u(t) \in L^2(\mathbb{R})$ that have the form $u(t) = A_u(t)\cos[\varphi_u(t)]$ with $A_u(t) \geq 0$ and $\varphi_u(t) \in [0, 2\pi)$, the associated analytic signal is approximated as:

$$Z_u(t) \approx A_u(t)e^{i\varphi_u(t)} \tag{4.15}$$

However this is not the case in general, but only for signals that are considered oscillatory enough. Those signals for which this statement is true are called *asymptotic signals*. Oscillatory enough means that the variations of $u(t)$ coming from the phase term $\cos[\varphi_u(t)]$ (i.e. change of phase) are much faster than the variations coming from the amplitude

$A_u(t)$ (i.e. amplitude modulation) [7]:

$$\left|\frac{d\varphi_u(t)}{dt}\right| \gg \left|\frac{1}{A_u(t)}\frac{dA_u(t)}{dt}\right| \tag{4.16}$$

This definition of asymptotic signals derives from the following lemma as taken from [2]:

Lemma 4.1. Let $u(t) \in L^2(\mathbb{R})$ be of the form $u(t) = A_u(t)\cos\left[\lambda\varphi_u(t)\right]$, where$\lambda \gg 1$ (i.e. large positive number), and $A_u(t) \in C_2(\mathbb{R})$ (space of twice continuously differentiable functions) and $\varphi_u(t) \in C_4(\mathbb{R})$ (space of four times continuously differentiable functions). Then, as $\lambda \to \infty$, the analytic signal associated with $u(t)$ is:

$$Z_u(t) = A_u(t)e^{i\lambda\varphi_u(t)} + O(\lambda^{-\frac{3}{2}}) \tag{4.17}$$

4.6 CWT of Asymptotic Signals - Method of Stationary Phase

Having expressed the asymptotic signal $u(t) = A_u(t)\cos\left[\varphi_u(t)\right]$ as it's associated analytic signal of the form $Z_u(t) \approx A_u(t)e^{i\varphi_u(t)}$, and assuming $\psi_{b,a}(t)$ to be a family of general progressive and asymptotic wavelets (progressive = a wavelet whose Fourier Transform is non-negative) of the form:

$$\psi(t) = A_\psi(t)e^{i\varphi_\psi(t)} \tag{4.18}$$

the CWT of $u(t)$ is then a Hardy function and will be expressed as:

$$T_\psi[u](b,a) = \langle u, \psi_{b,a}\rangle$$

$$= \frac{1}{a}\int_{-\infty}^{+\infty} u(t)\overline{\psi}\left(\frac{t-b}{a}\right)dt$$

$$= \frac{1}{2a}\int_{-\infty}^{+\infty} Z_u(t)\overline{\psi}\left(\frac{t-b}{a}\right)dt$$

$$= \frac{1}{2}T_\psi[Z_u](b,a) \tag{4.19}$$

Substituting equations 4.15, 4.18 into 4.19 gives:

$$T_\psi[u](b,a) = \frac{1}{2a}\int_{-\infty}^{+\infty} A_u(t)A_\psi\left(\frac{t-b}{a}\right)e^{i\left[\varphi_u(t)-\varphi_\psi\left(\frac{t-b}{a}\right)\right]}$$

$$= \frac{1}{2a}\int_{-\infty}^{+\infty} M_{b,a}(t)e^{i\Phi_{b,a}(t)}dt \tag{4.20}$$

where

$$M_{b,a}(t) = A_u(t)A_\psi\left(\frac{t-b}{a}\right) \tag{4.21}$$

and

$$\Phi_{b,a}(t) = \left[\varphi_u(t) - \varphi_\psi\left(\frac{t-b}{a}\right)\right] \tag{4.22}$$

If both the signal $u(t)$ and wavelet $\psi(t)$ are asymptotic, then the integrand in equation 4.20 is also asymptotic. Therefore the CWT integral of equation 4.20 is of the form:

$$I(\lambda) = \int_a^b A(t)e^{i\lambda\varphi(t)} \tag{4.23}$$

where $\lambda > 0$ is a large parameter and the function $A(x)$ is called the amplitude and the real-valued function $\varphi(x)$ is the phase, therefore I(λ) can be characterized as a generalized Fourier integral and the Method of Stationary Phase can be applied for its approximation.

Note. For equations 4.23 and 4.24, a and b symbolize the lower limit and the upper limit of the definite integral respectively and not the wavelet parameters.

4.6.1 *The method of stationary phase in 1-dimension*

Keeping in mind equation 4.23, some basic concepts and definitions of the method of stationary phase in 1-dimension are:

Definition 4.1 (Stationary points)**.** The endpoints of integration, i.e. places where the derivatives of $A(t)$ fail to be continuous, and places where the derivatives of $\varphi(t)$ vanish are called *critical points*. A simple critical point is a point $t = t_0$, where $\dot{\varphi}(t_0) = 0$ but $\ddot{\varphi}(t_0) \neq 0$. Such a simple critical point is also called a stationary point because this is the place where the phase function has a minimum or a maximum and is thus, stationary.

Theorem 4.1 (The Principal of Stationary Phase)**.** As $\lambda \to \infty$ (i.e. the integrand becomes very oscillatory) the dominant terms in the asymptotic expansion of $I(\lambda)$ arise from the immediate neighborhood of the end points and intermediate points at which $\lambda\varphi(t)$ is stationary.

The physical interpretation of this principle is as follows: When $\lambda \to \infty$ and $\lambda\dot{\varphi}(t_0) \neq 0$, then $\omega = \lambda\dot{\varphi}(t_0)$ is very large, which means that the signal is very oscillatory, so oscillatory that the amplitude $A(t)$ changes very little during one cycle and the integral in equation 4.23 evaluated over one cycle is zero. At points where $\varphi(t)$ is stationary, this cancellation does not occur. Consequently, only contributions from the stationary points and the boundary points add to the value of the integral.

Definition 4.2 (Stationary phase formula). For an interior stationary point $t = t_0$, where $a < t_0 < b$: If $A(t)e^{i\lambda\varphi(t)}$ has only one stationary point, $t = t_0$ (of first order), then the integral is estimated as:

$$\lim_{\lambda\to\infty} I(\lambda) = \lim_{\lambda\to\infty} \int_a^b A(t)e^{i\lambda\varphi(t)}dt$$

$$= \frac{\sqrt{2\pi}e^{isgn[\ddot{\varphi}(t_0)]\frac{\pi}{4}}}{\sqrt{\lambda|\ddot{\varphi}(t_0)|}} A(t_0)e^{i\lambda\varphi(t_0)} + O(\lambda^{-\frac{3}{2}}) \quad , \quad as \quad \lambda \to \infty \qquad (4.24)$$

4.6.2 *Application on the Continuous Wavelet Transform - "Marseille" Method*

Let $t = t_0$ be a stationary point of first order of the equation 4.20 integrand, i.e. such that:

$$\dot{\Phi}_{b,a}(t_0) = \left[\dot{\varphi}_u(t_0) - \frac{1}{a}\dot{\varphi}_\psi\left(\frac{t_0 - b}{a}\right)\right] = 0 \qquad (4.25)$$

and

$$\ddot{\Phi}_{b,a}(t_0) = \left[\ddot{\varphi}_u(t_0) - \frac{1}{a^2}\ddot{\varphi}_\psi\left(\frac{t_0 - b}{a}\right)\right] \neq 0 \qquad (4.26)$$

Applying the Method of Stationary Phase for the stationary point $t = t_0$ by substituting equation 4.20 to equation 4.24, $T_\psi[u](b,a)$ is approximated by :

$$T_\psi[u](b,a) \approx \frac{1}{2a} \frac{\sqrt{2\pi}e^{isgn[\ddot{\Phi}_{b,a}(t_0)]\frac{\pi}{4}}}{\sqrt{|\ddot{\Phi}_{b,a}(t_0)|}} M_{b,a}(t)e^{i\Phi_{b,a}(t)}$$

$$= \frac{1}{2a} \frac{\sqrt{2\pi}e^{isgn[\ddot{\Phi}_{b,a}(t_0)]\frac{\pi}{4}}}{\sqrt{|\ddot{\Phi}_{b,a}(t_0)|}} Z_u(t_0)\overline{\psi}\left(\frac{t_0 - b}{a}\right) \qquad (4.27)$$

which can be written as the value of the integrand of equation 4.19 at $t = t_0$ corrected by some factor, i.e.:

$$T_\psi[u](b,a) \approx \sqrt{\frac{\pi}{2}} \frac{Z_u(t_0)\overline{\psi}\left(\frac{t_0-b}{a}\right)}{corr(b,a)} \qquad (4.28)$$

where

$$corr(b,a) = a|\ddot{\Phi}_{b,a}(t_0)|^{1/2} \exp{-i(\pi/4)\operatorname{sgn}[\ddot{\Phi}_{b,a}(t_0)]} \qquad (4.29)$$

As it was presented in Chapter 3, with a proper choice of the parameter Q, mode decoupling can be achieved. Consequently, for multicomponent signals, any mode can be isolated and the modal identification procedure can be performed on the amplitude and phase of one component separately as it is for a monocomponent signal, allowing the anal-

ysis to be restricted to a domain where the wavelet coefficients of all but one component are negligible. Thus, it can be assumed that $t = t_0$ is a unique stationary point and that it is of first order.

- ***Ridge definition***

Focusing on the previously attained conclusions, the ridge $a_r(b)$ of the $T_\psi[u](b, a)$ now can be defined as the set of points (b, a) in the domain of the transform where the phase of $u(t)\overline{\psi}\left(\frac{t-b}{a}\right)$ is stationary, i.e. the points that satisfy $t_0(b, a) = b$.

Substituting $t_0 = b$, $a = a_r(b)$ and $\dot{\varphi}(t_0) = \omega_u(t_0) = \omega_u(b)$ in the stationary phase condition 4.25 gives:

$$\omega_u(b) = \frac{\dot{\varphi}_\psi(t_0)}{a_r(b)} \tag{4.30}$$

Consequently, once the ridge of the wavelet transform is determined, the *instantaneous frequency* can be determined easily from equation 4.1.

Example 4.1 (Instantaneous frequency for the complex Morlet wavelet and the Cauchy wavelet). Calculating the $\dot{\varphi}_\psi(t_0)$ for the complex Morlet wavelet and the Cauchy wavelet, utilized in this thesis:

For the Complex Morlet wavelet:

$$\psi(t) = e^{-t^2/(2\delta^2)} e^{i\beta t}$$

Thus, the wavelet's phase is equal to:

$$\varphi_\psi(t) = \beta t = \omega_\psi t,$$

$$\dot{\varphi}_\psi(t) = \omega_\psi$$

Therefore $\dot{\varphi}_\psi(0) = \omega_\psi$. Substituting in equation 4.1 gives for the Morlet wavelet:

$$\omega_u(b) = \frac{\omega_\psi}{a_r(b)}$$

For the Cauchy wavelet:

$$\psi(t) = \left(\frac{i}{t+i}\right)^{n+1} = \left(\frac{1}{\sqrt{t^2+1}}\right)^{n+1} e^{i(n+1)\arctan(t)}$$

Thus, the wavelet's phase is equal to:

$$\varphi_\psi(t) = (n+1)\arctan(t),$$

$$\dot{\varphi}_\psi(t) = \frac{n+1}{1+t^2}$$

Therefore $\dot{\varphi}_\psi(0) = n + 1$. Substituting in equation 4.1 gives for the Cauchy wavelet:

$$\omega_u(b) = \frac{n+1}{a_r(b)}$$

- ***Analytic signal from the skeleton of the CWT***

The skeleton of the $T_\psi[u](b, a)$ is the wavelet transform evaluated on the ridge, i.e. $T_\psi[u](b, a_r(b))$. The phase of the CWT $\Phi_{b,a}(t)$ on the ridge where $t_0 = b$, $a = a_r(b)$, (equation 4.22) then becomes:

$$\Phi_{b,a}(t) = [\varphi_u(t) - \varphi_\psi(0)] \tag{4.31}$$

where $\varphi_u(t)$ the phase of the analytic signal and $\varphi_\psi(0)$ the phase of the analyzing wavelet. Thus, if the equation of the analyzing wavelet is known, one can compute the *instantaneous phase* $\varphi_u(t)$ of the analytic signal on the ridge from the CWT.

Example 4.2 (Phase of the analytic signal for the complex Morlet wavelet and the Cauchy wavelet)**.** Consider from the previous example the phase of the Morlet and the Cauchy wavelet respectively:

$$\varphi_\psi(t) = \beta t = \omega_\psi t \quad \text{and} \quad \varphi_\psi(t) = (n+1)\arctan(t)$$

Therefore, for both the Morlet and the Cauchy wavelet: $\varphi_\psi(0) = 0$.
This leads to $\Phi_{b,a}(t) = \varphi_u(t) - 0 = \varphi_u(t)$. Consequently, when using the Morlet and the Cauchy wavelet the instantaneous phase of the analytic signal $\varphi_u(t)$ is equal to the phase of the CWT.

Continuing with the correction calculation, equation 4.32 implies that on the ridge where $t_0 = b$, $a = a_r(b)$:

$$T_\psi[u](b, a) \approx \sqrt{\frac{\pi}{2}} \frac{Z_u(b)\overline{\psi}(0)}{corr(b, a_r(b))} \tag{4.32}$$

Thus, one can conclude that the CWT on the ridge generally can be approximated as:

$$T_\psi[u](b, a_r(b)) \approx correction(b, a_r(b))Z_u(b) \tag{4.33}$$

which leads that the analytical signal on the ridge can be obtained by:

$$Z_u(b) \approx \frac{T_\psi[u](b, a_r(b))}{correction(b, a_r(b))} \tag{4.34}$$

The approximation of $T_\psi[u](b, a)$ by the equation 4.32 is the one followed by Carmona [2] and is of general sense. Focusing now on the $correction(b, a_r(b))$ calculation with wavelets that have constant frequency along the time axis, i.e. $\omega_\psi(t) = d\varphi_\psi(t)/dt = \dot{\varphi}_\psi(t) = constant$.
Therefore, $\ddot{\varphi}_\psi(t) = 0$ for all t. Applying this for $t = b$, $a = a_r(b)$, the ridge is defined as the

line $a = a_r(b)$. Consequently, ridges on the frequency axis can be represented in a Fourier line spectrum. Le-Argoul [13] employed this property and performed the approximate calculation of the CWT on the ridge as:

$$T_\psi[u](b, a_r(b)) \approx \frac{1}{2} Z_u(b) \widehat{\psi}\big(\dot\varphi_\psi(0)\big) \tag{4.35}$$

Thus, the analytic signal $Z_u(b)$ can be calculated from the skeleton of the CWT as:

$$Z_u(b) \approx \frac{2}{\widehat{\psi}(\dot\varphi_\psi(0))} T_\psi[u](b, a_r(b)) \tag{4.36}$$

with *instantaneous amplitude*:

$$A(b) = |Z_u(b)| \approx \left| \frac{2}{\widehat{\psi}(\dot\varphi_\psi(0))} T_\psi[u](b, a_r(b)) \right| \tag{4.37}$$

The correction term is equal to:

$$correction(b) = \frac{2}{\widehat{\psi}(\dot\varphi_\psi(0))} \tag{4.38}$$

and depends only on the ridge and on the analyzing wavelet.

Example 4.3 (Correction computation with the complex Morlet wavelet and the Cauchy wavelet). Continuing now the application for the Morlet and the Cauchy wavelet, the values of $\dot\varphi_\psi(0)$ where calculated in the previous example. The *correction*(b) then is:
For the Morlet wavelet with $\delta = 1$:

$$\widehat{\psi}(\omega) = \sqrt{2\pi} e^{-(\omega-\beta)^2/2}$$

As calculated, $\dot\varphi_\psi(0) = \beta$, thus the *correction*($b$) becomes:

$$correction(b) = \frac{2}{\widehat{\psi}(\dot\varphi_\psi(0))} = \frac{2}{\widehat{\psi}(\beta)} = \frac{2}{\sqrt{2\pi} e^{-(\beta-\beta)^2/2}} = \sqrt{\frac{2}{\pi}}$$

For the Cauchy wavelet:

$$\widehat{\psi}(\omega) = \frac{2\pi\omega^n e^{-\omega}}{n!}\Theta(\omega)$$

where $\Theta(\omega)$ is the Heaviside step function, but as $\psi(t)$ is progressive, $\Theta(\omega)$ can be ignored from the equation. As calculated, $\dot\varphi_\psi(0) = n + 1$, thus the *correction*($b$) becomes:

$$correction(b) = \frac{2}{\widehat{\psi}(\dot\varphi_\psi(0))} = \frac{2}{\widehat{\psi}(n+1)} = \frac{2}{\dfrac{2\pi(n+1)^n e^{-(n+1)}}{n!}} = \frac{n!}{\pi(n+1)^n e^{-(n+1)}}$$

However, for the Cauchy wavelet, the correction function contains a factorial (!), which

MATLAB does not calculate for large values of n, i.e. $(n > 140)$, but returns Inf. The problem is solved by handling large numbers using the natural logarithm and the gamma function that has the property: $\Gamma ln(n+1) = ln(n!)$ which can be implemented in MATLAB with the command gammaln(). Thus, the fraction is handled as follows:

$$\ln\big(correction(b)\big) = \ln\left(\frac{n!}{\pi(n+1)^n e^{-(n+1)}}\right)$$

$$= \ln(n!) - \big[\ln(\pi) + n\ln(n+1) - (n+1)\ln(e)\big]$$

$$= \ln(n!) - \ln(\pi) - n\ln(n+1) + (n+1)$$

$$= \Gamma ln(n+1) - \ln(\pi) - n\ln(n+1) + (n+1)$$

thus,

$$correction(b) = \exp\big[\Gamma ln(n+1) - \ln(\pi) - n\ln(n+1) + (n+1)\big]$$

In matlab the natural logarithm is called with the command log(). Validation test results:

Table 4.1: Large numbers handling validation test

n	factorial()	gammaln()
5	1.9817	1.9817
50	5.7074	5.7074
100	8.0253	8.0253
140	9.4800	9.4800
200	NaN	11.3167
1800 (Q=30)	NaN	33.8623

Listing 4.1: Handling the large factorials of the Cauchy wavelet

```
1  % set n value
2  n = 5
3
4  % Correction with natural logarithms
5  correction1 = exp(gammaln(n+1)-log(pi)-n*log(n+1)+(n+1))
6
7  % Correction as the original equation
8  correction2 = factorial(n)/(pi*exp(-(n+1))*(n+1)^n)
```

- *Ridge Estimation from the Phase of the Continuous Wavelet Transform*

As it was mentioned in the previous, the phase of the analytic signal can be obtained from the phase of the CWT. From equation 4.27, the phase of $T_\psi[u](b,a)$ is be defined as:

$$\angle\big(T_\psi[u](b,a)\big) = i\frac{\pi}{4}\,\mathrm{sgn}[\ddot{\Phi}_{b,a}(t_0)] + \Phi_{b,a}(t_0) \tag{4.39}$$

so, the derivatives of $\angle\big(T_\psi[u](b,a)\big)$ are essentially those of $\Phi_{b,a}(t_0)$.

Differentiation of equation 4.39 with respect to scale gives:

$$\frac{\partial\angle(T_\psi[u](b,a_r(b)))}{\partial a} = -\frac{t_0 - b}{a^2}\dot{\Phi}_{b,a}\left(\frac{t_0 - b}{a}\right) \tag{4.40}$$

on the intersection with the ridge, where $t_0 = b$:

$$\frac{\partial\angle(T_\psi[u](b,a_r(b)))}{\partial a} = 0 \tag{4.41}$$

Therefore, for a given time b, the ridge $a_r(b)$ can be found by iteration, as the fixed point of equation 4.41.

Similarly, differentiation of equation 4.39 with respect to b gives:

$$\frac{\partial\angle(T_\psi[u](b,a_r(b)))}{\partial b} = \frac{1}{a}\dot{\varphi}_\psi\left(\frac{t_0 - b}{a}\right) + \left[\frac{\partial a}{\partial b}\right]\frac{t_0 - b}{a^2}\dot{\varphi}_\psi\left(\frac{t_0 - b}{a}\right)$$

$$= \frac{\dot{\varphi}_\psi(0)}{a_r(b)} \tag{4.42}$$

the ridge $a_r(b)$ can be found by iteration, as the fixed point of equation 4.42.

Example 4.4 (Application for the Morlet and the Cauchy wavelet)**.** The fraction $\frac{\dot{\varphi}_\psi(0)}{a_r(b)}$ for the Morlet wavelet is equal to:

$$\frac{\partial\angle(T_\psi[u](b,a_r(b)))}{\partial b} = \frac{\omega_\psi}{a_r(b)}$$

and for the Cauchy wavelet is equal to:

$$\frac{\partial\angle(T_\psi[u](b,a_r(b)))}{\partial b} = \frac{n+1}{a_r(b)}$$

Example 4.5 (Illustration of the thought process of equation 4.41)**.** Consider a Cauchy wavelet with $Q = 8$. Employ the CWT of a monocomponent signal $u(t)$, find the ridge and plot a cross section of the modulus scalogram and a cross section of the phase diagram parallel to the scale axis. Compute the first derivative of the phase with respect to the scale a. Figure 4.4 shows the result where (a) is the cross section of the phase diagram parallel to the scale axis, (b) is the first derivative of the phase with respect to the scale

a and (c) is the cross section of the modulus scalogram parallel to the scale axis. As it can be observed, on the ridge $a_r(b) = 10.26$, there is a peak on (c), and on (b) the graph becomes a straight line equal to zero, confirming equation 4.41.
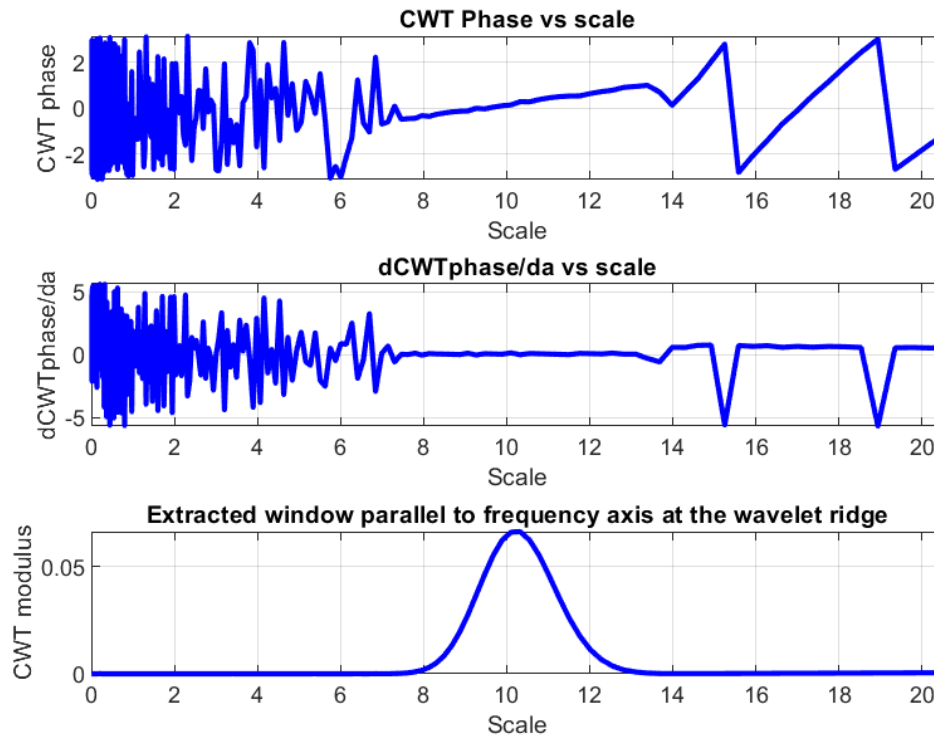

Figure 4.4: Example of the application of derivation of phase with respect to scale

4.7 Algorithms for the estimation of the instantaneous frequency

Once the ridge is determined, the instantaneous frequency can be calculated, from $\omega_b = \frac{\dot{\varphi}_\psi}{a_r(b)}$. Thus, the whole procedure is based on the identification of the ridge.

4.7.1 "Simple" method

This method is based on the heuristic that in a narrow time interval the energy of the signal is concentrated near its instantaneous frequency for that time interval. Particularly, this method is based on CWT's modulus scalogram and extracts a cross-section parallel to the scale (or frequency) axis of the plot, for a fixed value of the time variable b. If the signal is monocomponent, the ridge is unique ridge, thus the estimation of the ridge is obtained by looking for the global maxima in the scale variable, while for multicomponent signals where more than one ridge are present the estimation of each ridge focuses on local maxima, still with respect to the scale variable.

The basic algorithm is as follows:

1. Calculate the CWT matrix of the signal ut.

2. Based on the modulus scalogram, estimate a scale range $[a_{min}, a_{max}]$ that contains one candidate ridge.

3. Select a time value t_a to extract a cross-section of the modulus scalogram parallel to the scale axis. t_a must be such that the whole candidate ridge falls within the useful domain D outside the cone of influence.

4. Find the maximum value of the CWT modulus inside the range $[a_{min}, a_{max}]$

5. Repeat steps 2-4 if more than one ridges are present.

There are several ways to implement this algorithm in MATLAB and estimate directly the instantaneous frequency:

- *Finding the Modulus maxima manually using the max command:*

1. Calculate the CWT matrix of the signal ut:
```
[coefs,freq] = cwt(ut,scales,'wname',dt,'plot') ;
```

2. Based on the modulus scalogram, estimate a frequency range $[f_{min}, f_{max}]$ that contains one candidate ridge.

3. Select a time point to extract the cross section parallel to the frequency axis to be inside the domain D (The cone of influence) and find its index.
```
w_t = Q/2;
ind = round(w_t/dt);
```

4. Find maxima and it's indices [i,ind] at the coefs matrix.
```
disp('Simple method: - max():')
modulus=abs(coefs);
max_modulus = max(modulus(:,ind));
[i,~]=find(modulus==max_modulus);

f_modulus1=freq(i)
omega_modulus1=2*pi*f_modulus1
T_modulus1=1/f_modulus1
```

5. Repeat steps 2-4 if more than one ridges are present.

- *Finding the Modulus maxima manually using the findpeaks command from the Signal Processing Toolbox:*

The command pks=findpeaks(data) returns a vector with the local maxima (peaks) of the input signal vector, data. A local peak is a data sample that is either larger than its two neighboring samples or is equal to Inf.
The command [pks,locs] = findpeaks(data) additionally returns the indices at which the peaks occur.
Thus the application becomes simpler:

1. Calculate the CWT matrix of the signal ut:

```
[coefs,freq] = cwt(ut,scales,'wname',dt,'plot') ;
```

2. Select a time point to extract the the cross section parallel to the frequency axis to be inside the domain D (The cone of influence) and find its index.

```
w_t = Q/2;
ind = round(w_t/dt);
```

3. Find the local maximas of the cross section

```
disp('Simple method - findpeaks:')
freq_data = modulus(:,ind);
[~,locs] = findpeaks(freq_data,'MinPeakProminence',0.25);
f_modulus2 = freq(locs)
omega_modulus2=2*pi*f_modulus2
T_modulus2=1/f_modulus2
```

It it important to note that using the max command one can find better results than the findpeaks, because findpeaks is very sensitive to the "MinPeakProminence" setting and might return low frequency values that belong to noise. Additionally, it works well only for values inside the domain D.

4.7.2 "Marseille" method

This method is based on the definition of the ridges as the place where the frequency of the scaled mother wavelet is equal to the instantaneous frequency of the signal; therefore it can be calculated based on the fact:

$$\omega_b = \frac{\dot{\varphi}_\psi(0)}{a_r(b)} \approx \frac{\partial \angle(T_\psi[u](b, a_r(b)))}{\partial b}$$

Graphically the first derivative of a function provides the slope of a tangent line to the function's graph at any instant. Utilizing this property, ω_b can be calculated as the slope of the phase-time data extracted from the phase plot of the CWT on the time-frequency plane, at the wavelet's ridge.

The basic algorithm is as follows:

1. Calculate the CWT matrix of the signal ut.

2. Based on the modulus scalogram, estimate a scale range $[a_{min}, a_{max}]$ that contains one candidate ridge.

3. Set the indices k_{min} and k_{max} that correspond to the range $[a_{min}, a_{max}]$.

4. Select an initial value of scale: a_k.

5. Do for scale steps: k from k_{min} to k_{max}

   (a) Compute $dCWT_{phase} = \frac{\partial \angle(T_\psi[u](b,a_k))}{\partial b}$ as the slope of the phase plot in the time axis for the current scale a_k.

   (b) Calculate $a_{k_{new}} = \frac{\dot{\varphi}_\psi(0)}{dCWT_{phase}}$

(c) Check $|a_{k_{new}} - a_k| < \varepsilon$, where ε is the is the pre-defined accuracy. If the condition is true, $\omega(b) = dCWT_{phase}$ and end the iteration (break). If it is false, continue.

(d) Set next value $a_k = a_{k_{new}}$

Remark 4.2. This algorithm works only for values inside the domain D, outside the cone of influence. If tuned correctly, produces very accurate results.

This algorithm can be easily implemented in MATLAB:

Listing 4.2: Marseille method

```matlab
% Marseille method - using the phase of the CWT
disp('Marseille method:')
    % Set the frequency range
    fmin = 1.0;   % Hz
    fmax = 3.5;   % Hz
    freq = freq';
    indx_f = find(freq>fmin & freq<fmax);
    kmin = min(indx_f);
    kmax = max(indx_f);
    a_ridge = scales(1)*dt;

     for k=kmin:kmax

        dCWT_phase=median(abs(diff(unwrap(angle(coefs(k,indx_t))))/dt)));
        a_new = (n+1)/dCWT_phase;

        if abs(a_new-a_ridge) < 10^-4
            omega_marseille = (n+1)/a_new;
            f_marseille = omega_marseille/(2*pi);
            a_ridge = a_new;
        break
        end
            omega_marseille = (n+1)/a_new;
            f_marseille = omega_marseille/(2*pi);

        a_ridge = a_new;
    end
```

Remark 4.3. $\frac{\partial \angle (T_\psi[u](b,a_k))}{\partial b}$ is a continuous function. However, by definition, this quantity always belongs to the interval $[-\pi/2, \pi/2]$ and this will create discontinuities. Using the unwrap command in MATLAB removes these discontinuities.

Example 4.6 (Illustration of the thought process of equation 4.42)**.** Consider a Cauchy wavelet with $Q = 8$. Employ the CWT of a monocomponent signal $u(t)$, find the ridge and extract a cross section of the phase diagram parallel to the time axis. Compute the unwrapped phase. Figure 4.5 shows the result where (a) is the phase diagram on the time-frequency plane with the ridge illustrated, (b) is the extracted phase-time cross section of the phase diagram parallel to the time axis, and (c) is the unwrapped phase-time extracted cross section plot. The slope gives the instantaneous frequency which is
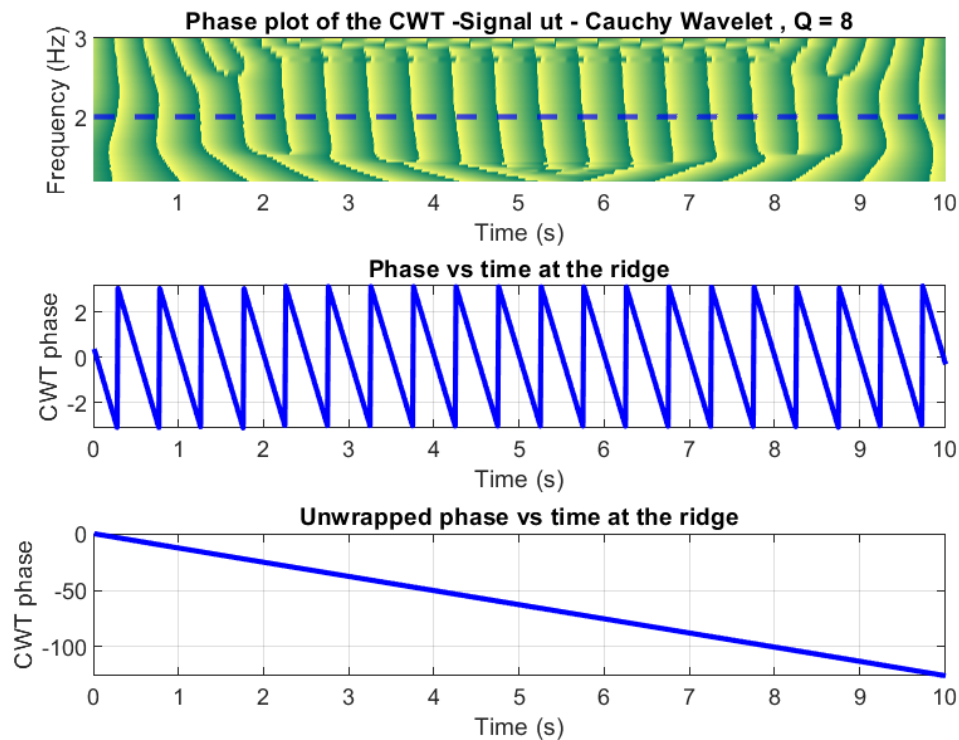
$f = 2Hz$, confirming the Marseille algorithm.

Figure 4.5: Example of the application of Marseille method. The slope gives the instantaneous frequency

4.7.3 *MATLAB tfridge*

MATLAB's Signal Processing Toolbox offers also the tfridge command. The function uses a penalized forward-backward greedy algorithm to extract the maximum-energy ridges from a time-frequency matrix, thus it can be considered to resemble an "integral" method.

The command fridge=tfridge(tfm,f) extracts the maximum-energy time-frequency ridge from the time-frequency matrix, tfm, and the frequency vector, f, and outputs the time-dependent frequency, fridge.

The command [fridge,iridge] = tfridge(tfm,f) also returns the row-index vector corresponding to the maximum-energy ridge. However, tfridge is very sensitive to the 'NumFrequencyBins' setting and might return low frequency values that belong to noise. Additionally, it works well only for values inside the domain D.

```
% Using the tfridge command from the Signal Processing Toolbox
disp('tfridge:')
[fridge,iridge] = tfridge(modulus(:,indx_t),freq,'NumRidges',4,...
     ...'NumFrequencyBins',Q); % values inside the domain D
f_tfridge = fridge(1,:)                % frequencies
i_ridge = iridge(1,:);                 % matrix index of ridges
omega_tfridge = 2*pi*f_tfridge
```

Chapter 5

Modal parameter identification using the CWT

This Chapter provides a basic theoretical background on structural dynamics and presents the techniques used in obtaining the modal parameters from the results of the CWT analysis. The systems considered are linear, with viscous proportional damping.

5.1 Structural Dynamics - Single Degree of Freedom (s.d.o.f.) systems

5.1.1 *Equation of motion*

Let $u(t)$, $\dot{u}(t)$, $\ddot{u}(t)$ denote respectively the displacement, velocity, and acceleration of a s.d.o.f. system. The equation of motion then is given by:

$$m\ddot{u}(t) + c\dot{u}(t) + ku(t) = p(t) \tag{5.1}$$

where m is the system's mass, c is the damping constant, k is the stiffness and $p(t)$ is the externally applied dynamic force.

5.1.2 *Viscoulsy damped free vibration of s.d.o.f. systems*

Free vibration is initiated by displacing the system from its static equilibrium position via imparting the mass an initial displacement $u(0)$ and velocity $\dot{u}(0)$ at time zero $t = 0$. If there is no externally applied dynamic force, then the free motion depends only on these initial conditions $u(0)$ and $\dot{u}(0)$. Setting $p(t) = 0$ in equation 5.1 gives the differential equation governing free vibration of s.d.o.f. systems with damping:

$$m\ddot{u}(t) + c\dot{u}(t) + ku(t) = 0 \tag{5.2a}$$

Dividing by the mass m gives:

$$\ddot{u}(t) + 2\xi\omega\ \dot{u}(t) + \omega^2 u(t) = 0 \tag{5.2b}$$

where
ω is the undamped angular natural frequency of the system, given by:

$$\omega = \sqrt{\frac{k}{m}} \tag{5.3}$$

ξ is the damping ratio or fraction of critical damping of the system, defined as:

$$\xi = \frac{c}{2m\omega} = \frac{c}{c_{cr}} \tag{5.4}$$

c, the damping constant, is a measure of the energy dissipated in a cycle of free vibration or in a cycle of forced harmonic vibration.

c_{cr} refers to the critical damping coefficient; it is the smallest value of c that inhibits oscillation completely, i.e. it is the dividing line between oscillatory and nonoscillatory motion and vise-versa. Consequently, c_{cr} defines the type of the system as:

i. *Underdamped systems*, where $c < c_{cr}$ or $\xi < 1$: the system oscillates about its equilibrium position with a progressively decreasing amplitude.

ii. *Critically damped systems*, where $c = c_{cr}$ or $\xi = 1$: the system returns to its equilibrium position without oscillating.

iii. *Overdamped systems*, where $c > c_{cr}$ or $\xi > 1$: the system does not oscillate and returns to its equilibrium position, as in the $\zeta = 1$ case, but at a slower rate.

As mentioned in Chapter 5, for the associated analytic signal to be approximated as $Z_u(t) \approx A_u(t)e^{i\varphi_u(t)}$, the assumption of weak damping $\xi \ll 1/\sqrt{2}$ is made, therefore the solution of the equation 5.2 that is presented in the following is for underdamped systems.

5.1.3 *Free response of underdamped s.d.o.f. system*

For underdamped systems where $c < c_{cr}$ or $\xi < 1$ the solution to the equation 5.2 subject to the initial conditions $u(0)$ and $\dot{u}(0)$ is:

$$u(t) = e^{-\xi\omega t}\left[u(0)\cos\widetilde{\omega}t + \frac{\dot{u}(0) + u(0)\xi\omega}{\widetilde{\omega}}\sin\widetilde{\omega}t\right] \tag{5.5}$$

where $\widetilde{\omega}$ is the damped angular natural frequency of the system, given by:

$$\widetilde{\omega} = \omega\sqrt{1 - \xi^2} \tag{5.6}$$

Setting

$$\rho = \sqrt{[u(0)]^2 + \left[\frac{\dot{u}(0) + u(0)\xi\omega}{\widetilde{\omega}}\right]^2} \tag{5.7}$$

and

$$\varphi = \arctan\left(\frac{\dot{u}(0) + u(0)\xi\omega}{u(0)\widetilde{\omega}}\right) \tag{5.8}$$

the equation 5.5 of displacement becomes:

$$u(t) = \rho e^{-\xi\omega t}\cos\left(\widetilde{\omega}t - \varphi\right) \tag{5.9}$$

The velocity and the acceleration are obtained by successively deriving the displacement $u(t)$:

The velocity is calculated as:

$$\dot{u}(t) = \rho\omega e^{-\xi\omega t}\Big[-\xi\cos\left(\widetilde{\omega}t - \varphi\right) - \sqrt{1 - \xi^2}\sin\left(\widetilde{\omega}t - \varphi\right)\Big]$$

$$= -\rho\omega e^{-\xi\omega t}\cos\left(\widetilde{\omega}t - \varphi - \delta\right) \tag{5.10}$$

where

$$\delta = \arctan\frac{\sqrt{1 - \xi^2}}{\xi} \tag{5.11}$$

and the acceleration is calculated as:

$$\ddot{u}(t) = \rho\omega e^{-\xi\omega t}(-\xi\omega)\Big[-\xi\cos\left(\widetilde{\omega}t - \varphi\right) - \sqrt{1 - \xi^2}\sin\left(\widetilde{\omega}t - \varphi\right)\Big]$$

$$+ \rho\omega e^{-\xi\omega t}\Big[\xi\widetilde{\omega}\sin\left(\widetilde{\omega}t - \varphi\right) - \sqrt{1 - \xi^2}\,\widetilde{\omega}\cos\left(\widetilde{\omega}t - \varphi\right)\Big]$$

$$= \rho\omega^2 e^{-\xi\omega t}\Big[(\xi^2 - (1 - \xi^2))\cos\left(\widetilde{\omega}t - \varphi\right) + 2\xi\sqrt{1 - \xi^2}\sin\left(\widetilde{\omega}t - \varphi\right)\Big]$$

$$= -\rho\omega^2 e^{-\xi\omega t}\cos\left(\widetilde{\omega}t - \varphi + \theta\right) \tag{5.12}$$

where

$$\theta = \arctan\frac{2\xi\sqrt{1 - \xi^2}}{1 - 2\xi^2} \tag{5.13}$$

It can be noted that the phase of the velocity and the phase of the acceleration are differentiated from the phase of the displacement by a quantity depending on the damping ratio ξ.

5.2 Structural Dynamics - Multi Degree of Freedom (m.d.o.f.) systems

5.2.1 *Equation of motion*

Let $\boldsymbol{u}(t)$, $\dot{\boldsymbol{u}}(t)$, $\ddot{\boldsymbol{u}}(t)$ denote respectively the displacement, velocity, and acceleration vectors of a m.d.o.f. system with N degrees of freedom. The equation of motion then is given by:

$$\mathbf{M}\ddot{\boldsymbol{u}}(t) + \mathbf{C}\dot{\boldsymbol{u}}(t) + \mathbf{K}\boldsymbol{u}(t) = \mathbf{P}(t) \tag{5.14}$$

where $\mathbf{M}$ is the system's mass matrix, $\mathbf{C}$ is the damping matrix, $\mathbf{K}$ is the stiffness matrix and $\mathbf{P}(t)$ is the externally applied dynamic force vector.

5.2.2 *Modal superposition*

Let $\boldsymbol{\Phi}$ be the modal matrix made of eigenvectors $\boldsymbol{\Phi}_j = [\Phi_{1j}, \Phi_{2j}, ..., \Phi_{Nj}]^T$. By definition, the mode shape vector $\boldsymbol{\Phi}_j$ describes the shape of the jth mode corresponding to the natural frequency ω_j. Then, the vector of displacements can be described mathematically by:

$$\boldsymbol{u}(t) = \sum_{j=1}^{N} \boldsymbol{\Phi}_j y_j(t) = \boldsymbol{\Phi} \mathbf{Y}(t) \tag{5.15}$$

The coupled equation of motion of equation 5.14 can be uncoupled after substituting $\boldsymbol{u}(t)$ using equation 5.15 and left multiplying it with $\boldsymbol{\Phi}^T$. This is achieved with the aid of the orthogonality condition, which makes $\mathbf{M}$, $\mathbf{K}$ and $\mathbf{C}$ diagonal, and is defined as:

$$\boldsymbol{\Phi}_j^T \mathbf{M} \boldsymbol{\Phi}_i = \begin{cases} M_j & \text{,if} \quad j = i \\ 0 & \text{,if} \quad j \neq i \end{cases} \tag{5.16}$$

$$\boldsymbol{\Phi}_j^T \mathbf{C} \boldsymbol{\Phi}_i = \begin{cases} C_j & \text{,if} \quad j = i \\ 0 & \text{,if} \quad j \neq i \end{cases} \tag{5.17}$$

$$\boldsymbol{\Phi}_j^T \mathbf{K} \boldsymbol{\Phi}_i = \begin{cases} K_j & \text{,if} \quad j = i \\ 0 & \text{,if} \quad j \neq i \end{cases} \tag{5.18}$$

5.2.3 *Viscoulsy damped free vibration of m.d.o.f. systems*

Considering again damped free vibration with initial conditions $\boldsymbol{u}(0)$, $\dot{\boldsymbol{u}}(0)$ at $t = 0$, then $\mathbf{P}(t) = 0$, the equation of motion becomes:

$$\mathbf{M}\ddot{\boldsymbol{u}}(t) + \mathbf{C}\dot{\boldsymbol{u}}(t) + \mathbf{K}\boldsymbol{u}(t) = 0 \tag{5.19}$$

Procedures to obtain the desired solution differ depending on the form of damping. The damping matrix $\mathbf{C}$ generally is not easy to calculate in practice. However, with condition 5.17, the transformation that diagonalizes both $\mathbf{M}$ and $\mathbf{K}$ will also diagonalize $\mathbf{C}$. So, by applying equation 5.15, equation 5.19 becomes:

$$\mathbf{M}\boldsymbol{\Phi}\ddot{\boldsymbol{Y}} + \mathbf{C}\boldsymbol{\Phi}\dot{\boldsymbol{Y}} + \mathbf{K}\boldsymbol{\Phi}\boldsymbol{Y} = 0 \tag{5.20}$$

Left multiplying by $\boldsymbol{\Phi}^T$ gives:

$$\boldsymbol{\Phi}^T \mathbf{M}\boldsymbol{\Phi}\ddot{\boldsymbol{Y}} + \boldsymbol{\Phi}^T \mathbf{C}\boldsymbol{\Phi}\dot{\boldsymbol{Y}} + \boldsymbol{\Phi}^T \mathbf{K}\boldsymbol{\Phi}\boldsymbol{Y} = 0 \tag{5.21}$$

Thus, the equations of motion can then be expressed as a N set of uncoupled s.d.o.f. equations:

$$M_j \ddot{y}_j + C_j \dot{y}_j + K_j y_j = 0 \qquad j = 1, 2, ..., N \tag{5.22}$$

Considering $C_j = 2\xi_j M_j \omega_j$ and $K_j = M_j \omega_j^2$, and dividing by M_j, the equations can be further simplified to:

$$\ddot{y}_j + 2\xi_j \omega_j \dot{y}_j + \omega_j^2 y_j = 0 \qquad j = 1, 2, ..., N \tag{5.23}$$

5.2.4 *Free response of underdamped m.d.o.f. system*

Consequently, the equations of 5.23 are of the same form as equation 5.2b governing the free vibration of a s.d.o.f system with viscous proportional damping. Adapting this result, the solution for equations 5.23 becomes:

$$y_j(t) = \rho_j e^{-\xi_j \omega_j t} \cos\left(\widetilde{\omega}_j t - \varphi_j\right) \tag{5.24}$$

$$\dot{y}_j(t) = -\rho_j \omega_j e^{-\xi_j \omega_j t} \cos\left(\widetilde{\omega}_j t - \varphi_j - \delta_j\right) \tag{5.25}$$

$$\ddot{y}_j(t) = -\rho_j \omega_j^2 e^{-\xi_j \omega_j t} \cos\left(\widetilde{\omega}_j t - \varphi_j + \theta_j\right) \tag{5.26}$$

where

$$\omega_j^2 = \frac{k_j}{m_j} \tag{5.27}$$

$$\widetilde{\omega}_j = \omega_j \sqrt{1 - \xi_j^2} \tag{5.28}$$

Therefore, for any degree of freedom $k = 1, ..., N$, the m.d.o.f. system's responses can be expressed as:

$$u_k(t) = \sum_{j=1}^{N} u_{kj}(t) = \sum_{j=1}^{N} \Phi_{kj} \rho_j e^{-\xi_j \omega_j t} \cos\left(\widetilde{\omega}_j t - \varphi_j\right) \tag{5.29}$$

$$\dot{u}_k(t) = \sum_{j=1}^{N} \dot{u}_{kj}(t) = -\sum_{j=1}^{N} \Phi_{kj} \rho_j \omega_j e^{-\xi_j \omega_j t} \cos\left(\widetilde{\omega} t_j - \varphi_j - \delta_j\right) \tag{5.30}$$

$$\ddot{u}_k(t) = \sum_{j=1}^{N} \ddot{u}_{kj}(t) = -\sum_{j=1}^{N} \Phi_{kj} \rho_j \omega_j^2 e^{-\xi_j \omega_j t} \cos\left(\widetilde{\omega}_j t - \varphi_j + \theta_j\right) \tag{5.31}$$

5.3 Modal Parameters Identification Procedure

5.3.1 *Relations between obtained data and modal parameters*

As it was presented in the previous Chapter, employing a ridge estimation method allows the identification of the instantaneous frequencies ω_j and the analytical signal $Z_{\cdot_{kj}}$. The next step is to find a relation to extract the damping ratio and the mode shapes (the modal parameters in general) from the analytical signal. At this point it is assumed that the CWT has been applied on the measured free responses $u_k(t)$, $\dot{u}_k(t)$, and $\ddot{u}_k(t)$ of the k DOF, and each signal has been decomposed into its N components in the form of

instantaneous functions:

$$\sum_{j=1}^{N} A_{\cdot_{kj}}(t) \cos\left[\varphi_{\cdot_{kj}}(t)\right] \tag{5.32}$$

Then, to be able to identify the modal parameters, equations 5.29, 5.30 and 5.31 are expressed in the form of equation 5.32:

$$u_k(t) = \sum_{j=1}^{N} u_{kj}(t) = \sum_{j=1}^{N} A_{u_{kj}}(t) \cos\left[\varphi_{u_{kj}}(t)\right] \tag{5.33}$$

where:

$$\begin{cases} \varphi_{u_{kj}}(t) & = \widetilde{\omega}_j t - \varphi_j + \dfrac{\pi}{2}(1 - \mathrm{sgn}(\Phi_{kj})) \\ A_{u_{kj}}(t) & = |\Phi_{kj}|\rho_j e^{-\xi_j \omega_j t} \end{cases} \tag{5.34}$$

$$\dot{u}_k(t) = \sum_{j=1}^{N} \dot{u}_{kj}(t) = \sum_{j=1}^{N} A_{\dot{u}_{kj}}(t) \cos\left[\varphi_{\dot{u}_{kj}}(t)\right] \tag{5.35}$$

where:

$$\begin{cases} \varphi_{\dot{u}_{kj}}(t) & = \widetilde{\omega}_j t - \varphi_j - \delta_j + \dfrac{\pi}{2}(1 + \mathrm{sgn}(\Phi_{kj})) \\ A_{\dot{u}_{kj}}(t) & = |\Phi_{kj}|\rho_j \omega_j e^{-\xi_j \omega_j t} \end{cases} \tag{5.36}$$

$$\ddot{u}_k(t) = \sum_{j=1}^{N} \ddot{u}_{kj}(t) = \sum_{j=1}^{N} A_{\ddot{u}_{kj}}(t) \cos\left[\varphi_{\ddot{u}_{kj}}(t)\right] \tag{5.37}$$

where:

$$\begin{cases} \varphi_{\ddot{u}_{kj}}(t) & = \widetilde{\omega}_j t - \varphi_j + \theta_j + \dfrac{\pi}{2}(1 + \mathrm{sgn}(\Phi_{kj})) \\ A_{\ddot{u}_{kj}}(t) & = |\Phi_{kj}|\rho_j \omega_j^2 e^{-\xi_j \omega_j t} \end{cases} \tag{5.38}$$

Le-Argoul [13] used these instantaneous functions to get linear or constant relations between data and modal parameters. They defined these relations by performing a parametric identification technique based on the minimization by the least squares method of an error criterion. This error criterion was defined as the difference between the instantaneous functions that are derived from the processed data $R^{measure}(t)$ and those obtained from the theory $R^{model}(t)$. The results are the following relations:

- **Using the phases of the obtained analytical signals**

As it was presented in the previous Chapter, the time evolution of the phase ($\varphi_{u_{kj}}(t)$, or $\varphi_{\dot{u}_{kj}}(t)$, or $\varphi_{\ddot{u}_{kj}}(t)$) is a straight line with slope ω_j; the estimation of ω_j then leads then to a straight line inverse problem. Additionally, the time evolution of the ridge $a_r(t)$ was shown to be constant, thus the damped natural angular frequency $\widetilde{\omega}_j$ is related with the instantaneous frequency $\dot{\varphi}_{\cdot_{kj}}$ by:

$$\widetilde{\omega}_j = \dot{\varphi}_{u_{kj}}(t) = \frac{\dot{\varphi}_\psi(0)}{a_{r\,u_{kj}}(t)} \tag{5.39}$$

$$\widetilde{\omega}_j = \dot{\varphi}_{\dot{u}_{kj}}(t) = \frac{\dot{\varphi}_\psi(0)}{a_{r\,\dot{u}_{kj}}(t)} \tag{5.40}$$

$$\widetilde{\omega}_j = \dot{\varphi}_{\ddot{u}_{kj}}(t) = \frac{\dot{\varphi}_\psi(0)}{a_{r\,\ddot{u}_{kj}}(t)} \tag{5.41}$$

The damping ratio can be obtained directly by:

$$\xi_j = |\cos(\delta_j - \pi \operatorname{sgn}(\Phi_{kj}))| = \left|\cos\left(\varphi_{u_{kj}}(t) - \varphi_{\dot{u}_{kj}}(t)\right)\right| \tag{5.42}$$

$$\xi_j = \left|\cos\left(\frac{\theta_j + \pi \operatorname{sgn}(\Phi_{kj})}{2}\right)\right| = \left|\cos\left(\frac{\varphi_{\ddot{u}_{kj}}(t) - \varphi_{u_{kj}}(t)}{2}\right)\right| \tag{5.43}$$

The sign of Φ_{kj} can be obtained in relation with a reference Φ_{mj}. The phase difference d_j^{km} between a dof k and a dof m on the j mode is equal to:

$$d_j^{km}(t) = \varphi_{u_{kj}}(t) - \varphi_{u_{mj}}(t) = -(\varphi_{\dot{u}_{kj}}(t) - \varphi_{\dot{u}_{mj}}(t)) = -(\varphi_{\ddot{u}_{kj}}(t) - \varphi_{\ddot{u}_{mj}}(t)) \tag{5.44}$$

is either zero or equal to $\pm\pi$:

$$d_j^{km}(t) = \frac{\pi}{2}\left(\operatorname{sgn}(\Phi_{mj}) - \operatorname{sgn}(\Phi_{kj})\right) \tag{5.45}$$

Therefore, Φ_{kj} and Φ_{mj} have the same sign if $d_j^{km}(t) = 0$ and opposite signs if $d_j^{km}(t) = \pm\pi$.

- **Using the amplitudes of the obtained analytical signals**

The undamped natural angular frequency ω_j can be expressed as:

$$\omega_j = \frac{A_{\dot{u}_{kj}}(t)}{A_{u_{kj}}(t)} \tag{5.46}$$

$$\omega_j = \frac{A_{\ddot{u}_{kj}}(t)}{A_{\dot{u}_{kj}}(t)} \tag{5.47}$$

The time evolution of the logarithm of the amplitude ($\log(A_{u_{kj}}(t))$, or $\log(A_{\dot{u}_{kj}}(t))$, or $\log(A_{\ddot{u}_{kj}}(t))$) is a straight line with slope $-\xi_j \omega_j$ as it can be observed by:

$$\log(A_{u_{kj}}(t)) = \log(|\Phi_{kj}|\rho_j) - \xi_j \omega_j t \tag{5.48}$$

$$\log(A_{\dot{u}_{kj}}(t)) = \log(|\Phi_{kj}|\rho_j \omega_j) - \xi_j \omega_j t \tag{5.49}$$

$$\log(A_{\ddot{u}_{kj}}(t)) = \log(|\Phi_{kj}|\rho_j \omega_j^2) - \xi_j \omega_j t \tag{5.50}$$

The identification of the absolute value of Φ_{kj} is again a straight line inverse problem. The ratio $A_{u_{kj}}(t)/A_{u_{mj}}(t)$ of the amplitude of the jth component of the response of the dof k upon that of the dof m is a constant in time which is the absolute value of the kth component of mode j. Consequently:

$$|\Phi_{kj}| = \frac{A_{u_{kj}}(t)}{A_{u_{mj}}(t)} \tag{5.51}$$

5.4 Algorithm for modal parameter identification

Summarizing and combining now all the theory that has been developed in Chapters 3, 4 and this Chapter, an identification procedure is presented to obtain the values of modal parameters. These methods include a technique that requires only the displacement response vector $\boldsymbol{u}(t)$ as well as techniques that require the acceleration $\ddot{\boldsymbol{u}}(t)$, the velocity $\dot{\boldsymbol{u}}(t)$ and the displacement response vector $\boldsymbol{u}(t)$. The algorithm presented employs the displacement response, but can be easily extended to velocity or acceleration ones. All the identification methods are linear and lead to a direct estimation without iteration and initial conditions. The algorithm is as follows:

1. Choose a mother wavelet. (The factors that define a proper mother wavelet for the analysis have been presented in section 3.3.5).

2. Apply the FFT and obtain rough estimates of the modal frequencies. This is done firstly due to the fact that the computation of the bounds of Q and the edge effect delimiting equations include the values of ω_j and secondly because the methods presented are based on the the analysis of a single component, so when dealing with a multicomponent signal a range of frequencies where the candidate frequency is located is needed. (FFT has been presented in section 3.2.3).

3. Choose a value for the Q factor. (The choice of Q has been analyzed in section 3.3.8).

$$c_f \frac{\omega_j}{2d\omega_j} \leq Q \leq \frac{L\omega_j}{2c_t}$$

4. Compute the edge effect delimiting lines. (As presented in section 3.3.7).

$$\omega_1 = \frac{1}{t}2c_tQ\mu_\psi \quad , \quad \omega_2 = \frac{1}{L-t}2c_tQ\mu_\psi \quad , \quad \omega_3 = 0 \quad , \quad \omega_4 = \frac{2\pi f_{Nyquist}}{1 + c_f\frac{1}{2Q}}$$

5. Choose a dof k and obtain its responses $u_k(t)$, $\dot{u}_k(t)$ and $\ddot{u}_k(t)$.

6. Compute the CWT of $u_k(t)$, $T_\psi[u_k](b,a)$, the CWT of $\dot{u}_k(t)$, $T_\psi[\dot{u}_k](b,a)$, and the CWT of $\ddot{u}_k(t)$, $T_\psi[\ddot{u}_k](b,a)$. (Algorithms presented in section 3.3.9).

7. Identify the ridges $a_{r_{u_{kj}}}(b)$. (As presented in Chapter 4).

8. Construct the analytical signal $Z_{u_{kj}}(b)$ for each ridge (As presented in Chapter 4). Each ridge corresponds to a mode j.

$$\dot{\varphi}_{u_{kj}}(b) = \frac{\dot{\varphi}_\psi(0)}{a_{r_{u_{kj}}}(b)}$$

$$Z_{u_{kj}}(b) = A_{u_{kj}}(t)e^{i[\varphi_{u_{kj}}(t)]} \approx \frac{2}{\widehat{\psi}(\dot{\varphi}_\psi(0))}T_\psi[u_{kj}](b, a_{r_{u_{kj}}}(b))$$

Apply the same for $Z_{\dot{u}_{kj}}(b)$ and $Z_{\ddot{u}_{kj}}(b)$.

9. Identify the angular frequency $\widetilde{\omega}_j$ or ω_j as:

   i. From ridge (and phase): $\widetilde{\omega}_j = \dot{\varphi}_{u_{kj}}(b)$.

   ii. From modulus: $\omega_j = \frac{A_{\dot{u}_{kj}}(b)}{A_{u_{kj}}(b)} = \frac{|Z_{\dot{u}_{kj}}(b)|}{|Z_{u_{kj}}(b)|}$ then, $\widetilde{\omega}_j = \omega_j\sqrt{1 - \xi_j^2}$

10. Identify the damping ratio ξ_j as:

   i. From modulus: as the slope of $\log(A_{u_{kj}}(b)) = |Z_{u_{kj}}(b)|$.

   ii. From phase (a): $\xi_j = \left|\cos\left(\varphi_{u_{kj}}(t) - \varphi_{\dot{u}_{kj}}(t)\right)\right| = |\angle Z_{u_{kj}}(b) - \angle Z_{\dot{u}_{kj}}(b)|$.

   iii. From phase (b): $\xi_j = \left|\cos\left(\frac{\varphi_{\ddot{u}_{kj}}(t) - \varphi_{u_{kj}}(t)}{2}\right)\right| = \left|\cos\left(\frac{\angle Z_{\ddot{u}_{kj}}(b) - \angle Z_{u_{kj}}(b)}{2}\right)\right|$

11. Identify the mode shape vector $\mathbf{\Phi}_j$ as:

   i. Choose a reference dof m (usually the top dof) and impose $\Phi_{mj} = 1$.

   ii. Compute the absolute value $|\Phi_{kj}| = \frac{A_{u_{kj}}(b)}{A_{u_{mj}}(b)} = \frac{|Z_{u_{kj}}(b)|}{|Z_{u_{mj}}(b)|}$.

iii. Compute the sign $\text{sgn}(\Phi_{kj})$ as:

Calculate $d_j^{km}(b) = |\varphi_{u_{kj}}(b) - \varphi_{u_{mj}}(b)| = |\angle Z_{u_{kj}}(b) - \angle Z_{u_{mj}}(b)|$.

If $d_j^{km}(t) = 0$, then Φ_{kj} and Φ_{mj} have the same sign, if else, then Φ_{kj} and Φ_{mj} have opposite signs.

iv. Finally, $\Phi_{kj} = |\Phi_{kj}| \, \text{sgn}(\Phi_{kj})$.

v. The signal $u_k(t)$ can be reconstructed from the analytic signal as:

$$u_k(t) = \sum_{j=1}^{N} Re\left[Z_{u_{kj}}(b) \right]$$

.

Remark 5.1. This algorithm can be summarized into three steps:

1. Compute the CWT of the signal.

2. Identify ridges, the corresponding skeletons and compute the analytic signals.

3. Identify the modal parameters.

Chapter 6

Numerical Applications

The algorithm presented in section 5.4 is now employed for modal identification of two examples: a s.d.o.f. system and a m.d.o.f. system. The algorithm is implemented in MATLAB version 2021a and use the built in cwt command with some modifications as mentioned in section 3.3.10.

The two chosen mother wavelets are the Complex Morlet wavelet and the Cauchy wavelet of order n. These two wavelets where selected because of the following reasons:

1. They are admissible.

2. They are both complex,progressive wavelets. Consequently, the CWT results are also complex, which allows to extract the information about the modulus of the CWT to implement the Simple method and the the phase of the CWT to implement the Marseille method, and to reconstruct the signal $u(t)$.

3. They have good time and frequency localization properties.

4. They reflect the type of features present in the time series as they are waveforms with an increased number of oscillations.

5. They have parameters in their definitions that strongly influence the localization properties, which enables their tuning with the Q factor.

6.1 Single Degree of Freedom System

6.1.1 *The s.d.o.f. model*

Consider the mass-spring-damper system of figure 6.1, with the characteristics presented in table 6.1. In order to obtain the free responses $u(t)$, $\dot{u}(t)$ and $\ddot{u}(t)$, the system is subjected to initial conditions:

$$u(0) = 0.5m \quad and \quad \dot{u}(0) = 0m/s$$

The duration of the obtained signal is L=10 sec and the sampling period is dt=0.01 sec. The displacement response is shown in figure 6.2.

Table 6.1: Characteristics of the test s.d.o.f. system

Natural period	T = 0.5 sec
Natural frequency	f = 1/T = 2 Hz
Natural damped angular frequency	ω = 2π/T = 12.57 rad/sec
Mass	m = 1 kg
Damping ratio	ξ = 2 %
Stiffness	k = mω^2 = 157.9 N/m
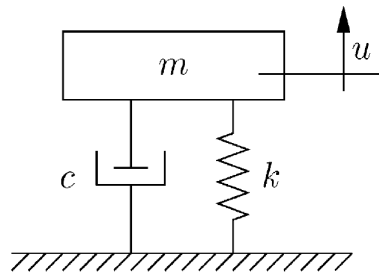
Figure 6.1: The test s.d.o.f. system

6.1.2 *Choice of Q*

The FFT results are $f = 1.998\ Hz \rightarrow \omega = 12.55\ rad/sec$, illustrated in figure 6.3. Considering $c_f = c_t = 5$ and $d\omega = \omega - 0 = \omega$, the Q value is bounded as:

$$2.5 \leq Q \leq 12.55$$

After some tests so that $Re\left[Z_{u_{kj}}(b)\right] = u(t)$, $Q = 2.5$ is selected for the Cauchy wavelet and $Q = 9.0$ is selected for the Morlet wavelet.
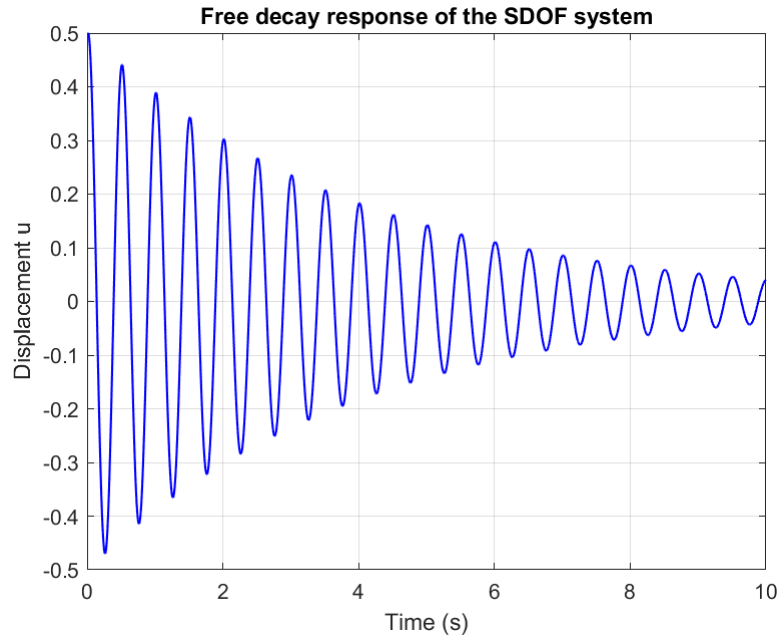
Figure 6.2: Displacement response $u(t)$ of the test s.d.o.f. system
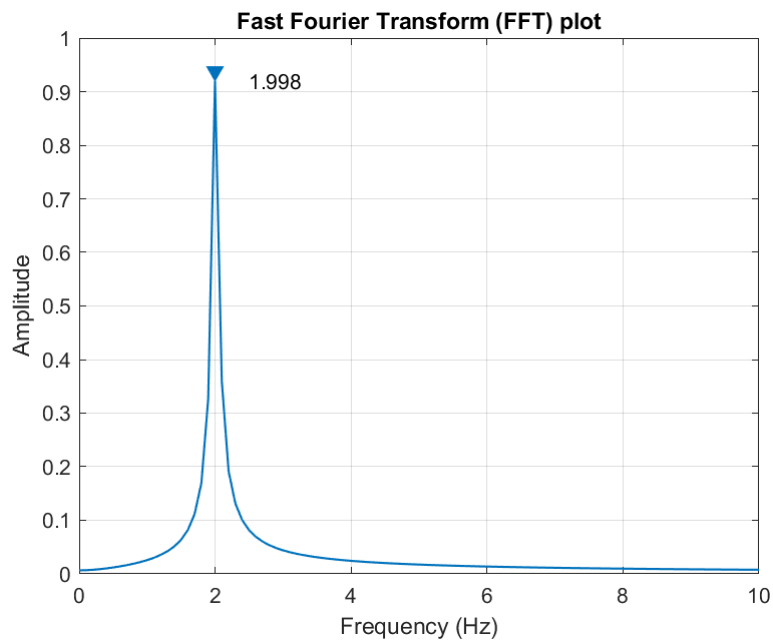
Figure 6.3: FFT results of the test s.d.o.f. system

6.1.3 CWT results

- **Cauchy wavelet**

The CWT of the signal $u(t)$ is then calculated, the results are the figures 6.5, 6.6, 6.7, where the CWT Scalogram, the time-frequency modulus plot and time-frequency phase plot of signal $u(t)$ with Cauchy mother wavelet for $Q = 2.5$ are illustrated respectively.
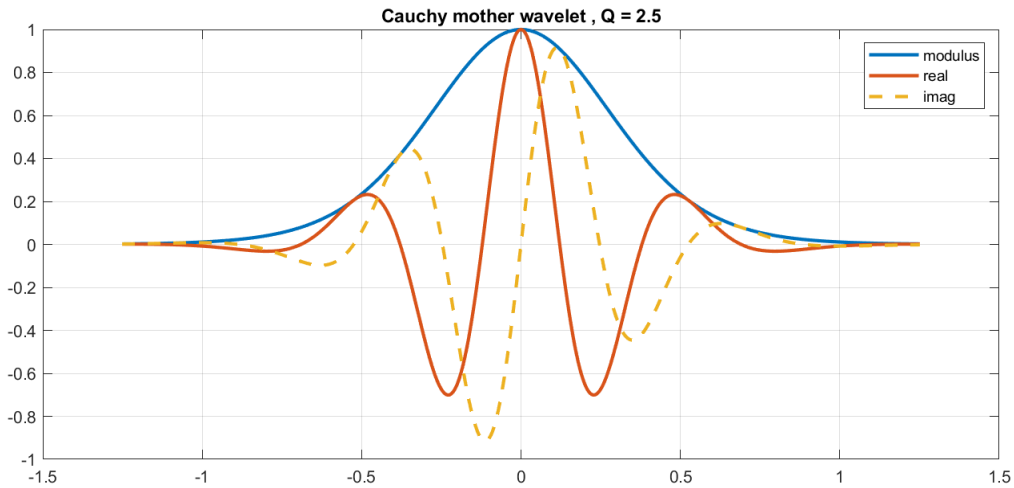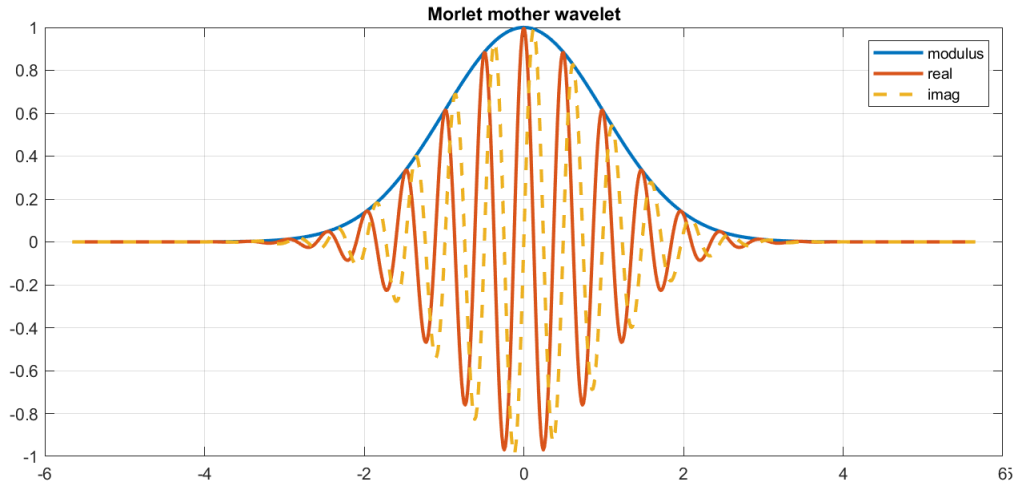
Figure 6.4: The Cauchy mother wavelet for $Q = 2.5$

As it can be observed in figures 6.5 and 6.6, there is only one ridge, corresponding to the fact that the signal is component. Additionally the edge effects outside of the domain D are clearly visible on the region of the plot with small time values. Edge effects can be observed also in figure 6.7, for low frequencies.
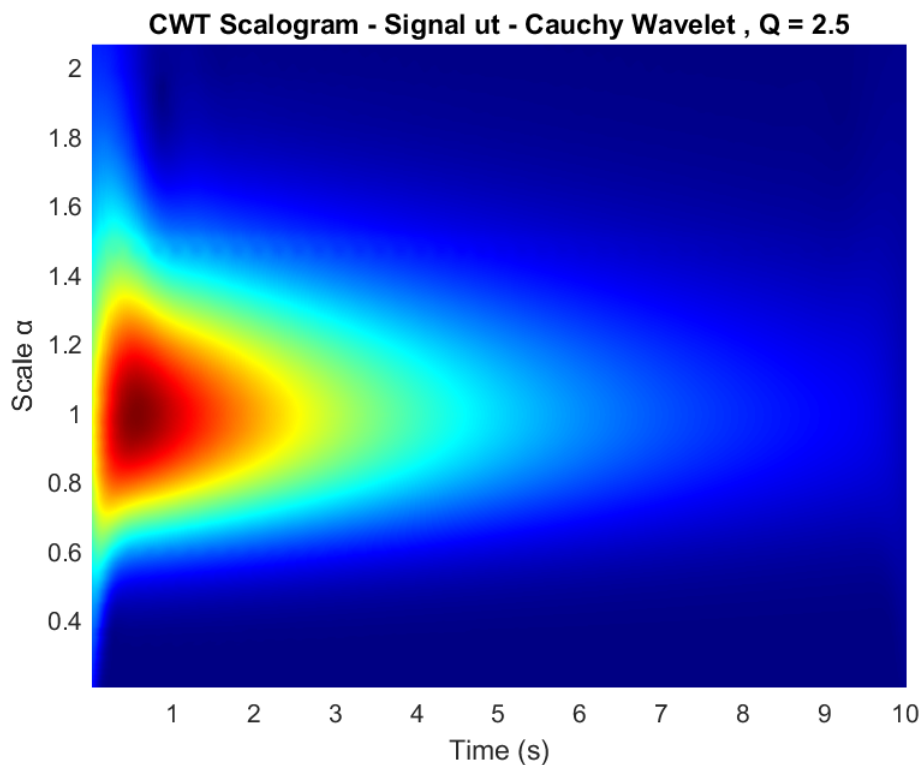
Figure 6.5: CWT Modulus Scalogram of signal $u(t)$, Cauchy mother wavelet, $Q = 2.5$
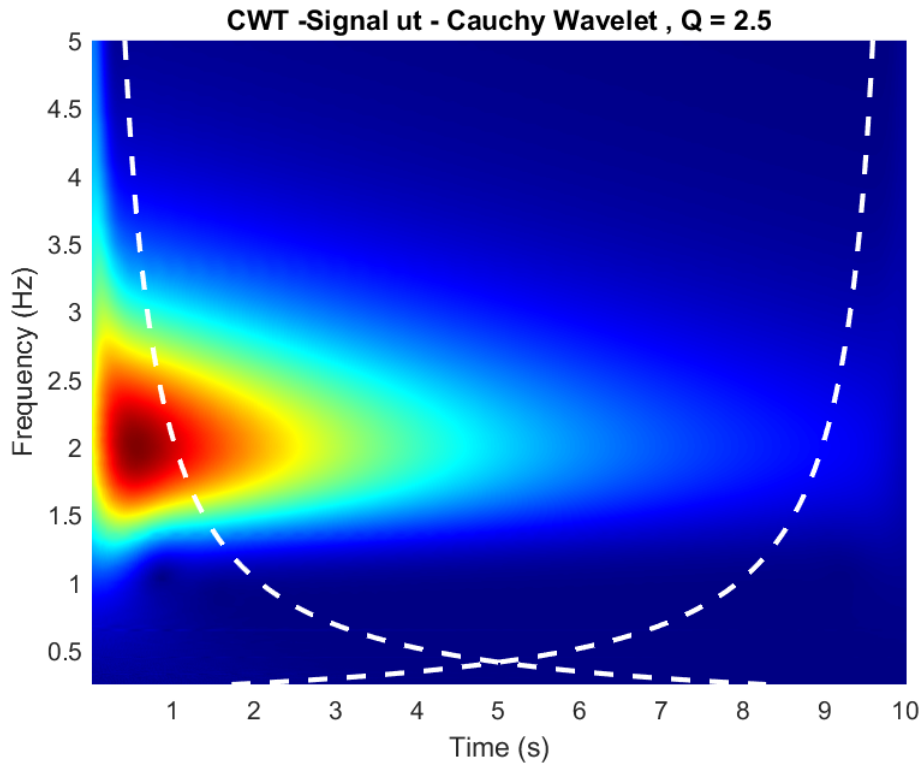
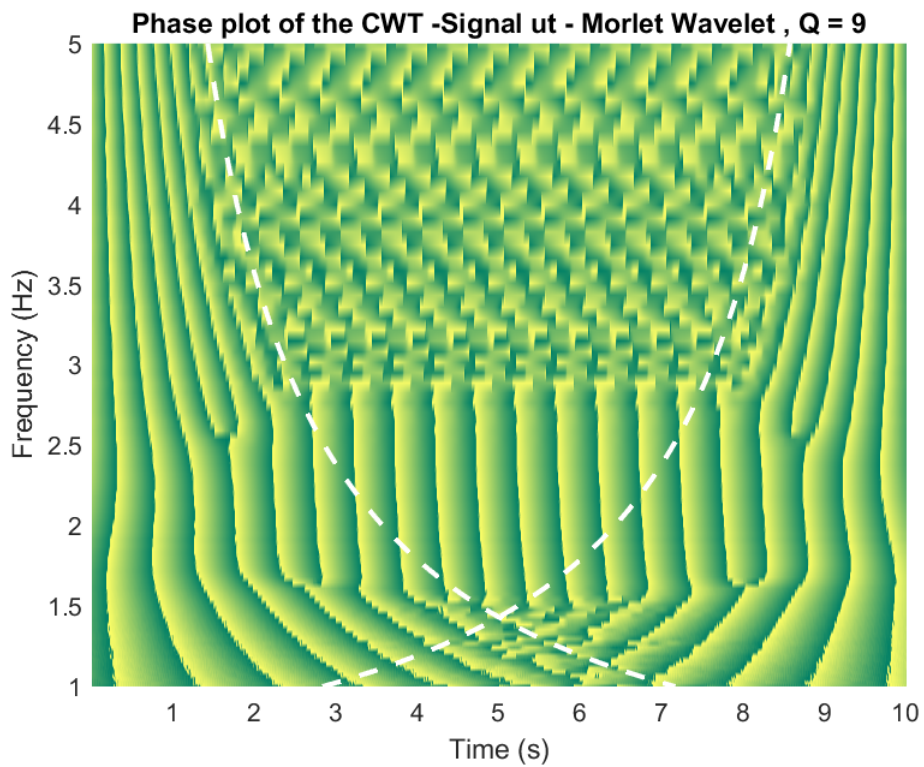Figure 6.6: CWT time-frequency modulus plot of signal $u(t)$, Cauchy mother wavelet, $Q = 2.5$
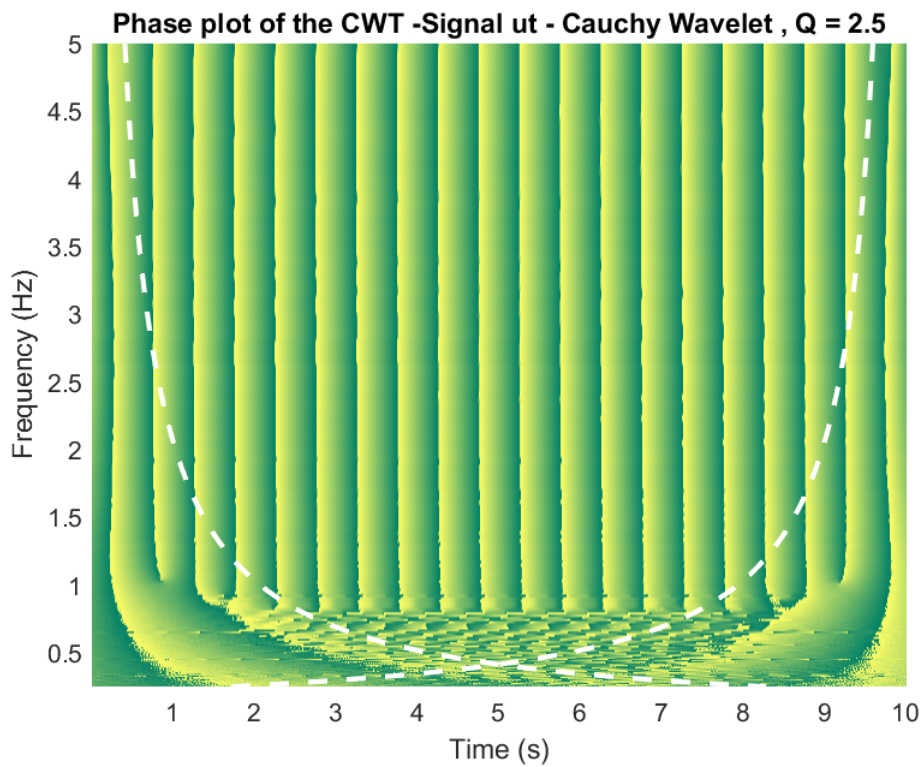
Figure 6.7: CWT time-frequency phase plot of signal $u(t)$, Cauchy mother wavelet, $Q = 2.5$

111

- ## *Morlet wavelet*

The CWT of the signal $u(t)$ is then calculated, the results are the figures 6.9, 6.10, 6.11, where the CWT Scalogram, the time-frequency modulus plot and time-frequency phase plot of signal $u(t)$ with Morlet mother wavelet for $Q = 9.0$ are illustrated respectively.

Figure 6.8: The Morlet mother wavelet for $Q = 9.0$

Same observations with the Cauchy wavelet CWT can be done, as seen in figures 6.9 and 6.10, and 6.11. One extra thing that can be observed is that as for the Morlet wavelet Q is higher, the edge effects become more significant.
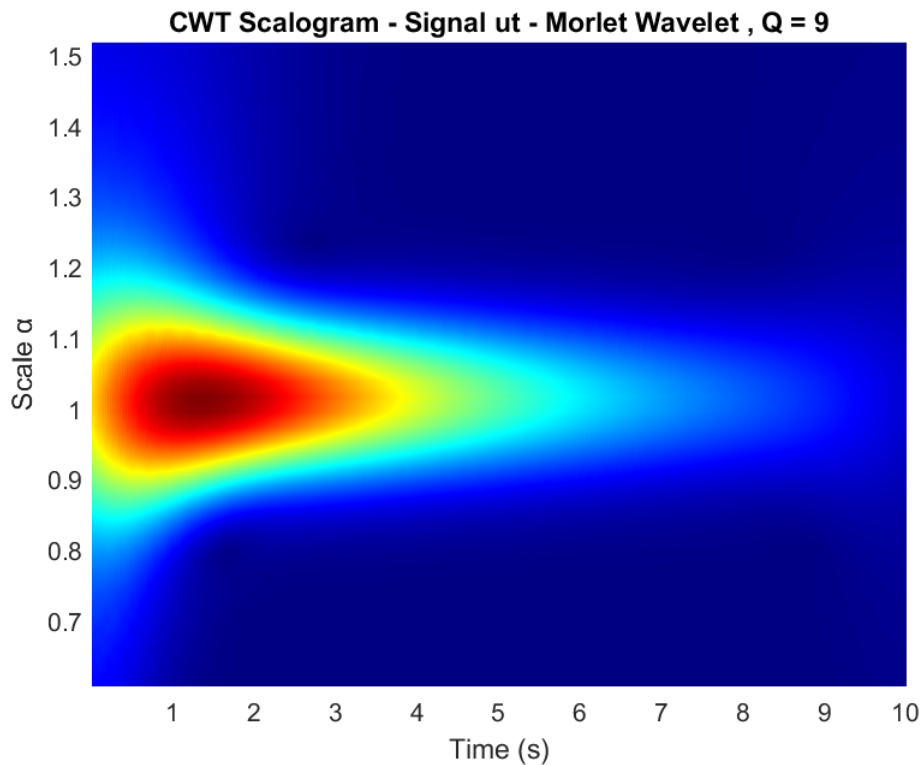
Figure 6.9: CWT Modulus Scalogram of signal $u(t)$, Morlet mother wavelet, $Q = 9.0$

112
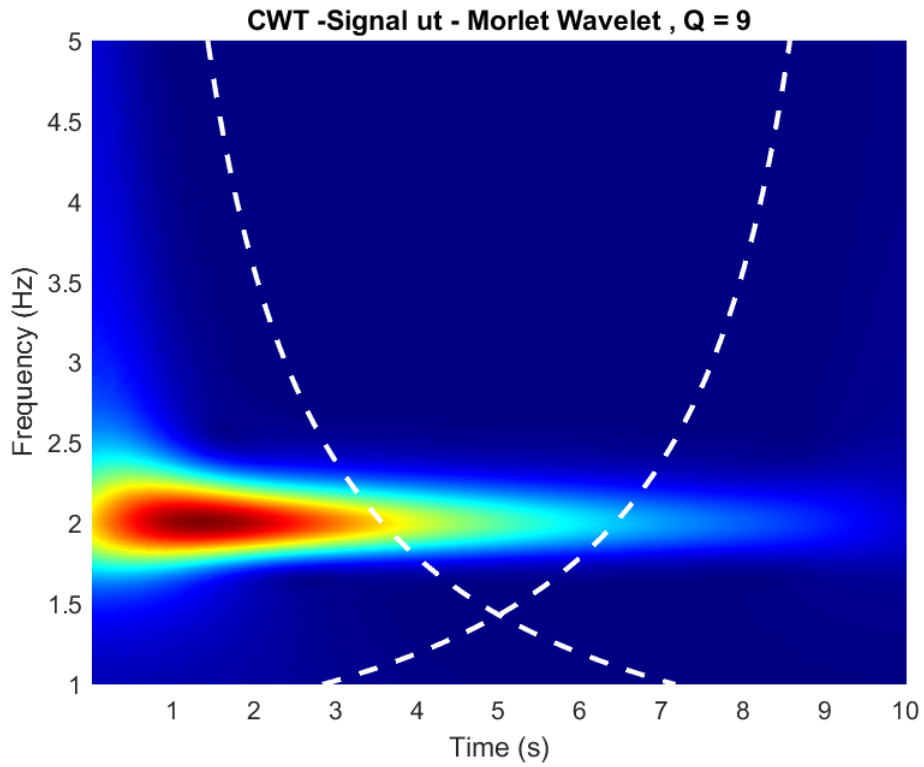
Figure 6.10: CWT time-frequency modulus plot of signal $u(t)$, Morlet mother wavelet, $Q = 9.0$

Figure 6.11: CWT time-frequency phase plot of signal $u(t)$, Morlet mother wavelet, $Q = 9.0$

113

6.1.4 *Frequency Estimation*

- **Estimation from modulus max**

As there is only one ridge, frequency can be estimated searching for the global maximum employing the methods presented in Chapter 4, see figures 6.12 and 6.13. Observe that the maximum is at $f = 2\ Hz$. Also, for low frequencies, outside the domain D, a small distortion can be observed, which is due to the edge effects.
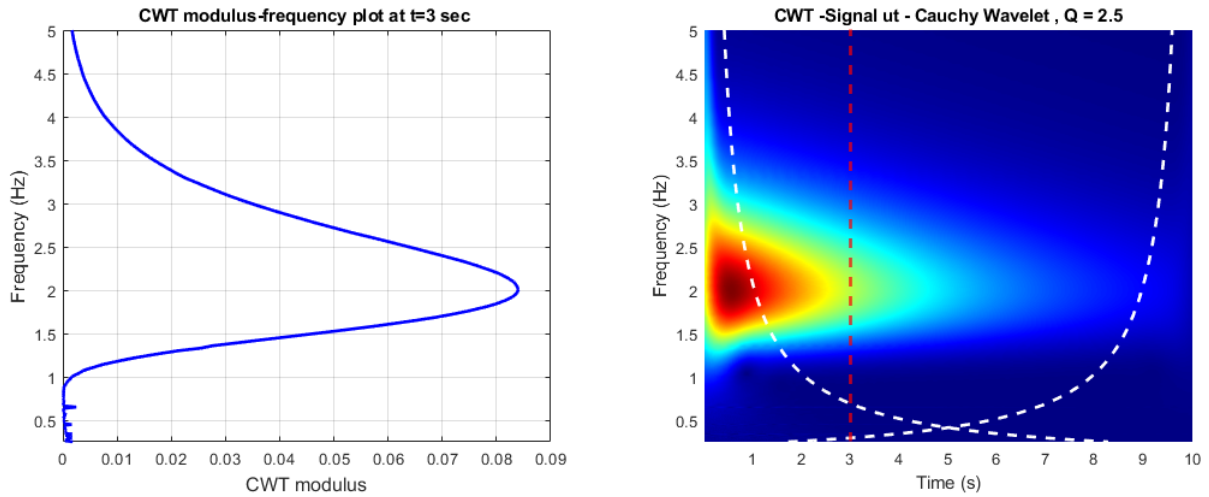
Figure 6.12: Cross section of the modulus plot parallel to the frequency axis, signal $u(t)$, Cauchy mother wavelet, $Q = 2.5$
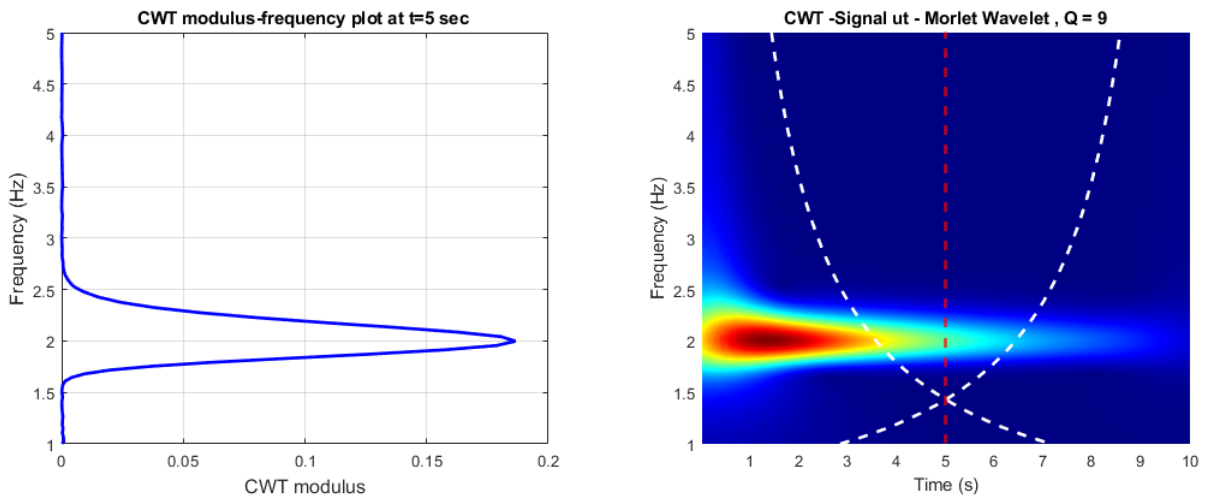
Figure 6.13: Cross section of the modulus plot parallel to the frequency axis, signal $u(t)$, Morlet mother wavelet, $Q = 9.0$

- **Estimation from phase**

The Marseille method is applied, as presented in Chapter 4, see figures 6.14 and 6.15. The slope of the phase-time data extracted from the phase plot of the CWT on the time-frequency plane, at the wavelet's ridge, is the natural angular frequency ω.
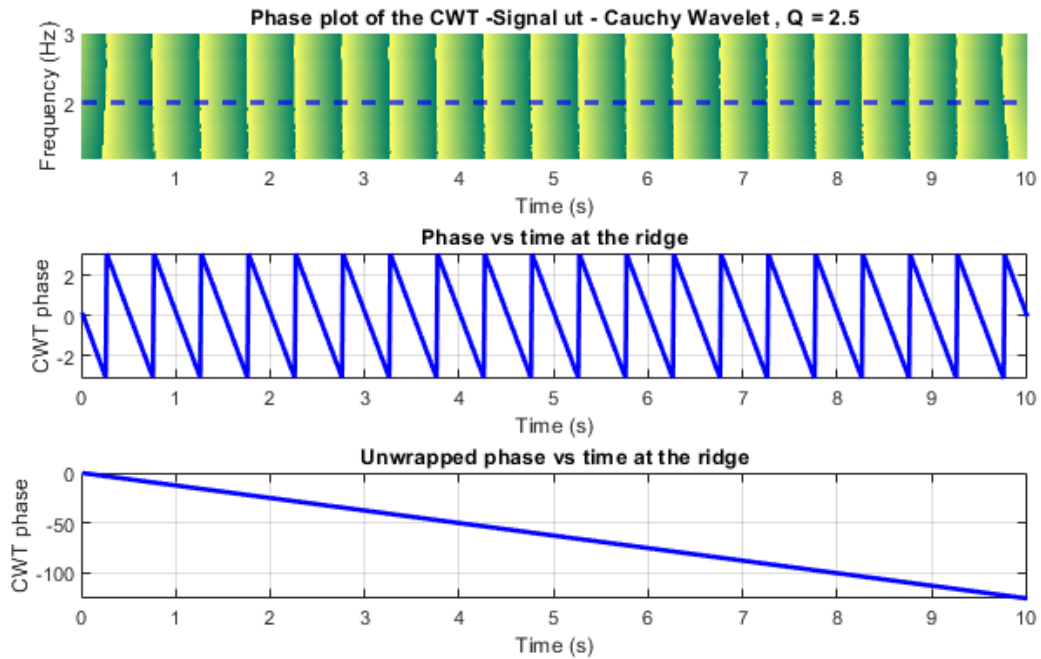

Figure 6.14: Cross section of the phase plot parallel to the time axis at the ridge, signal $u(t)$, Cauchy mother wavelet, $Q = 2.5$
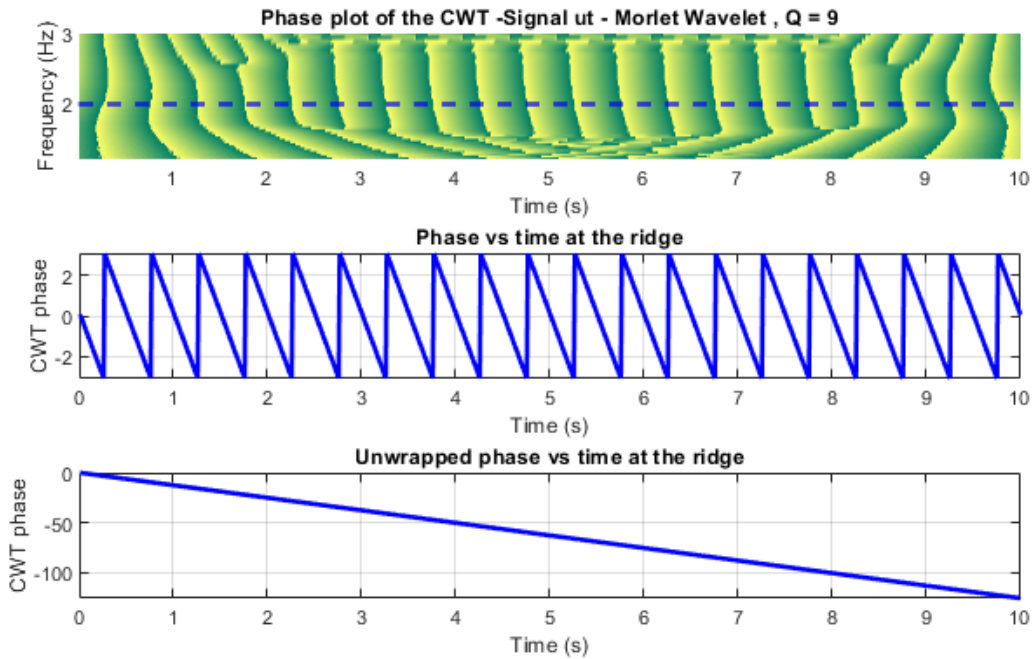

Figure 6.15: Cross section of the phase plot parallel to the time axis at the ridge, signal $u(t)$, Morlet mother wavelet, $Q = 9.0$

6.1.5 *Damping Ratio Estimation*

- **Estimation from modulus**

As it was presented in Chapter 5, the slope of the logarithm of the modulus-time data extracted from the modulus plot of the CWT on the time-frequency plane at the wavelet's ridge, is equal to $-\xi\omega$. Having ω estimated, the damping ratio ξ then can be estimated, see figures 6.16 and 6.17.
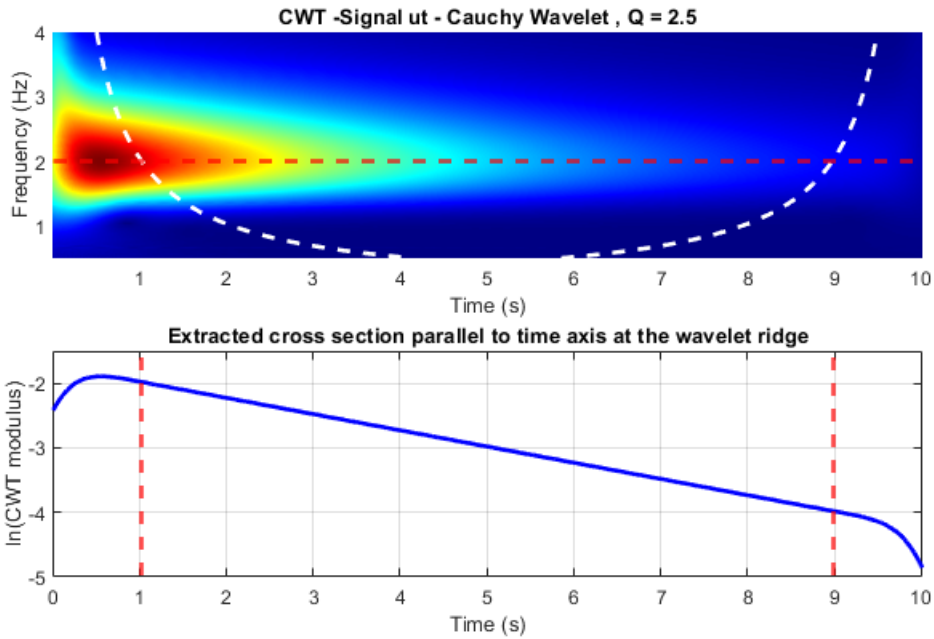

Figure 6.16: Logarithm of the cross section of the modulus plot parallel to the time axis at the ridge, signal $u(t)$, Cauchy mother wavelet, $Q = 2.5$.
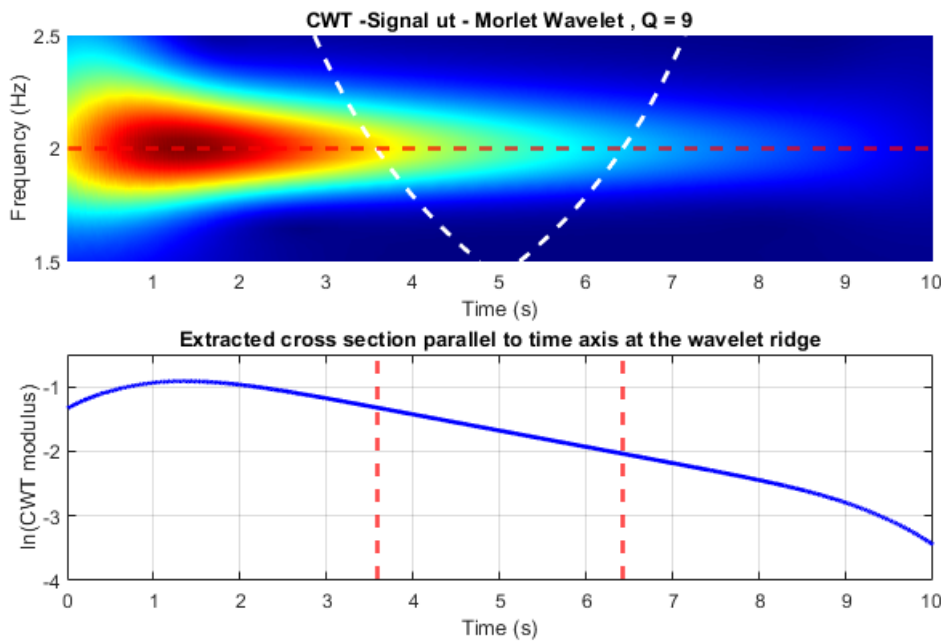

Figure 6.17: Logarithm of the cross section of the phase plot parallel to the time axis at the ridge, signal $u(t)$, Morlet mother wavelet, $Q = 9.0$

- **Estimation from phase**

The equations of Chapter 5 they can be visualized and illustrated in figures 6.18 and 6.19, where (a) is estimated as $\xi_j = |\angle Z_{u_{kj}}(b) - \angle Z_{\dot{u}_{kj}}(b)|$ and (b): $\xi_j = \left| \cos\left(\dfrac{\angle Z_{\ddot{u}_{kj}}(b) - \angle Z_{u_{kj}}(b)}{2} \right) \right|$.

It can be observed that only the values inside the domain D give the correct estimation.
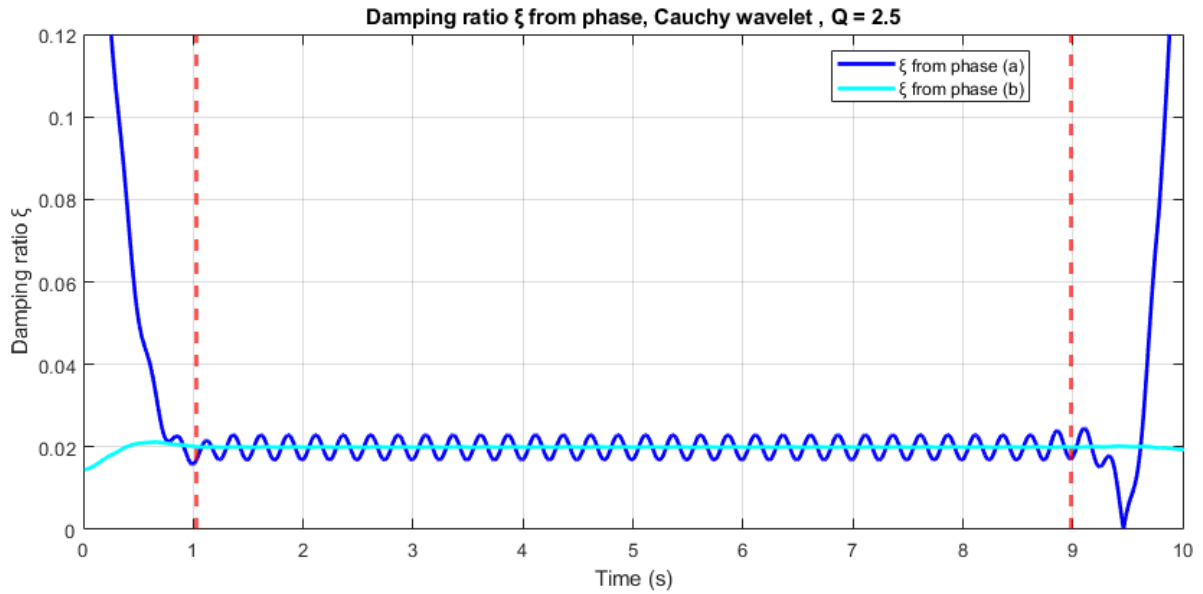

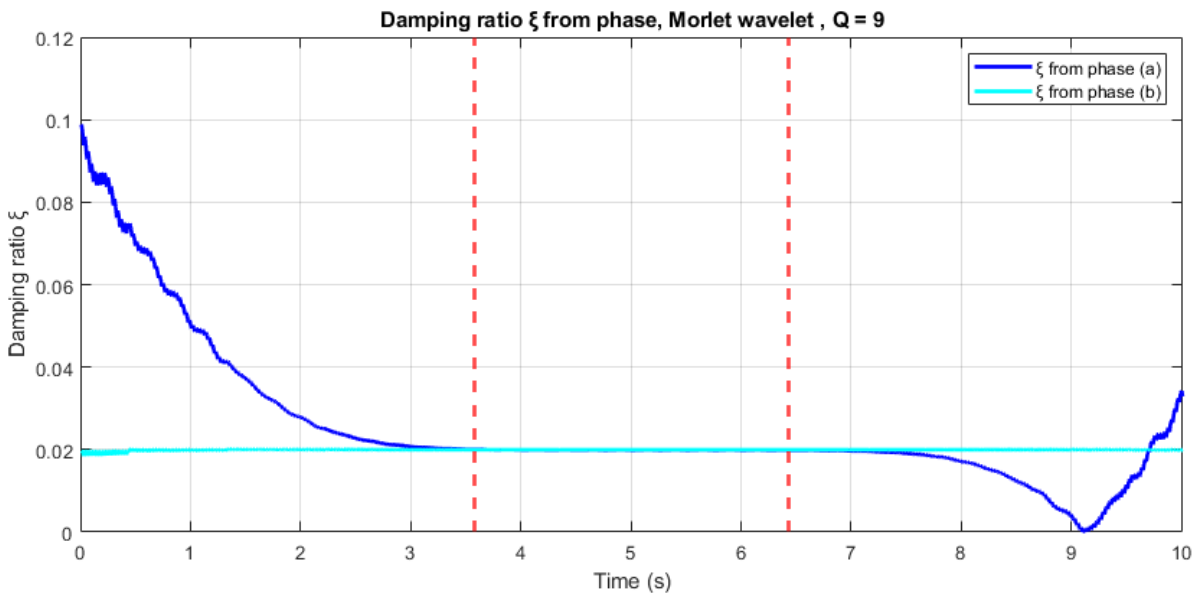Figure 6.18: Damping ratio ξ using the phase , Cauchy mother wavelet, $Q = 2.5$

Figure 6.19: Damping ratio ξ using the phase, signal $u(t)$, Morlet mother wavelet, $Q = 9.0$

6.1.6 *Signal* $u(t)$ *and* $Re\left[Z_{u_{kj}}(b)\right]$

The base of the whole definition of analytic signals is that $u(t) = Re\left[Z_{u_{kj}}(b)\right]$. This is confirmed in figures 6.20 and 6.21. As it can be observed the results are very close: the frequency modulation fits exactly, while the amplitudes for all values, except from the beginning because of the edge effects in the calculation of the CWT.
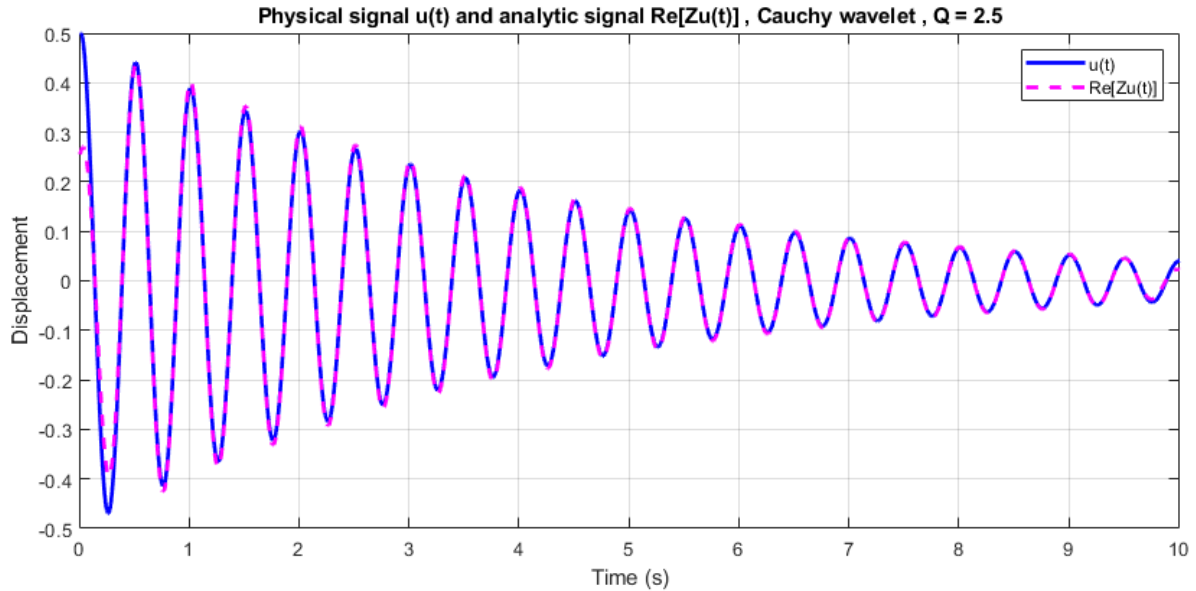

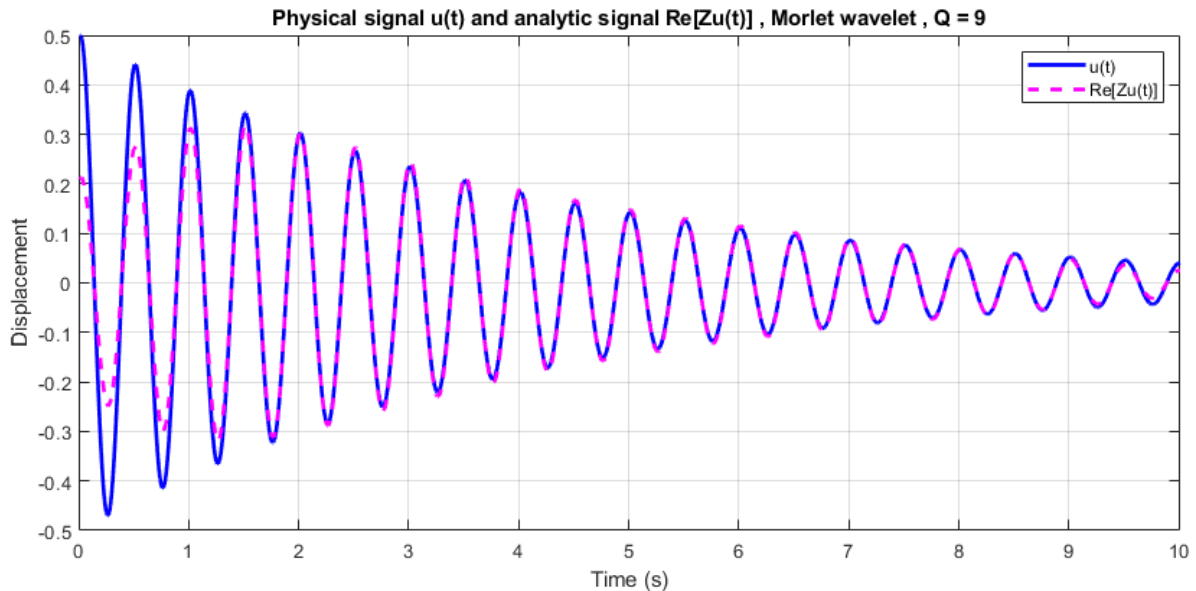Figure 6.20: Physical signal u(t) and Re[Zu(t)] comparison, Cauchy mother wavelet, $Q = 2.5$

Figure 6.21: Physical signal u(t) and Re[Zu(t)] comparison, signal $u(t)$, Morlet mother wavelet, $Q = 9.0$

6.1.7 *Modal parameter identification results*

The results obtained from the analysis are summarized in tables 6.9 and 6.10. As it can be observed, the estimated results for both mother wavelets are very close to the exact values, practically the same. Changing the values of Q (inside it's calculated bounds) the modal parameter identification results vary only on the third decimal point, therefore the methods and equations applied give steady results.

Table 6.2: s.d.o.f. modal parameter identification results - Natural frequency

Natural frequency f (Hz)						
Exact	Simple method		Marseille method		Z_u modulus eqn.	
	Cauchy	Morlet	Cauchy	Morlet	Cauchy	Morlet
2.0000	2.0072	1.9983	2.0012	2.0009	1.9956	1.9957

Table 6.3: s.d.o.f. modal parameter identification results - Damping ratio

Damping ratio ξ						
Exact	Slope method		Phase eqn.(a)		Phase eqn.(b)	
	Cauchy	Morlet	Cauchy	Morlet	Cauchy	Morlet
0.0200	0.0201	0.0200	0.0199	0.0199	0.0200	0.0200

Remark 6.1. The wavy form of (a) in figure 6.18 can be remedied by setting $Q = 3$, however the results are not affected.
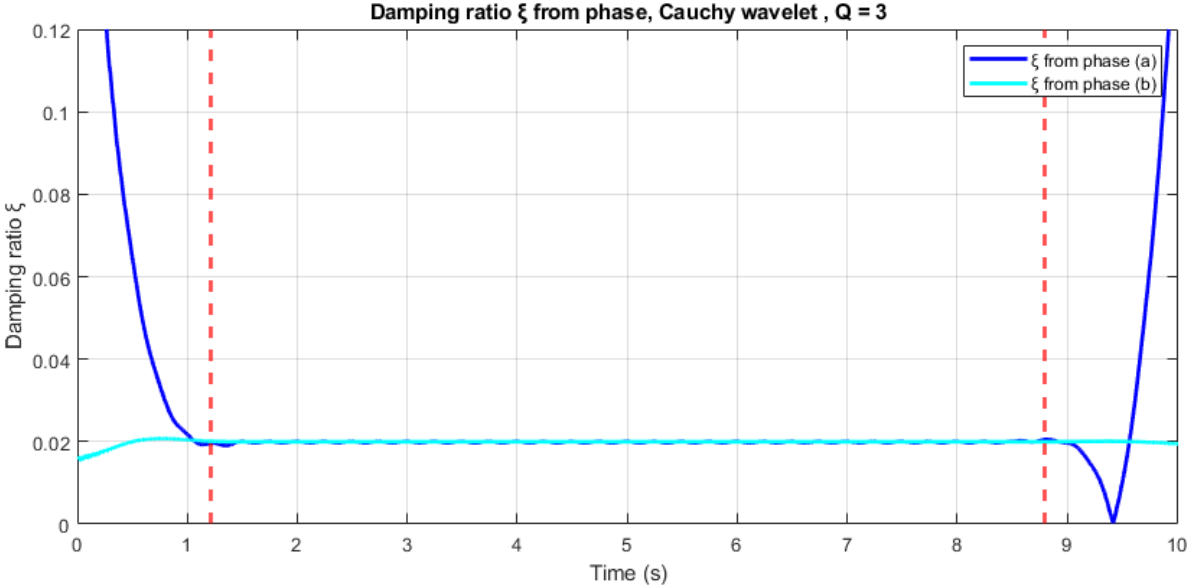

Figure 6.22: Damping ratio ξ using the phase, signal $u(t)$, Cauchy mother wavelet, $Q = 3$

6.2 Multi Degree of Freedom System

6.2.1 *The m.d.o.f. model*

Consider the mass-spring-damper system with four degrees of freedom, as shown in figure 6.23, with the characteristics presented in table 6.4. In order to obtain the free responses $u_k(t)$, $\dot{u}_k(t)$ and $\ddot{u}_k(t)$, $1 \leq k \leq 4$ of the four masses, the system is subjected to initial conditions:

$$\boldsymbol{u}(0) = [u_1(0) = 1.00,\ u_2(0) = 0.75,\ u_3(0) = 0.50,\ u_4(0) = 0.25]^T\ m$$
$$\dot{\boldsymbol{u}}(0) = 0 m/s.$$

The duration of the obtained signal is L=5 sec and the sampling period is dt=0.0049 sec. The displacement response is shown in figure 6.24.
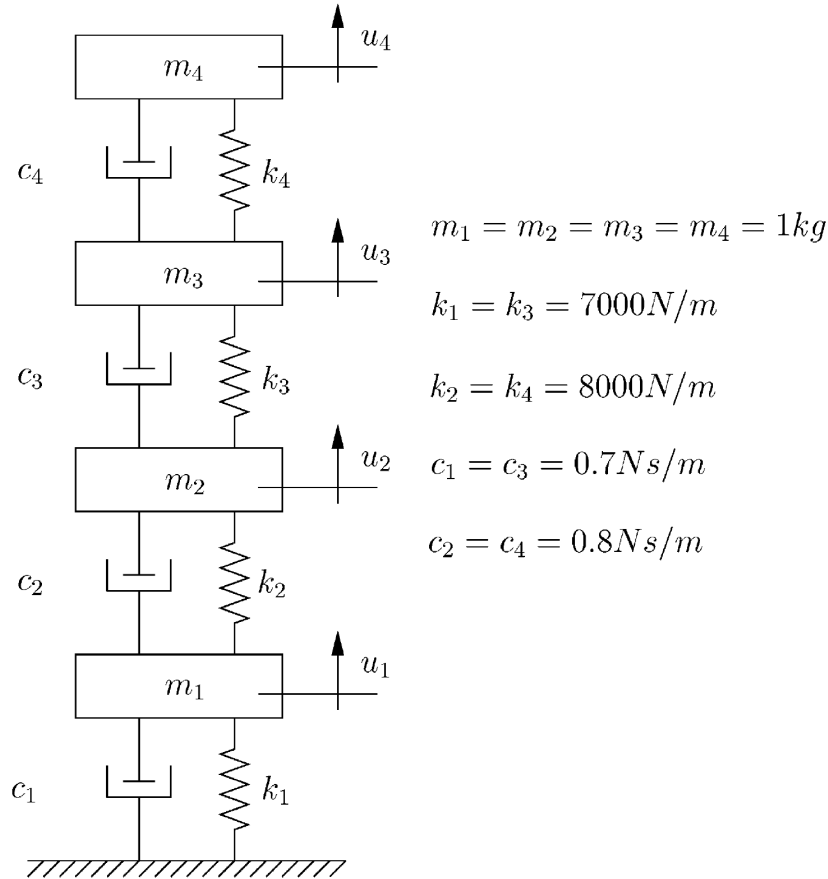

$$m_1 = m_2 = m_3 = m_4 = 1 kg$$

$$k_1 = k_3 = 7000 N/m$$

$$k_2 = k_4 = 8000 N/m$$

$$c_1 = c_3 = 0.7 N s/m$$

$$c_2 = c_4 = 0.8 N s/m$$

Figure 6.23: The test 4 d.o.f. system

<center>Table 6.4: Characteristics of the test 4 d.o.f. system</center>

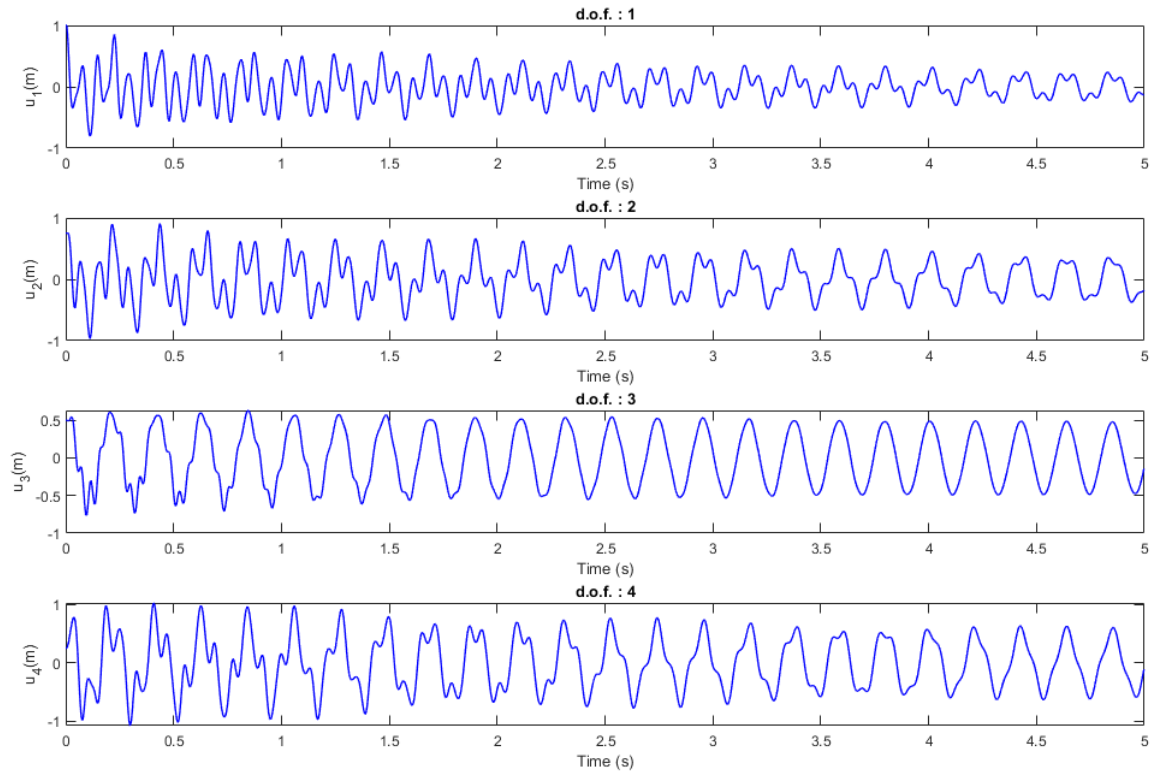|	
Natural frequencies	$f_1 = 4.7397\ Hz$ $f_2 = 13.5900\ Hz$ $f_3 = 21.5035\ Hz$ $f_4 = 25.9414\ Hz$
Damping ratios	$\xi_1 = 0.15\ \%$ $\xi_2 = 0.43\ \%$ $\xi_3 = 0.68\ \%$ $\xi_4 = 0.81\ \%$
Mode shapes $\boldsymbol{\Phi}=$	$\begin{bmatrix} 0.3683 & -1.0848 & 1.3441 & -1.8620 \\ 0.6498 & -1.0453 & -0.5468 & 2.6923 \\ 0.8891 & 0.0886 & -1.2818 & -2.3209 \\ 1.0000 & 1.0000 & 1.0000 & 1.0000 \end{bmatrix}$
Masses	$m_1 = m_2 = m_3 = m_4 = 1 kg$
Damping coefficients	$c_1 = c_3 = 0.7\ Ns/m$ $c_2 = c_4 = 0.8\ Ns/m$
Stiffness	$k_1 = k_3 = 7000\ N/m$ $k_2 = k_4 = 8000\ N/m$

Figure 6.24: Displacement responses $u_k(t)$ of the test 4 d.o.f. system

6.2.2 *Choice of Q*

The FFT results are illustrated in figure 6.25. Considering $c_f = c_t = 5$ and $d\omega_j = min[(\omega_j - \omega_{j-1}), (\omega_{j+1} - \omega_j)]$ for $1 \leq j \leq N$ with $\omega_0 = 0$, $\omega_{N+1} = 2\pi f_{Nyquist}$, the Q value is bounded and chosen for each mode as in table 6.5.
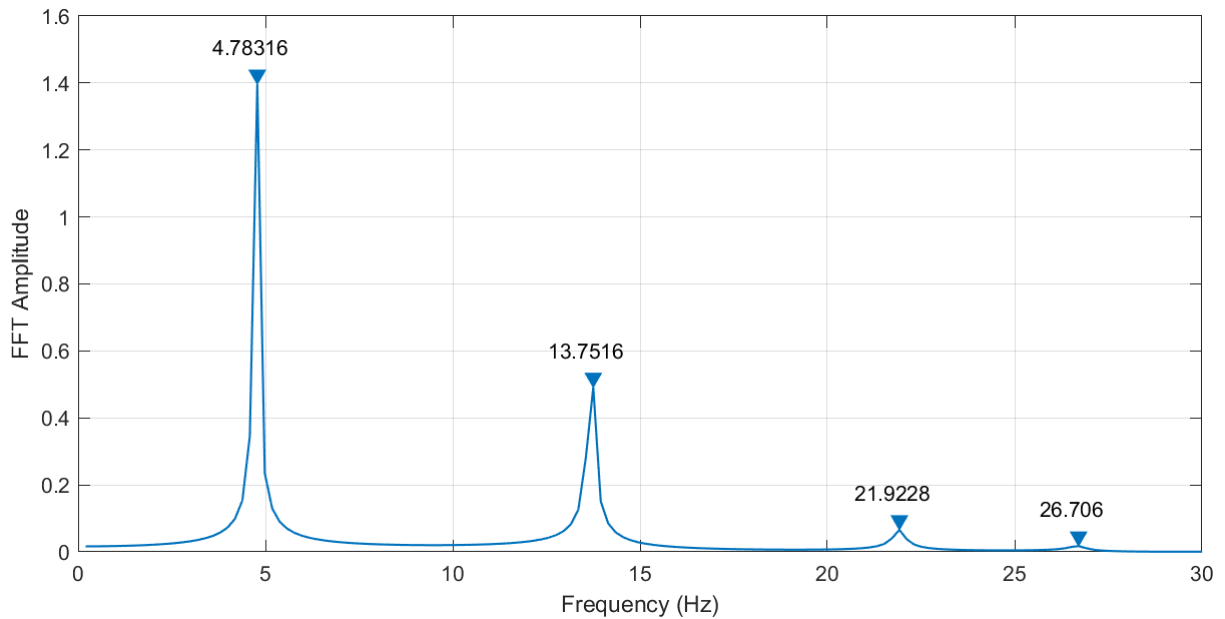

Figure 6.25: FFT results of the test 4 d.o.f. system

Table 6.5: Q values choice for the test 4 d.o.f. system

ω_j (rad/s)	$d\omega_j$ (rad/s)	bounds	Q_j
10π	10π	$2.500 \leq Q \leq 15.708$	$Q_1 = 8$
27π	17π	$3.971 \leq Q \leq 42.412$	$Q_2 = 20$
42π	10π	$10.500 \leq Q \leq 65.973$	$Q_3 = 30$
52π	10π	$13.000 \leq Q \leq 81.681$	$Q_4 = 30$

6.2.3 CWT results

The CWT of the signal $u(t)$ is then calculated, the results are the following:
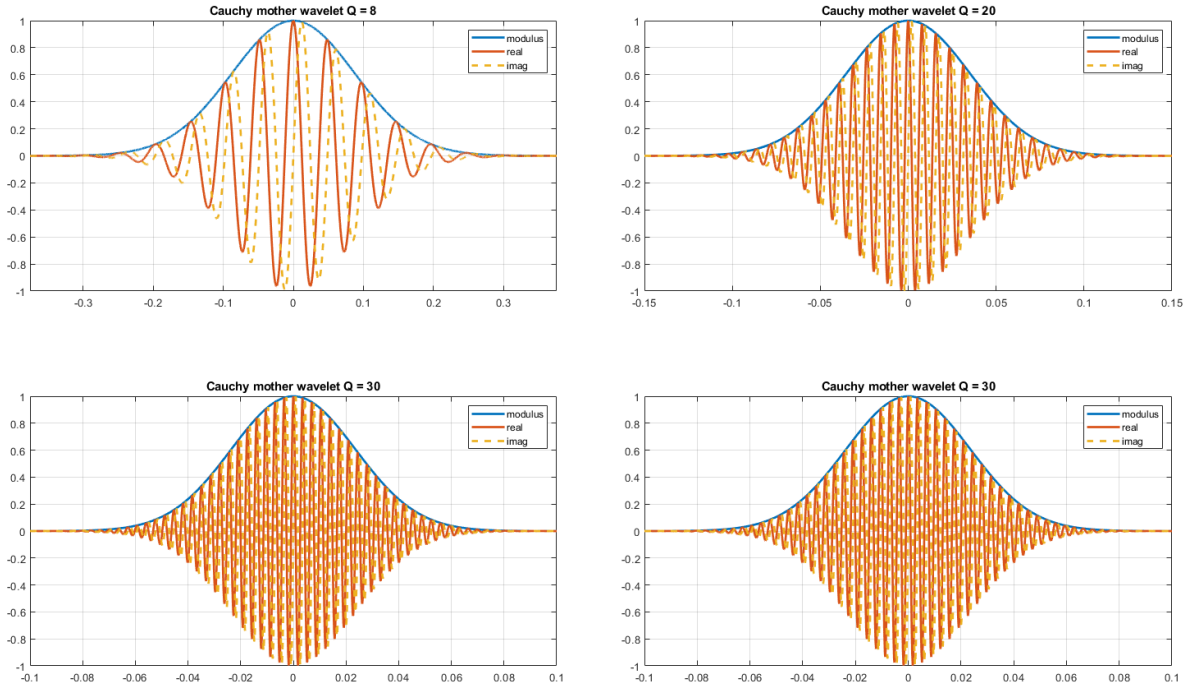
- **Cauchy wavelet**

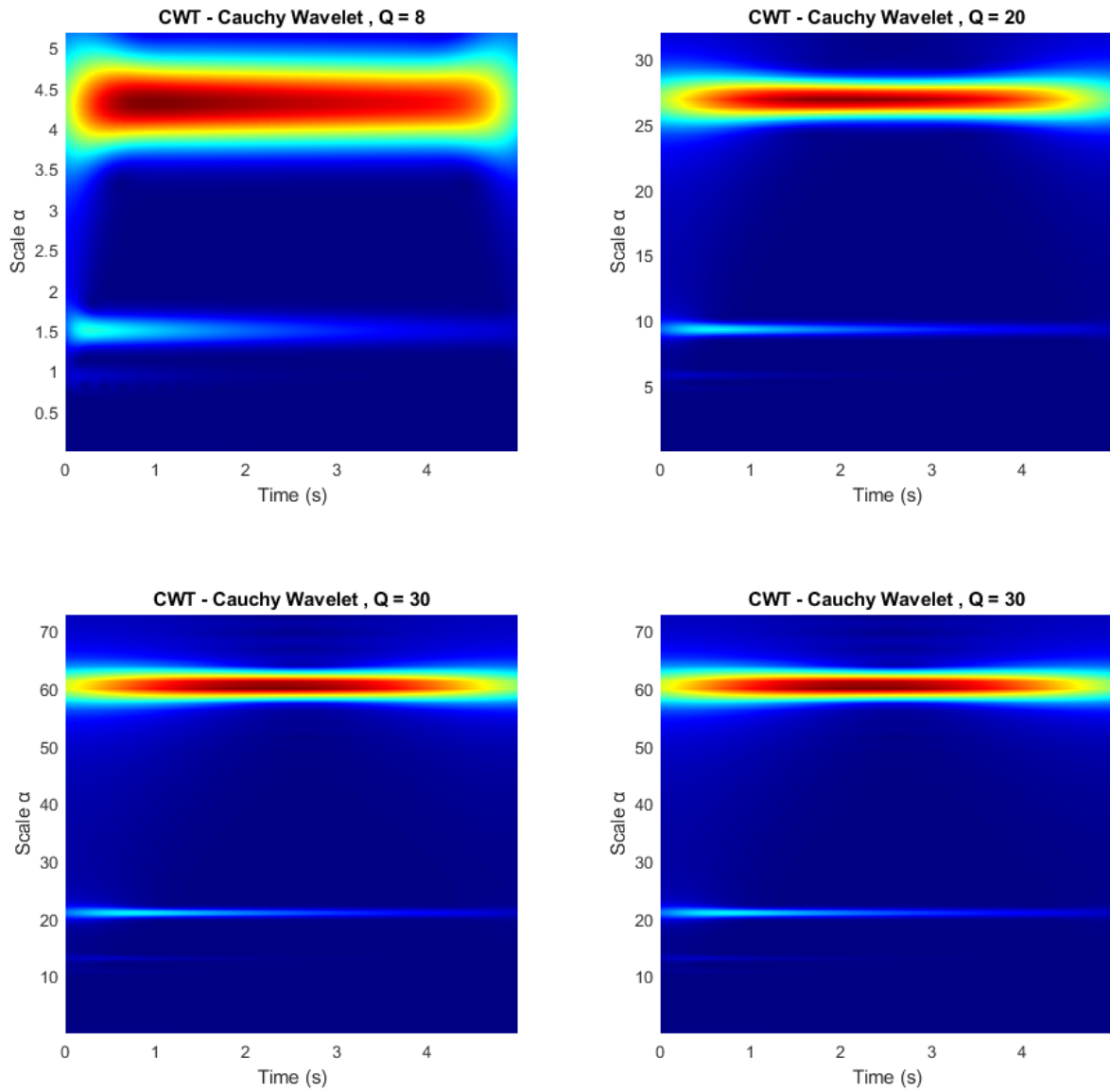Figure 6.26: The Cauchy mother wavelets for different Q values

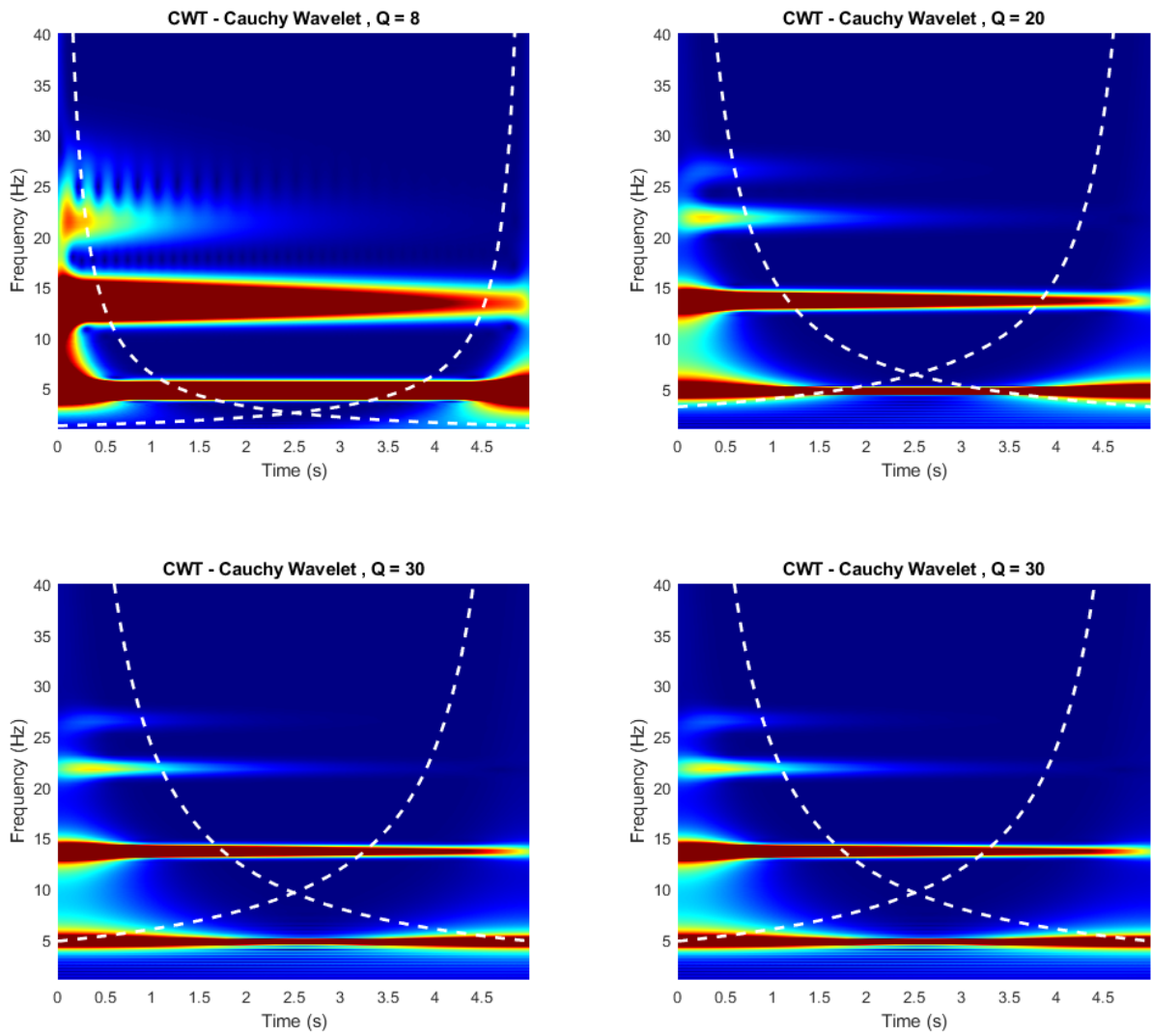Figure 6.27: CWT Modulus Scalogram for each mode, signal $u(t)$, Cauchy mother wavelet

Figure 6.28: CWT Modulus Time-Frequency plot for each mode, signal $u(t)$, Cauchy mother wavelet
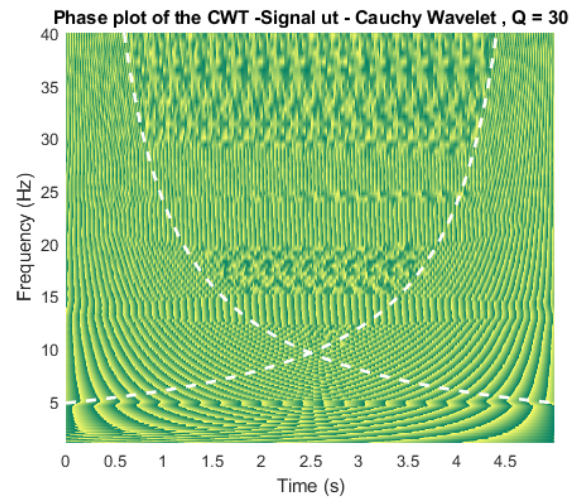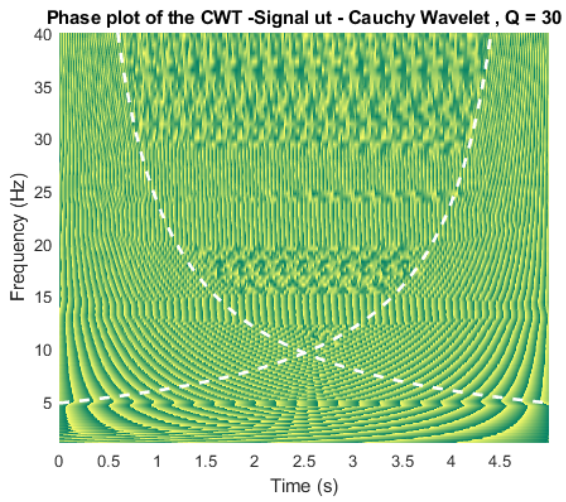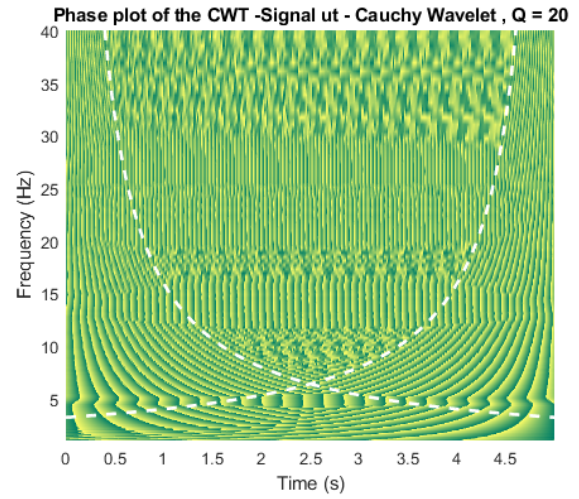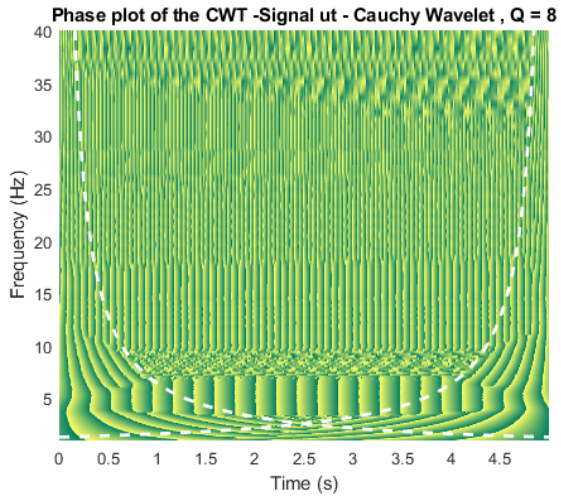
Figure 6.29: CWT Phase Time-Frequency plot for each mode, signal $u(t)$, Cauchy mother wavelet

6.2.4 Frequency Estimation

- **Estimation from modulus**
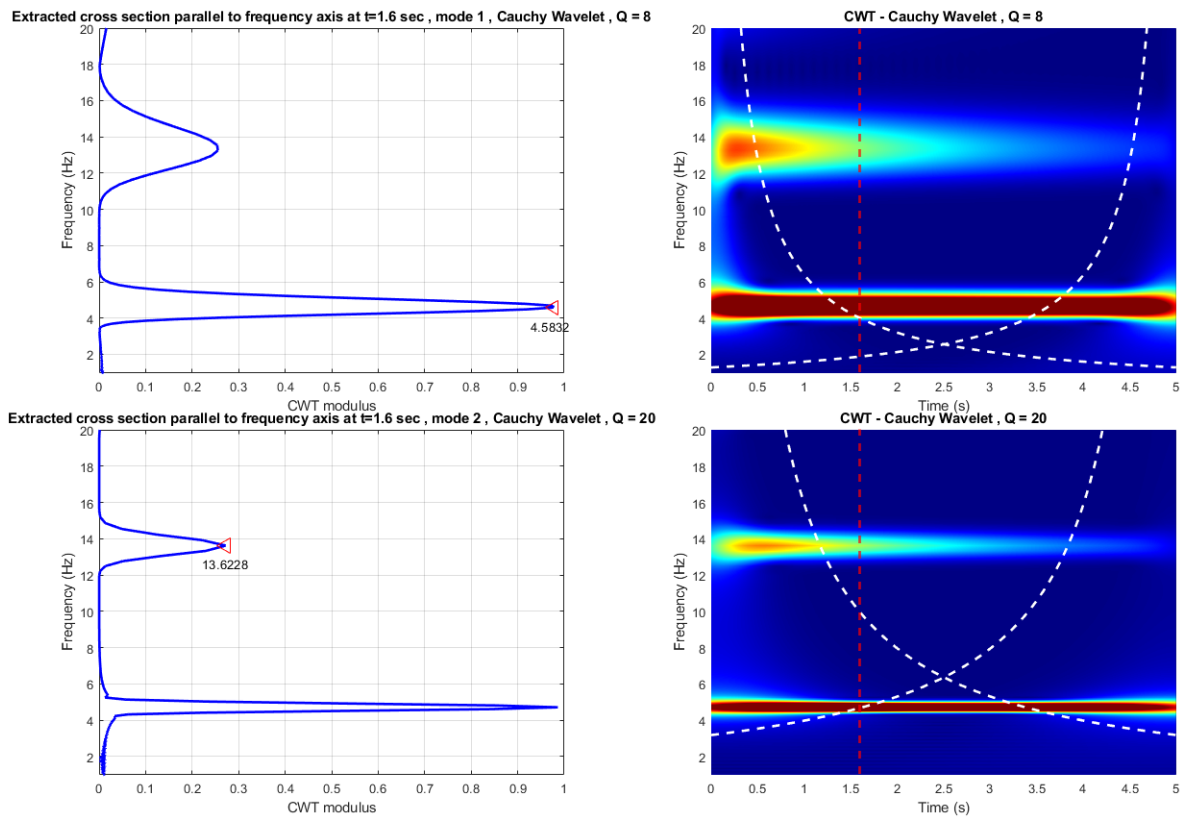
Figure 6.30: Cross section of the modulus plot parallel to the frequency axis for modes 1 and 2, signal $u(t)$, Cauchy mother wavelet
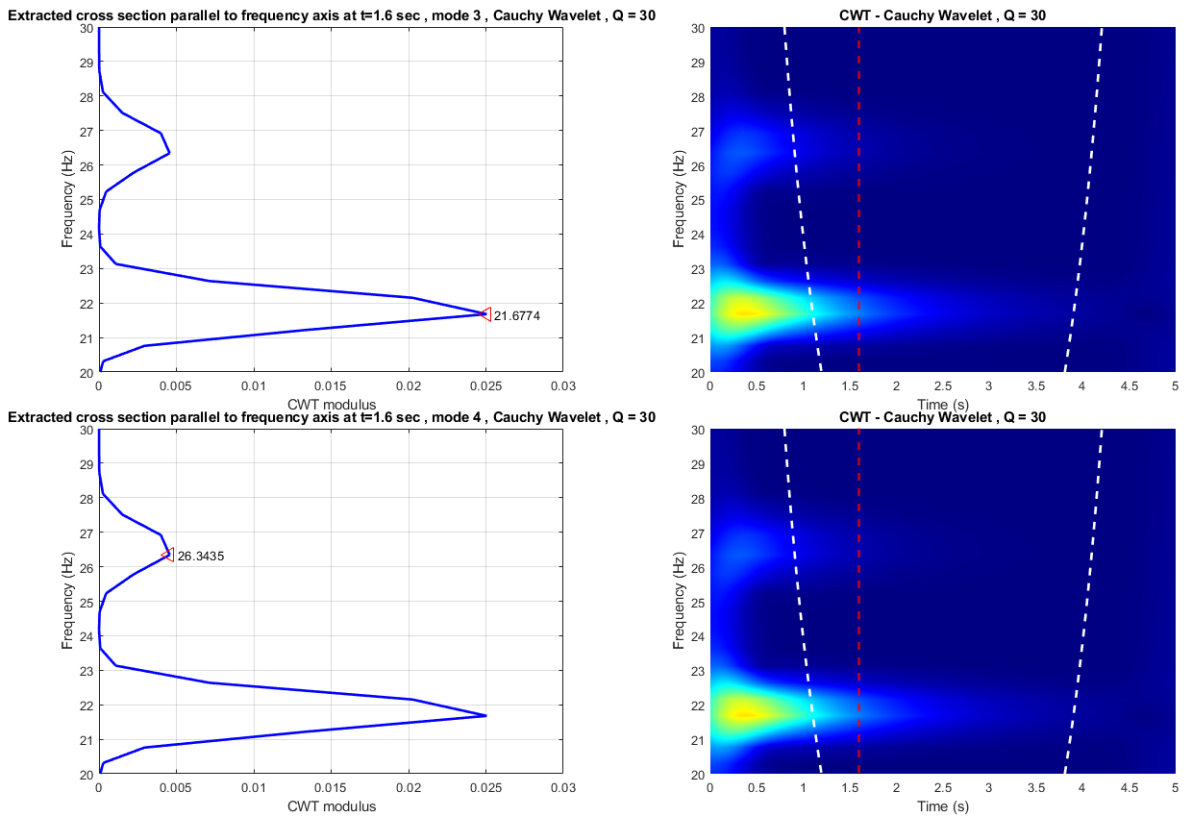
Figure 6.31: Cross section of the modulus plot parallel to the frequency axis for modes 3 and 4, signal $u(t)$, Cauchy mother wavelet

- **_Estimation from phase_**
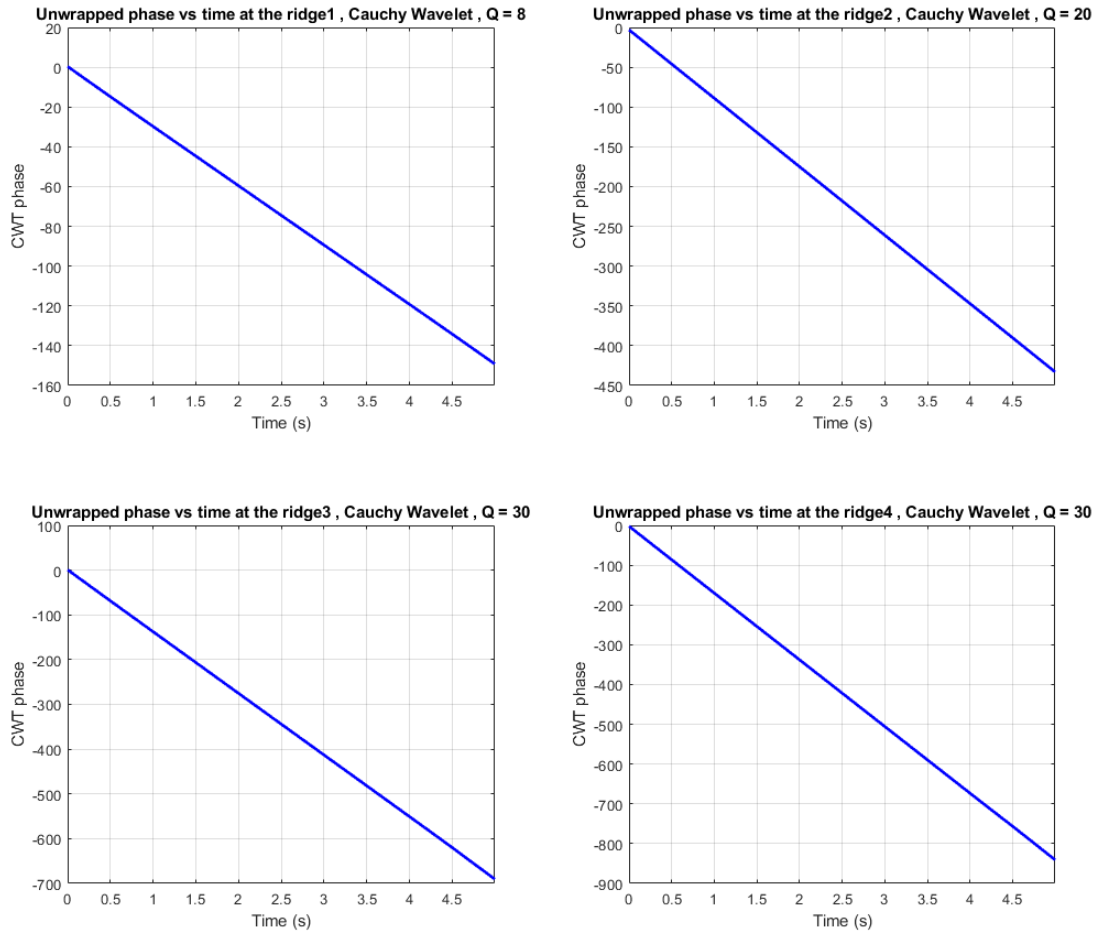
Figure 6.32: Damping ratio ξ for all the modes using the phase, Cauchy mother wavelet

6.2.5 Damping Ratio Estimation

- **Estimation from modulus**
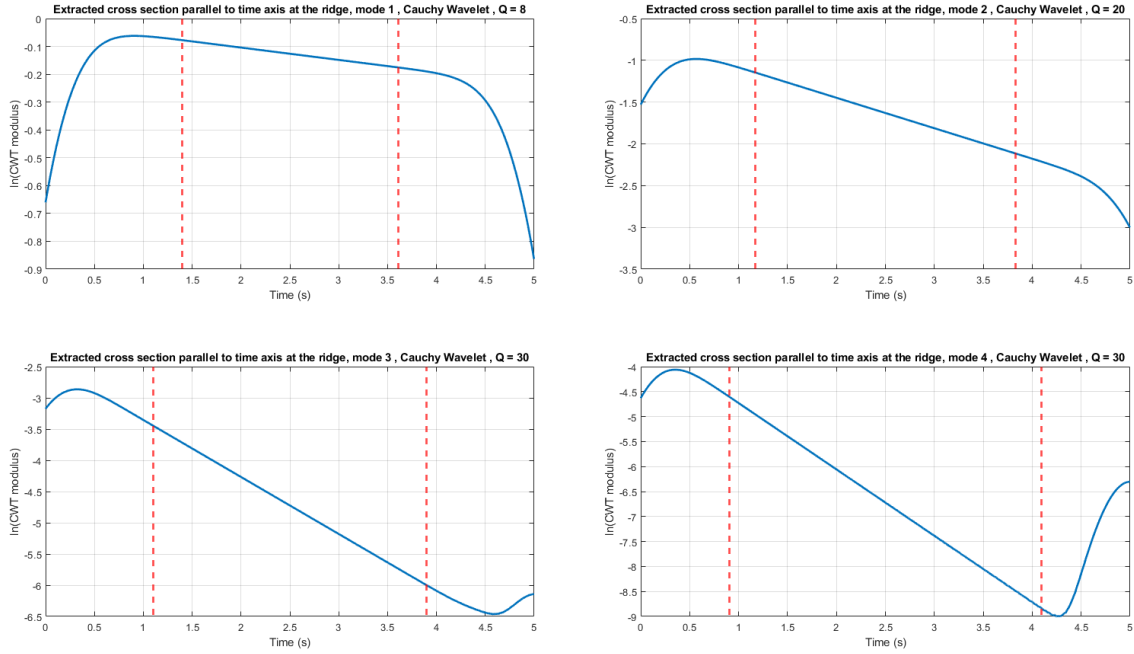
Figure 6.33: Logarithm of the cross section of the modulus plot parallel to the time axis at the ridge for all the modes, signal $u(t)$, Cauchy mother wavelet

- **Estimation from phase**
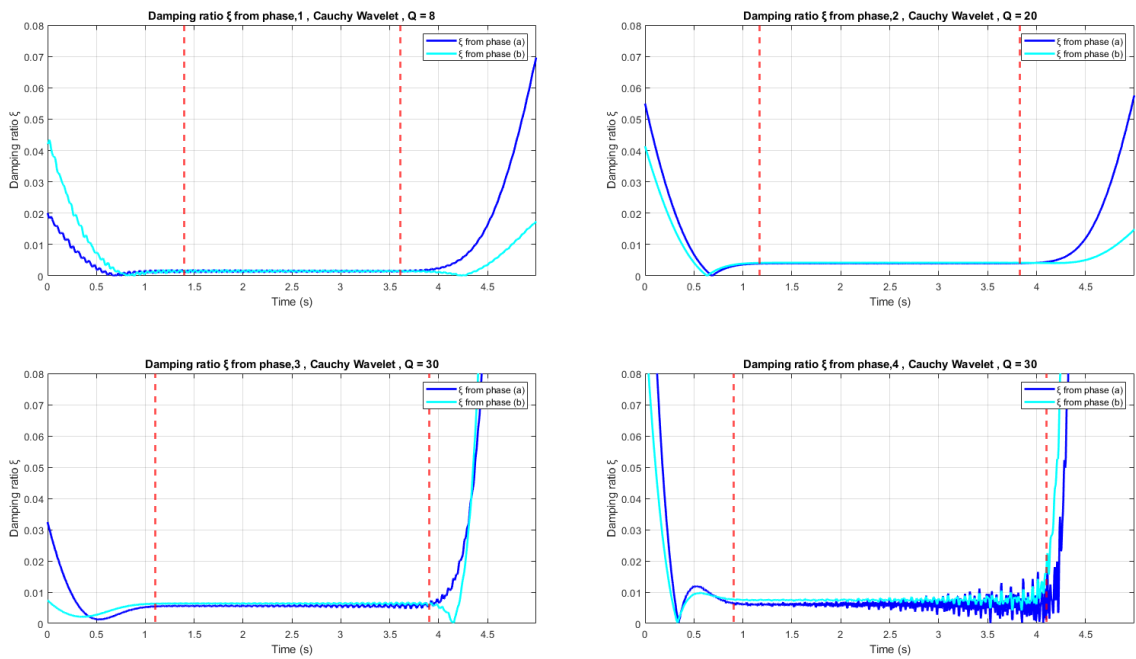
Figure 6.34: Damping ratio ξ for all the modes using the phase, Cauchy mother wavelet

6.2.6 Mode Shape Estimation
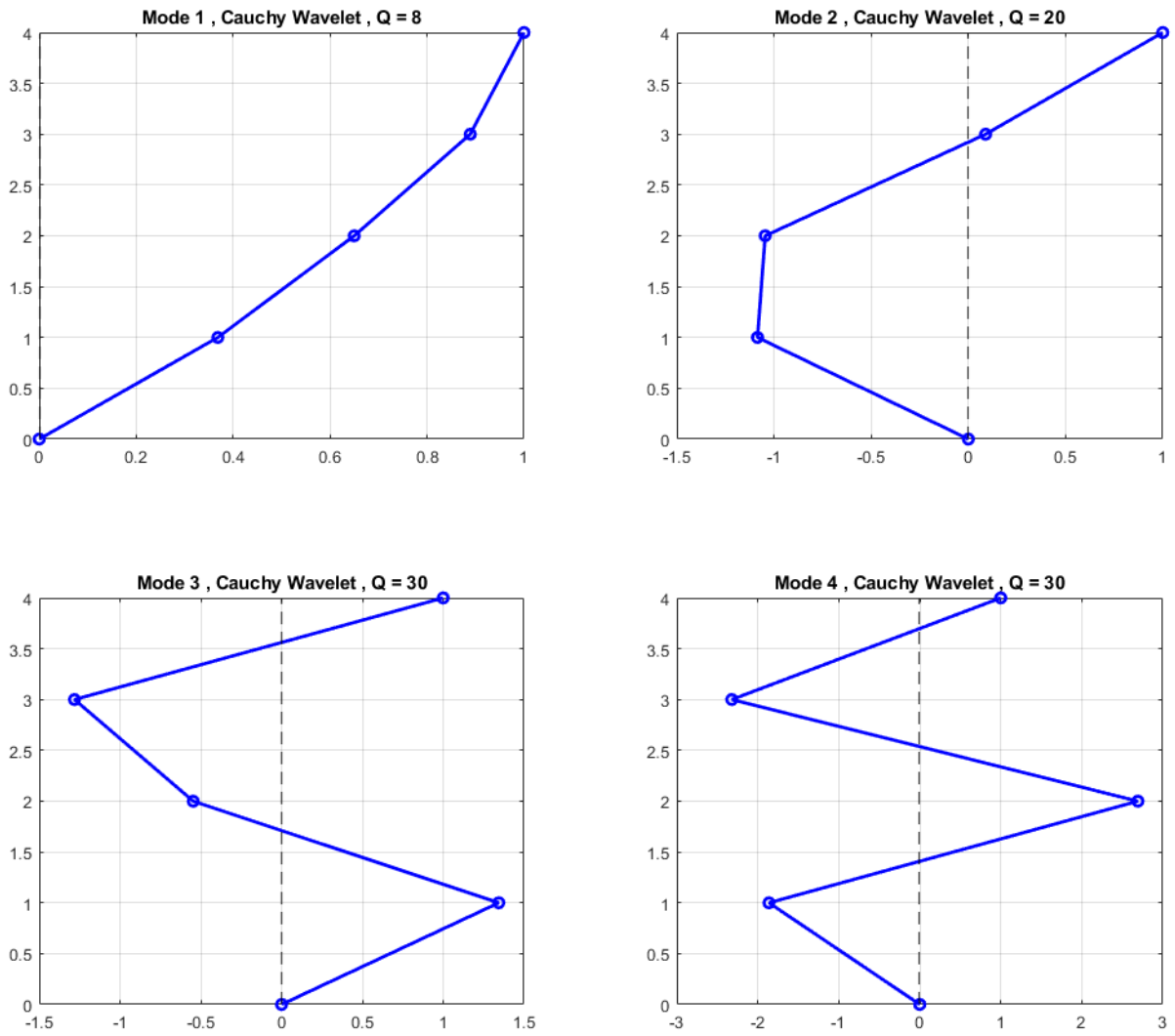
Figure 6.35: Estimated mode shapes, signal $u(t)$, Cauchy mother wavelet

6.2.7 *Modal parameter identification results*

Table 6.6: m.d.o.f. modal parameter identification results - Natural frequencies

Natural frequencies f (Hz)				
Cauchy wavelet				
Mode	**Exact**	**Simple method**	**Marseille method**	Z_u **modulus eqn.**
1	4.74	4.58	4.74	4.73
2	13.59	13.63	13.69	13.23
3	21.50	21.68	21.92	20.29
4	25.94	26.34	26.67	23.78

Table 6.7: m.d.o.f. modal parameter identification results - Damping ratios

Damping ratios ξ				
Cauchy wavelet				
Mode	**Exact**	**Slope method**	**Phase eqn.(a)**	**Phase eqn.(b)**
1	0.0015	0.0015	0.0015	0.0015
2	0.0043	0.0042	0.0040	0.0042
3	0.0068	0.0066	0.0056	0.0064
4	0.0081	0.0079	0.0061	0.0075

Table 6.8: Mode shapes of the test 4 d.o.f. system

Mode shapes Φ	
Cauchy wavelet	
Exact values	Estimated values

$$\begin{bmatrix} 0.3683 & -1.0848 & 1.3441 & -1.8620 \\ 0.6498 & -1.0453 & -0.5468 & 2.6923 \\ 0.8891 & 0.0886 & -1.2818 & -2.3209 \\ 1.0000 & 1.0000 & 1.0000 & 1.0000 \end{bmatrix} \qquad \begin{bmatrix} 0.3683 & -1.0848 & 1.3441 & -1.8617 \\ 0.6498 & -1.0453 & -0.5469 & 2.6922 \\ 0.8891 & 0.0886 & -1.2819 & -2.3207 \\ 1.0000 & 1.0000 & 1.0000 & 1.0000 \end{bmatrix}$$

Consequently, one can make the following remarks:

1. In figure 6.28 can be observed that Q factor affects the edge effects: The higher the Q, the more significant the edge effects, confirming the theory.

2. In figure 6.28 can also be observed that Q factor allows for mode uncoupling: For $Q = 8$, modes 1 and 2 can be easily distinguished, but modes 3 and 4 are coupled. For a higher Q these two modes start to uncouple, but the lower modes are found outside the domain D. Consequently, the first mode is estimated for $Q = 8$, the second for $Q = 20$, and the third and the fourth for $Q = 30$ where these two modes are clearly distinguishable.

3. The estimated natural frequencies are very close to the exact values. Some small differences appear for the 4th mode.

4. Simple method and Marseille method work very well. Conversely, the built in MATLAB commands findpeaks and tfridge do not detect the frequencies of mode 3 and 4.

5. The estimated damping ratios with the slope method are very close to the exact values. The estimated damping ratios from phase do have a small difference with the exact values for higher modes, especially for equation a.

6. One additional observation is that equations (a) $\xi_j = |\angle Z_{u_{kj}}(b) - \angle Z_{\dot{u}_{kj}}(b)|$ and (b) $\xi_j = \left| \cos\left(\frac{\angle Z_{\ddot{u}_{kj}}(b) - \angle Z_{u_{kj}}(b)}{2} \right) \right|$ are very sensitive to the value of the Q, i.e. as the Q increases, they become more distorted.

7. Mode shape identification is very successful as the estimated values are practically the same with the exact values.

8. Similar results for the same problem are obtained from Le-Argoul [13].

6.2.8   Signal $u(t)$ and $Re\left[Z_{u_{kj}}(b)\right]$

The value of Q affects only the amplitude of the analytic signal, thus for a particular value of Q, $u(t) = Z_u(t)$. One example is shown in figure 6.36 for the 4th d.o.f.
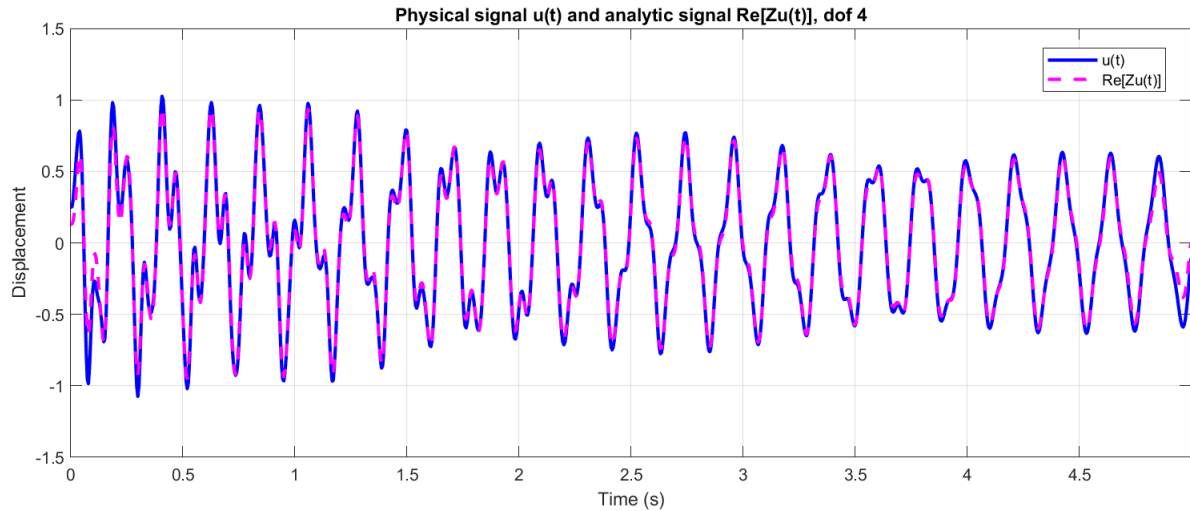
Figure 6.36: Signal $u(t)$ and $Re\left[Z_{u_{kj}}(b)\right]$ of the 4th d.o.f., Cauchy mother wavelet

6.2.9   Morlet Wavelet

For the Morlet wavelet, the previously selected values of Q do not perform well. New values $Q_1 = 9$, $Q_2 = 15$, $Q_3 = 20$ and varying Q_4, are selected and the following conclusions are obtained:

1. The Simple method estimates accurately the frequencies for all the modes.

2. The Marseille method estimates accurately the frequencies for modes 1,2,3 and fails completely for mode 4.

3. Using the modulus ratio of the analytic signals also estimates accurately the frequencies for modes 1,2,3 but has a difference for mode 4 (but the same happens with the Cauchy wavelet too in this case).

4. The damping ratios are estimated accurately only for modes 1 and 2.

5. The mode shapes are estimated accurately.

Table 6.9: m.d.o.f. modal parameter identification results - Natural frequencies

Natural frequencies f (Hz)				
Morlet wavelet				
Mode	**Exact**	**Simple method**	**Marseille method**	Z_u **modulus eqn.**
1	4.74	4.74	4.74	4.73
2	13.59	13.63	13.69	13.29
3	21.50	21.95	21.92	20.29
4	25.94	26.56	11.7244	23.23

Table 6.10: m.d.o.f. modal parameter identification results - Damping ratios

Damping ratios ξ				
Morlet wavelet				
Mode	**Exact**	**Slope method**	**Phase eqn.(a)**	**Phase eqn.(b)**
1	0.0015	0.0016	0.0016	0.0015
2	0.0043	0.0042	0.0040	0.0042
3	0.0068	0.0086	0.0081	0.0067
4	0.0081	0.1945	0.0843	0.0506

Table 6.11: Mode shapes of the test 4 d.o.f. system

Mode shapes Φ	
Morlet wavelet	
Exact values	**Estimated values**

$$\begin{bmatrix} 0.3683 & -1.0848 & 1.3441 & -1.8620 \\ 0.6498 & -1.0453 & -0.5468 & 2.6923 \\ 0.8891 & 0.0886 & -1.2818 & -2.3209 \\ 1.0000 & 1.0000 & 1.0000 & 1.0000 \end{bmatrix} \qquad \begin{bmatrix} 0.3683 & -1.0848 & 1.3443 & -1.8467 \\ 0.6498 & -1.0453 & -0.5468 & 2.6735 \\ 0.8891 & 0.0886 & -1.2824 & -2.3073 \\ 1.0000 & 1.0000 & 1.0000 & 1.0000 \end{bmatrix}$$

Chapter 7

Conclusions and Remarks

7.1 Mother wavelet choice

The two chosen mother wavelets were the Complex Morlet wavelet and the Cauchy wavelet of order n. These two wavelets were selected because of the following reasons:

1. They are admissible.

2. They are both complex,progressive wavelets. Consequently, the CWT results are also complex, which allows to extract the information about the modulus of the CWT to implement the Simple method and the the phase of the CWT to implement the Marseille method, and to reconstruct the signal $u(t)$.

3. They have good time and frequency localization properties.

4. They reflect the type of features present in the time series as they are waveforms with an increased number of oscillations.

5. They have parameters in their definitions that strongly influence the localization properties, which enables their tuning with the Q factor.

Both wavelets worked well on the s.d.o.f. system, however, for the m.d.o.f. system, the Cauchy wavelet estimates all modal parameters for all modes accurately, while the Morlet wavelet had some differences for the damping ratios of the 3rd and 4^{rth} mode. Therefor, they are appropriate for modal parameter identification.

7.2 Methods evaluation

Time-frequency analysis of vibration responses with the CWT is effective, as:

1. CWT is an effective tool for the modal parameter identification of s.d.o.f. and m.d.o.f. damped systems from their free decay responses.

2. CWT is a linear transform by definition and thus, appropriate for the analysis of multi-component signals.

3. CWT has an inherent multi-resolution ability. This property enables the separation of the close frequency components of a coupled frequency signal.

4. CWT can be used to analyze effectively non-stationary vibration measurements as the free responses of a damped system.

5. CWT can identify multiple structural parameters from a single signal without knowledge of the applied force acting on the structure.

6. CWT with complex mother wavelets allows to determine the time variation of instantaneous amplitude and phase of each component within the signal a property that facilitates the modal parameter identification procedure.

Factors to be considered in the implementation of the CWT are:

1. The choice of proper sampling frequency to avoid aliasing.

2. The choice of proper scale range to cover all the frequency content of the signal.

3. The mother wavelet choice.

4. The effective delimitation of the edge effects.

7.3 Q factor

The role of the Q parameter in the CWT analysis can be summarized as:

1. Q is a useful parameter that can be utilized to define the parameters of mother wavelets, in order to ameliorate the modal parameter identification using the CWT. Higher Q produce narrower wavelets, with more oscillations within their waveform. Consequently, the application of the CWT with a high Q factor allows a multiscale analysis with high frequency resolution (at the expense of a lower time resolution), making it appropriate for analyzing oscillatory signals such as the responses of a structure.

2. With a proper choice of the parameter Q, mode decoupling can be achieved. Consequently, for multicomonent signals, any mode can be isolated and the modal identification procedure can be performed on the amplitude and phase of one component separately as it is for a monocomponent signal.

3. Q factor affects the edge effects: The higher the Q, the more significant the edge effects. However, by expressing the delimiting equations in relation to Q the useful domain D can be defined correctly.

7.4 Additional work

This thesis can be further developed by exploring the addition of noise, the use of ambient vibrations, forced vibrations and the insertion of structural damage (e.g. decrease of stiffness) in the analysis.

Chapter 8

Bibliography

[1] Boashash B., (2016). "Time-Frequency Signal Analysis and Processing, A Comprehensive Reference", 2nd Ed., Academic Press.

[2] Carmona R., Hwang W-L., Torrésani B. (1998). "Practical Time–Frequency Analysis, Gabor and Wavelet Transforms with an Implementation in S", Wavelet Analysis and its Applications, Vol. 9, Academic Press.

[3] Chui C.K., in: Charles K. Chui (Ed.) (1991). "An Introduction to Wavelets", Academic Press.

[4] Chopra A.K. (2011). "Dynamics of Structures: Theory and Applications to Earthquake Engineering", 4rth Ed., Pearson Education Inc, New Jersey.

[5] Daubechies, I. (1990). "The wavelet transform time-frequency localization and signal analysis", IEEE Trans. Inform. Theory, 36, 961–1004.

[6] Debnath L. (2002). "Wavelet Transforms and Their Applications", Birkhäuser Boston.

[7] Delprat N., Escudie B., Guillemain P., Ronland-martinet R.K., Tchamichian Ph., Torrésani B. (1992). "Asymptotic wavelet and Gabor analysis: extraction of instantaneous frequencies", IEEE 38 , 644–664.

[8] Fragiadakis M., "Nonlinear Analysis of Frame Structures under Seismic Loading", lecture notes, October 2020, ADERS 2020-2021.

[9] Gram-Hansen K., Dorize K., "On the choice of parameters for time–frequency analysis", in: Y. Meyer (Ed.), Wavelets and Applications, Proceedings of the International Conference, Masson, Parts, 1991, pp. 86–92.

[10] Harris F.J. (1978). "On the Use of Windows for Harmonic Analysis with the Discrete Fourier Transform", Proceedings of the IEEE 66, no. 1, 51–83.

[11] Kaiser G. (2011). "A Friendly Guide to Wavelets", 1st Ed., Modern Birkhäuser Classics, Birkhäuser Boston.

[12] LaTeX – A document preparation system.

[13] Le T-P., Argoul P. (2004). "Continuous wavelet transform for modal identification using free decay response", Journal of Sound and Vibration , 277, 73-100.

[14] Le T-P. (2003). "Auscultation Dynamique des Structures á l'Aide de l'Analyse continue en Ondelettes" , Ph.D. Thesis, ENPC.

[15] Lilly J. M. (2017). "Element analysis: a wavelet-based method for analysing time-localized events in noisy time series." Proceedings of the Royal Society A. Volume 473: 20160776, pp. 1–28.

[16] Liner C. (2010). An overview of wavelet transform concepts and applications, University of Houston, 1–17, 26.

[17] Ljung L., Glover K. (1981). Frequency domain versus time domain methods in system identification, Automatica, Volume 17, Issue 1,Pages 71-86.

[18] Stein E.M., Shakarchi R. (2011). Functional Analysis, Introduction to Further Topics in Analysis, Princeton University Press.

[19] Maia N.M.M., Silva J.M.M., He N., Jlieven N.A., Lin R.M. , Skingle G.W., To W-M., Urgueira A.P.V., (1998) *"Theoretical and Experimental Modal Analysis"*, Research Studies Press Ltd., Hertfordshire.

[20] MathWorks, MATLAB version 2021a [Computer Program].

[21] MathWorks Official Site : MATLAB documentation, answers, file exchanges.

[22] Misiti M., Misiti Y., Oppenheim G., Poggi J.M.: Wavelet Toolbox: Getting started ver.R2021b, MathWorks.

[23] Misiti M., Misiti Y., Oppenheim G., Poggi J.M.: Wavelet Toolbox: User's guide ver.R2021b, MathWorks.

[24] MathWorks: Signal Processing Toolbox: User's guide ver.R2021b, MathWorks.

[25] Morlet J., (1980). "Sampling theory and wave propagation", Proceedings of the 51st Annual Meeting Soc. Explor. Geophys. Los Angeles.

[26] Grossmann A., Morlet J. (1985). "Decomposition of functions into wavelets of constant shape, and related transforms", In: Mathematics and Physics, Lecture on Recent Results L. Streit, Editor. World Scientific Publishing (Singapore).

[27] Najmi A.-H., Sadowsky J. (1997). "The Continuous Wavelet Transform and Variable Resolution Time-Frequency Analysis",Johns Hopkins APLTech. Dig.,18, 134–140.

[28] Nobach H., Tropea C., Cordier L., Bonnet J. P., Delville J., Lewalle J., Farge M., Schneider K., and R. J. Adrian (2007). "Review of Some Fundamentals of Data Processing." Springer Handbook of Experimental Fluid Mechanics (C. Tropea, A. L. Yarin, and J. F. Foss, eds.). Berlin, Heidelberg: Springer, pp. 1337–1398.

[29] Pérez-Ramírez C., Amezquita-Sanchez J., Adeli H., Valtierra-Rodriguez M., Romero-Troncoso R., Dominguez - Gonzalez A., Osornio-Rios R. (2016). Time-frequency techniques for modal parameters identification of civil structures from acquired dynamic signals, Journal of Vibroengineering, Vol. 18, Issue 5, 2016, p. 3164-3185.

[30] Signal Processing in Earthquake Engineering, lecture notes, course taught by Fragiadakis M. and Taflampas I., ADERS 2020-2021.

[31] Proakis J.G., Manolakis D.G. (1996). "Digital Signal Processing: principles, algorithms and applications, 3rd Ed., Prentice-Hall, Inc., New Jersey.

[32] Reda Taha M. M. (2006). "Wavelet Transform for Structural Health Monitoring: A Compendium of Uses and Features", International Journal - STRUCT HEALTH MONIT. 5. 267-295.

[33] Todorovska M. (2001). "Estimation of Instantaneous Frequency of Signals Using the Continuous Wavelet Transform" , Technical Report CE 01-07, University of Southern California, Los Angeles.

[34] Torrence C., Compo G.P. (1998). "A Practical Guide to Wavelet Analysis", Bulletin of the American Meteorological Society, Vol. 79(1):61-78.

[35] Tuzlukov V. (2010), "Signal Processing Noise", Electrical Engineering and Applied Signal Processing Series, CRC Press.

Additional literature on modal parameter identification with the CWT in chronological order:

[36] Staszewski W.J., Cooper J.E. (1995). "Flutter data analysis using the wavelet transform", Proceedings of the international congress MV2: new advances in modal synthesis of large structures, non linear, damped and non deterministic cases. Lyon, France, 5–6 October 2 1995, 549–561.

[37] Staszewski W.J. (1997). "Identification of damping in mdof systems using time-scale decomposition", J. Sound Vib.203 , 283–305.

[38] Staszewski W.J. (1998). Identification of non-linear systems using multi-scale ridges and skeletons of the wavelet transform, Journal of Sound and Vibration 214 , 639–658.

[39] Ruzzene M., Fasana A., Garibaldi L., Piombo B. (1997). "Natural frequencies and dampings identification using wavelet transform: application to real data", Mech. Syst. Signal Process. 11 (2),207–218.

[40] Argoul P., Hans S., Conti F., Boutin C. (2000). Time–frequency analysis of free oscillations of mechanical structures. Application to the identification of the mechanical behavior of buildings under shocks, in: Proceedings of the COST F3 Conference: System Identification and Structural Health Monitoring, Madrid, Spain, pp. 283–292.

[41] Lamarque C.H., Pernot S., Cuer A. (2000). "Damping identification in multi-degree-of-freedom systems via a wavelet-logarithmic decrement – Part 1 theory", J. Sound Vib. 235 (3) 361–374.

[42] Lardies J., Gouttebroze S. (2002). "Identification of modal parameters using the wavelet transform", Int. J. Mech. Sci. 44 (11) 2263–2283.

[43] Argoul P., Le T-P. (2003). Instantaneous indicators of structural behaviour based on continuous Cauchy wavelet, transform, Mechanical Systems and Signal Processing 17 , 243–250.

[44] Kijewski T., Kareem T. (2003). "Wavelet transforms for system identification in civil engineering", Comput.-Aided Civ. Infrastruct. Eng. 18 (5) 339–355.

[45] Slavic I., Simonovski I, Boltezar M. (2003). "Damping identification using a continuous wavelet transform: application to real data", J. Sound Vib. 262 (2) 291–307.

[46] Erlicher, S., Argoul, P. (2007). Modal identification of linear non-proportionally damped systems by wavelet transform, Mechanical Systems and Signal Processing, 21(3), 1386–1421.

[47] Chen S.-L., J. Liu J., Lai H.-C. (2009). "Wavelet analysis for identification of damping ratios and natural frequencies", J. Sound Vib. 323 (1) 130–147.

[48] Le T.P., Paultre P. (2012) "Modal identification based on continuous wavelet transform and ambient excitation tests", J. Sound Vib. 331 (9) 2023–2037.

[49] Sarparast H., Ashory M.R., Hajiazizi M., Afzali M., Khatibi M.M. (2014). "Estimation of modal parameters for structurally damped systems using wavelet transform", Eur. J. Mech. ASolids 47 82–91.

[50] Dziedziech K., Staszewski W.J., Basu B,. Uhl T. (2015). "Wavelet-based detection of abrupt changes in natural frequencies of time-variant systems", Mech. Syst.Signal Process. 64–65 347–359.

[51] Wijesundara K.K., Negulescu C., Foerster E. (2015). "Estimation of Modal Properties of Low-Rise Buildings Using Ambient Excitation Measurements", Shock and Vibration. Article ID 173450.

[52] Wang, S., Zhao, W., Zhang, G., Xu, H., Du, Y. (2021). "Identification of structural parameters from free vibration data using Gabor wavelet transform", Mechanical Systems and Signal Processing, Volume 147.